JSCSEN 78(1)1–154(2013)

ISSN 1820-7421(Online)

Journal of the Serbian Chemical Society

Electronic version

VOLUME 78

No 1

BELGRADE 2013

Available on line at

www.shd.org.rs/JSCS/

The full search of JSCS is available through

DOAJ DIRECTORY OF OPEN ACCESS JOURNALS

www.doaj.org

Journal of the Serbian Chemical Society
JSCS-info@shd.org.rs • www.shd.org.rs/JSCS

J. Serb. Chem. Soc. Vol. 78, No. 1 (2013)

CONTENTS

Published by the Serbian Chemical Society
Karnegijeva 4/III, 11000 Belgrade, Serbia
Printed by the Faculty of Technology and Metallurgy
Karnegijeva 4, P.O. Box 35-03, 11120 Belgrade, Serbia

Journal of the Serbian Chemical Society
JSCS-info@shd.org.rs • www.shd.org.rs/JSCS

J. Serb. Chem. Soc. 78 (1) 1–13 (2013)
JSCS–4391

UDC 547.447:66.094.2+546.47'273'11+
546.62'214+542.913:547.43
Original scientific paper

$Zn(BH_4)_2/Al_2O_3$: A new synthetic method for the efficient and convenient reduction of organic carbonyl compounds to their corresponding alcohols

DAVOOD SETAMDIDEH*, BEHROOZ KHEZRI and MEHDI RAHMATOLLAHZADEH

Department of Chemistry, Faculty of Sciences, Mahabad Branch, Islamic Azad University, Mahabad, 59135-443, Iran

(Received 11 January 2012)

Abstract: $Zn(BH_4)_2$ (0.5–2 mmol) in the presence of Al_2O_3 (1 mmol) reduces a variety of organic carbonyl compounds such as aldehydes, ketones, acyloins, α-diketones and α,β-unsaturated carbonyl compounds to their corresponding alcohols. The reduction reactions were realized in THF at room temperature affording high to excellent yields of the products. The chemoselective reduction of aldehydes over ketones was successfully accomplished with this reducing system. In addition, regioselectivity and exclusive 1,2-reduction of conjugated carbonyl compounds to their corresponding allylic alcohols in high to excellent yields was successfully accomplished.

Keywords: $Zn(BH_4)_2$; Al_2O_3; reduction; carbonyl compounds; chemoselective; regioselectivity.

INTRODUCTION

It is well known that sodium borohydride reduces organic carbonyl compounds to their corresponding alcohols using enormously different reducing systems.[1] In order to control the reducing power of the reagent, hundreds of substituted borohydrides have been introduced in the chemical literature and many are now commercially available, *e.g.*, $Li(BH_4)$,[2a–c] $K(BH_4)$,[2d] $Ca(BH_4)_2$,[3a] $Cu(BH_4)_2$,[3b–d] $Ti(BH_4)_3$,[4] $Zr(BH_4)_4$,[5a,b] $LiBH_4$, $Ca(BH_4)_2$ and $Zn(BH_4)_2$ are the modified borohydride agents that have better solubility in aprotic solvents, so their uses and applications are of interest in organic synthesis. Among these reagents, zinc borohydride is unique because: a) Zn^{2+} is a soft Lewis acid in comparison to Ca^{2+}, Li^+ and Na^+, which are hard acids and b) better coordination ability of Zn^{2+}, which imparts selectivity in hydride transfer reactions. In addition, reduction of aldehydes and ketones with $NaBH_4$ impregnated on neutral

* Corresponding author. E-mail: davood.setamdideh@gmail.com
doi: 10.2298/JSC120111044S

Al_2O_3 under microwave irradiation has been reported. Although the reported method is fast for the reduction of aldehydes, in the case of ketones, the need for large amounts of $NaBH_4$ (eightfold) and the moderate yields of the products are major limitations.[5c–d] On the other hand, zinc tetrahydroborate, $Zn(BH_4)_2$, as a non-conventional hydride transfer agent, has been reported to effect very efficient chemo-, regio- and stereoselective reductions. This potential reducing agent is neutral and can be used in a range of aprotic solvents, such as ether, THF and DMF. In spite of this, zinc tetrahydroborate has been used less than regular reducing agents in laboratories for the reduction of organic compounds, probably because of its non-availability as a commercial reagent, being freshly prepared in solution, and the problem of controlling its reducing power. To overcome these limitations, stable modifications of $Zn(BH_4)_2$ in the form of tertiary amino or phosphinoligand complexes, such as $[Zn(BH_4)_2(dabco)]$ (dabco: 1,4-diazabicyclo [2.2.2.] octane,[2,6] $[Zn(BH_4)_2(pyz)]_n$ (pyz: pirazin),[7] $[Zn(BH_4)_2(Ph_3P)_{1-2}]$,[8] $[Zn(BH_4)_2(bpy)]$ (bpy: bipyrdine),[9] $[Zn(BH_4)_2(py)]$ (py: pyridine),[10] $[Zn(BH_4)_2–XP_4]$ (XP_4: crosslinked 4-polyvinylpiridine),[11] $[Zn(BH_4)_2(nmi)]$[12a] (nmi: *N*-methylimidazole) and $[Zn(BH_4)_2(nic)]$ (nic: nicotine)[12b] have been made and used for the reduction of organic compounds. The challenge in chemistry to develop efficient processes, reaction media and conditions are some of the most important issues in the scientific community in this matter. In this context and in continuation of previous studies with modified reducing systems,[12] herein, $Zn(BH_4)_2/Al_2O_3$ is introduced as a new combination reducing system for the efficient and convenient reduction of carbonyl compounds to their corresponding alcohols.

RESULTS AND DISCUSSION

Ranu *et al.* reported $Zn(BH_4)_2$ to be a reducing agent capable of reducing some organic carbonyl compounds.[13a–c] To investigate the influence of alumina on the rate of reduction and the lack of systematic information on the reduction of carbonyl compounds with zinc borohydride in the presence of alumina without using any other agent directed the focus of the present study to an investigation of the influence of alumina as a moderator catalyst on this transformation. The preliminary experiments showed that the reduction of benzaldehyde (1 mmol) as a model compound with $Zn(BH_4)_2$ (1 mmol) in THF or CH_3CN was not completed after 1 h at room temperature. However, when this reaction was performed in the presence of neutral alumina (1 mmol), the rate of reduction was dramatically accelerated and the reaction was completed within 1 min (Scheme 1).

These results prompted an investigation of the optimum reaction conditions to examine the influence of alumina as a catalyst. For the selection of the appropriate solvent(s) and amount of catalyst in such reductions, a set of experiments was performed on the reduction of benzaldehyde and acetophenone as model compounds, the results of which are given in Tables I and II, respectively.

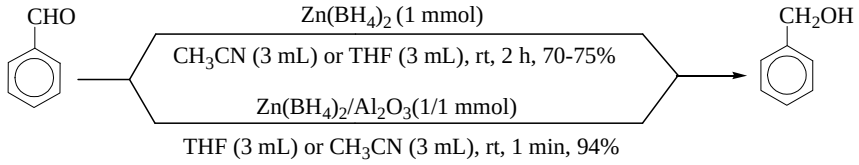

Scheme 1. Comparison of the reduction of benzaldehyde by $Zn(BH_4)_2$ in the presence and absence of neutral alumina.

TABLE I. Optimization reaction conditions for reduction of benzaldehyde with the $Zn(BH_4)_2$, neutral Al_2O_3 system at room temperature

Entry	Molar ratio[a]	Solvent (3 mL)	Time, h	Conversion[b], %
1	(1/0.5/0)	THF	1	<100 [c]
2	(1/1/0)	THF	2	<100 [c]
3	(1/1/0)	CH_3CN	2	<100 [c]
4	(1/0.5/1) [d]	THF	0.08	100
5	(1/0.5/2)	THF	1.5	100
6	(1/0.5/1) [d]	CH_3CN	0.08	100
7	(1/1/1)	THF	0.016	100

[a]Molar ratio benzaldehyde/$Zn(BH_4)_2$/Al_2O_3; [b]completion of the reaction was monitored by TLC (eluent, CCl_4, Et_2O: 5/2); [c]the yields of isolated pure products were 50 % for entry 1, 75 % for entry 2 and 70 % for entry 3; [d]the reduction reactions were performed in the presence of acidic, basic or neutral alumina and the same results were obtained

TABLE II. Optimization reaction conditions for the reduction of acetophenone with the $Zn(BH_4)_2$, neutral Al_2O_3 system at room temperature

Entry	Molar ratio[a]	Solvent (3 mL)	Time, h	Conversion[b], %
1	(1/1/0)	THF	1	<100[c]
2	(1/1/1)[d]	THF	1	100
3	(1/1/2)	THF	1	<100[c]
4	(1/2/1)[d]	THF	0.8	100
5	(1/2/2)	THF	1.2	100

[a]Molar ratio acetophenone/$Zn(BH_4)_2$/Al_2O_3; [b]completion of the reaction was monitored by TLC (eluent, CCl_4, Et_2O: 5/2), [c]the yield of isolated pure products were 60 % for entry 1 and 80 % for entry 3; [d]the reduction reactions were performed in the presence of acidic, basic or neutral alumina and the same results were obtained

The results showed that the reduction of benzaldehyde at room temperature with 0.5 molar amount of $Zn(BH_4)_2$ in the presence of 1 molar amount of neutral Al_2O_3 was very efficient (Table I, entries 4 and 6). In addition, it is noteworthy that the reduction reactions were performed in the presence of acidic and basic Lalumina and the same results were obtained. Then these optimal conditions were applied for the reduction of structurally different aliphatic and aromatic aldehydes with neutral alumina. All the reactions were performed with 0.5 mol $Zn(BH_4)_2$ per mol aldehyde at room temperature and the corresponding primary alcohols were obtained in high to excellent yields (83–97 %), as could be seen in Table III.

TABLE III. Reduction of aldehydes (1 mmol) with the $Zn(BH_4)_2$ (0.5 mmol)/Al_2O_3 (1 mmol) system in THF (3 mL) at room temperature; the reduction reactions were realized in the presence of neutral alumina

Entry	Substrate	Product	Time h	Yield[a] %	M.p. or B.p., °C	
					Found	Reported[14]
1	Benzaldehyde	Benzyl alcohol	0.08	94	203–204	205
2	4-Chlorobenzaldehyde	4-Chlorobenzyl alcohol	0.08	92	71–73	70–72
3	3-Chlorobenzaldehyde	3-Chlorobenzyl alcohol	0.08	96	238	237
4	2,4-Dichlorobenzaldehyde	2,4-Dichlorobenzyl alcohol	0.08	90	56–58	55–58
5	4-Methylbenzaldehyde	4-Methylbenzyl alcohol	0.1	93	60–62	59–61
6	4-Methoxybenzaldehyde	4-Methoxybenzyl alcohol	0.1	93	258	259
7	4-Hydroxybenzaldehyde	4-Hydroxybenzyl alcohol	0.1	97	119–122	118–122
8	2-Hydroxybenzaldehyde	2-Hydroxybenzyl alcohol	0.1	92	84–85	83–85
9	3-Nitrobenzaldehyde	3-Nitrobenzyl alcohol	0.08	94	31–33	30–32
10	4-Nitrobenzaldehyde	4-Nitrobenzyl alcohol	0.08	94	92–94	92–94
11	4-Hydroxy-3-methoxy benzaldehyde	4-Hydroxy-3-methoxybenzyl alcohol	0.1	97	114–115	113–115
12	Furfural	Furfuryl alcohol	0.1	88	169–170	170
13	1-Naphthaldehyde	1-Naphthylmethanol	0.1	90	61–62	61–63
14	2,6-Dimethylhept-5-enal	2,6-Dimethylhept-5-en-1-ol	0.08	90	225–227	225–226
15	Heptanal	1-Heptanol	0.08	83	177	176

[a]Yields refer to isolated pure products

Next, attention was turned to the reduction of ketones using this reducing system. The low reactivities of ketones relative to those of aldehydes led to the reduction reactions being performed under different conditions, *i.e.*, the reductions were performed with 1 molar amounts of $Zn(BH_4)_2$ at room temperature in the presence of 1 molar amounts of neutral Al_2O_3 in THF (Table II, entry 2). The utility of this reducing system was further explored with the reduction of structurally different aliphatic and aromatic ketones using 1 mol $Zn(BH_4)_2$ in the presence of 1 mol neutral Al_2O_3 per mol ketone in THF at room temperature. Such reductions were also efficient and the corresponding secondary alcohols were obtained in high to excellent yields (87–98 %) (Table IV).

The synthetic applications of vicinal diols are well known and their preparations from the reduction of acyloins or α-diketones have attracted a great deal of attention. Reduction of α-diketones usually gives a mixture of α-hydroxy ketones and vicinal diols. Selective reduction of α-diketones to acyloins[15] or vicinal diols[16] can be undertaken with some chemical or biochemical reagents. Reduction of α-diketones to vicinal diols with modified hydroborate agents is also a subject of interest[12,17] and this goal was easily achieved by $Zn(BH_4)_2$ (2 mol) in the presence of 1 mol neutral Al_2O_3 in THF at room temperature. The

reduction reactions were performed efficiently in short reaction times (20–40 min) (92–95 %) (Table V). Under different conditions, attempts to reduce α-diketones into acyloins were unsatisfactory and only vicinal diols were identified as the sole products. In addition, reduction of acyloins to vicinal diols is also a subject of interest in organic synthesis. The applications of non-hydridic reductants[18] and modified hydroborate[12,17] have also been reported for such reductions. Using $Zn(BH_4)_2$ (1 mol) in the presence of neutral Al_2O_3 (1 mol) in THF also easily provided this transformation at room temperature. Acyloin compounds were reduced to their corresponding vicinal diols in high to excellent yields with this reducing system (90–94 %) (Table V, entries 2 and 4).

TABLE IV. Reduction of ketones (1 mmol) with the $Zn(BH_4)_2$ (1 mmol)/Al_2O_3 (1 mmol) system in THF (3 mL) at room temperature; the reduction reactions were realized in the presence of neutral alumina

Entry	Substrate	Product	Time	Yield[a]	M.p. or B.p., °C	
			h	%	Found	Reported[14]
1	Benzophenone	Diphenylmethanol	3	96	65–67	65–67
2	Acetophenone	1-Phenylethanol	1	93	203	204
3	4-Bromoacetophenone	1-(4-Bromophenyl)ethanol	1	98	37–38	36–37
4	4-Methylacetophenone	1-(4-Methylphenyl)-ethanol	3	93	219–221	218–220
5	4-Methoxybenzo-phenone	(4-Methoxyphenyl)-(phenyl)methanol	4	90	68–69	67–69
6	2,3-Dihyro-1*H*-inden--1-one	2,3-Dihydro-1*H*-inden-1-ol	1.5	95	52–55	50–54
7	9*H*-Fluoren-9-one	9*H*-Fluoren-9-ol	1.6	93	153–154	153–154
8	4-Phenylcyclohexanone	4-Phenylcyclohexanol	1	87	58–60	58
9	4-Phenyl-2-butanone	4-Phenylbutan-2-ol	0.8	90	131–132	132

[a]Yields refer to isolated pure products

The chemoselective reduction of one functional group without affecting the other one is a well-known strategy for the preparation of molecules with ever-increasing complexity in organic synthesis.

This subject is of great interest and numerous modified hydroborate systems have been reported for it.[6,8–10a–c,12,13b,17,19] Since under the defined conditions, the reduction of aldehydes and ketones with $Zn(BH_4)_2$ in the presence of Al_2O_3 is dependent on the molar ratio of $Zn(BH_4)_2$ to Al_2O_3, it was thought that this system could have a chemoselectivity towards the reduction of aldehydes over ketones. This fact was demonstrated with the selective reduction of benzaldehyde in the presence of acetophenone using 0.5 mol $Zn(BH_4)_2$ in the presence of 1 mol neutral Al_2O_3 at room temperature in THF (Table VI, entry 3) (Scheme 2).

TABLE V. Reduction of acyloins and α-diketones with the $Zn(BH_4)_2/Al_2O_3$ (1 mmol) in THF (3 mL) at room temperature; the reduction reactions were realized in the presence of neutral alumina

Entry	Substrate	Product	$Zn(BH_4)_2$/ Substrate	Time h	Yield[a] %	M.p. or B.p., °C Found	M.p. or B.p., °C Reported[14]
1	Benzyl[b]	1,2-Diphenyl-ethane-1,2-diol	2/1	0.33	95	–	–
2	Benzoin[b]	1,2-Diphenyl-ethane-1,2-diol	1/1	0.33	90	–	–
3	1,2-Bis(4-methoxyphe-nyl)ethane-1,2-dione[b]	1,2-Bis(4-me-thoxyphenyl)-ethane-1,2-diol	2/1	0.58	92	–	–
4	2-Hydroxy-1,2-bis(4--methoxyphenyl)-ethanone[b]	1,2-Bis(4-me-thoxyphenyl)-ethane-1,2-diol	1/1	0.5	94	–	–
5	1,3-Diphenylpro-pane-1,2-dione	1,3-Diphenyl-propane-1,2-diol	2/1	0.67	95	63–64	63–64

[a]Yields refer to isolated pure products; [c]the pinacols were formed as dl-*meso* mixtures that were not separated

TABLE VI. Optimization of the reaction conditions for the competitive reduction of benzaldehyde (1 mmol) and acetophenone (1 mmol) with the $Zn(BH_4)_2$, Al_2O_3 system in THF (3 mL) at room temperature; the reduction reactions were performed in the presence of neutral alumina

Entry	Molar ratio[a]	Time, h	Yield of benzyl alcohol[b], %	Yield of 1-phenylethanol[b], %
1	1/1/0.5/0	1	50	30
2	1/1/0.5/0.5	1	79	6
3[c]	1/1/0.5/1	0.08	97	0
4	1/1/1/1	1	94	30
5	1/1/2/1	1	96	51

[a]Molar ratio as benzaldehyde, acetophenone, $Zn(BH_4)_2$, Al_2O_3; [b]yields refer to isolated pure products by PLC (eluent, CCl_4, Et_2O: 5/2); [c]GC analysis was also performed

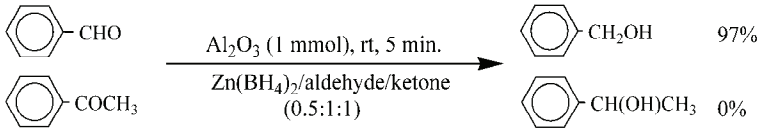

Scheme 2. Competitive reduction of benzaldehyde and acetophenone with $Zn(BH_4)_2$/neutral Al_2O_3 system in THF; the ratio in parentheses is in mmol.

The usefulness of this chemoselectivity of the reduction was further examined with the reduction of benzaldehyde in the presence of other ketones. As shown in Table VII, benzaldehyde was reduced exclusively, or nearly so.

Reduction of unsaturated carbonyl compounds with sodium borohydride, one of the most widely utilized reducing agents, is highly solvent dependent and generally does not result in useful regioselectivity.[20a,b] To control the reducing potential and selectivity of $NaBH_4$ into regioselective 1,2-reduction of conju-

gated enones, numerous hydroborate agents have been developed in the following ways: a) by the replacement of hydride(s) with sterically bulky substituents or electron-withdrawing/releasing groups in order to discriminate between the structural and electronic environments of carbonyl groups;[20c–f] b) combination with Lewis acids[20g–k,3a] and mixed solvent systems;[20a] c) use of transition metal hydroborates and their new modifications;[20l] d) use of quaternary ammonium and phosphonium tetrahydroborates;[19e–f,20m–n] e) and finally immobilization on an anion exchange resin.[20o]

TABLE VII. Competitive reduction of benzaldehyde (1 mmol) in the presence of ketones (1 mmol) to their corresponding alcohols with $Zn(BH_4)_2$ (0.5 mmol), neutral Al_2O_3 (1 mmol) in THF (3 mL) at room temperature

Entry	Ketone	Time, h	Yield1[a], %	Yield2[b], %
1	Acetophenone	0.08	97	0
2	Benzophenone	0.08	93	2
3	9*H*-Fluoren-9-one	0.08	95	3
4	4-Phenylbutan-2-one	0.08	91	8

[a]Yield1 of benzyl alcohol refers to isolated pure products by PLC (eluent, CCl_4, Et_2O: 5/2); [b]yields of corresponding alcohols for ketones refer to isolated pure products by PLC (eluent, CCl_4, Et_2O: 5/2)

The usefulness of the studied reducing system was further investigated with the regioselective 1,2-reduction of *α*,*β*-unsaturated carbonyl compounds. Thus, the reduction of cinnamaldehyde was examined. The reduction reaction occurred with 0.5 mmol $Zn(BH_4)_2$ in the presence of 1 mmol neutral Al_2O_3 in 5 min at room temperature in THF with a perfect regioselectivity and the product cinnamyl alcohol was obtained in high yield (Table VIII, entry 1). This procedure was also applied for the reduction of citral at room temperature and geraniol was obtained in 92 % yield (Table VIII, entry 2).

Furthermore, the reductions of conjugated enones with the studied reducing system were investigated. The results showed that the procedure was also regioselective and efficient, but the reduction reactions were performed using 1 molar amounts of $Zn(BH_4)_2$ in the presence of 1 molar amounts of neutral Al_2O_3 at room temperature in THF. Regioselective 1,2-reductions of benzylideneacetone and chalcone were successfully achieved, with high to excellent yields of the corresponding allylic alcohols (Table VIII, entries 3 and 4).

In order to show the efficiency of the reducing system $Zn(BH_4)_2/Al_2O_3$, the results obtained in the present were compared with those of reported in the literature for $NaBH_4/MoCl_5$,[21a] $NaBH_4$/Dowex1-x8,[21b] $[Zn(BH_4)_2(bpy)]$,[9] $[Zn(BH_4)_2(py)]$,[10] $[Zn(BH_4)_2(Ph_3P)_2]$,[8] $Ph_3PMe(BH_4)$[20m] and $[PhCH_2(dabco)]BH_4$[19e], as given in Table IX.

TABLE VIII. Reduction of conjugated carbonyl compounds with $Zn(BH_4)_2$, Al_2O_3 (1 mmol) in THF (3 mL) at room temperature; the reduction reactions were performed in the presence of neutral alumina

Entry	Substrate	Product	$Zn(BH_4)_2$/ Substrate	Time h	Yield[a] %	M.p. or B.p., °C Found	Reported[14]
1	Cinnamaldehyde	3-Phenyl-2-propen--1-ol	0.5/1	0.08	96	33–34	33–35
2	*Cis* and *trans* citral	*Cis* and *trans*-3,7-dimethyl-2,6-octadien--1-ol[b]	0.5/1	0.08	92	–	–
3	Benzylideneacetone	4-Phenyl-3-butene--2-ol	1/1	1	95	55–56	55–57
4	Chalcone	1,3-Diphenylprop-2--en-1-ol	1/1	3	91	33–34	33–34

[a]Yields refer to isolated pure products; [b]*cis* and *trans* geraniol were not separated

TABLE IX. Comparison of the reductions of aldehydes and ketones with $Zn(BH_4)_2/Al_2O_3$ system and with other reported reducing systems; I – $Zn(BH_4)_2/Al_2O_3$, II – $NaBH_4/MoCl_5$, III – $NaBH_4$/Dowex1-x8, IV – $[Zn(BH_4)_2(bpy)]$, V – $[Zn(BH_4)_2(py)]$, VI – $[Zn(BH_4)_2(Ph_3P)_2]$, VII – $Ph_3PMe(BH_4)$, VIII – $[PhCH_2(dabco)]BH_4$

Entry	Substrate	Molar ratio (reagent/substrate), time, h, yield, % I	II[21a]	III[21b]	IV[9]	V[10]	VI[8]	VII[20m]	VIII[19e]
1	Benzaldehyde	0.5, 0.08, 94	0.5, 0.03, 96	1, 0.05, 96	0.25, 0.02, 95	1, 0.5, 91	–	1, Im[a], 90	1, 0.25, 90
2	4-Methoxybenzaldehyde	0.5, 0.1, 93	1.5, 3, 99	1.5, 3, 99	0.35, 0.17, 99	1, 1.3, 96	1, 0.17, 89	1, Im, 83	2, 0.8, 85
3	4-Chlorobenzaldehyde	0.5, 0.08, 92	1, 0.15, 99	1, 0.15, 99	0.25, 0.08, 98	1, 0.2, 99	1, Im, 88	1, Im, 86	1, 0.23, 90
4	Benzophenone	1, 3, 96	3, 3.2, 98	3, 3.2, 98	1, 0.75, 99	2, 4.3, 97	–	–	2, 21.5, 90
5	9*H*-Fluoren-9-one	1, 1.6, 93	2, 1.8, 94	2, 1.8, 94	1, 1.5, 94	2, 5.3, 98	2, 0.33, 85	1.6, 18, 80	–
6	Benzoin	1, 0.33, 90	2, 0.17, 96	2, 0.17, 96	0.5, 0.08, 91	0.5, 0.5, 97	–	–	–

[a]Immediately

EXPERIMENTAL

All substrates and reagents of the best available quality were purchased from commercial sources and used without further purification. IR and ^{1}H-NMR spectra were recorded on a PerkinElmer FT-IR RXI and a 300 MHz Bruker spectrometers, respectively. Agilent 6890N gas chromatograph equipped with a FID detector was used in this study. The products were characterized by their ^{1}H-NMR or IR spectra and comparison with authentic samples (melting points or boiling points). The organic layers were dried over anhydrous sodium sulfate. All

yields refer to isolated pure products. TLC on silica gel 60 F_{254} aluminum sheets was applied for purity determination of the substrates and products and to monitor the reactions.

A typical procedure for reduction of aldehydes with the $Zn(BH_4)_2/Al_2O_3$ system in THF

$Zn(BH_4)_2$ was prepared from $ZnCl_2$ and $NaBH_4$ according to an established procedure from the literature.[5] In a round-bottomed flask (10 mL) equipped with a magnetic stirrer, a solution of benzaldehyde (0.106 g, 1 mmol) in THF (3 mL) was prepared. To this solution, $Zn(BH_4)_2$ (0.048 g, 0.5 mmol) and then neutral Al_2O_3 (0.101 g, 1 mmol) were added and the mixture was stirred at room temperature for 5 minutes. Completion of the reaction was monitored by TLC (eluent, CCl_4/Et_2O: 5/2). Then, distilled water (1 mL) was added to the reaction mixture and stirring was continued stirred for 5 min.. The mixture was extracted with CH_2Cl_2 (3×6 mL) and dried over anhydrous Na_2SO_4. Evaporation of the solvent and a short column chromatography of the resulting crude material over silica gel (0.015–0.040 mm, eluent, CCl_4/Et_2O: 5/3) afforded the pure liquid benzyl alcohol (0.102 g, 94 %, Table III, entry 1).

A typical procedure for reduction of ketones to alcohols with the $Zn(BH_4)_2/Al_2O_3$ system in THF

In a round-bottomed flask (10 mL) equipped with a magnetic stirrer, a solution of acetophenone (0.121 g, 1 mmol) in THF (3 mL) was prepared. To this solution, $Zn(BH_4)_2$ (0.095 g, 1 mmol) and then neutral Al_2O_3 (0.101 g, 1 mmol) were added. The resulting mixture was stirred at room temperature for 60 min. The progress of the reaction was monitored by TLC (eluent, CCl_4/Et_2O: 5/2). After completion of the reaction, distilled water (1 mL) was added to the reaction mixture and then stirring was continued for an additional 5 min. The mixture was extracted with CH_2Cl_2 (3×8 mL) and dried over anhydrous sodium sulfate. Evaporation of the solvent and short column chromatography of the resulting crude material over above mentioned silica gel afforded pure crystals of 1-phenylethanol (0.11 g, 93 % yield, Table IV, entry 2).

A typical procedure for reduction of α-diketones and acyloins with the $Zn(BH_4)_2/Al_2O_3$ system in THF

In a round-bottomed flask (10 mL) equipped with a magnetic stirrer, a solution of benzil (0.21 g, 1 mmol) in THF (3 mL was prepared. To this solution, $Zn(BH_4)_2$ (0.190 g, 2 mmol) and then neutral Al_2O_3 (0.101 g, 1 mmol) were added. The resulting mixture was stirred at room temperature for 20 min. The progress of the reaction was monitored by TLC (eluent, CCl_4/Et_2O: 5/2). After completion of the reaction, distilled water (1 mL) was added to the reaction mixture and stirring was continued for an additional 5 min. The mixture was extracted with CH_2Cl_2 (3×10 mL) and dried over anhydrous sodium sulfate. Evaporation of the solvent and short column chromatography of the resulting crude material over above mentioned silica gel afforded pure crystals of 1,2-diphenylethane-1,2-diol (0.20 g, 95 % yield, Table V, entry 1).

A typical procedure for the competitive reduction of aldehydes and ketones with the $Zn(BH_4)_2/Al_2O_3$ system in THF (method A)

In a round-bottomed flask (10 mL) equipped with a magnetic stirrer, a solution of benzaldehyde (0.106 g, 1 mmol) and acetophenone (0.120 g, 1 mmol) in THF (3 mL) was prepared. To this solution, $Zn(BH_4)_2$ (0.048 g, 0.5 mmol) and then neutral Al_2O_3 (0.101 g, 1 mmol) were added and the mixture was stirred at room temperature. The progress of the reaction was monitored by TLC. After 5 min, the reaction mixture was quenched by addition of distilled water (1 mL) and this mixture was then stirred for an additional 5 min. The mixture was extracted with CH_2Cl_2 (3×8 mL) and dried over anhydrous sodium sulfate. After

the evaporation of solvent, the resulting crude products (0.223 g) were separated by plate layer chromatoghraphy (PLC) over silica gel (60 F_{254} (0.063–0.200 mm), eluent, CCl_4/Et_2O: 5/2), which afforded pure liquid benzyl alcohol as the sole product (0.106 g, 97 %) and acetophenone (0.108 g, 89 %) as intact material (Table VI, entry 3).

A typical procedure for competitive reduction of aldehydes and ketones with $Zn(BH_4)_2/Al_2O_3$ system in THF (method B)

In a round-bottomed flask (10 mL) equipped with a magnetic stirrer, a solution of benzaldehyde (0.106 g, 1 mmol) and acetophenone (0.121 g, 1 mmol) in THF (3 mL) was prepared. A sample of reaction mixture in THF is injected (0.1 μL) onto a HP5 30 m×25 μm capillary column. The initial column temperature (100 °C) was held for 2 min, then increased at 15 °C min^{-1} to 240 °C and held for 15 min. Benzaldehyde eluted first (7.28 min) followed by acetophenone (10.29 min) with a relative response ratio of about 1:1 (Instrument parameters: injector temperature, 250 °C; detector temperature, 300 °C; flow rate (He), 45 mL min^{-1}, with He as the make-up gas). Then, to this solution, $Zn(BH_4)_2$ (0.048 g, 0.5 mmol) and then neutral Al_2O_3 (0.101 g, 1 mmol) were added and the mixture was stirred at room temperature. The progress of the reaction was monitored by TLC. After 5 min, the reaction mixture was quenched by the addition of distilled water (0.5 mL) and the stirring was continued for an additional 5 min. and dried over anhydrous sodium sulfate. Again, a sample of reaction mixture in THF is injected (0.1 μL) onto the GC column under the same conditions. Benzyl alcohol eluted first (9.71 min) followed by acetophenone (10.29 min) with a relative response ratio of about 1:1. The reduction procedure afforded pure liquid benzyl alcohol as the sole product and acetophenone as unreacted material.

The typical procedure for the regioselective 1,2-reduction of conjugated carbonyl compounds with the $Zn(BH_4)_2/Al_2O_3$ system in THF

In a round-bottomed flask (10 mL) equipped with a magnetic stirrer, a solution of benzylideneacetone (0.146 g, 1 mmol) in THF (3 mL) was prepared. To this solution, $Zn(BH_4)_2$ (0.0.95 g, 1 mmol) and then neutral Al_2O_3 (0.101 g, 1 mmol) were added. The resulting mixture was stirred at room temperature. The progress of the reaction was monitored by TLC (eluent, CCl_4/Et_2O: 5/2). After completion of the reaction within 60 min, distilled water (1 mL) was added to the reaction mixture and this mixture was then stirred for an additional 5 min. The mixture was extracted with CH_2Cl_2 (3×10 mL) and dried over anhydrous sodium sulfate. Evaporation of the solvent and short column chromatography of the resulting crude material over silica gel (eluent, CCl_4/Et_2O: 5/2) afforded pure liquid 4-phenyl-3-buten-2-ol (0.140 g, 95 % yield, Table VIII, entry 3).

CONCLUSIONS

In this investigation, it was shown that the combination system of $Zn(BH_4)_2$/ /Al_2O_3 in THF reduces a variety of carbonyl compounds to their corresponding alcohols in high to excellent yields. The reduction reactions were performed with 0.5–2 mmol $Zn(BH_4)_2$ in the presence of 1 mmol Al_2O_3 in THF. Reduction of acyloins and α-diketones by this reducing system also efficiently produced the corresponding vicinal diols**.** In addition, the chemoselective reduction of aldehydes over ketones was successfully accomplished with this reducing system. Regioselectivity of this system was also investigated with exclusive 1,2-reduction of conjugated carbonyl compounds to their corresponding allylic alcohols in high

to excellent yields. All reductions were realized at room temperature. The high efficiency of the reductions, short reaction times and easy work-up procedure makes this combined reductant an attractive new protocol for the reduction of carbonyl compounds and it could be a useful addition to the existing methodologies.

Acknowledgments. The authors gratefully appreciate the financial support of this work by the Research Council of the Islamic Azad University Branch of Mahabad, Iran. The assistance of Mr. Avat Ali Poramjad and Mr. Chalak Azimi for running the FT-IR spectra is also acknowledged.

И З В О Д

$Zn(BH_4)_2/Al_2O_3$: НОВ СИНТЕТИЧКИ ПОСТУПАК ЗА ЕФИКАСНУ РЕДУКЦИЈУ ОРГАНСКИХ КАРБОНИЛНИХ ЈЕДИЊЕЊА ДО ОДГОВАРАЈУЋИХ АЛКОХОЛА

DAVOOD SETAMDIDEH, BEHROOZ KHEZRI и MEHDI RAHMATOLLAHZADEH

Department of Chemistry, Faculty of Sciences, Mahabad Branch, Islamic Azad University, Mahabad, 59135-443, Iran

$Zn(BH_4)_2$ (0,5–2 mmol) у присуству Al_2O_3 (1 mmol) редукује различита карбонилна једињења, као што су алдехиди, кетони, ацилоини, *α*-дикетони и *α*,*β*-незасићена карбонилна једињења, до одговарајућих алкохола. Реакција се одвија у тетрахидрофурану као растварачу, на собној температури, а принос производа је висок до одличан. Хемиоселективна редукција алдехида у присуству кетона извршена је успешно. Осим тога, постигнута је региоселективност и селективна 1,2-редукција конјугованих карбонилних једињења до одговарајућих алилних алкохола у високом до одличном приносу.

(Примљено 11. јануара 2012)

REFERENCES

1. a) H. O. House, *Modern Synthetic Reaction*, Benjamin, Menlo Park, CA, USA, 1972; b) S. D. Burk, R. L. Danheiser, *Handbook of Reagents for Organic Synthesis, Oxidising and Reducing Agents*, Wiley-VCH, New York, 1999; c) J. Seyden-Penne, *Reductions by the Alumino and Borohydrides in Organic Synthesis*, Wiley-VCH, New York, 1997; d) M. Hudlicky, *Reductions in Organic Chemistry*, Ellis Horwood, Chichester, UK, 1984.
2. a) H. C. Brown, S. Narasimhan, Y. M. Choi, *J. Org. Chem.* **47** (1982) 4702; b) K. Oai, A. Ookawa, *J. Org. Chem.* **51** (1986) 4000; c) A. Arase, Y. Nunokawa, Y. Masuda, Y. M. Hoshi, *J. Chem. Soc., Chem. Commun.* (1991) 205; d) I. Nishiwaki, F. Fujiyama *Synthesis* (1972) 569
3. a) H. Fujii, K. Oshima, K. Utimoto, *Chem. Lett*. (1991) 1847; b) M. E. Osborn, J. F. Pegues, L. A. Paquett, *J. Org. Chem.* **45** (1980) 167; c) G. W. J. Fleet, P. J. C. Harding, *Tetrahedron Lett.* **22** (1981) 675; d) J. A. Cowan, *Tetrahedron Lett.* **27** (1986) 1205
4. a) K. Ravikumar, S. S. Baskaran, S. Chandrasekaran, *Tetrahedron Lett.* **34** (1993) 171; b) T. J. Marks, J. R. Kolb, *Chem. Rev*. **77** (1977) 263
5. a) W. J. Gensler, F. Johnson, A. D. B. Sloan, *J. Am. Chem. Soc*. **82** (1960) 6074; b) P. Crabbe, G. A. Garcia, C. Rius, *J. Chem. Soc., Perkin Trans. 1* (1973) 810; c) H. C. Brown, S. Krishnamurthy, *Tetrahedron* 35 (1979) 567; d) R. S. Varma, R. K. Saini, *Tetrahedron Lett.* 38 (1997) 4337

6. H. Firouzabadi, M. Adibi, B. Zeynizadeh, *Synth. Commun.* **28** (1998) 1257
7. B. Tamami, M. M. Lakouraj, *Synth. Commun.* **25** (1995) 3089
8. H. Firouzabadi, M. Adibi, M. Ghadami, *Phosphorus Sulfur Silicon Relat. Elem.* **142** (1998) 191
9. B. Zeynizadeh, *Bull. Chem. Soc. Jpn.* **76** (2003) 317
10. a) B. Zeynizadeh, F. Faraji, *Bull. Korean Chem. Soc.* **24** (2003) 453; b) B. Zeynizadeh, K. Zahmatkesh, *J. Chin. Chem. Soc.* **50** (2003) 267; c) B. Zeynizadeh, K. Zahmatkesh, *J. Chin. Chem. Soc.* **51** (2004) 801; d) B. Zeynizadeh, K. Zahmatkesh, *J. Chin. Chem. Soc.* **52** (2005) 109; f) B. Zeynizadeh, D. Setamdideh, F. Faraji, *Bull. Korean Chem. Soc.* **29** (2008) 76
11. H. Firouzabadi, B. Tamami, N. Goudarzian, *Synth. Commun.* **21** (1991) 2275
12. a) B. Zeynizadeh, D. Setamdideh, *Asian J. Chem*. **21** (2009) 3603; b) D. Setamdideh, M. Rafig, *E-J. Chem*. **9** (2012) 2338; c) B. Zeynizadeh, D. Setamdideh, *J. Chin. Chem. Soc.* **52** (2005) 1179; d) D. Setamdideh, B. Zeynizadeh, *Zeit. Naturforsch.* **61b** (2006) 1275; e) B. Zeynizadeh, D. Setamdideh, *Synth. Commun*. **36** (2006) 2699; f) D. Setamdideh, B. Khezri, *Asian J. Chem*. **22** (2010) 5566; g) D. Setamdideh, B. Khezri, M. Mollapour, *Orient. J. Chem.* **27** (2011) 991
13. a) B. C. Ranu, *Synlett.* (1993) 885; b) B. C. Ranu, R. Chakraborty, *Tetrahedron Lett*. **31** (1990) 7663; c) D. C. Sarkar, A. R. Das, B. C. Ranu, *J. Org. Chem.* **55** (1990) 5799
14. a) *Dictionary of organic compounds*, 5th ed., Chapman & Hall, New York, 1982; b) *Fluka Catalogue of Fine Chemicals*, 2003; c) *Aldrich Catalogue of Fine Chemicals*, 2003
15. a) W. Kreiser, *Ann. Chem*. **745** (1971) 164; b) V. H. Pechmann, F. Dahl, *Chem. Ber*. **23** (1890) 2421; c) T. L. Ho, G. A. Olah, *Synthesis* (1976) 815; d) T. Mori, T. Nakahara, H. Nozaki, *Can. J. Chem*. **47** (1969) 3266; e) R. Mayer, G. Hiller, M. Nitzschke, J. Jentzsch, *Angew. Chem.* **75** (1963) 370; f) M. B. Rubin, J. M. Ben-Bassat, *Tetrahedron Lett*. **12** (1971) 3403
16. M. Imuta, H. Ziffer, *J. Org. Chem.* **43** (1978) 3530
17. a) B. Zeynizadeh, F. Shirini, *J. Chem. Res.* (2003) 335; b) B. Zeynizadeh, S. Yahyaei, *Zeit. Naturforsch.* **59b** (2004) 704
18. A. T. Blomquist, A. Goldstein, *Org. Synth.* **36** (1956) 12
19. a) J. S. Cha, E. J. Kim, O. O. Kwon, J. M. Kim, *Bull. Korean Chem. Soc*. **17** (1996) 50; b) J. S. Cha, O. O. Kwon, S. Y. Kwen, J. M. Kim, W. W. Seo, S. W. Chang, *Bull. Korean Chem. Soc*. **17** (1996) 221; c) J. S. Cha, O. O. Kwon, J. M. Kim, *Bull. Korean Chem. Soc*. **17** (1996) 725; d) J. S. Cha, O. O. Kwon, J. M. Kim, H. Song, *Bull. Korean Chem. Soc*. 17 (1996) 900; e) H. Firouzabadi, G. R. Afsharifar, *Bull. Chem. Soc. Jpn.* **68** (1995) 2595; f) H. Firouzabadi, G. R. Afsharifar, *Synth. Commun.* **22** (1992) 497; j) C. F. Nutaitis, G. W. Gribble, *Tetrahedron Lett*. **24** (1983) 4287; h) S. Kim, Y. J. Kim, C. H. Oh, K. H. Ahn, *Bull. Korean Chem. Soc*. **5** (1984) 202
20. a) R. S. Varma, G. W. Kabalka, *Synth. Commun.* **15** (1985) 985; b) C. F. Nutaitis, J. E. Bernardo, *J. Org. Chem*. **54** (1989) 5629; c) S. Krishnamurthy, H. C. Brown, *J. Org. Chem*, **40** (1975) 1864; d) S. Krishnamurthy, H. C. Brown, *J. Org. Chem.* **42** (1977) 1197; e) S. Kim, Y. C. Moon, K. H. Ahn, *J. Org. Chem*. **47** (1982) 3311; f) E. J. Corey, K. B. Becker, R. K. Varma, *J. Am. Chem. Soc.* **94** (1972) 8616; g) J. C. Fuller, E. L. Stangeland, C. T. Goralski, B. Singaram, *Tetrahedron Lett.* **34** (1993) 257; h) B. Ganem, *J. Org. Chem*. **40** (1975) 146; i) J. M. Fortunato, B. Ganem, *J. Org. Chem*. **41** (1976) 2194; j) J. L. Luche, *J. Am. Chem. Soc*. **100** (1978) 2226; k) A. L. Gemal, J. L. Luche, *J.*

Am. Chem. Soc. **103** (1981) 5454; l) K. S. Ravikumar, S. Baskaran, S. Chandrasekaran, *J. Org. Chem*. **58** (1993) 5981; m) H. Firouzabadi, M. Adibi, *Synth. Commun*. **26** (1996) 2429; n) H. Firouzabadi, M. Adibi, *Phosphorus, Sulfur, Silicon Relat. Elem*. **142** (1998) 125; o) A. R. Sande, M. H. Agadale, R. B. Mane, M. M. Salunkhe, *Tetrahedron Lett.* **25** (1984) 3501

21. a) B. Zeynizadeh, S. Yahyaei, *Bull. Korean Chem. Soc*. **24** (2003) 1664; b) H. C. Brown, B. C. Subba Rao, *J. Am. Chem. Soc.* **78** (1956) 2582.

Journal of the Serbian Chemical Society
JSCS-info@shd.org.rs • www.shd.org.rs/JSCS
J. Serb. Chem. Soc. 78 (1) 15–25 (2013)
JSCS–4392
UDC *norcantharidin+547.75–125+547.6–334
Original scientific paper

Antioxidant and radical scavenging activities of some norcantharidin and bridged perhydroisoindole derivatives

AYSEGUL PEKSEL[1]*, CUMALI CELIK[1,2], NUKET OCAL[1] and REFIYE YANARDAG[3]

[1]Department of Chemistry, Faculty of Arts and Science, Yildiz Technical University, Davutpasa, Istanbul-34210, Turkey, [2]Community College, Yalova University, Yalova-77100, Turkey and [3]Department of Chemistry, Faculty of Engineering, Istanbul University, Avcilar, İstanbul-34320, Turkey

(Received 23 January, revised 15 March 2012)

Abstract: A series of norcantharidin and bridged perhydroisoindole derivatives were evaluated for their antioxidant and radical scavenging activities. Different *in vitro* methodologies, such as total reducing power, 1,1-diphenyl-2-picryl-hydrazil (DPPH$^{\bullet}$) free radical scavenging, superoxide anion radical scavenging and metal chelating activities were used. Among the 11 tested compounds, 7 compounds showed potent reducing power activity and 7 compounds showed potent superoxide anion radical scavenging activity. All the tested compounds exhibited potent free radical scavenging ability. The results showed that the synthesized compounds have effective antioxidant power.

Keywords: norcantharidin; bridged perhydroisoindole; reducing power; superoxide anion radical.

INTRODUCTION

The imide moiety is an integral structural part of various important bioactive molecules, such as fumaramidmycin, granulatimide, isogranulatimide and rebeccamycin. These molecules are reported to exhibit antitumour, anti-inflammatory and antimicrobial activities.[1–3] A literature search revealed that certain compounds with antitumour activity, and in particular molecules able to interact with DNA, are characterized by the presence of both an extended π-system and an imide function. In addition, *N*-substituted imides, such as maleimides,[4] isohematinic acids[5] and especially bicyclic and tricyclic derivatives such as tandospirone derivatives[3,6] are known for their broad spectrum of pharmacological properties, thus showing antibiotic, fungicidal, analgesic, anxiolytic and cytostatic effects.

On the other hand, derivatives of the tricyclic anhydride *exo*-5,6-dehydronorcantharidin (**2**, Fig. 1) are also pharmacologically active.[7] This compound shows

* Corresponding author. E-mail: peksel@yildiz.edu.tr
doi: 10.2298/JSC120123036P

a comparable activity to that of cantharidin (**1**, Fig. 1), which is the major effective ingredient in pharmaceuticals for the treatment of certain malignant tumours in China. Norcantharidin is a synthetic demethylated analogue of cantharidin, a traditional Chinese herb, now being worldwide used as an antitumour agent for its safety without myelosuppression in patients and effectiveness against cells with a multidrug resistance phenotype. It was reported that norcantharidin could induce cell apoptosis and inhibit the proliferation of a variety of human tumour cell lines *in vitro*, including colorectal cancer, oral cancer, cervical cancer, breast cancer, hepatoma, leukaemia, melanoma and gall bladder carcinoma, and it was proved to block tumour invasion, metastasis and angiogenesis.[8] Norcantharidin and *exo*-5,6-dehydro-norcantharidin (**2**) have been widely employed in clinical practice, as they are less toxic and much easier to synthesize.[9,10] Perhydroisoindoles are also selective sigma receptor antagonists and have a low potential for movement disorder side effects associated with typical antipsychotic agents.[11,12]

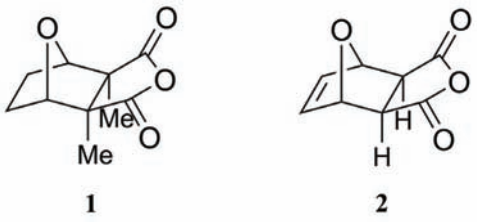

Fig. 1. The structures of cantharidin (**1**) and *exo*-5,6-dehydronorcantharidin (**2**).

Therefore, the synthesis of bioactive norcantharidin analogues, that represent aryl-modified bicyclic imide systems, was also considered to be of interest. Thus, *N*-(4-methoxyphenyl)-7-oxabicyclo[2.2.1]hept-5-ene-2-*exo*-3-*exo*-dicarboximide (**3**) and the *p*-chlorophenyl derivative **4** were prepared as the starting compounds in good yields (70 and 72 %, respectively).[9,13] Then, their hydroarylation reactions with aryl- and heteroaryl iodides in the presence of triphenylarsine (Scheme 1) and subsequent reduction by $NaBH_4$ were investigated to open new access to perhydroisoindole derivatives.[14] The synthesized compounds were evaluated for antioxidant and free radical scavenging activities.

Reactive oxygen species (ROS) are chemical entities that include oxygen free radicals. They can be generated in metabolic pathways within body tissues, and can also be introduced from external sources, such as drugs, food, UV radiation and environmental pollution. *In vivo*, such species are securely coupled at their site of generation or are detoxified by endogenous anti-oxidative defences so as to preserve the optimal cellular function. In pathological conditions, however, the detoxifying mechanisms are often inadequate as excessive quantities of ROS can be generated. This resulting pro-oxidant shift, a process known as oxidative stress, can result in the degradation of cellular components such as DNA, carbohydrates, polyunsaturated lipids and proteins, or precipitate enzyme inacti-

vation, irreversible cellular dysfunction and ultimately cell death if the pro-oxidant–antioxidant balance is not restored.[15,16] Thus, antioxidants are important inhibitors against oxidative damage.[17–19] Antioxidants interfere with the oxidation process by reacting with free radicals, chelating catalytic metals and also by acting as oxygen scavengers. Therefore, the preparation of more effective new antioxidants is a very important area of research.

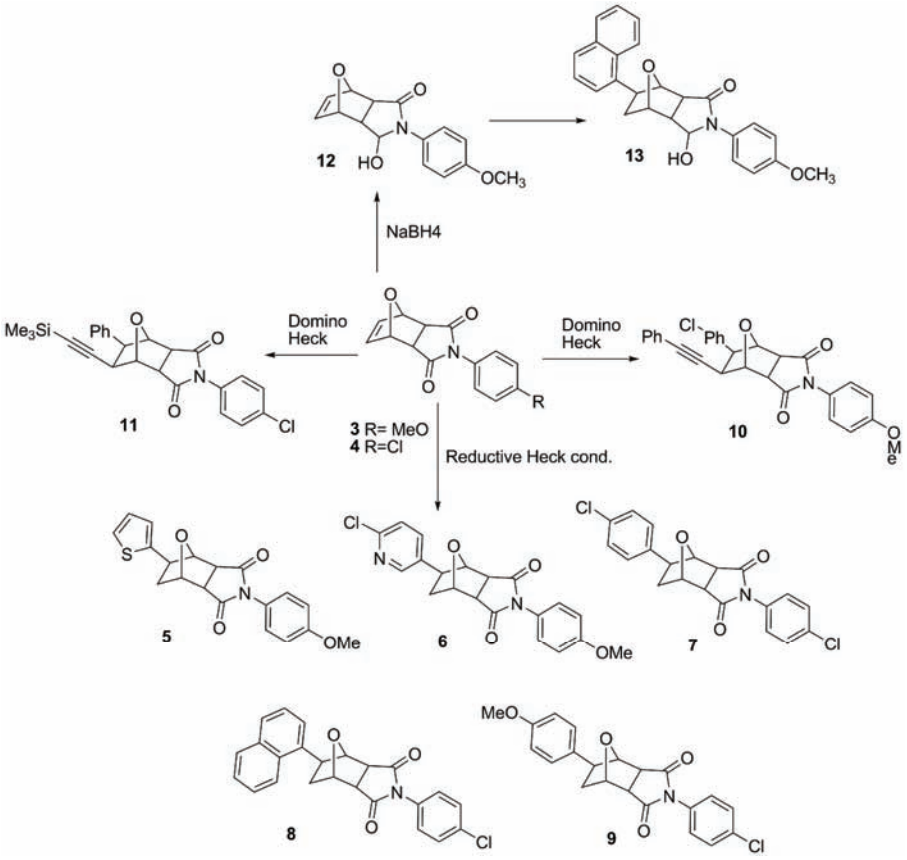

Scheme 1. Synthesis of bioactive norcantharidin analogues and the perhydroisoindole derivatives used in this work. *N*-(4-Methoxyphenyl)-7-oxabicyclo[2.2.1]hept-5-ene-2-*exo*--3-*exo*-dicarboximide (**3**) and the *p*-chlorophenyl derivative **4** were synthesized as the starting compounds.

The aim of this study was to investigate the reducing power, free radical scavenging, superoxide anion radical scavenging and metal chelating activities of some norcantharidin and bridged perhydroisoindole derivatives. The results were

compared to commercial and standard antioxidants, such as Trolox, butylated hydroxyanisole (BHA) and butylated hydroxytoluene (BHT).

EXPERIMENTAL

Chemicals

Reduced nicotinamide adenine dinucleotide (NADH), 6-hydroxy-2,5,7,8-tetramethylchroman-2-carboxylic acid (Trolox), nitroblue tetrazolium (NBT), phenazine methosulphate (PMS), the stable free radical 1,1-diphenyl-2-picrylhydrazil (DPPH$^{\bullet}$) and trichloroacetic acid (TCA) were obtained from Sigma-Aldrich (Germany). Butylated hydroxyanisole (BHA) and butylated hydroxytoluene (BHT) were provided by Fluka (Buchs, Switzerland). All other employed chemicals were of analytical grade and obtained from either Sigma-Aldrich, Fluka or Merck.

Norcantharidin and the bridged perhydroisoindole derivatives were prepared according to previously reported procedures and characterized by comparing their spectral data to those reported earlier.[14]

Evaluation of antioxidant and radical scavenging activities

Reducing power assay. The reducing power capacity of norcantharidin and the bridged perhydroisoindole derivatives was measured according to the method of Oyaizu.[20] Various amounts of the samples (10–50 μg) were mixed with 2.5 mL of phosphate buffer (0.2 M, pH 6.6) and 2.5 mL potassium ferricyanide, $K_3[Fe(CN)_6]$ (1 %, w/v), and the mixture was incubated at 50 °C for 30 min. Then, after addition of 2.5 mL of trichloroacetic acid (10 %, w/v), the mixture was centrifuged at 3000 rpm for 10 min. Finally, 2.5 mL of the upper-layer solution was mixed with 2.5 mL distilled water and 0.5 mL $FeCl_3$ (0.1 %, w/v) and the absorbance was measured at 700 nm. α-Tocopherol, BHA and BHT were used as standard antioxidants. Higher absorbance of the reaction mixture indicated greater reducing power.

Free radical scavenging activity assay. The free radical scavenging activity of norcantharidin and the bridged perhydroisoindole derivatives was measured with DPPH$^{\bullet}$ using a slightly modified method of Brand-Williams *et al.*[21] Briefly, 20 mg/L DPPH$^{\bullet}$ solution in methanol was prepared and 1.5 mL of this solution was added to 0.75 mL of the sample, butylated hydroxyanisole (BHA), butylated hydroxytoluene (BHT), Trolox or ascorbic acid (5–20 μg mL^{-1}). The mixture was shaken vigorously and the decrease in absorbance at 517 nm was measured after 30 min. Water (0.75 mL) instead of the sample was used as the control. The percent inhibition activity was calculated using the following equation:

$$\text{Free radical scavenging activity (\%)} = 100(A_0 - A_1)/A_0 \quad (1)$$

where A_0 is the absorbance of the control reaction and A_1 is the absorbance in the presence of a sample solution. The radical scavenging activity was expressed as the IC_{50} value, the concentration required for a 50 % reduction in the DPPH$^{\bullet}$ concentration, which was determined from a calibration curve for each compound.

Superoxide anion scavenging activity assay. Measurement of superoxide anion scavenging activity of norcantharidin and the bridged perhydroisoindole derivatives were based on the method described by Liu *et al.*[22] Superoxide anions were generated in a non-enzymatic phenazine methosulphate–nicotinamide adenine dinucleotide (PMS–NADH) system by oxidation of NADH and assayed by reduction of NBT. In this experiment, the superoxide anion was generated in 3 mL of tris–HCl buffer (16 mM, pH 8.0) containing 1 mL of NBT (50 μM) solution, 1 mL of NADH (78 μM) solution and 100 μg mL^{-1} concentration of a sample solution. The reaction was started by adding 1 mL of PMS solution (10 μM) to the mixture. The reac-

tion mixture was incubated at 25 °C for 5 min and absorbance at 560 nm was recorded against blank samples in a spectrophotometer. BHA, BHT, and Trolox were used as standard samples (100 μg mL^{-1}). The inhibition of superoxide anion radical generation (%) was calculated using Eq. (1).

Metal chelating activity assay. The chelating activity of norcantharidin and the bridged perhydroisoindole derivatives on ferrous ions was measured according to the method of Decker and Welch.[23] Aliquots of 1 mL of different concentrations (25, 50, 75 and 100 μg mL^{-1}) of the samples were mixed with 3.7 mL of deionised water. The mixture was incubated with $FeCl_2$ (2 mM, 0.1 mL) for 30 min. After incubation, the reaction was initiated by addition of ferrozine (5 mM and 0.2 mL) and after 10 min at room temperature, the absorbance was measured at 562 nm in a spectrophotometer. A lower absorbance indicates a higher chelating power. The chelating activity of the extract on Fe^{2+} was compared with that of EDTA at same concentrations. Chelating activity was calculated using the following formula:

$$\text{Metal chelating activity (\%)} = 100(1 - A_S/A_{EDTA}) \quad (2)$$

where A_S and A_{EDTA} are the absorbances in the presence of a sample and EDTA, respectively.

A control test was performed without addition of a sample.

RESULTS AND DISCUSSION

Three 5,6-dehydronorcantharidin, eight norcantharidin and bridged perhydroisoindole compounds (Fig. 2, Table I) were investigated for their antioxidant and radical scavenging activities. Reducing power is used as one of the indicators of antioxidant capability. In the reducing power assay, the presence of reductants (antioxidants) in the tested samples resulted in a reduction of the Fe^{3+}/ferricyanide complex to the ferrous form (Fe^{2+}). The amount of Fe^{2+} complex can therefore be monitored by measuring the formation of the Perls' Prussian Blue at 700 nm. The reducing power of norcantharidin and the bridged perhydroisoindole derivatives and standard antioxidants are given in Table II. The results show that the reducing power of the samples was not concentration dependent. Based on a comparison of the absorbance at 700 nm, compounds **7**, **11**–**13** showed the lowest reducing power. Compounds **8** and **9** exhibited moderate reducing power. Compounds **4**–**6** and **10** gave similar results. A higher activity was found for compound **3**. The tested compounds **3**–**6** and **10** exhibited higher activity than BHA, BHT and α-tocopherol at a 10 μg mL^{-1} concentration. A correlation was found between the reducing capabilities and the substituents. The reason for the higher reducing power capacity of the compounds can be explained by considering the structure of the compounds. The presence of a carbonyl group and an alkene or alkyne on the ring system seems to increase the reductive capacity of the com-

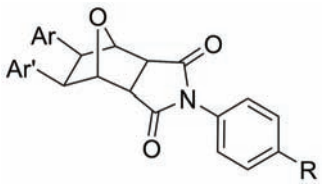

Fig. 2. Structure of the bridged perhydroisoindole derivatives used in this study.

pounds. These results revealed that these 5,6-dehydronorcantharidin, norcantharidin and the bridged perhydroisoindole derivatives were good electron and hydrogen donors and could terminate a radical chain reaction, converting the free radicals to more stable products.

TABLE I. The three 5,6-dehydronorcantharidins (**3**,**4** and **12**) and eight norcantharidins and bridged perhydroisoindole derivatives investigated in this study

Compound	R	Ar	*Ar'*
3	OMe	–	–
4	Cl	–	–
5	OMe	(2-thienyl)	–
6	OMe	(6-chloropyridin-3-yl)	–
7	Cl	(*p*-chlorophenyl)	–
8	Cl	(1-napthyl)	–
9	Cl	(*p*-methoxyphenyl)	–
10	OMe	(*p*-chlorophenyl)	(phenylethynyl)
11	Cl	(phenyl)	(trimethylsilyl)ethynyl
12	OMe	–	–
13	OMe	(1-napthyl)	–

TABLE II. Reducing power (absorbance at 700 nm) of different concentrations (10, 20, 30, 40 and 50 μg mL^{-1}) of norcantharidin and the bridged perhydroisoindole derivatives. BHA, BHT and α-tocopherol were used as reference antioxidants. The given values are means ± *SD* (*n* = 3). A higher absorbance indicates a greater reducing power

Compound	*c* / μg mL^{-1}				
	10	20	30	40	50
3	0.14±0.01	0.14±0.01	0.15±0.01	0.15±0.00	0.15±0.01
4	0.10±0.01	0.10±0.01	0.11±0.01	0.11±0.01	0.11±0.01
5	0.10±0.01	0.10±0.00	0.10±0.01	0.11±0.01	0.11±0.01
6	0.10±0.01	0.10±0.01	0.10±0.00	0.10±0.00	0.11±0.01
7	0.01±0.00	0.01±0.00	0.01±0.00	0.01±0.00	0.01±0.00
8	0.03±0.00	0.04±0.01	0.04±0.01	0.04±0.00	0.04±0.00
9	0.04±0.00	0.04±0.00	0.04±0.00	0.04±0.00	0.04±0.00
10	0.09±0.01	0.09±0.01	0.10±0.00	0.10±0.01	0.11±0.01
11	0.01±0.00	0.01±0.00	0.01±0.00	0.01±0.00	0.01±0.00
12	0.01±0.00	0.01±0.00	0.01±0.00	0.01±0.00	0.01±0.00
13	0.01±0.00	0.01± 0.00	0.01±0.00	0.01±0.00	0.01±0.00
BHA	0.09±0.02	0.17±0.02	0.25±0.01	0.33±0.03	0.41±0.02
BHT	0.03±0.00	0.06±0.00	0.09±0.01	0.14±0.01	0.16±0.01
α-Tocopherol	0.04±0.00	0.07±0.01	0.12±0.01	0.12±0.01	0.18±0.01

Hydrogen-donating ability is an index of primary antioxidants. These antioxidants donate a hydrogen to a free radical, leading to non-toxic species and therefore to inhibition of the propagation phase of lipid oxidation. 1,1-Diphenyl--2-picrylhydrazil (DPPH$^{\bullet}$) is a stable free radical and accepts an electron or hydrogen radical to become a stable diamagnetic molecule. DPPH· has been used as

a free radical to evaluate the anti-oxidative activity of some natural and synthetic sources. The DPPH radical scavenging effects of norcantharidin and the bridged perhydroisoindole derivatives are presented in Table III. Their comparable scavenging activities were also expressed as IC_{50} values (Table IV). All the tested compounds showed lower free radical scavenging activities when compared to BHA, BHT, Trolox and ascorbic acid. Compounds **5**–**8** exhibited similar activity to BHT at 5 and 10 μg mL^{-1} concentrations. The DPPH free radical scavenging activity was improved by the presence of N, S and Cl on the heterocyclic ring and alkene groups. From these results, it could be stated that the tested compounds have a moderate ability to scavenge free radicals and could serve as free radical inhibitors or scavengers according to the synthetic antioxidants. From the inhibition concentration IC_{50} values of the compounds, it was seen that compounds **4**, **5**, **7**, **8**, **12** and **13** had the highest activities, as shown by the lowest values of IC_{50}, followed by compound **6**, **9** and **10**, while compound **3** and **11** had the lowest activities. A higher DPPH radical scavenging activity is associated with a lower IC_{50} value. It was evident that the compounds did show hydrogen-donating ability to act as antioxidants.

TABLE III. Free radical scavenging activity (%) of different concentrations (5, 10, 15 and 20 μg mL^{-1}) of norcantharidin and the bridged perhydroisoindole derivatives. BHA, BHT, Trolox and ascorbic acid were used as reference antioxidants. The given values are means ± *SD* (*n* = 3)

Compound	*c* / μg mL^{-1}			
	5	10	15	20
3	17.9±0.3	18.7±0.6	18.7±0.9	18.7±0.1
4	16.3±0.5	16.7±1.4	17.5±0.1	19.9±0.1
5	30.1±2.2	31.7±1.4	31.7±0.8	32.1±1.2
6	30.9±1.2	30.9±0.6	31.7±0.9	32.1±1.0
7	30.5±0.4	30.9±0.1	31.7±1.4	32.1±1.2
8	30.1±0.1	31.7±0.5	31.7±0.5	32.1±0.5
9	31.3±0.8	31.7±1.0	32.1±1.2	32.5±0.8
10	17.9±0.9	17.9±0.9	18.3±0.8	20.7±0.4
11	18.3±0.8	18.7±0.7	19.1±0.7	19.1±0.7
12	16.7±0.6	16.7±0.6	18.3±0.8	20.7±0.4
13	15.9±0.1	18.3±0.7	18.3±0.8	19.5±0.6
BHA	68.3±2.7	78.9±2.5	88.2±2.1	92.7±1.5
BHT	31.7±2.0	36.6±1.5	42.3±0.6	45.5±2.7
Trolox	95.5±1.7	95.9±0.6	96.8±0.6	97.2±1.7
Ascorbic acid	95.9±1.7	96.3±1.0	96.3±0.6	96.3±0.6

The superoxide anion radical is known to be very harmful to cellular components as a precursor of more reactive oxygen species, such as hydrogen peroxide, hydroxyl radical and singlet oxygen, which induce oxidative damage in lipids, proteins and DNA. In a biological system, its toxic role can be eliminated by superoxide dismutase.[14] In the PMS–NADH–NBT system, the superoxide an-

ion derived from dissolved oxygen by the PMS–NADH coupling reaction reduces NBT. The decrease in the absorbance at 560 nm with antioxidants indicates the consumption of the superoxide anion in the reaction mixture. The superoxide radical scavenging activities by 100 μg mL^{-1} of norcantharidin and the bridged perhydroisoindole derivatives in comparison to the same amount of BHA, BHT and Trolox are given in Table V. Compounds **5**–**7** and **10** showed lower superoxide radical scavenging activity than BHA, BHT and Trolox, while compounds **3**, **4**, **11**–**13** showed higher activity than BHT. It is important to mention that compounds **8** and **9** exhibited more potent activity when compared to those of all the tested standard antioxidants, *i.e.*, BHA, BHT and Trolox at the same concentration. These results clearly indicate that the Cl atom present in the structure and the alkene group seems to induce the activity of the compounds and they act as good superoxide radical scavengers.

TABLE IV. Free radical scavenging activity (IC_{50} / μg mL^{-1}) of norcantharidin and the bridged perhydroisoindole derivatives. BHA, BHT and Trolox were used as reference antioxidants. A higher DPPH radical scavenging activity is associated with a lower IC_{50} value

Compound	IC_{50} / μg mL^{-1}
3	130.6±8.2
4	29.9±5.1
5	33.1±3.9
6	44.1±2.5
7	35.3±4.5
8	33.1±5.2
9	46.9±2.6
10	37.4±5.1
11	112.8±6.8
12	25.6±1.3
13	31.7±2.3
BHA	2.3±0.1
BHT	4.8±0.3
Trolox	4.5±0.3

TABLE V. Superoxide anion radical scavenging activity of norcantharidin and the bridged perhydroisoindole derivatives at a concentration of 100 μg mL^{-1}. BHA, BHT and Trolox acid were used as the reference antioxidants. The given values are the means ± *SD* (n = 3)

Compound	Superoxide anion radical scavenging activity, %
3	75±0.8
4	72±0.5
5	36±2.9
6	25±0.5
7	26±1.3
8	95±1.3
9	91±0.8
10	57±1.2

TABLE V. Continued

Compound	Superoxide anion radical scavenging activity, %
11	75±1.1
12	74±1.7
13	63±1.1
BHA	78±0.8
BHT	59±2.8
Trolox	81±1.7

Chelating agents are effective as secondary antioxidants because they reduce the redox potential thereby stabilizing the oxidized form of the metal ion. Iron is known as the most important lipid oxidation pro-oxidant due to its high reactivity. Especially Fe^{2+} is the most powerful pro-oxidant among the various species of metal ions. The ferrous ion chelating effects of norcantharidin and the bridged perhydroisoindole derivatives are presented in Table VI. Compounds **3**–**7** exhibited no chelating activity on ferrous ions at any of the tested concentrations. Compound **8**–**13** showed moderate chelating activity on ferrous ions after an incubation time of 30 min. The results were compared with EDTA at the same concentrations. At a concentration of 100 μg mL^{-1}, EDTA had a 96 % chelating effect on ferrous ions after an incubation time of 30 min. The data obtained from this study revealed that compounds **8**–**13** had a slightly effective capacity for iron binding, suggesting that their action as antioxidants might be related to their iron binding capacity. It is known that compounds with structures containing two or more functional groups, such as OH, SH, COOH, N, S and O, can show metal chelating activity.

TABLE VI. Metal chelating activity (%) of different concentrations (25, 50, 75 and 100 μg mL^{-1}) of norcantharidin and the bridged perhydroisoindole derivatives. EDTA was used as a standard compound. The reported values are the mean ± *SD* (*n* = 3)

Compound	*c* / μg mL^{-1}			
	25	50	75	100
3	0	0	0.6±0.0	1.8±0.0
4	0	0	0	0
5	0	0	0	0
6	0	0	1.1 ± 0.0	1.9±0.1
7	0	0	0	1.1±0.0
8	10.7±0.2	14.3±0.1	15.5±0.2	19.9±0.1
9	13.9±0.2	14.9±0.3	17.3±0.1	23.5±0.6
10	4.2±0.2	6.3±0.1	11.3±0.2	15.2±0.7
11	16.7±0.6	16.7±0.2	17.9±0.3	22.6±2.3
12	16.1±0.0	16.4±0.1	16.9±0.1	19.1±0.1
13	9.8±0.4	11.9±0.2	14.3±0.0	14.9±0.1
EDTA	85.0±1.2	95.0±2.7	96.0±2.1	96.0±1.2

CONCLUSIONS

A series of norcantharidin and bridged perhydroisoindole derivatives (**3**–**13**) were synthesized and their antioxidant properties were evaluated. The results showed that most of the synthesized derivatives exhibited significant antioxidant and radical scavenging activities *in vitro*. According to the obtained results, a correlation exists between the radical scavenging and antioxidant activities of the compounds and the substituents. Among the synthesized compounds, compounds **3**–**6** and **8**–**10** were found to be the most active reducing agents. Compound **3**, **4**, **8**, **9** and **11**–**13** were determined to have the highest superoxide anion radical scavenging ability in addition to being potent antioxidants and thus they represent a new class of antioxidant and antiradical agents.

ИЗВОД

АНТИОКСИДАТИВНА АКТИВНОСТ И СПОСОБНОСТ ХВАТАЊА СЛОБОДНИХ РАДИКАЛА НЕКИХ НОРКАНТАРИДИНСКИХ И ПЕРХИДРОИЗОИНДОЛНИХ ДЕРИВАТА СА МОСТОМ

AYSEGUL PEKSEL[1], CUMALI CELIK[1,2], NUKET OCAL[1] и REFIYE YANARDAG[3]

[1]*Department of Chemistry, Faculty of Arts and Science, Yildiz Technical University, Davutpasa, Istanbul-34210, Turkey,* [2]*Community College, Yalova University, Yalova-77100, Turkey и* [3]*Department of Chemistry, Faculty of Engineering, Istanbul University, Avcilar, Istanbul-34320, Turkey*

Утврђивана је антиоксидативна активност и способност хватања слободних радикала серије норкантаридинских и перхидроизоиндолних деривата са мостом. Одређиван је укупни редукујући капацитет, способности хватања радикала методом DPPH, способност хватања супероксидног анјона и способност хелатирања метала. Од 11 анализираних једињења, 7 је испољило велики редукујући потенцијал, а 8 способност хватања супероксидног анјона. Сва тестирана једињења су могла везивати слободне радикале, потврђујући њихову антиоксидативну активност.

(Примљено 23. јануара, ревидирано 15. марта 2012)

REFERENCES

1. M. F. Brana, A. Gradillas, A. Gomez, N. Acero, F. Llinares, D. Munoz-Mingarro, C. Abradelo, F. Rey-Stolle, M. Yuste, J. Campos, M. A. Gallo, A. Espinosa, *J. Med. Chem.* **47** (2004) 2236
2. S. M. Sondhi, R. Rani, P. Roy, S. K. Agrawal, A. K. Saxena, *Bioorg. Med. Chem. Lett.* **19** (2009) 1534
3. J. Kossakowski, M. Jarocka, *Farmaco* **56** (2001) 785
4. F. Zentz, A. Valla, R. Le Guillou, R. Labia, A. Mathot, D. Sirot, *Farmaco* **57** (2002) 421
5. R. M. Di Pardo, M. A. Patane, R. C. Newton, R. Price, T. P. Broten, R. S. L. Chang, R. W. Ransom, J. Di Salvo, R. M. Freidinger, M. G. Bock, *Bioorg. Med. Chem. Lett.* **11** (2001) 1959
6. J. Kossakowski, A. Bielenica, B. Miroslaw, A. E. Koziol, I. Dybala, M. Struga, *Molecules* **13** (2008) 1570
7. M. E. Hart, A. R. Chamberlin, C. Walkom, J. A. Sakoff, A. McCluskey, *Bioorg. Med. Chem. Lett.* **14** (2004) 1969

8. L. Ying, G. Yan, L. Fu You, P. You Ming, L. Sun, L. Jun, C. Qiong, S. Yan, Y. Kun, *Mol. Cell Biochem.* **361** (2012) 79
9. L. P. Deng, H. Yongzhou, *J. Heterocycl. Chem.* **44** (2007) 597
10. L. P. Deng, F. M. Liu, H. Y Wang, *J. Heterocycl. Chem.* **42** (2005) 13
11. E. Ciganek (Du Pont Merck Pharmaceutical Company), US 5216018 (1993)
12. P. J. Gilligan (Du Pont Merck Pharmaceutical Company) US 5532243 (1996)
13. L. S. Oswal, S. N. Sarkar, K. V. Bhandari, B. H. Oza, B. C. Patel, *Iran. Polym. J.* **13** (2004) 297
14. C. Celik, I. Kulu, N. Ocal, D. E. Kaufmann, *Helv. Chim. Acta* **92** (2009) 1092
15. G. Miliauskas, P. R. Venskutonis, T. A. van Beek, *Food Chem.* **85** (2004) 231
16. B. Halliwell, J. M. C. Gutteridge, *Free Radicals in Biology and Medicine*, 2nd ed., Clarendon Press, Oxford, 1989, p. 617
17. Y. C. Chung, S. J. Chen, C. K. Hsu, C. T. Chang, S. T. Chou, *Food Chem.* **91** (2005) 419
18. T. Juntachote, E. Berghofer, *Food Chem.* **92** (2005) 193
19. C. S. Ku, S. P. Mun, *Biores. Technol.* **99** (2008) 4503
20. M. Oyaizu, *Jpn. J. Nutr.* **44** (1986) 307
21. W. Brand-Williams, M. E. Cuvelier, C. Berset, *Lebensm. Wiss. Technol.* **28** (1995) 25
22. F. Liu, V. F. C. Ooi, S. T. Chang, *Life Sci.* **60** (1997) 763
23. E. A. Decker, B. Welch, *J. Agr. Food Chem.* **38** (1990) 674.

Journal of the Serbian Chemical Society
JSCS-info@shd.org.rs • www.shd.org.rs/JSCS

J. Serb. Chem. Soc. 78 (1) 27–37 (2013)
JSCS–4393

UDC 633.94:665.52/.54:615.27/.28
Original scientific paper

Composition, and antioxidant and antimicrobial activities of the essential oils of a full-grown *Pinus cembra* L. tree from the Calimani Mountains (Romania)

CRISTINA LUNGU APETREI[1], ADRIAN SPAC[2], MIHAI BREBU[3], CRISTINA TUCHILUS[4] and ANCA MIRON[5]*

[1]*Department of Plant and Animal Biology, School of Pharmacy, University of Medicine and Pharmacy "Grigore T. Popa" – Iasi, Romania,* [2]*Department of Physical Chemistry, School of Pharmacy, University of Medicine and Pharmacy "Grigore T. Popa" – Iasi, Romania,* [3]*Physical Chemistry of Polymers Laboratory, Petru Poni Institute of Macromolecular Chemistry, Iasi, Romania,* [4]*Department of Microbiology, School of Medicine, University of Medicine and Pharmacy "Grigore T. Popa" – Iasi, Romania and* [5]*Department of Pharmacognosy, School of Pharmacy, University of Medicine and Pharmacy "Grigore T. Popa" – Iasi, Romania*

(Received 9 April, revised 21 June 2012)

Abstract: The chemical composition and the antioxidant and antimicrobial effects of the essential oils of *Pinus cembra* L. needles and twigs were investigated in this study. The chemical composition was analyzed using both the GC and GC–MS techniques. α-Pinene (69.14 %) was the major constituent of the needle essential oil while the twig essential oil was characterized by a high content of limonene+β-phellandrene (40.97 %) and α-pinene (24.94 %). The needle and twig essential oils showed weak DPPH radical scavenging effects. In the antimicrobial assays, both essential oils showed high activity against *Sarcina lutea* and *Staphylococcus aureus* but no activity against *Bacillus cereus*, *Escherichia coli* and *Pseudomonas aeruginosa*. The needle and twig essential oils had similar antimicrobial effects against *Sarcina lutea*. The twig essential oil was more active against *S. aureus* than the needle essential oil and also exhibited a moderate activity against *Candida albicans*.

Keywords: cembran pine; α-pinene; limonene; DPPH radical; *Staphylococcus aureus*; *Candida albicans*.

INTRODUCTION

Pinus cembra L. (Pinaceae), commonly known as cembran pine, Swiss stone pine or Arolla pine, is a glacial relict growing in the European Alps (Switzerland, Austria, northern Italy and south-eastern France) and the Carpathian Mountains

* Corresponding author. E-mail: ancamiron@yahoo.com
doi: 10.2298/JSC120409075A

(Poland, Slovakia, Ukraine and Romania). It grows at high altitudes ranging from 900 to 2850 and 1985 m in the Alps and the Carpathian Mountains, respectively, and is very resistant to the conditions of high abiotic stress in the alpine timberline (UV-B irradiation, frosts and strong winds).[1–3]

The chemistry and the biological effects of essential oils of different pine species have been intensively studied.[4–9] In contrast, there are only a few studies on cembran pine essential oils.[10,11] Dormont *et al.* studied the volatiles emitted by the cones and foliage (ramets with one-year-old needles from the apical parts of branches) and reported α- and β-pinene together with a mixture of limonene and β-phellandrene as the major volatile constituents; other monoterpene hydrocarbons (myrcene, camphene, sabinene, terpinolene and bornyl acetate) were identified in traces. In addition, traces of tricyclene were found in the cone volatiles.[10] Ochocka *et al*. separated, identified and quantified the enantiomers of four monoterpene hydrocarbons (α- and β-pinene, camphene and limonene) in the needle essential oil. The authors reported the occurrence of both enantiomers of camphene, α- and β-pinene and the (–)isomer of limonene. (–)Limonene and α-pinene as sum of the (–) and (+)isomers dominated in the needle essential oil.[11] A literature survey revealed no studies on the biological effects of cembran pine volatiles. In this context, the main objectives of the present study were to investigate the chemical composition of the needle and twig essential oils of *P. cembra* and to evaluate their antioxidant and antimicrobial effects in order to find some possible therapeutic uses.

EXPERIMENTAL

Plant material

The needles with twigs were sampled from a full-grown cembran pine in a natural stand located at approximately 1650 m altitude on the Calimani Mountains (Romania) in June 2011. The plant material was authenticated in the Department of Plant and Animal Biology, School of Pharmacy, University of Medicine and Pharmacy "Grigore T. Popa" – Iasi, Romania. Before extraction of the essential oils, the needles and twigs were separated and dried in the shade at 20±2 °C. Herbarium voucher samples have been deposited in the Department of Pharmacognosy, School of Pharmacy, University of Medicine and Pharmacy "Grigore T. Popa" – Iasi, Romania.

Chemicals

An alkane standard solution C_8–C_{20}, butylated hydroxyanisole (BHA) and 2,2-diphenyl--1-picrylhydrazyl (DPPH) radical were purchased from Sigma-Aldrich (Steinheim, Germany). Mueller Hinton agar and broth were obtained from Merck (Darmstadt, Germany). Sabouraud 4 % glucose agar was obtained from Fluka Biochemika (Buchs, Switzerland). Sabouraud dextrose broth was procured from Oxoid (Basingstoke, UK). The antibiotic discs were purchased from Himedia (Mumbai, India). All other reagents and solvents were of analytical grade.

Microorganisms

Gram-positive bacteria (*Staphylococcus aureus* ATCC 25923, *Sarcina lutea* ATCC 9341 and *Bacillus cereus* ATCC 14579), Gram-negative bacteria (*Escherichia coli* ATCC 25922 and *Pseudomonas aeruginosa* ATCC 27853) and pathogenic yeasts (*Candida albicans* ATCC 10231) were obtained from the Culture Collection of the Department of Microbiology, School of Medicine, University of Medicine and Pharmacy "Grigore T. Popa" – Iasi, Romania.

Isolation of the essential oils

100 g of each sample (needles or twigs) were ground with a grinder, mixed with 1000 mL of doubly distilled water and subjected to hydrodistillation for 4 h in a modified Clevenger-type apparatus.[9] The essential oils were collected, dried over anhydrous sodium sulphate and kept in a sealed glass tube at 4 °C until studied. Yields of the essential oils (v/w %) were calculated on a dry weight basis and are expressed as average values of the results from several extractions.

GC and GC–MS analyses

The GC-FID analysis of the essential oils was performed on an Agilent 6890 gas chromatograph. Separation of the constituents of the essential oils was realised on a DB-5MS capillary column (30 m×0.25 mm i.d., film thickness 0.25 μm). A volume of 0.3 μL was injected in the split mode (split ratio 1:100). The carrier gas was helium at a flow rate of 1.0 mL min^{-1}. The oven temperature was programmed from 40 to 280 °C at a rate of 3 °C min^{-1}; the final temperature was held for 8 min.[7] The injector and detector temperatures were maintained at 250 °C. The GC–MS analysis was performed using an Agilent 7890A gas chromatograph equipped with an Agilent 5975C inert mass selective detector with electron impact ionization. The same column and temperature program as described for GC-FID analysis were used. The carrier gas was helium (1.0 mL min^{-1}) and the split ratio was 1:100. The injector, MS source and MS quadrupole temperatures were set at 250, 230 and 150 °C, respectively. Mass spectra were acquired in the scan mode (mass range 15–450 *m*/*z*). In order to determine the retention indices, standard solutions of *n*-alkanes (C_8–C_{20}) were analyzed under the same chromatographic conditions. The volatile constituents were identified by comparison of their mass spectral data with those in the Wiley 275 mass spectra library stored in the GC–MS database and with those of pure standards. The identity of the constituents was confirmed by comparison of calculated retention indices with those reported in the literature[12-16] and with those of pure standards. The relative percentages of the essential oils constituents were obtained from the FID peak areas without the use of correction factors.

DPPH radical scavenging assay

DPPH radical scavenging activity was evaluated as described by Mighri *et al.*[17] Briefly, 1 mL of each essential oil dilution in methanol (concentration range from 20 to 60 mg mL^{-1}) was mixed with 1 mL DPPH solution in methanol (0.004 %, w/v). The mixtures were vortexed and kept in the dark. After 30 min, the absorbance was measured at 517 nm. BHA was used as a positive control. DPPH radical scavenging activity (%) was calculated using the following formula:

$$100(A_0 - A_t)/A_0$$

where A_0 is the absorbance of the blank and A_t is the absorbance in the presence of an essential oil or positive control. All the experiments were performed in triplicate; the results are expressed as means ± *SD*. The EC_{50} (the concentration that gives half-maximal response) values were calculated by linear interpolation between the values above and below 50 % activity.

Agar diffusion assay

The antimicrobial activities were screened using the agar diffusion assay.[18,19] Each microbial suspension was adjusted to a turbidity equivalent to 0.5 McFarland turbidity standard. Aliquots (0.1 mL) of each microbial suspension were spread in Mueller Hinton agar (antibacterial tests) and Sabouraud agar (antifungal tests). Sterile stainless steel cylinders (5 mm internal diameter; 10 mm height) were placed on the agar surface and filled with 30 µL of each essential oil. Discs (6 mm diameter) containing ampicillin (25 µg disc^{-1}), chloramphenicol (30 µg disc^{-1}) and nystatin (100 µg disc^{-1}) were used as positive controls. The plates were incubated at 37 °C for 24 h (antibacterial tests) and at 24 °C for 48 h (antifungal tests). After incubation, the diameters of the inhibition zones were measured. All experiments were performed in triplicate and the results are expressed as means ± *SD*.

Broth microdilution assay

The minimum inhibitory concentrations (*MIC*s) and the minimum bactericidal/fungicidal concentrations (*MBC*s/*MFC*s) were determined using a broth microdilution assay.[17,20] The microbial suspensions were adjusted to a turbidity of 0.5 McFarland standard. The essential oils were dissolved in 50 % dimethyl sulphoxide at a concentration of 250 mg mL^{-1} and then subjected to serial two-fold dilutions in Mueller Hinton broth (antibacterial tests) and Sabouraud broth (antifungal tests) in 96-well plates (concentration range from 250 to 0.12 mg mL^{-1}; final volume in each well 100 µL). Other 95 µL of broth and 5 µL of microbial inoculum were further dispensed into each well. The plates were incubated at 37 °C (antibacterial tests) and 24 °C (antifungal tests) for 24 h. The essential oils were screened twice against each microorganism. The lowest concentration of the essential oil that inhibited the visible growth of microorganisms was recorded as the *MIC*.[21] The *MBC*/*MFC* values (the lowest concentration of an essential oil killing completely the microorganisms being tested)[21] were determined by transferring 10 µL of samples showing inhibition of visible growth on the surface of an agar plate. The subcultures were incubated at 37 °C (antibacterial tests) and 24 °C (antifungal tests) for 24 h. The *MIC* and *MBC*/*MFC* values of ampicillin/nystatin towards bacteria/yeast strains were also evaluated.

Statistical analysis

Statistical analyses were performed using the Kruskal–Wallis and Mann–Whitney U tests. Values of *P* less than 0.05 were considered statistically significant.

RESULTS AND DISCUSSION

Essential oils analysis

The essential oils from needles (EON) and twigs (EOT) of cembran pine were obtained in yields of 1.96 and 2.45 %, respectively and analyzed by both GC and GC–MS. A list of the constituents in order of elution on a DB-5MS column, their retention indices and percentages are reported in Table I. It is noteworthy that in both essential oils, limonene co-eluted with *β*-phellandrene and the two compounds were quantified as a single peak. 27 compounds accounting for 91.59 % of the total essential oil composition were identified in EON. *α*-Pinene (69.14 %) was the most abundant compound. Other main constituents were limonene+*β*-phellandrene (4.64 %), *α*-cadinene (3.71 %), *γ*-cadinene (2.61 %), camphene (2.59 %), bicyclogermacrene (2.44 %) and cadina-1,4-diene (1.36 %). The

amount of β-pinene was found to be 0.89 %. Monoterpene hydrocarbons (78.93 %) were the major class of compounds followed by sesquiterpene hydrocarbons (12.09 %). GC analysis of EOT revealed 28 compounds representing 92.22 % of the total essential oil composition. The main constituents of EOT were limonene+β-phellandrene (40.97 %), α-pinene (24.94 %) and β-pinene (10.38 %), followed by camphene (5.55 %), myrcene (1.7 %) and γ-terpinene (1.52 %). Monoterpene hydrocarbons (87.24 %) were the most abundant while sesquiterpene hydrocarbons (3.35 %) were present in lower amounts.

TABLE I. Chemical composition (%) of cembran pine essential oils

Compound	*RI*[a]	*RI*[b]	EON	EOT
2-Hexenal	850	850	0.17	–
Tricyclene	921	926	0.14	0.30
α-Thujene	925	924	–	tr[c]
α-Pinene	936	935	69.14	24.94
Camphene	950	953	2.59	5.55
Sabinene	970	975	tr	–
β-Pinene	979	979	0.89	10.38
Myrcene	990	990	0.58	1.7
α-Phellandrene	1006	1004	–	0.23
δ-3-Carene	1008	1009	0.69	1.03
p-Cymene	1023	1024	tr	–
Limonene+β-phellandrene	1028	1029	4.64	40.97
γ-Terpinene	1058	1058	–	1.52
α-Terpinolene	1084	1084	0.16	0.56
Linalool	1099	1101	tr	–
Nonanal	1105	1102	–	0.49
trans-Pinocarveol	1139	1139	–	0.10
Terpineol-4	1179	1177	–	0.10
Estragole	1197	1200	0.23	0.21
trans-Carveol	1218	1219	–	0.14
Carvone	1242	1243	–	0.23
Bornyl acetate	1283	1283	0.16	0.20
α-Cubebene	1344	1349	tr	–
α-Copaene	1372	1375	tr	–
β-Caryophyllene	1415	1415	0.96	0.34
α-Humulene	1452	1451	0.17	0.81
γ-Muurolene	1472	1475	tr	tr
Germacrene D	1478	1480	tr	–
β-Selinene	1485	1484	0.22	0.15
Bicyclogermacrene	1492	1488	2.44	–
α-Muurolene	1495	1499	0.24	0.21
γ-Cadinene	1510	1514	2.61	0.23
δ-Cadinene	1516	1523	0.31	0.38
Cadina-1,4-diene	1529	1531	1.36	0.41
α-Cadinene	1533	1537	3.71	0.73
Caryophyllene oxide	1578	1581	–	0.16

TABLE I. Continued

Compound	*RI*[a]	*RI*[b]	EON	EOT
Monoterpene hydrocarbons			78.93	87.24
Oxygenated monoterpenes			0.24	0.78
Sesquiterpene hydrocarbons			12.09	3.35
Oxygenated sesquiterpenes			–	0.16
Others			0.33	0.69
Total identified			91.59	92.22

[a]Retention indices relative to C_8–C_{20} *n*-alkanes calculated on DB-5MS capillary column; [b]retention indices reported in the literature;[12-16] [c]traces (<0.1 %)

A previous study made by Dormont *et al.* reported α-pinene, β-pinene and a mixture limonene+β-phellandrene as the major constituents in the volatiles emitted by cembran pine cones and foliage (ramets with one-year-old needles from the apical parts of the branches). α-Pinene (67.1 %) dominated in the cone volatiles while β-pinene (18.2 %) and limonene+β-phellandrene (11.1 %) were in lower amounts. Regarding foliage volatiles, the authors reported differences between samples collected from forest trees (α-pinene 38.9 %, β-pinene 20.7 %, limonene+β-phellandrene 34.0 %) and planted trees (α-pinene 26.4 %, β-pinene 10.1 %, limonene+β-phellandrene 57.9 %).[10] Ochocka *et al.* studied a commercially manufactured essential oil from cembran pine needles. This study revealed that α-pinene as the sum of enantiomers and limonene as the (–)isomer were present in similar amounts (34.3 and 32.7 %, respectively); in case of β-pinene, the sum of both enantiomers was only 12.5 %.[11] On the contrary, in the present study, α-pinene was identified in the highest percentage (69.14 %) in the needle essential oil while limonene+β-phellandrene and β-pinene were in significantly lower amounts (4.64 and 0.89 %, respectively). These differences in the chemical composition of essential oils from cembran pine needles can most probably be explained by different environmental conditions and time of collection.

Antioxidant activity

The antioxidant activities of cembran pine essential oils were evaluated by the DPPH radical scavenging assay, which is a simple, rapid and highly reproducible method widely used in antioxidant screening.[22] The results of the assay are given in Table II. According to the EC_{50} values, both EON (19.93±0.75 mg mL^{-1}) and EOT (18.66±0.70 mg mL^{-1}) were less active than the positive control, BHA (3.3±0.1 μg mL^{-1}). The weak antioxidant activity of cembran pine essential oils might be related to the high content of non-phenolic compounds (monoterpenes and sesquiterpenes). Among plant secondary metabolites, polyphenols are known to have a high capacity to scavenge free radicals due to the hydrogen and electron donating abilities of their hydroxyl groups.[22]

There are very few literature reports on DPPH scavenging effects of the essential oils from other *Pinus* species. Different experimental protocols in DPPH

assay make it difficult to compare the present results with those of other studies. However, it should be pointed out that a weak DPPH scavenging activity (less than 20 %) was reported for the essential oil from *P. radiata* (10 μL) after 70 min reaction time.[23] On the contrary, high DPPH scavenging effects were reported for the essential oils from *P. densiflora* and *P. thunbergii* needles (EC_{50} = 120 and 30 μg mL^{-1}, respectively) in comparison to *α*-tocopherol (EC_{50} = 12.6 μg mL^{-1}) and butylated hydroxytoluene (EC_{50} = 14.3 μg mL^{-1}); the scavenging effects were assessed after 30 min reaction time at 37 °C.[24] These contradictory results might be due to different experimental conditions in the DPPH assay, but also to differences in the chemical composition and possible interactions between the volatile constituents.[25]

TABLE II. DPPH Radical scavenging activity of cembran pine essential oils; different letters in the column indicate values significantly different ($P \leq 0.05$)

Essential oil/positive control	EC_{50}
EON	19.93±0.75 mg mL^{-1}[a] (b)
EOT	18.66±0.70 mg mL^{-1}[a] (b)
BHA	3.3±0.1 μg mL^{-1}[a] (a)

Antimicrobial activity

The antimicrobial activities were initially tested by the agar diffusion method in comparison to ampicillin, chloramphenicol and nystatin (Table III). EON and EOT showed high activity against *S. aureus* and *S. lutea* with inhibition zones larger than 14 mm but no activity against *B. cereus*, *E. coli* and *P. aeruginosa*. The EOT also had moderate activity against *C. albicans* (inhibition zone of 9.66 mm).[26] Unlike EOT, EON showed no antifungal activity.

TABLE III. Antimicrobial activity (diameter of inhibition zone, mm) of cembran pine essential oils determined by the agar diffusion method; different letters in the column indicate values significantly different ($P \leq 0.05$)

Microorganism	EON (30 μL)	EOT (30 μL)	Ampicillin (25 μg $disc^{-1}$)	Chloramphenicol (30 μg $disc^{-1}$)	Nystatin (100 μg $disc^{-1}$)
S. aureus ATCC 25923	22[a] (a)	24.7±0.6[a] (b)	27.7±0.6[a] (c)	26±1[a] (bc)	Not determined
S. lutea ATCC 9341	31±1[a] (a)	30±1[a] (a)	36[a] (b)	35.3±0.6[a] (b)	Not determined
B. cereus ATCC 14579	No zone	No zone	No zone	25.7±0.6	Not determined
E. coli ATCC 25922	No zone	No zone	19±1[b] (a)	26[b] (b)	Not determined
P. aeruginosa ATCC 27853	No zone	No zone	No zone	18	Not determined
C. albicans ATCC 10231	No zone	9.7±0.6[b] (a)	Not determined	Not determined	29.3±0.6[b] (b)

The *MIC* and *MBC*/*MFC* values of cembran pine essential oils against the sensitive microbial strains were determined by a broth microdilution assay in comparison to ampicillin and nystatin (Table IV). Both essential oils showed similar antimicrobial effects against *S. lutea* with *MIC* and *MBC* values of 0.12 and 0.24 mg mL^{-1}, respectively. *S. aureus* was less susceptible to cembran pine essential oils. According to the *MIC* and *MBC* values, EOT (1.95 and 3.9 mg mL^{-1}, respectively) was more active than EON (3.9 and 15.62 mg mL^{-1}, respectively). The broth microdilution assay confirmed the antifungal activity of EOT (*MIC* = 7.81 mg mL^{-1} and *MFC* = 15.62 mg mL^{-1}).

TABLE IV. Antimicrobial activity of cembran pine essential oils determined by the broth microdilution method

Microorganism	EON		EOT		Ampicillin		Nystatin	
	MIC	*MBC*/*MFC*	*MIC*	*MBC*/*MFC*	*MIC*	*MBC*/*MFC*	*MIC*	*MBC*/*MFC*
	mg mL^{-1}				μg mL^{-1}			
S. aureus ATCC 25923	3.9	15.62	1.95	3.9	0.25	0.5	n.d.[a]	n.d.
S. lutea ATCC 9341	0.12	0.24	0.12	0.24	0.25	0.5	n.d.	n.d.
C. albicans ATCC 10231	n.d.	n.d.	7.81	15.62	n.d.	n.d.	1	2

[a]Not determined

Among volatile constituents, phenolics (thymol, carvacrol and eugenol) and oxygenated monoterpenes (*α*-terpineol, terpinen-4-ol and linalool) have been reported to possess not only strong antimicrobial effects, but also a wide spectrum of activity.[27] The lack of activity against some microbial strains might be due to the high content of monoterpene hydrocarbons in the cembran pine essential oils. The low antimicrobial activity of hydrocarbons has been attributed to their low hydrogen bonding capacity and water solubility.[28] Both EON and EOT are dominated by monoterpene hydrocarbons; they contain low amounts of oxygenated monoterpenes (< 1 %) and no phenolics. EOT proved to be more effective than EON. The higher percentages of limonene+*β*-phellandrene and *β*-pinene are not solely responsible for the antimicrobial potency of EOT; synergistic, additive or antagonistic interactions between volatile constituents may also affect the antimicrobial activity.

There are many literature reports on the antimicrobial effects of other pine needle essential oils, some of them giving contradictory results. The essential oil isolated from the needles of *P. nigra* ssp. *dalmatica* was reported to have a high effect against *S. aureus* (*MIC* = 0.03 %, v/v) and less pronounced effects against *P. aeruginosa* (*MIC* = 0.25 %, v/v), *E. coli* (*MIC* = 2.50 %, v/v) and *C. albicans* (*MIC* = 0.25 %, v/v).[8] Hong *et al*. reported that the essential oil from *P. koraiensis* needles showed no activity against *S. aureus* and *E. coli* but exhibited

antifungal activity against *C. albicans* (28.9–31.5 % *vs*. control); the essential oil from *P. densiflora* needles inhibited the growth of *S. aureus* (66.7–77.8 % *vs*. control) while it had no activity against *E. coli* and *C. albicans*.[29] On the contrary, Park and Lee reported that the essential oil from *P. densiflora* needles exhibited antibacterial effects against *E. coli*, *S. aureus* and *P. aeruginosa* with *MIC* values of 0.8, 1.7 and 26.3 mg mL^{-1}, respectively. Against the same bacterial strains, the *MIC* values of the essential oil from *P. thunbergii* needles were 6.6, 13.2 and 26.3 mg mL^{-1}, respectively.[24] These differences in antimicrobial effects of pine essential oils might be attributed to different antimicrobial screening assays, variations in chemical composition and possible interactions between the constituents.[30]

CONCLUSIONS

This is the first report on the antioxidant and antimicrobial effects of the essential oils of cembran pine needles and twigs and also the first report on the chemical composition of the latter. The results of the present study indicate that both essential oils are rich in monoterpene hydrocarbons. α-Pinene was the major constituent of the needle essential oil while the twig essential oil was dominated by limonene+β-phellandrene and α-pinene. Cembran pine essential oils showed weak free radical scavenging activity but displayed high antibacterial activity against *S. lutea* and *S. aureus*. Twig essential oil was more active against *S. aureus* than needle essential oil and, in addition, it was active against *C. albicans*. Further research is required to evaluate the spectrum of activity of cembran pine essential oils and the possible interactions (synergistic, additive and antagonistic) in the case of association with antibiotics and other essential oils.

Acknowledgements. The authors express their gratitude to Professor Constantin Toma (Faculty of Biology, Al. I. Cuza University of Iasi, Romania) and to the administrative staff of Calimani National Park (Romania) for their valuable help in the acquisition of the plant material.

ИЗВОД

САСТАВ, АНТИОКСИДАТИВНА И АНТИМИКРОБНА АКТИВНОСТ ЕТАРСКИХ УЉА ДРВЕТА *Pinus cembra* СА ПЛАНИНА КАЛИМАНИ (РУМУНИЈА)

CRISTINA LUNGU APETREI[1], ADRIAN SPAC[2], MIHAI BREBU[3], CRISTINA TUCHILUS[4] и ANCA MIRON[5]

[1]Department of Plant and Animal Biology, School of Pharmacy, University of Medicine and Pharmacy „Grigore T. Popa“ – Iasi, Romania, [2]Department of Physical Chemistry, School of Pharmacy, University of Medicine and Pharmacy „Grigore T. Popa“ – Iasi, Romania, [3]Physical Chemistry of Polymers Laboratory, Petru Poni Institute of Macromolecular Chemistry, Iasi, Romania, [4]Department of Microbiology, School of Medicine, University of Medicine and Pharmacy „Grigore T. Popa“ – Iasi, Romania и [5]Department of Pharmacognosy, School of Pharmacy, University of Medicine and Pharmacy „Grigore T. Popa“ – Iasi, Romania

Испитиван је хемијски састав, антиоксидативна и антимикробна активност етарских уља из иглица и грана дрвета *Pinus cembra* L. Хемијски састав је утврђиван мето-

дама GC и GC–MS. α-Пинен је био главни састојак етарског уља из иглица (69,14 %), док је етарско уље грана највише имало лимонена и β-феландрена (укупно 40,97 %) и α-пинена (24,94 %). Етарска уља иглица и грана су исказала малу активност у DPPH тесту. Оба уља су испољила велику активност према бактеријама *Sarcina lutea* и *Staphylococcus aureus*, али не према *Bacillus cereus*, *Escherichia coli* и *Pseudomonas aeruginosa*. Етарска уља иглица и грана су имала сличну антимикробну активност према *S. lutea*. Етарско уље из грана је било активније према *S. aureus* него уље из иглица, а испољавало је извесну активност и према гљивици *Candida albicans*.

(Примљено 9. априла, ревидирано 21. јуна 2012)

REFERENCES

1. I. Blada, *Ann. For. Res.* **51** (2008) 115
2. S. Casalegno, G. Amatulli, A. Camia, A. Nelson, A. Pekkarinen, *Forest Ecol. Manag.* **259** (2010) 750
3. G. Wieser, W. J. Manning, M. Tausz, A. Bytnerowicz, *Environ. Pollut.* **139** (2006) 53
4. P. K. Koukos, K. I. Papadopoulou, D. Th. Patiaka, A. D. Papagiannopoulos, *J. Agr. Food Chem.* **48** (2000) 1266
5. P. K. Koukos, K. I. Papadopoulou, A. D. Papagiannopoulos, D. Th. Patiaka, *Holz Roh Werkst.* **58** (2001) 437
6. M. Krauze-Baranowska, M. Mardarowicz, M. Viwart, L. Pobłocka, M. Dynowska, *Z. Naturforsch., C* **57** (2002) 478
7. F. Macchioni, P. L. Cioni, G. Flamini, I. Morelli, S. Maccioni, M. Ansaldi, *Flavour Frag. J.* **18** (2003) 139
8. O. Politeo, M. Skocibusic, A. Maravic, M. Ruscic, M. Milos, *Chem. Biodivers.* **8** (2011) 540
9. T. Stevanovic, F.-X. Garneau, F.-I. Jean, H. Gagnon, D. Vilotic, S. Petrovic, N. Ruzic, A. Pichette, *Flavour Frag. J.* **20** (2005) 96
10. L. Dormont, A. Roques, C. Malosse, *Phytochemistry* **49** (1998) 1269
11. J. R. Ochocka, M. Asztemborska, D. Sybilska, W. Langa, *Pharm. Biol.* **40** (2002) 395
12. J. G. S. Maia, E. H. A. Andrade, M. G. B. Zoghbi, *J. Food Compos. Anal.* **13** (2000) 227
13. M. Mardarowicz, D. Wianowska, A. L. Dawidowicz, R. Sawicki, *Z. Naturforsch., C* **59** (2004) 641
14. J. G. S. Maia, E. H. A. Andrade, A. C. M. da Silva, J. Oliveira, L. M. M. Carreira, J. S. Araújo, *Flavour Frag. J.* **20** (2005) 474
15. C. I. G. Tuberoso, A. Kowalczyk, V. Coroneo, M. T. Russo, S. Dessi, P. Cabras, *J. Agr. Food Chem*. **53** (2005) 10148
16. A. Angioni, A. Barra, V. Coroneo, S. Dessi, P. Cabras, *J. Agr. Food Chem.* **54** (2006) 4364
17. H. Mighri, H. Hajlaoui, A. Akrout, H. Najjaa, M. Neffati, *C. R. Chim.* **13** (2010) 380
18. CLSI M02-A11, *Performance Standards for Antimicrobial Disk Susceptibility Tests*, Approved Standard, 11th ed., Wayne, PA, 2012
19. G. Del-Vechio-Vieira, O. V. Sousa, C. H. Yamamoto, M. A. C. Kaplan, *Rec. Nat. Prod.* **3** (2009) 52
20. CLSI M07-A9, *Methods for Dilution Antimicrobial Susceptibility Tests for Bacteria that Grow Aerobically*, Approved Standard, 9th ed., Wayne, PA, 2012
21. J. Yu, J. Lei, H. Yu, X. Cai, G. Zou, *Phytochemistry* **65** (2004) 881

22. D. Villaño, M. S. Fernández-Pachón, M. L. Moyá, A. M. Troncoso, M. C. García-Parrilla, *Talanta* **71** (2007) 230
23. G. Sacchetti, S. Maietti, M. Muzzoli, M. Scaglianti, S. Manfredini, M. Radice, R. Bruni, *Food Chem.* **91** (2005) 621
24. J.-S. Park, G.-H. Lee, *J. Sci. Food Agr.* **91** (2011) 703
25. W. Wang, N. Wu, Y. G. Zu, Y. J. Fu, *Food Chem.* **108** (2008) 1019
26. M. Yousefzadi, M. H. Mirjalili, N. Alnajar, A. Zeinali, M. Parsa, *J. Serb. Chem. Soc.* **76** (2011) 857
27. H. J. D. Dorman, S. G. Deans, *J. Appl. Microbiol.* **88** (2000) 308
28. M. Soković, P. D. Marin, D. Brkić, L. J. L. D. van Griensven, *Food* **1** (2007) 220
29. E.-J. Hong, K.-J. Na, I.-G. Choi, K.-C. Choi, E.-B Jeung, *Biol. Pharm. Bull.* **27** (2004) 863
30. Y. Fu, Y. Zu, L. Chen, X. Shi, Z. Wang, S. Sun, T. Efferth, *Phytother. Res.* **21** (2007) 989.

Journal of the Serbian Chemical Society
JSCS-info@shd.org.rs • www.shd.org.rs/JSCS

J. Serb. Chem. Soc. 78 (1) 39–55 (2013)
JSCS–4394

UDC 546.562'742'732'712'472'481'492'722'
963+547.298.61+542.913:543.42:615.28+88
Original scientific paper

Metal complexes of *N'*-[2-hydroxy-5-(phenyldiazenyl)-benzylidene]isonicotinohydrazide. Synthesis, spectroscopic characterization and antimicrobial activity

ABDOU S. EL-TABL[1]*, MOHAMAD M. E. SHAKDOFA[2,3] and ADEL M. E. SHAKDOFA[1]

[1]*Department of Chemistry, Faculty of Science, El-Menoufia University, Shebin El-Kom, Egypt,* [2]*Inorganic Chemistry Department, National Research Center, P. O. Box 12622, Dokki, Cairo, Egypt and* [3]*Department of Chemistry, Faculty of Sciences and Arts, King Abdulaziz University, Khulais, Saudi Arabia*

(Received 7 March 2011, revised 12 June 2012)

Abstract: A new series of Cu(II), Ni(II), Co(II), Mn(II), Zn(II), Cd(II), Hg(II), VO(II), UO_2(II), Fe(III) and Ru(III) complexes of *N'*-[2-hydroxy-5-(phenyldiazenyl)benzylidene]isonicotinohydrazide (H_2L) was synthesized and characterized by elemental analysis, ^{1}H-NMR, IR, UV–Vis and ESR spectroscopy, magnetic and thermogravimetric (TG) analyses, and conductivity measurements. The spectral data showed that the ligand behaved as a neutral bidentate (complexes **2**, **4**–**6** and **14**), monobasic bidentate (complexes **7** and **9**), monobasic tridentate (complexes **3**, **8**, **10**, **11** and **16**) or dibasic tridentate (complexes **12**, **13** and **15**) and was bonded to the metal ions *via* the carbonyl oxygen atom in the ketonic or enolic form, the azomethine nitrogen atom and/or the deprotonated phenolic hydroxyl oxygen. The ESR spectrum of the solid vanadyl(II) complex **2** showed an axially anisotropic spectrum with eight lines in the low field region and with $g_\perp > g_\parallel$ and $A_\parallel >> A_\perp$ relationships, which are characteristics of a distorted octahedral structure with a d_{xy} ground state. However, the copper(II) complexes **4**–**6**, and the manganese(II) complex **10** showed an isotropic type symmetry, while the copper(II) complexes **3** and **7** showed an axial symmetry type with $g_\parallel > g_\perp > g_e$, indicating a covalent bond character. The antibacterial and antifungal activities of the ligand and its metal complexes showed low activity compared with the standard drugs (tetracycline for the bacteria and amphotricene B for the fungi).

Keywords: metal complexes; syntheses; spectral; isonicotinohydrazide; biological activities.

* Corresponding author. E-mail: asaeltabl@yahoo.com
doi: 10.2298/JSC110307062E

INTRODUCTION

There has been growing interest in studying hydrazones and their metal complexes due to their application as antifungal,[1–3] antibacterial,[1–4] anticonvulsant,[5] anti-inflammatory,[3] antimalarial,[6] analgesic,[7] antiplatelets,[8] antituberculosis,[9] anticancer activities,[10] and their use in the treatment of leprosy and mental disorder diseases.[11] Hydrazones act as herbicides, insecticides, nematocides, rodenticides and plant growth regulators, plasticizers and stabilizers for polymers, and polymerization initiators and antioxidants. In analytical chemistry, hydrazones are used in the detection, determination and isolation of compounds containing a carbonyl group. More recently, they have been extensively used for the detection and determination of several metals.[12] Metal complexes of 2-acetylpyridine benzoylhydrazone were synthesized and crystallographically characterized.[13] The Mn(II), Fe(III), Ni(II), Co(II) and Zn(II) complexes of 2,6-diformyl-4-methylphenol bis(benzoylhydrazone) were prepared and characterized by elemental and spectroscopic measurements.[14] The Co(II), Mn(II), Cu(II) complexes of 2-acetylpyridine salicyloylhydrazone and 2-benzoylpyridine salicyloylhydrazone were also synthesized and characterized.[15] Moreover, zinc(II) complexes of 2-benzoylpyridinephenylhydrazone, 2-benzoylpyridine*para*-chlorophenylhydrazone and 2-benzoylpyridine*para*-nitrophenylhydrazone were prepared and characterized by elemental, spectral and single-crystal X-ray diffraction analyses.[16] Much work on metal complexes of hydrazones with different functional groups has been reported.[17] However, little research has been devoted to metal complexes of azo-hydrazone ligands; hence, the synthesis, characterization and antimicrobial activities of copper(II), nickel(II), cobalt(II), manganese(II), zinc(II), cadmium(II), mercury(II), vanadyl(II), uranyl(II), iron(III) and ruthenium(III) complexes of *N*′-[2--hydroxy-5-(phenyldiazenyl)benzylidene]isonicotinohydrazide were undertaken in the reported study.

EXPERIMENTAL

Materials and measurements

The starting chemicals were of analytical grade and provided by Merck. 2-Hydroxy-5-(phenyldiazenyl)benzaldehyde was prepared by a published method.[18] Elemental analyses were determined by the Analytical Unit of the Cairo University of Egypt. Standard analytical methods were used to determine the metal ion contents.[19] All metal complexes were dried in vacuum over anhydrous $CaCl_2$. The IR spectra were measured as KBr discs using a JASCO FT/IR 6100 spectrophotometer (400–4000 cm^{-1}). The electronic spectra in dimethyl sulphoxide (DMSO) solutions (10^{-3} M) were recorded on a Perkin-Elmer 550 spectrophotometer. The molar conductance of 10^{-3} M solutions of the complexes in DMSO was measured at 25 °C with a Bibby conductometer type MCl. The resistance measured in ohms and the molar conductivities were calculated according to the equation: $\Lambda_M = VKg/M_wR_\Omega$, where: Λ_M is the molar conductivity (Ω^{-1} cm^2 mol^{-1}), V is the volume of the complex solution (mL), K is the cell constant (0.92 cm^{-1}), M_w is the molecular weight of the complex, g is the weight of the complex (g), R_Ω is the resistance (Ω). The ^{1}H-NMR spectra were recorded in DMSO-d_6-using

a JEOL EX-270 MHz FT-NMR spectrometer. The mass spectrum was recorded using a JEOL JMS-AX-500 mass spectrometer provided with a data system. The thermal analysis (TG) was performed under nitrogen on a Shimadzu DT-30 thermal analyzer from 23–800 °C at a heating rate of 10 °C min^{-1}. The magnetic moments (μ_B) were measured at room temperature by the Gouy method $\mu_{eff} = 2.84(\chi_{m,corr}T)^{1/2}$ using mercuric tetracyanatocobaltate(II) as the magnetic susceptibility standard. Diamagnetic corrections were estimated from the Pascal constant.[20] ESR Measurements of the solid complexes at room temperature were realized using a Varian E-109 spectrophotometer, with di(phenyl)-(2,4,6-trinitrophenyl)imino-azanium (DPPH) as the standard material. Thin layer chromatography (TLC) was used to confirm the purity of the compounds.

Preparation of ligand [H_2L]

The ligand, *N*′-[2-hydroxy-5-(phenyldiazenyl)benzylidene]isonicotinohydrazide (H_2L) was prepared (Scheme 1) by adding equimolar amounts of isonicotinic hydrazide (1.37 g, 1.0 mmol, in 20 mL of absolute ethanol) to 2-hydroxy-5-(phenyldiazenyl)benzaldehyde (2.26 g, 1.0 mmol, in 20 mL of absolute ethanol). The mixture was refluxed under stirring for 1 h. The solid product which formed was filtered off, washed with cold ethanol, followed by crystallization from ethanol and finally dried under vacuum over anhydrous $CaCl_2$.

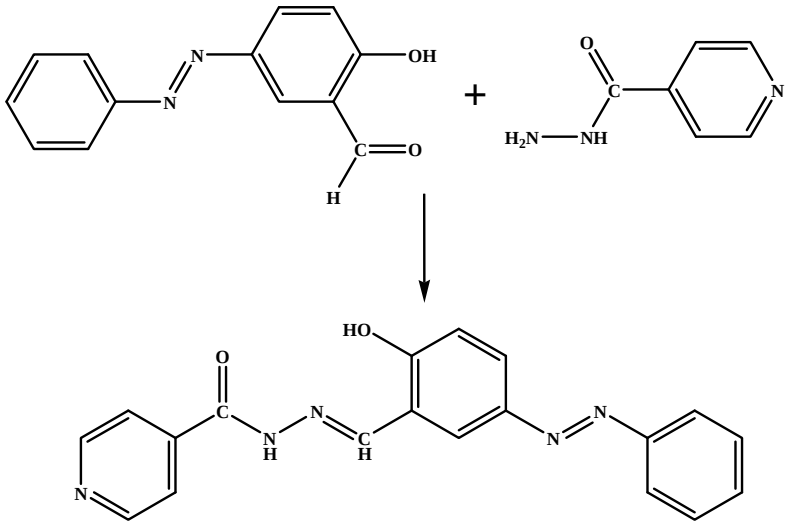

Scheme 1. Preparation of the ligand, *N*′-[2-hydroxy-5-(phenyldiazenyl)-benzylidene]isonicotinohydrazide (H_2L).

*Preparation of the metal complexes **2–16***

The metal complexes were prepared by mixing a hot ethanolic solution of the required metal acetate: $Cu(CH_3COO)_2 \cdot H_2O$, $Ni(CH_3COO)_2 \cdot 4H_2O$, $Co(CH_3COO)_2 \cdot 4H_2O$, $Mn(CH_3COO)_2 \cdot 4H_2O$, $Zn(CH_3COO)_2 \cdot 2H_2O$, $Cd(CH_3COO)_2 \cdot 2H_2O$, $Hg(CH_3COO)_2 \cdot H_2O$, and $UO_2(CH_3COO)_2 \cdot H_2O$, metal chloride: $CuCl_2 \cdot 2H_2O$, $FeCl_3 \cdot 6H_2O$, $RuCl_3 \cdot 3H_2O$ or metal sulphate: $CuSO_4 \cdot 5H_2O$, $VOSO_4 \cdot H_2O$ and $Cu(NO_3)_2 \cdot 2.5H_2O$ with a suitable amount of a hot ethanolic solution of the ligand to form 1:1 or 1:2, M:L (metal:ligand) complexes in the

presence of 2 mL of triethylamine (TEA). The reaction mixture was then refluxed for a time depending on the metal salt used (2–4 h). The formed precipitates were filtered off, washed with ethanol, then with diethyl ether and dried under vacuum over anhydrous $CaCl_2$.

In vitro *antibacterial and antifungal activities*

The biological activities of the newly synthesized hydrazone ligand, its metal complexes and metal salts were performed in the Botany Department, Laboratory of Microbiology, Faculty of Science, El-Menoufia University, Egypt. They were studied for their antibacterial and antifungal activities by the disc diffusion method.[21,22] The antimicrobial activities were realized using the bacteria *Escherichia coli* and *Bacillus subtilis*, and the fungus *Aspergillus niger* at 10 mg mL^{-1} concentrations in DMSO. The bacteria were subcultured in nutrient agar medium which contained 5 g L^{-1} NaCl, 5 g L^{-1} peptone, 3 g L^{-1} beef extract and 20 g L^{-1} agar in distilled water. The fungus was subcultured in Dox medium which contained (in distilled water): 1 g L^{-1} yeast extract, 30 g L^{-1} sucrose, 3 mg L^{-1} $NaNO_3$, 20 g L^{-1} agar, 0.5 g L^{-1} KCl, 1 g L^{-1} KH_2PO_4, 0.5 g L^{-1} $MgSO_4 \cdot 7H_2O$ (0.5 g) and a trace of $FeCl_3 \cdot 6H_2O$ in distilled water. These mediums were then sterilized by autoclaving at 120 °C for 15 min. After cooling to 45 °C, the medium was poured into 90 mm diameter Petri dishes and incubated at 37 or 28 °C, for the bacteria and the fungus, respectively. After a few hours, the Petri dishes were stored at 4 °C. The micro-organisms were spread over each dish using a sterile bent loop rod. The test was performed by placing filter paper disks (3 mm diameter) with a known concentration of the compounds on the surface of the agar plates inoculated with a test organism. DMSO was used as the negative control. The standard antibacterial drug tetracycline, antifungal drug amphotericin B and solution of metal salts were also screened under similar conditions for comparison. The Petri dishes were incubated for 48 h at 37 or 28 °C for the bacteria and the fungus, respectively. The zone of inhibition was carefully measured in millimetres. All determinations were made in duplicate for each of the compounds. The average of the two independent readings for each compound was recorded.

RESULTS AND DISSCUSSION

The ligand, *N*'-[2-hydroxy-5-(phenyldiazenyl)benzylidene]isonicotinohydrazide (H_2L) and its metal complexes **2**–**16** are stable at room temperature. They are non-hygroscopic and insoluble in common organic solvents, such as ethanol, methanol, chloroform and acetone, but completely soluble in DMF and DMSO. The elemental analyses showed that the complexes **3**–**6**, **8**, **10**, **11**, **14** and **16** were formed in a 2L:1M molar ratio, while the complexes **2**, **7**, **9**, **12**, **13** and **15** were formed in a 1L:1M molar ratio. The ^{1}H-NMR, IR and UV–Vis spectral data were compatible with the suggested structures (Figs. 1–3). The physical, analytical and spectral data for the ligand and its metal complexes are given in the Supplementary material to this paper, together with selected spectra of the ligand and its complexes, *i.e.*, the IR spectra of **1**, **6** and **8** (Figs. S-1–S-3), the ^{1}H-NMR spectra of **1** and **13** (Figs. S-4 and S-5), the mass spectrum of **1** (Fig. S-6) and the ESR spectra of **2**, **3** and **6** (Figs. S-7–S-9).

Infrared spectra

The spectrum of the ligand (H_2L) showed a strong band at 1658 cm^{-1} due to the carbonyl group of the hydrazide moiety, whereas the medium band at 3174

cm^{-1} may be assigned to the N–H group.[23,24] This observation indicates that the ligand is present in the ketonic form in the solid state.[25] The spectrum showed two broad bands in the 3300–3550 cm^{-1} and 2550–3000 cm^{-1} ranges which may be assigned to the stretching vibration of the phenolic hydroxyl groups associated through intra- and intermolecular hydrogen bonding.[23] The relatively strong and medium bands located at 1605, 1468 and 1004 cm^{-1} corresponded to the azomethine group,[26] the azo group[27] and ν(N–N),[23] respectively. The band which appeared at 1289 cm^{-1} is due to the ν(C–OH) of the phenolic moiety.[25]

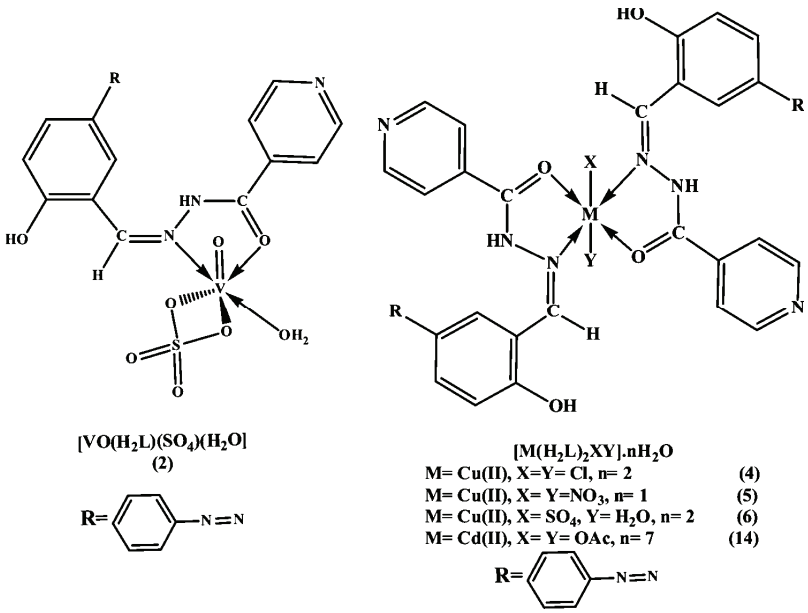

Fig. 1. Structure of the vanadyl(II), copper(II) and cadmium(II) complexes (**2**, **4**–**6** and **14**, respectively).

By comparison of the spectra of the complexes with that of the free ligand, the mode of bonding between the ligand and the metal ions could be established. The spectra of complexes **7**, **9**, **12**, **13**, and **15** showed the disappearance of bands that are characteristic to ν(C=O) and ν(N–H), indicating that the ligand bonded to the metal ions in its enolate form through the enolic carbonyl oxygen atom. This mode of bonding was supported by the appearance of new bands in the 1507–1546 cm^{-1} and 1207–1258 cm^{-1} ranges, corresponding to ν(N=C–O) and ν(C–O), respectively.[28] In the case of complexes **2**–**6**, **8**, **10**, **11**, **14** and **16**, the band characteristic of ν(N–H) was still present and the band of the carbonyl group was shifted to lower frequencies by 43–52 cm^{-1} indicating that, the ligand in these complexes coordinated to the metal ions in its ketonic form *via* the oxy-

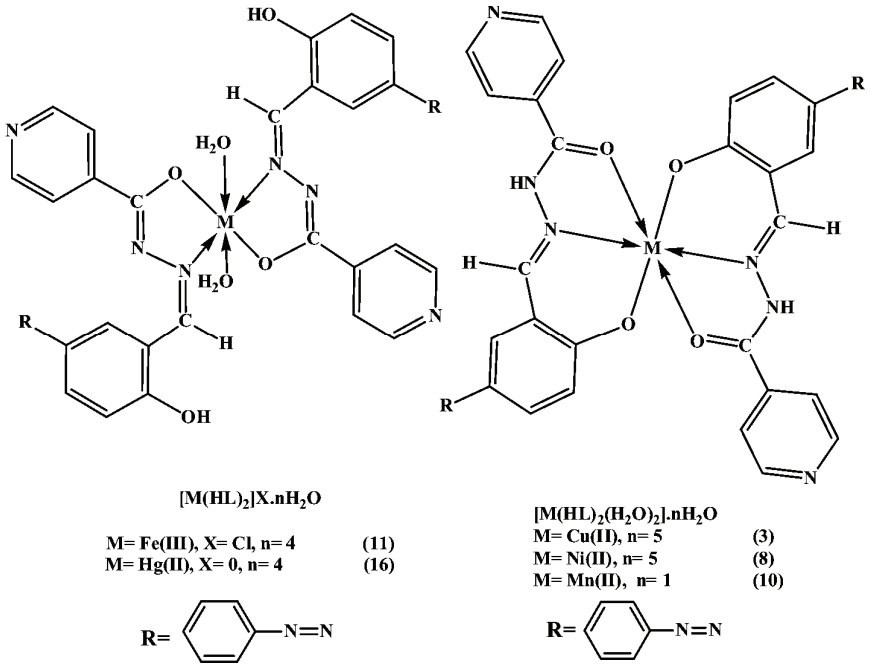

Fig. 2. Structure of the copper(II), nickel(II), manganese(II), iron(III) and mercury complexes (**3**, **8**, **10**, **11** and **16**, respectively).

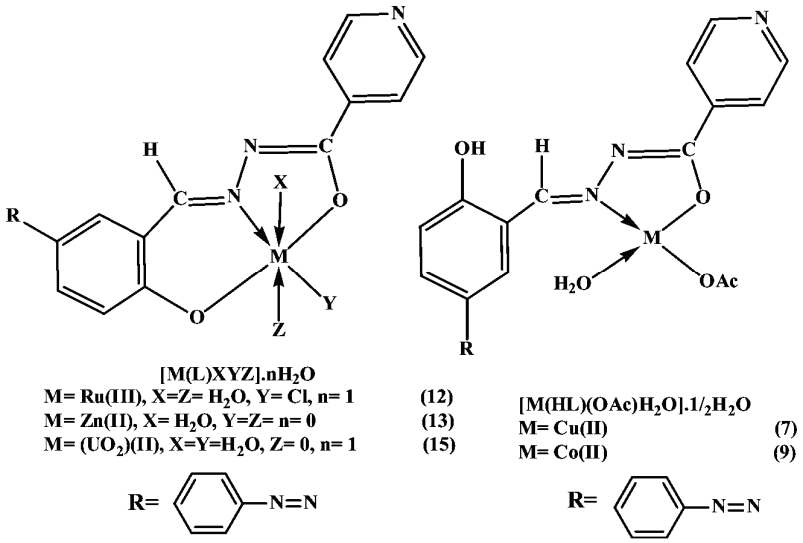

Fig. 3. Structure of the copper(II), cobalt(II), ruthenium(III), zinc(II) and uranyl(II) complexes (**7**, **9**, **12**, **13** and **15**, respectively).

gen atom of the carbonyl group. In all complexes, the band characteristic of the azomethine group was shifted to lower frequencies, appearing in the 1538–1603 cm^{-1} range. At the same time, the band due to ν(N–N) was shifted to a higher frequency. The increasing in the frequency of this band ν(N–N) is a clear indication that an increase in the double bond character is compensating for the loss of electron density *via* electron donation to the metal ions, which if further confirmation of the coordination of the ligand *via* the azomethine group. In complexes **3**, **8**, **10**–**13**, **15** and **16**, the small shifts in the band characteristic of the phenolic oxygen atom indicate that the bonding occurred *via* the deprotonated phenolic oxygen atom. The appearance of new bands in the 573–610 cm^{-1}, 510–575 cm^{-1} and 467–509 cm^{-1} ranges for complexes **2**–**16** may be assigned to the ν(M–O), ν(M←O) and ν(M←N), respectively.[29] The appearance of these bands was taken as confirmation that the bonding of the ligand with the metal ions occurred *via* the carbonyl oxygen atom in the enolic or ketonic form, azomethine nitrogen atom and/or the deprotonated phenolic hydroxyl oxygen atom. The IR spectrum of the nitrate complex (**5**) showed bands at ν_5 (1415), ν_1 (1330) and ν_2 (954), indicating that the nitrate group coordinated to the metal ion. The difference between the two high bands (ν_5–ν_1) was 85 cm^{-1} indicating that the nitrate ion bonded to the copper(II) ion in an unidentate manner.[30–32] In the case of sulphate complexes **2** and **6,** new bands appeared at 1258, 1143, 1112 and 984 cm^{-1}, and at 1192, 1058 and 962 cm^{-1} for the two complexes, respectively. The bands of the first complex **2** indicated that the sulphates were coordinated to the vanadyl(II) ion in a chelating bidentate fahion,[30,33] while the bands of complex **6** indicated that the sulphates were coordinated to the copper(II) ion in a chelating unidentate fahion.[30,32] In the acetate complexes, the acetates may be coordinated to the metal ion in unidentate, bidentate or bridging bidentate manner. The $\nu_{as}(CO_2^-)$ and $\nu_s(CO_2^-)$ of the free acetate ion are at *ca*. 1560 and 1416 cm^{-1} respectively. In the unidentate acetate complexes, ν(C=O) was higher than $\nu_s(CO_2^-)$ and ν(C–O) was lower than $\nu_{as}(CO_2^-)$. As a result, the separation between the two ν(C–O) was much larger in the unidentate than in the free ion but in the bidentate, the separation was lower than in the free ion while in the bridging bidentate, the two ν(CO) were closer to the free ion.[30] In the case of complexes **7**, **9** and **14** two new bands appeared in the 1546–1561 cm^{-1} and 1358–1387 cm^{-1} ranges, which were attributed to the symmetric and asymmetric stretching vibration of the acetate group. The difference between these two bands are in the 159–194 cm^{-1} range, which indicates that the acetates coordinate to the metal ion in a unidentate manner.[30,34] The infrared spectra of the vanadyl and uranyl complexes **2** and **15** revealed a medium band at 997 and 910 cm^{-1}, which may be attributed to ν(V=O)[35] and ν(O=U=O),[29] respectively.

^{1}H-NMR spectra

The ^{1}H-NMR spectrum of the ligand (H_2L) shows the absence of the signal of the amino group (NH_2) characteristic of the starting material (hydrazide). The spectrum shows three sets of peaks, the first one observed as singlet at 12.41 (*s*, 1H) and 11.65 (*s*, 1H) ppm which may be assigned to the hydroxyl (OH) and (NH) protons, respectively.[23,24,36] These hydrogen resonances appear at high δ values because of their attachment to highly electronegative atoms, oxygen and nitrogen, respectively; hence, they are in a low electron density environment. This assignment was confirmed by the deuterated spectra in which the intensity of these bands was considerably decreased. The position of these peaks in the downfield region indicates the possibility of extensive hydrogen bonding involving these groups.[36] The second set appeared as a singlet at 8.60 (1H, *s*) ppm and corresponded to the azomethine proton (H–C=N).[36] The third group appeared as multiplets in the 7.14–8.31 (12H, *m*) ppm range, which were attributed to aromatic protons. It is clear from the ^{1}H-NMR spectrum of the ligand that it exists in the keto form only with no evidence for the presence of the enol form. This result was confirmed by the appearance of the signal of the (NH) and phenolic (OH) only and the absence of the (OH) signal of the enolic form. The same conclusion was reported by many authors.[24,36]

Comparing the ^{1}H-NMR spectra of the zinc(II) and uranyl(II) complexes, **13** and **15**, respectively, with that of the free ligand, it could be noticed that the signals of the NH and OH groups had disappeared, indicating that the ligand bonded to the zinc(II) and uranyl(II) ions as a dibasic ligand *via* the enolic carbonyl oxygen and the deprotonated hydroxyl oxygen atoms. This observation was confirmed by the absence of the signal of the acetate proton. A significant downfield shift of the azomethine proton signal in the complexes relative to the corresponding signal of the free ligand confirmed the coordination of the azomethine nitrogen atom.

Mass spectra

The mass spectrum of the ligand (H_2L) revealed a molecular ion peak at *m*/*z* 345, which is consistent with the formula weight (345.36) for this ligand. This result confirmed the identity of the ligand structure.

Molar conductivity

The molar conductivity of 1×10^{-3} M solution of the metal complexes in DMSO at room temperature are in the 3.5–22.5 Ω^{-1} cm^2 mol^{-1} range, except for complex **11**, indicating the non-electrolytic nature of these complexes. These results confirmed that the anion is coordinated to the metal ion. The considerably high values of some complexes may be due to partial solvolysis by DMSO. However, complex **11** has a molar conductivity value of 80.5 Ω^{-1} cm^2 mol^{-1}, indi-

cating the electrolytic nature of this complex.[37] These data are in agreement with the results of Greenwood *et al*.[38] They suggested 50–70 Ω^{-1} cm^2 mol^{-1} as the range for a 1:1 electrolyte in DMSO.

Electronic absorption spectra

The structure of the ligand reveals that the two lone pairs of electrons of the azo group are not the only interacting non-bonding electrons, since the hydrazone part of the ligand also contains nitrogen and oxygen atoms, which may be extra sources of lone pair of electrons. Thus, another n→π* transition is expected to occur from these non-bonding orbitals to different π* molecular orbitals extending over such large molecules.[39] The electronic absorption spectral bands of the ligand and its metal complexes in DMSO in the 200–1100 nm range are reported in the Supplementary material to this article. The data reveals that the spectrum of the ligand comprises three sets of bands in the UV and visible regions. The first set of shortest wavelength appeared at 270 and 320 nm and may be assigned to the π→π* transition in the benzenoid and pyridine moieties and the intra ligand π→π* transition.[24,40] The second set appears at 350 and 375 nm and may be assigned to n→π* of the azomethine and carbonyl group.[24,40] The third set located at 420 nm may correspond to π→π* transition involving the π-electrons of the azo group.[39,41] The band located in the visible region at 455 nm can be assigned to π→π* transition involving the whole electronic system of the compounds with a considerable charge transfer character arising mainly from the phenolic moiety.[39,41]

The spectrum of vanadyl(II) complex **2** in DMSO solution showed that there are three bands at 700, 575 and 520 nm, which may be assigned to $^2B_2(d_{xy})\rightarrow E(d_{xz},d_{zy})$, $^2B_2(d_{xy})\rightarrow{}^2B_1(d_{x^2-y^2})$ and $^2B_2(d_{xy})\rightarrow{}^2A_1(d_{z^2})$ transitions, indicating that the vanadyl(II) complex has a distorted octahedral structure (Fig. 1).[42–44] The spectra of copper(II) complexes **3**–**6** were nearly identical, showing a broad band centered in the 630–675 nm range. The position and the broadness of this band indicated that copper(II) ion has a tetragonally distorted octahedral geometry (Figs. 1 and 2). This broad band may consist of three superimposed transitions $^2B_{1g}\rightarrow{}^2E_g$, $^2B_{1g}\rightarrow\ \rightarrow{}^2A_{1g}$ and $^2B_{1g}\rightarrow{}^2B_{2g}$.[42,45] This could be due to the Jahn Teller effect that operates on the d^9 electronic ground state of six-coordinated system, elongating one *trans* pair of coordinate bonds and shortening the remaining four. However, the electronic spectrum of the copper complex **7** showed a broad band with shoulders at 650 and 730 nm. This spectrum is similar to that reported for square planar copper(II) complexes (Fig. 3).[42,46] The electronic spectrum of the nickel(II) complex **8** exhibited three bands located at 850 (ν_1), 660 (ν_2) and 580 (ν_3) nm, which may be assigned to $^3A_{2g}\rightarrow{}^3T_{2g}$, $^3A_{2g}\rightarrow{}^3T_{1g}$ and $^3A_{2g}\rightarrow{}^3T_{1g}(p)$ spin-allowed transitions, respectively, which are characteristic of the nickel(II) ion in an octahedral structure (Fig. 2).[42,45–48] The

ν_2/ν_1 ratio of 1.29 is lower than the usual range 1.50–1.75, indicating a distorted nickel(II) complex.[48] The electronic spectrum of the cobalt(II) complex **9** showed two bands appearing at 650 and 505 nm. These bands may be assigned to $^4A_2(F)\rightarrow{}^4T_{1g}(p)$ transitions, suggesting that a tetrahedral geometry around the cobalt(II) ion (Fig. 3).[42,49] This assignment is supported by the μ_{eff} value 4.42 μ_B, which is consistent with a tetrahedral structure.[49] A weak band at 590 nm may be due to spin–spin coupling.[49] The electronic absorption spectrum of manganese(II) complex **10** displayed weak absorption bands at 650, 600, 540 and 465 nm. These bands may corresponded to $^6A_{1g}\rightarrow{}^4T_{1g}(^4G)$ (ν_1), $^6A_{1g}\rightarrow{}^4E_g(^4G)$ (ν_2), $^6A_{1g}\rightarrow{}^4E_g(^4D)$ (ν_3) and $^6A_{1g}\rightarrow\ \rightarrow{}^4T_{1g}(^4p)$ (ν_4) transitions, respectively. These transitions are characteristic of a manganese(II) ion in an octahedral geometry (Fig. 2).[50] The electronic absorption spectrum of iron(III) complex **11** showed bands at 640 and 580 nm, which may be assigned to $^6A_{1g}\rightarrow{}^4T_{2g}(G)$ and $^6A_1(G)\rightarrow{}^4T_1(G)$ transitions, respectively. These bands are characteristic of an octahedral iron(III) complex (Fig. 2).[51] However, the electronic absorption spectrum of ruthenium(III) complex **12** in DMSO solution displayed two bands, at 560 and 650 nm. The first band is due to a ligand-to-metal charge-transfer (LMCT) transition and the second is assigned to a $^2T_{2g}\rightarrow{}^2A_{2g}$ transition. The band positions are similar to those observed for other octahedral ruthenium(III) complexes (Fig. 3).[52] The electronic spectrum of the uranyl complex **15** exhibits one band at 530 nm which may be assigned to ligand-to-uranium charge-transfer transitions (Fig 3).[53] The diamagnetic zinc(II), cadmium(II) and mercury(II) complexes (**13**, **14** and **16**) have a d^{10} system, so they do not show d–d transitions.

Magnetic moments

The magnetic moments of the complexes **2**–**16** at room temperature are presented in the Supplementary material to this article. The results showed that all these complexes **2**–**12** are paramagnetic. The vanadyl complex **2** shows a magnetic value equal to 1.73 μ_B, which corresponds to one unpaired electron.[28,32] The copper(II) complexes **3**–**7** showed values in the 1.68–1.88 μ_B range, which are consistent with a one-unpaired electron system in an octahedral or square planar structure.[24] The nickel(II) complex **8** showed a value of 3.01 μ_B, which is consistent with a two-unpaired electron system of an octahedral nickel(II) complex.[24] The cobalt(II) complex **9** showed a value of 4.42 μ_B; this value indicates a high-spin tetrahedral cobalt(II) complex.[49] The magnetic moment values of the manganese(II) complex **10** and iron(III) complex **11** are 4.87 and 5.34 μ_B, respectively. These values are compatible with high-spin manganese(II) and iron(III) complexes, respectively.[40] The magnetic moment value of ruthenium(III) complex **12** is 1.65 μ_B, which is characteristic for a d^5 low-spin ruthenium(III) complex.[40]

Electron spin resonance of the copper(II), nickel(II), cobalt(II), manganese(II) and vanadyl(II) complexes

The ESR spectrum of the solid vanadyl(II) complex **2** (d^1, ^{51}V, $I = 7/2$) is an axially anisotropic eight-line spectrum with $g_\perp > g_\parallel$ and $A_\parallel >> A_\perp$ relationships, which are characteristics of a distorted octahedral structure with a d_{xy} ground state.[54] The spectrum shows two types of resonance components, one set is due to parallel features ($g_\parallel$) and the other set due to perpendicular features ($g_\perp$), which indicate axially symmetric anisotropy, characteristic of interaction between the electron spin and vanadium nuclear spin. Ligand nitrogen superhyperfine splitting was not observed on vanadium line, indicating interaction occuring between the electron spin and the ligand.[55–57] These values are typical for VO^{2+} in a distorted octahedral complex.[58,59] The molecular orbital coefficients α^2 and β^2 were also calculated for the complexes using the following equations.:

$$\alpha^2 = \frac{E(2.0023 - g_\parallel)}{8\lambda\beta^2} \quad (1)$$

$$\beta^2 = -1.17\frac{A_\parallel}{P} + \frac{A_\perp}{P} + g_\parallel - 0.36g_\perp - 0.64g_e \quad (2)$$

where $P = 128\times10^{-4}$ cm^{-1}, $\lambda = 135$ cm^{-1} and E is the electronic transition energy of $^2B_2 \rightarrow {}^2E$. The lower values for α^2 compared to β^2 indicate that in-plane σ bonding is more covalent than in-plane π-bonding.[60] The in-plane π-bonding parameter β^2 observed are consistent with those observed by McGarvey and Kivelson for vanadyl complexes of acetylacetone.[61]

The ESR spectra of the solid copper(II) complexes **4**–**6** at room temperature exhibit high field signals, which are isotropic due to the tumbling motion of the molecules. The g_{iso} values of the complexes are 2.080, 2.055 and 2.104, respectively.[32,62] The ESR spectra of the solid copper(II) complexes **3** and **7** at room temperature are characteristic for a d^9 configuration, having an axial symmetry type of a $d_{(x^2-y^2)}$ ground state, which is the most common state for copper(II) complexes.[63,64] The g values of $g_\parallel = 2.235$ and 2.198, $g_\perp = 2.045$ and 2.056 with $g_{iso} = 2.108$ and 2.104, respectively, suggest an elongated tetragonal octahedral geometry for **3** and square planar for **7**.[65] The trend of the g-values, *i.e.*, $g_\parallel > g_\perp > g_{e(2.0023)}$ confirmed the tetragonal distortion around the copper(II) ion in **3** and the square planar geometry in **7**,[66] which correspond to elongation of the fourfold symmetry axis z. In addition, exchange coupling interactions between the copper(II) ion are explained by the Hathaway Expression $G = (g_\parallel - 2)(g_\perp - 2)$. If the value of G is < 4.0, a considerable exchange coupling is present in the solid complex. If G is > 4.0, the exchange interactions are negligible, which is typical as in the case of complexes **3** and **7** ($G = 5.22$ and 4.15, respectively). This confirmed the tetragonal octahedral and square planar structures in **3** and **7**, respec-

tively.[67,68] Kivelson and Neiman showed that for an ionic environment, $g_{\|}$ is ≥ 2.3, but for a covalent environment $g_{\|} < 2.3$. The $g_{\|}$-values for complexes **3** and **7** are 2.235 and 2.225, respectively; consequentially, the environments are considerably covalent.[67,68]

The ESR spectra of the solid nickel(II) and cobalt(II) complexes **8** and **9** at room temperature do not show any ESR signals as rapid spin lattice relaxation of nickel(II) and cobalt(II) tends to broaden the lines at higher temperatures.[40] The ESR spectra of the solid manganese(II) complex **10** and ruthenium(III) complex **12** give isotropic signals centred at 1.997 and 2.150, respectively. The broadening of the spectra is due to spin relaxation.[40] The spectrum of ruthenium(III) complex shows an additional weak signal at 2.00, which may be due to the free radical.

Thermal analysis of some of the complexes

The thermogravimetric (TG) analysis was realised in the temperature range 20–800 °C under nitrogen. The results (Table I) show good agreement between the calculated and experimental weight losses. The results showed that the complexes **2**, **5**–**7** and **12** generally decomposed in several steps. The first step is the elimination of water of hydration or solvent molecules, as in complexes **5**–**7** and **12**, in the temperature range 30–117 °C. The second step is the loss of water of coordination, as in complexes **2**, **6**, **7** and **12**, in the 100–350 °C range. The observed loss of coordinated water at high temperatures may be due to hydrogen bonding with the hydroxyl group. The third step is the loss of the anions (sulphate, nitrate, chloride and acetate) in the temperature range 240–380 °C. The fourth step is the complete decomposition of the complexes through degradation of the ligand in temperature range 300–680 °C, leaving metal oxide as the residue.

TABLE I. The results of the thermogravimetric analysis of some of the complexes

No.	Temp. range, °C	Loss in weight Found (Calcd.), %	Assignment	Composition of the residue
2	140–175	3.6 (3.4)	Loss of one molecule of coordinated water	$[VO(H_2L)_2(SO_4)]$
	320–380	18.0 (18.2)	Loss of sulphate group	$[VO(HL)_2]$
	400–490	66.7 (65.6)	Decomposition of the complex forming V_2O_5	V_2O_5
5	50–90	2.3 (2.0)	Dehydration process (H_2O)	$[Cu(H_2L)_2(NO_3)_2]$
	300–350	13.9 (13.8)	Loss of two nitrate groups ($2HNO_3$)	$[Cu(HL)_2]$
	360–680	72.2 (75.3)	Decomposition of the complex forming CuO	CuO

TABLE I. Continued

No.	Temp. range, °C	Loss in weight Found (Calcd.), %	Assignment	Composition of the residue
6	50–117	3.8 (4.0)	Dehydration process (H_2O)	$[Cu(H_2L)_2(SO_4)H_2O]$
	130–260	2.0 (2.0)	Loss of one molecule of coordinated water	$[Cu(H_2L)_2(SO_4)]$
	270–350	10.8 (10.6)	Loss of one sulphate group (H_2SO_4)	$[Cu(HL)_2]$
	370–650	57.0 (61.2)	Decomposition of the complex forming CuO	CuO
7	50–110	3.5 (3.6)	Dehydration process (H_2O)	$[Cu(HL)(OAc)(H_2O)]$
	205–250	3.5 (3.6)	Loss of one molecule of coordinated water	[Cu(HL)(OAc)]
	270–356	12.4 (11.3)	Loss of one acetate group (HOAc)	[Cu(L)]
	360–580	68.1 (58.6)	Decomposition of the complex forming CuO	CuO
12	50–105	3.5 (3.4)	Dehydration process (H_2O)	$[Ru(L)Cl(H_2O)_2]$
	110–230	6.4 (6.7)	Loss of two molecule of coordinated water	[Ru(L)Cl]
	240–280	6.9 (6.6)	Loss of one chlorine (HCl)	[Ru(L–H)]
	300–430	56.7 (59.2)	Decomposition of the complex forming Ru_2O_3	Ru_2O_3

Antibacterial and antifungal screening

The results of screening of antimicrobial activities of the ligand and its metal complexes are listed in Table II. The results show that all the metal complexes exhibited inhibitory effects towards the gram-positive bacterium *B. subtilis* and the gram-negative bacterium *E. coli*. Moreover, the complexes **4** and **13**–**16** exhibited inhibitory effects towards the fungus *A. niger*. In comparison, the parent organic ligand and the solutions of the metal salts had low activity against the bacteria and were inactive against fungus under the experimental conditions. The order of the activity of the compounds against *B. subtilis* was tetracycline > **3** > **2** = **4** > **14** = **16** > **8** > **12** > **6** = **7** = **10** = **13** = **15** > **1** = **5** = **9** > **11**, Table II. The order of the activity against *E. coli* was **2** > tetracycline > **4** > **14** > **15** > **11** > **7** > **6** > **1** = **8** = **13** = **16** > **12** > **3** > **5** > **9** = **10**, Table II. However, the order of the activity against the fungus *A. niger* was **16** > **4** > **14** > amphotericin B = **15** > **13**, Table II. The results show that the activity of complexes against the tested microorganisms was significantly enhanced on coordination. This enhancement in the activity may be rationalized on the basis that their structures mainly possess an additional C=N bond. The most interesting point of the biological measurements is that the azohydrazone had a mild biological effect while other types of hydrazones, such as *N*-phenylglycine 2-(1-methyl-3-oxobutylidene)hydrazide,[69] 3-hydroxy-2-naphthalenecarboxylic acid, [1-(2-pyridinyl)ethylidene]hydrazide,[70]

p-aminoacetophenone isonicotinoylhydrazone[2] and Schiff bases[4,71–73] are biologically strongly active. In addition, their metal complexes showed higher biological activity than the azohydrazone complexes. Hence, it may be stated that the lower activity of azohydrazone and its complexes against both bacteria and fungi could be attributed to the presence of the azo group.

TABLE II. Biological activities of the ligand and its metal complexes against bacteria and a fungus; inhibition zone, mm

Compound	*A. niger*	*E. coli*	*B. subtitles*
DMSO	0	0	0
Amphotericin B	17	–	–
Tetracycline	–	35	40
Ligand (**1**)	0	15	15
2	0	42	24
3	0	13	28
4	20	32	24
5	0	12	15
6	0	17	17
7	0	18	17
8	0	15	21
9	0	11	15
10	0	11	17
11	0	19	11
12	0	14	20
13	12	15	17
14	18	25	22
15	17	20	17
16	40	15	22

CONCLUSIONS

The Cu(II), Ni(II), Co(II), Mn(II), Zn(II), Cd(II), Hg(II), VO(II), UO_2(II), Fe(III) and Ru(III) complexes of *N*′-[2-hydroxy-5-(phenyldiazenyl)benzylidene]-isonicotinohydrazide (H_2L) were characterized by elemental analysis, ^{1}H-NMR, IR, UV–Vis and ESR spectroscopy, thermogravimetric analyses and magnetic and conductivity measurements. The analyses revealed that the ligand bonded in one of four modes, neutral bidentate, monobasic bidentate, monobasic tridentate or dibasic tridentate with the different metal ions *via* the oxygen atom of the carbonyl group in the ketonic or enolic form, the nitrogen atom of the azomethine group or the deprotonated hydroxyl oxygen atom of the azo moiety. The analytical and spectral data showed the prepared complexes had either octahedral or square planar geometry. Some of the metal complexes exhibited inhibitory effects towards gram-positive (*B. subtilis)* and gram-negative (*E. coli*) bacteria and the complexes **4**, **13**–**16** exhibited inhibitory effects towards the fungus *A. niger*.

SUPPLEMENTARY MATERIAL

Physical and spectral data of the synthesized compounds are available electronically from http://www.shd.org.rs/JSCS/, or from the corresponding author on request.

ИЗВОД

КОМЛЕКСИ МЕТАЛА СА *N'*-[2-ХИДРОКСИ-5-(ФЕНИЛДИАЗЕНИЛ)-БЕНЗИЛИДЕН]--ИЗОНИКОТИНОХИДРАЗИДОМ. СИНТЕЗА, СПЕКТРОСКОПСКА КАРАКТЕРИЗАЦИЈА И АНТИМИКРОБНА АКТИВНОСТ

ABDOU S. EL-TABL[1], MOHAMAD M. E. SHAKDOFA[2,3] и ADEL M. E. SHAKDOFA[1]

[1]Department of Chemistry, Faculty of Science, El-Menoufia University, Shebin El-Kom, Egypt, [2]Inorganic Chemistry Department, National Research Center, P.O. Box 12622, Dokki, Cairo, Egypt and [3]Department of Chemistry, Faculty of Sciences and Arts, King Abdulaziz University, Khulais, Saudi Arabia

Синтетизована је нова серија Cu(II), Ni(II), Co(II), Mn(II), Zn(II), Cd(II), Hg(II), VO(II), UO_2(II), Fe(III) и Ru(III) комплекса са *N'*-[2-хидрокси-5-(фенилдиазенил)-бензилиден]-изоникотинохидразидом (H_2L) као лигандом. За карактеризацију комплекса употребљени су елементална микроанализа, ^{1}H-NMR, IR, UV–Vis, ESR, термогравиметријска (TG) анализа, магнетна и кондуктометријска мерења. Спектроскопска мерења су показала да се у случају комплекса **2**, **4**–**6** и **14** H_2L координује као неутрални бидентатни лиганд код комплекса **7** и **9** као монобазни бидентатни лиганд, код комплекса **3**, **8**, **10**, **11** и **16** као монобазни тридентатни лиганд и код комплекса **12**, **13** и **15** као двобазни тридентатни лиганд. Координација лиганда за јон метала се одвија преко карбонилног кисеониковог атома у енолној или кето форми, азометинског атома азота, или депротонованог фенолног атома кисоника. ESR мерења ванадил(II) комплекса у чврстом стању (**2**) показују аксијално-анизотропски облик спектра са осам линија у области ниже енергије $g_\perp > g_\parallel$ и $A_\parallel >> A_\perp$, што одговара дисторгованој октаедарској структури комплекса са d_{xy} основним стањем. Међутим, ова мерења код комплекса бакра(II) (**4**–**6**), као и код комплекса мангана(II) (**10**) показују изотропски облик ESR спектра, док у случају комплекса бакра(II) (**3** и **7**) ови спектри показују аксијалну симетрију са $g_\parallel > g_\perp > g_e$, што указује на присуство ковалентног карактера везе. Резултати испитивања антибактеријске и антифунгалне активности за H_2L лиганд и испитиване комплексе одговарају активности средње јачине у поређењу са стандардним агенсима.

(Примљено 7. марта 2011, ревидирано 12. јуна 2012)

REFERENCES

1. V. P. Singh, A. Katiyar, S. Singh, *Biometals* **21** (2008) 491
2. V. P. Singh, A. Katiyar, S. Singh, *J. Coord. Chem.* **62** (2009) 1336
3. K. V. Sharma, V. Sharma, R. K. Dubey, U. N. Tripathi, *J. Coord. Chem.* **62** (2009) 493
4. K. M. Ibrahim, I. M. Gabr, G. M. Abu El-Reash, R. R. Zaky, *Monatsh. Chem.* **140** (2009) 625
5. Ş. G. Küçükgüzel, A. Mazi, F. Sahin, S. Öztürk, J. Stables, *Eur. J. Med. Chem.* **38** (2003) 1005
6. P. Melnyk, V. Leroux, C. Sergheraert, P. Grellier, *Bioorg. Med. Chem. Lett.* **16** (2006) 31
7. P. C. Lima, L. M. Lima, K. C. M. da Silva, P. H. O. Léda, A. L. P. de Miranda, C. A. M. Fraga, E. J. Barreiro, *Eur. J. Med. Chem.* **35** (2000) 187

8. A. C. Cunha, J. M. Figueiredo, J. L. M. Tributino, A. L. P. Miranda, H. C. Castro, R. B. Zingali, C. A. M. Fraga, M. C. B. V. de Souza, V. F. Ferreira, E. J. Barreiro, *Bioorg. Med. Chem.* **11** (2003) 2051
9. K. K. Bedia, O. Elçin, U. Seda, K. Fatma, S. Nathaly, R. Sevim, A. Dimoglo, *Eur. J. Med. Chem.* **41** (2006) 1253
10. N. Terzioglu, A. Gürsoy, *Eur. J. Med. Chem.* **38** (2003) 781
11. C. Loncle, J. M. Brunel, N. Vidal, M. Dherbomez, Y. Letourneux, *Eur. J. Med. Chem.* **39** (2004) 1067
12. S. H. Guzar, J. Qin-Hang, *Chem. Res. Chin. Univ.* **24** (2008) 143
13. Y. J. Jang, U. Lee, B. K. Koo, *Bull. Korean Chem. Soc.* **26** (2005) 925
14. P. Cheng, D. Liao, S. Yan, Z. Jiang, G. Wang, *Polyhedron* **14** (1995) 2355
15. S. Shit, J. Chakraborty, B. Samanta, A. M. Z. Slawin, V. Gramlich, S. Mitra, *Struct. Chem.* **20** (2010) 633
16. A. A. Recio Despaigne, J. G. da Silva, A. C. M. do Carmo, O. E. Piro, E. E. Castellano, H. Beraldo, *Inorg. Chim. Acta* **362** (2009) 2117
17. A. S. El-Tabl, R. M. El-Bahnasawy, A. E. Hamdy, *J. Chem. Res.* (2009) 659
18. J.-N. Liu, B.-W. Wu, B. Zhang, Y. Liu, *Turk. J. Chem.* **30** (2006) 41
19. G. Svehla, *Vogel's textbook of macro and semi micro quantitative inorganic analysis*, 5th ed., Longman, New York, 1979
20. L. Lewis, R. G. Wilkins, *Modern coordination chemistry*, Interscience, New York, 1960
21. E. O. Offiong, S. Martelli, *Farmaco* **49** (1994) 513
22. *Practical Medical Microbiology*, J. G. Collee, J. P. Duguid, A. G. Farser, B. D. Marmion, Eds., Churchill Livingstone, New York, 1989
23. M. R. Maurya, S. Khurana, C. Schulzke, D. Rehder, *Eur. J. Inorg. Chem.* (2001) 779
24. R. Gup, B. Kirkan, *Spectrochim. Acta, A* **62** (2005) 1188
25. G. C. Xu, L. Zhang, L. Liu, G. F. Liu, D. Z. Jia, *Polyhedron* **27** (2008) 12
26. B. Samanta, J. Chakraborty, S. Shit, S. R. Batten, P. Jensen, J. D. Masuda, S. Mitra, *Inorg. Chim. Acta* **360** (2007) 2471
27. H. Tezcan, E. Uzluk, *Dyes Pigm.***77** (2008) 626
28. B. Singh, P. Srivastava, *Transition Met. Chem.* **12** (1987) 475
29. Z. H. Abd El-Wahab, M. M. Mashaly, A. A. Salman, B. A. El-Shetary, A. A. Faheim, *Spectrochim. Acta, A* **60** (2004) 2861
30. K. Nakamto, *Infrared and Raman spectra of inorganic and coordination compounds*, 3rd ed., Wiley, New York, 1977, p. 244
31. E. Katsoulakou, V. Bekiari, C. P. Raptopoulou, A. Terzis, P. Lianos, E. M. Zoupa, S. P. Perlepes, *Spectrochim. Acta, A* **61** (2005) 1627
32. S. Chandra, L. K. Gupta, *Spectrochim. Acta, A* **61** (2005) 1181
33. B. Singh, A. K. Srivastav, P. Srivastava, *Transition Met. Chem.* **13** (1988) 463
34. L. K. Gupta, U. Bansal, S. Chandra, *Spectrochim. Acta, A* **66** (2007) 972
35. P. N. Remya, C. H. Suresh, M. L. P. Reddy, *Polyhedron* **26** (2007) 5016
36. B. N. B. Raj, M. R. P. Kurup, E. Suresh, *Spectrochim. Acta, A* **71** (2008) 1253
37. W. J. Geaey, *Coord. Chem. Rev.***7** (1971) 81
38. N. N. Greenwood, B. P. Straughan, A. E. Wilson, *J. Chem. Soc. A* (1968) 2209
39. N. M. Rageh, A. M. Abdel Mawgoud, H. M. Mostafa, *Chem. Papers* **53** (1999) 107
40. M. F. R. Fouda, M. M. Abd-Elzaher, M. M. E. Shakdofa, F. A. El Saied, M. I. Ayad, A. S. El Tabl, *J. Coord. Chem.* **61** (2008) 1983
41. R. Gup. E. Giziroglu, B. Kirkan, *Dyes Pigm.***73** (2007) 40

42. A. B. P. Lever, *Inorganic electronic spectroscopy*, Elsevier, Amsterdam, 1968
43. R. N. Jadeja, J. R. Shah, *Polyhedron* **26** (2007) 1677
44. A. M. B. Bastos, J. G. da Silva, P. I. Da. S. Maia, V. M. Deflon, A. A. Batista, A. V. M. Ferreira, L. M. Botion, E. Niquet, H. Beraldo, *Polyhedron* **27** (2008) 1787
45. B. Graham, L. Spiccia, B. W. Skelton, A. H. White, D. C. R. Hockless, *Inorg. Chim. Acta* **358** (2005) 3974
46. R. C. Khulbe, R. P. Singh Y. K. Bhoon, *Transition Met. Chem.* **8** (1983) 59
47. S.-X. Hui, Y.-X. Zeng, L. Cun, X.-R. Gen, *Transition Met. Chem.* **20** (1995) 191
48. K. R. Krishnapriya, M. Kandaswamy, *Polyhedron* **24** (2005) 113
49. K. Gudasi, R. V. Shenoy, R. S. Vadavi, S. A. Patil, M. Nethaji, *J. Mol. Struct.* **788** (2006) 22
50. R. Sharma, S. K. Agarwal, S. Rawat, M. Nagar, *Transition Met. Chem.* **31** (2006) 201
51. M. Tiliakos, P. Cordopatis, A. Terzis, C. P. Raptopoulou, S. P. Perlepes, E. M. Zoupa, *Polyhedron* **20** (2001) 2203
52. A. N. Al-Hakimi, A. S. El-Tabl, M. M. E. Shakdofa, *J. Chem. Res.* (2009) 770
53. J. B. Gandhi, N. D. Kulkarni, *Transition Met. Chem.* **26** (2001) 96
54. G. R. Hauson, T. A. Kabanos, A. D. Keramidas, D. Mentzafos, A. Terzis, *Inorg. Chem.* **31** (1992) 2587
55. D. Kevelson, S.-K. Lee, *J. Chem. Phys.* **41** (1964) 1896
56. F. A. Walker, R. L. Carlin, P. H. Rieger, *J. Chem. Phys.* **45** (1966) 4181
57. D. Kivelson, *J. Chem. Phys.* **33** (1960) 1094
58. Y. Dong, R. K. Narla, E. Sudbeck, F. M. Uckun, *J. Inorg. Biochem.* **78** (2000) 321
59. S. S. Dodward, R. S. Dhamnaskar, P. S. Prabhu, *Polyhedron* **8** (1989) 1748
60. N. Raman, Y. P. Raja, A. Kulandaisamy, *Proc. Indian Acad. Sci. (Chem. Sci.)* **113** (2001) 183
61. P. B. Sreeja, M. R. P. Kurup, *Spectrochim. Acta, A* **61** (2005) 331
62. K. B. Gudasi, R. S. Vadavi, R. V. Shenoy, S. A. Patil, M. Nethaji, *Transition Met. Chem.* **31** (2006) 374
63. A. S. El-Tabl, *Bull. Korean Chem. Soc.* **25** (2004) 1757
64. B. J. Hathaway, D. E. Billing, *Coord. Chem. Rev.* **5** (1970) 143
65. A. S. El-Tabl, *Transition Met. Chem.* **27** (2002) 166
66. A. S. El-Tabl, *Transition Met. Chem.* **23** (1998) 63
67. R. K. Ray, G. B. Kauffman, *Inorg. Chim. Acta* **174** (1990) 237
68. R. K. Ray, G. B. Kauffman, *Inorg. Chim. Acta* **174** (1990) 257
69. A. S. El-Tabl, F. A. El-Saied, A. N Al-Hakimi, *J. Coord. Chem.* **61** (2008) 2380
70. K. M. Ibrahim, I. M. Gabr, R. R. Zaky, *J. Coord. Chem.* **62** (2009) 1100
71. G. B. Bagihalli, S. A. Patil, *J. Coord. Chem.* **62** (2009) 1690
72. A. Kulkarni, P. G. Avaji, G. B. Baghialli, S. A. Patil, P. S. Badami, *J. Coord. Chem.* **62** (2009) 481
73. K. V. Sharma, V. Sharma, R. K. Dubey, U. N. Tripathi, *J. Coord. Chem.* **62** (2009) 506.

Journal of the Serbian Chemical Society
JSCS@tmf.bg.ac.rs • www.shd.org.rs/JSCS
J. Serb. Chem. Soc. *78* (1) S1–S8 (2013) *Supplementary material*

SUPPLEMENTARY MATERIAL TO

Metal complexes of *N′*-[2-hydroxy-5-(phenyldiazenyl)-benzylidene]isonicotinohydrazide. Synthesis, spectroscopic characterization and antimicrobial activity

ABDOU S. EL-TABL[1]*, MOHAMAD M. E. SHAKDOFA[2,3] and ADEL M. E. SHAKDOFA[1]

[1]*Department of Chemistry, Faculty of Science, El-Menoufia University, Shebin El-Kom, Egypt,* [2]*Inorganic Chemistry Department, National Research Center, P. O. Box 12622, Dokki, Cairo, Egypt and* [3]*Department of Chemistry, Faculty of Sciences and Arts, King Abdulaziz University, Khulais, Saudi Arabia*

J. Serb. Chem. Soc. 78 (1) (2013) 39–55

PHYSICAL, ANALYTICAL AND SPECTRAL DATA FOR THE LIGAND AND ITS COMPLEXES

N′-*[2-Hydroxy-5-(phenyldiazenyl)benzylidene]isonicotinohydrazide (*H_2L*)* (***1***). Yellow color; yield: 95 %; Anal. Calcd. for $C_{19}H_{15}N_5O_2$ (FW: 345.35): C, 66.08; H, 4.38; N, 20.28 %. Found: C, 65.85; H, 4.37; N, 20.22 %. IR (KBr, cm^{-1}): 3300–3550, 2540–3000 (br) (H_2O/O–H), 3174 (N–H), 1658 (C=O), 1605 (C=N), 1468 (N=N), 1289 (C–O_{ph}), 1004 (N–N); ^{1}H-NMR (270 MHz, DMSO-d_6, δ/ ppm): 12.41 (1H, *s*, OH), 11.65 (1H, *s*, NH), 8.76 (1H, *s*, H–C=N), 7.14–8.31 (12H, *m*, aromatic); MS (*m*/*z*): 345 (M^+); UV–Vis (DMSO, 10^{-3} M) (λ / nm): 270, 320, 350, 375, 420, 455.

[VO(H_2L*)(*SO_4*)(*H_2O*)]* (***2***). Light brown color; yield: 75 %; Anal. Calcd. for $C_{19}H_{17}N_5O_8SV$ (FW: 526.37): C, 43.35; H, 3.26; N, 13.30; V, 12.72 %. Found: C, 43.29; H, 3.67; N, 13.51; V, 12.89 %. 3426 (br) (H_2O/O–H), 3239 (N–H), 1607 (C=O), 1553 (C=N), 1470 (N=N), 1290 (C–O_{ph}), 1041 (N–N), 575 (V–O), 509 (V–N); UV–Vis (DMSO, 10^{-3} M) (λ / nm): 290, 345, 360, 395, 425, 450, 520, 575, 700; Magnetic moment (μ_{eff} / μ_B): 1.73; Molar conductivity (Ω^{-1} cm^2 mol^{-1}): 22.5.

[Cu(HL)$_2$*]·5*H_2O (***3***). Yellowish green color; yield: 55 %; Anal. Calcd. for $C_{38}H_{38}CuN_{10}O_9$ (FW: 842.33): C, 54.18; H, 4.55; N, 16.63; Cu, 7.54 %. Found: C, 54.00; H, 4.87; N, 16.32; Cu, 7.42 %; IR (KBr, cm^{-1}): 3391(br) (H_2O/O–H), 1601 (C=N), 1507 (N=C–O), 1464 (N=N), 1285 (C–O_{ph}), 1208 (C–O_{amide}),

* Corresponding author. E-mail: asaeltabl@yahoo.com
doi: 10.2298/JSC110307062E

1026 (N–N), 593 (Cu–O), 538 (Cu←O), 466 (Cu←N); UV–Vis (DMSO, 10^{-3} M) (λ / nm): 265, 330, 350, 380, 420, 450, 630; magnetic moment (μ_{eff} / μ_B): 1.79; molar conductivity (Ω^{-1} cm^2 mol^{-1}): 6.9.

[Cu(H$_2$L)$_2$Cl$_2$]·2H$_2$O (***4***). Olive color; yield: 70 %; Anal. Calcd. for $C_{38}H_{34}Cl_2CuN_{10}O_6$ (FW: 861.19): C, 53.00; H, 3.98; N, 16.26; Cl, 8.23, Cu, 7.38 %. Found: C, 52.56; H, 4.01; N, 16.88; Cl, 7.98; Cu, 7.04 %; 3426 (br) (H$_2$O/O–H), 3198 (N–H), 1611 (C=O), 1570 (C=N), 1476 (N=N), 1278 (C–O$_{ph}$), 1047 (N–N), 551 (Cu–O), 464 (Cu–N); UV–Vis (DMSO, 10^{-3} M) (λ / nm): 280, 345, 365, 390, 435, 470, 675; Magnetic moment (μ_{eff} / μ_B): 1.68; Molar conductivity (Ω^{-1} cm^2 mol^{-1}): 15.4.

[Cu(H$_2$L)$_2$(NO$_3$)$_2$]·H$_2$O (***5***). Olive color; yield: 65 %; Anal. Calcd. for $C_{38}H_{32}CuN_{12}O_{11}$ (FW: 896.28): C, 50.92; H, 3.60; N, 18.75; Cu, 7.09 %. Found: C, 50.81; H, 3.78; N, 18.46; Cu, 7.10 %; IR (KBr, cm^{-1}): 3428 (br) (H$_2$O/O–H), 3187 (N–H), 1606 (C=O), 1577 (C=N), 1465 (N=N), 1290 (C–O$_{ph}$), 1031 (N–N), 534 (Cu–O), 462 (Cu–N); UV-Vis (DMSO, 10^{-3} M) (λ / nm): 265, 330, 350, 390, 405, 440, 650; magnetic moment (μ_{eff} / μ_B): 1.75; molar conductivity (Ω^{-1} cm^2 mol^{-1}): 13.1.

[Cu(H$_2$L)$_2$(SO$_4$)(H$_2$O)]·2H$_2$O (***6***). Olive color; yield: 63 %; Anal. Calcd. for $C_{38}H_{36}CuN_{10}O_{11}S$ (FW: 904.36): C, 50.47; H, 4.01; N, 15.49; Cu, 7.03 %. Found: C, 50.43; H, 4.04; N, 15.11; Cu, 6.89 %; IR (KBr, cm^{-1}): 3425 (br) (H$_2$O/O–H), 3174 (N–H), 1606 (C=O), 1546 (C=N), 1468 (N=N), 1292 (C–O$_{ph}$), 1031 (N–N), 533 (Cu–O), 457 (Cu–N); UV–Vis (DMSO, 10^{-3} M) (λ / nm): 275, 325, 340, 355, 375, 420, 470, 660; magnetic moment (μ_{eff} / μ_B): 1.77; molar conductivity (Ω^{-1} cm^2 mol^{-1}): 19.9.

[Cu(HL)(OAc)(H$_2$O)]·1/2H$_2$O (***7***). Green color; yield: 60 %; Anal. Calcd. for $C_{21}H_{20}CuN_5O_{5.5}$ (FW: 493.96): C, 51.06; H, 4.08; N, 14.18; Cu, 12.86 %. Found: C, 51.08; H, 4.31; N, 14.01; Cu, 12.65 %. IR (KBr, cm^{-1}): 3367 (br) (H$_2$O/O–H), 1602 (C=N), 1507 (N=C–O), 1463 (N=N), 1281 (C–O$_{ph}$), 1218 (C–O$_{amide}$), 1026 (N–N), 592 (Cu–O), 538 (Cu←O), 467 (Cu←N); UV–Vis (DMSO, 10^{-3} M) (λ / nm): 240, 266, 326, 344, 3598, 475, 650 and 740; magnetic moment (μ_{eff} / μ_B): 1.88; molar conductivity (Ω^{-1} cm^2 mol^{-1}): 12.4.

[Ni(HL)]·5H$_2$O (***8***). Beige color; yield: 61 %; Anal. Calcd. for $C_{38}H_{38}N_{10}NiO_9$ (FW: 837.49): C, 54.50; H, 4.57; N, 16.73; Ni, 7.01 %. Found: C, 54.42; H, 5.01; N, 16.58; Ni, 6.91 %; IR (KBr, cm^{-1}): 3362(br) (H$_2$O/O–H), 1600 (C=N), 1525 (N=C–O), 1465 (N=N), 1299 (C–O$_{ph}$), 1207 (C–O$_{amide}$), 1059 (N–N), 573 (Ni–O), 506 (Ni←O), 476 (Ni←N); UV-Vis (DMSO, 10^{-3} M) (λ / nm): 265, 350, 390, 405, 430, 465, 580, 660, 850; magnetic moment (μ_{eff} / μ_B): 3.01; molar conductivity (Ω^{-1} cm^2 mol^{-1}): 5.3.

[Co(HL)(OAc)(H$_2$O)]·1/2H$_2$O (***9***). Reddish brown color; yield: 58 %, Anal. Calcd. for $C_{21}H_{20}CoN_5O_{5.5}$ (FW: 489.35): C, 51.54; H, 4.12; N, 14.31; Co, 12.04 %. Found: C, 51.71; H, 4.03; N, 14.18; Co, 12.59 %; IR (KBr, cm^{-1}): 3383

(br) (H_2O/O–H), 1603 (C=N), 1512 (N=C–O), 1464 (N=N), 1293 (C–O_{ph}), 1215 (C–O_{amide}), 1026 (N–N), 595 (Co–O), 563 (Co←O), 480 (Co←N); UV–Vis (DMSO, 10^{-3} M) (λ / nm): 270, 330, 360, 395, 435, 450, 505, 590, 650; magnetic moment (μ_{eff} / μ_B): 4.42; molar conductivity (Ω^{-1} cm^2 mol^{-1}): 13.3.

[Mn(HL)$_2$]·H$_2$O ***(10)***. Dark yellow color; yield: 55 %, Anal. Calcd. for $C_{38}H_{30}MnN_{10}O_5$ (FW: 761.66): C, 59.92; H, 3.97; N, 18.39; Mn, 7.21 %. Found: C, 60.08; H, 4.04; N, 18.27; Mn, 7.16 %; IR (KBr, cm^{-1}): 3446 (br) (H_2O/O–H), 1603 (C=N), 1546 (N=C–O), 1467 (N=N), 1312 (C–O_{ph}), 1258 (C–O_{amide}), 1019 (N–N), 594 (Mn–O), 561 (Mn←O), 473 (Mn←N); UV–Vis (DMSO, 10^{-3} M) (λ / nm): 280, 325, 350, 380, 405, 450, 465, 540, 600, 650; magnetic moment (μ_{eff} / μ_B): 4.87; molar conductivity (Ω^{-1} cm^2 mol^{-1}): 6.8.

[Fe(HL)$_2$Cl]·4H$_2$O ***(11)***. Dark brown color; yield: 66 %; Anal. Calcd. for $C_{38}H_{36}ClFeN_{10}O_8$ (FW: 852.05): C, 53.57; H, 4.26; N, 16.44; Cl, 4.16, Fe, 6.55 %. Found: C, 53.44; H, 4.20; N, 16.45; Cl, 3.99; Fe, 6.30 %; IR (KBr, cm^{-1}): 3385 (br) (H_2O/O–H), 3211 (N–H), 1607 (C=O), 1538 (C=N), 1458 (N=N), 1244 (C–O_{ph}), 1020 (N–N), 610 (Fe–O), 566 (Fe←O), 502 (Fe←N); UV–Vis (DMSO, 10^{-3} M) (λ / nm): 280, 330, 350, 385, 415, 460, 580, 640; magnetic moment 5.34; molar conductivity: 80.5 Ω^{-1} cm^2 mol^{-1}.

[Ru(L)Cl(H$_2$O)$_2$]·H$_2$O ***(12)***. Dark brown color; yield: 72 %; Anal. Calcd. for $C_{19}H_{19}ClN_5O_5Ru$ (FW: 533.91): C, 42.74; H, 3.59; N, 13.12; Cl, 6.64, Ru, 18.93 %. Found: C, 42.84; H, 3.96; N, 13.28; Cl, 6.54; Ru, 18.72 %; IR (KBr, cm^{-1}): 3433 (br) (H_2O/O–H), 1602 (C=N), 1489 (N=N), 1272 (C–O_{ph}), 1019 (N–N), 593 (Ru–O), 525 (Ru←O), 482 (Ru←N); UV–Vis (DMSO, 10^{-3} M) (λ / nm): 260, 320, 345, 375, 430, 460, 560, 650; magnetic moment (μ_{eff} / μ_B): 65; molar conductivity: 21.5 Ω^{-1} cm^2 mol^{-1}.

[Zn(L)(H$_2$O)] ***(13)***. Dark yellow color; yield: 63 %; Anal. Calcd. for $C_{19}H_{15}N_5O_3Zn$ (FW: 426.73): C, 53.48; H, 3.54; N, 16.41; M, 15.32 %. Found: C, 53.90; H, 3.70; N, 16.42; M, 15.20 %; IR (KBr, cm^{-1}): 3447 (br) (H_2O/O–H), 1606 (C=N), 1515 (N=C–O), 1479 (N=N), 1228 (C–O_{ph}), 1207 (C–O_{amide}), 1035 (N–N), 586 (Zn–O), 510 (Zn←O), 469 (Zn←N); ^{1}H-NMR (270 MHz, DMSO-d_6, δ / ppm): 8.76 (1H, *s*, H–C=N), 6.70–7.96 (12H, *m*, aromatic); UV–Vis (DMSO, 10^{-3} M) (λ / nm): 280, 320, 360, 400, 430, 475; magnetic moment (μ_{eff} / / μ_B): diamagnetic; molar conductivity (Ω^{-1} cm^2 mol^{-1}): 6.4.

[Cd(H$_2$L)$_2$(OAc)$_2$]·7H$_2$O ***(14)***. Deep yellow color; yield: 51 %; Anal. Calcd. for $C_{42}H_{50}CdN_{10}O_{15}$ (FW: 1047.32): C, 48.17; H, 4.81; N, 13.37; Cd, 10.73 %. Found: C, 48.29; H, 4.65; N, 13.55; Cd, 11.21 %; IR (KBr, cm^{-1}): 3369 (br) (H_2O/O–H), 3176 (N–H), 1607 (C=O), 1546 (C=N), 1464 (N=N), 1292 (C–O_{ph}), 1020 (N–N), 592 (Cd–O), 533 (Cd←O), 492 (Cd←N); UV–Vis (DMSO, 10^{-3} M) (λ / nm): 280, 330, 365, 405, 425, 465; magnetic moment (μ_{eff} / μ_B): diamagnetic; molar conductivity (Ω^{-1} cm^2 mol^{-1}): 8.5.

[(UO$_2$)(L)(H$_2$O)$_2$]·H$_2$O (***15***). Orange color; yield: 77 %; Anal. Calcd. for $C_{19}H_{19}N_5O_7U$ (FW: 667.41): C, 34.19; H, 2,87; N10.49; UO_2, 40.48 %. Found: C, 34.77; H, 3.39; N, 8.54; U, 37.05 %; IR (KBr, cm^{-1}): 3401(br) (H_2O/O–H), 1603 (C=N), 1522 (C=N–O), 1472 (N=N), 1257 (C–O_{ph}), 1017 (N–N), 590 (U–O), 549 (U←O), 505 (U←N); ^{1}H-NMR (270 MHz, DMSO-d_6, δ / ppm): 7.17–8.25 (12H, *m*, aromatic), 9.01 (1H, *s*, H–C=N); UV–Vis (DMSO, 10^{-3} M) (λ / nm): 270, 325, 360, 395, 440, 480, 530; magnetic moments (μ_{eff} / μ_B): diamagnetic; molar conductivity (Ω^{-1} cm^2 mol^{-1}): 9.5.

[Hg(HL)$_2$]·4H$_2$O (***16***). Reddish brown color; yield: 72 %; Anal. Calcd. for $C_{38}H_{36}HgN_{10}O_8$ (FW: 962.27): C, 47.48; H, 3.77; N, 14.57; Hg, 20.87 %. Found: C, 47.47; H, 3.69; N, 14.68; Hg, 20.25 %; IR (KBr, cm^{-1}): 3432 (br) (H_2O/O–H), 3207 (N–H), 1615 (C=O), 1549 (C=N), 1455 (N=N), 1227 (C–O_{ph}), 1039 (N–N), 601 (Hg–O), 536 (Hg←O), 496 (Hg←N); UV–Vis (DMSO, 10^{-3} M) (λ / nm): 270, 330, 355, 380, 420, 460; magnetic moment (μ_{eff} / μ_B): diamagnetic; molar conductivity (Ω^{-1} cm^2 mol^{-1}): 10.5.

SOME SPECTRA OF THE LIGAND AND SELECTED COMPLEXES

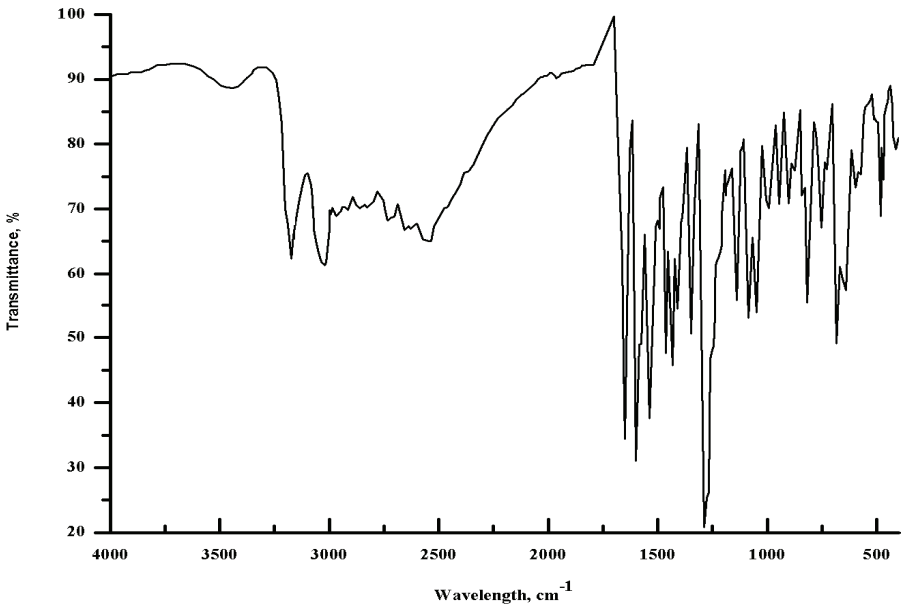

Fig. S-1. The IR spectrum of the ligand [H_2L] (**1**).

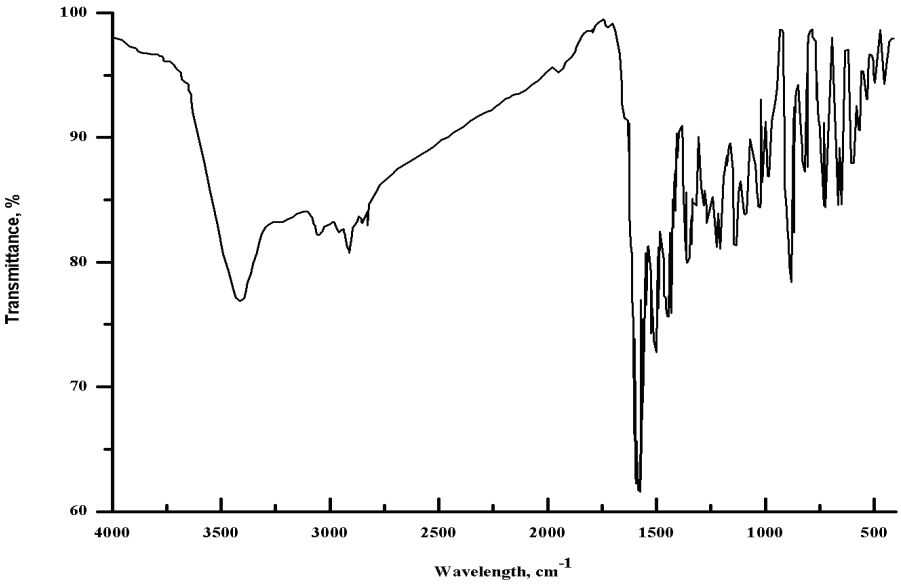

Fig. S-2. The IR spectrum of the complex $[Cu(H_2L)_2(SO_4)(H_2O)]\cdot 2H_2O$ (**6**).

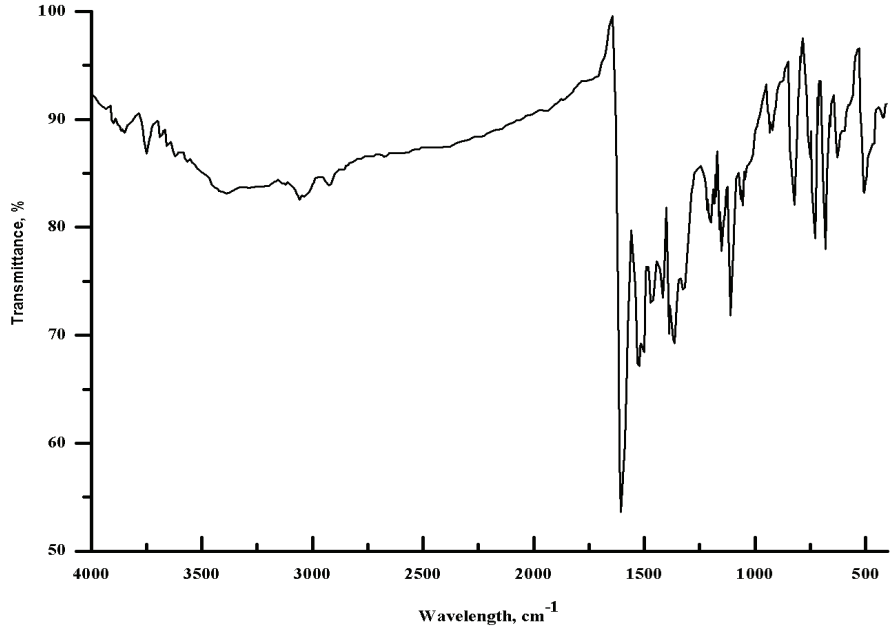

Fig. S-3.The IR spectrum of the complex $[Ni(HL)_2]\cdot 5H_2O$ (**8**).

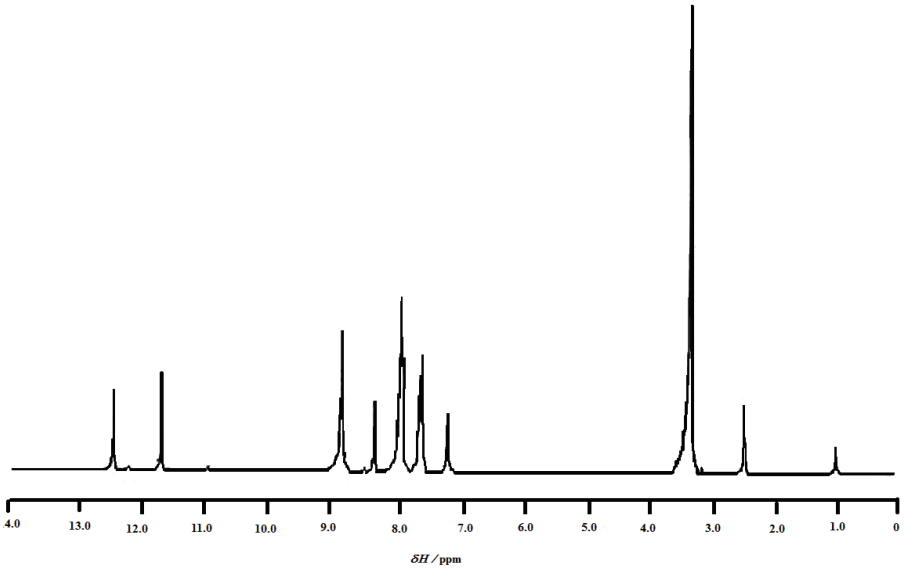

Fig. S-4. The ^{1}H-NMR spectrum of the ligand (H_2L) (**1**).

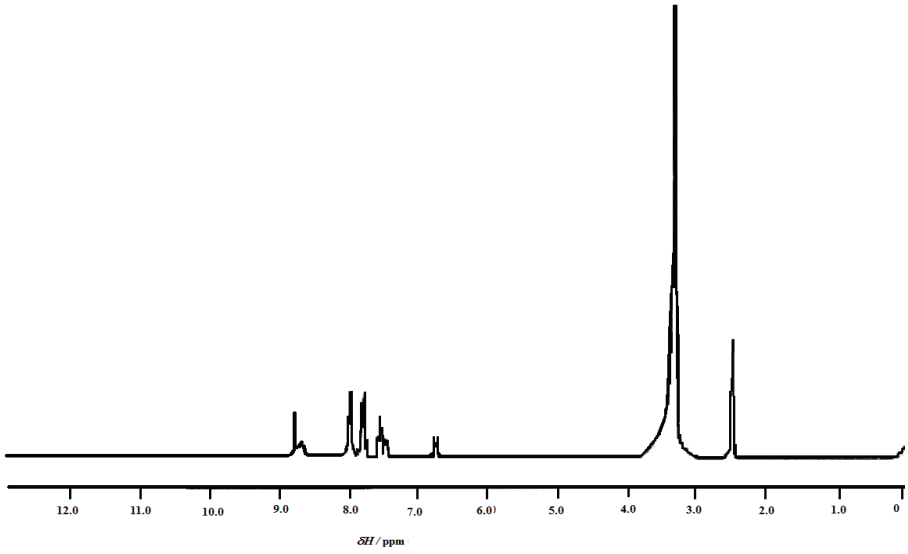

Fig. S-5. The ^{1}H-NMR spectrum of the complex [Zn(L)(H_2O)] (**13**).

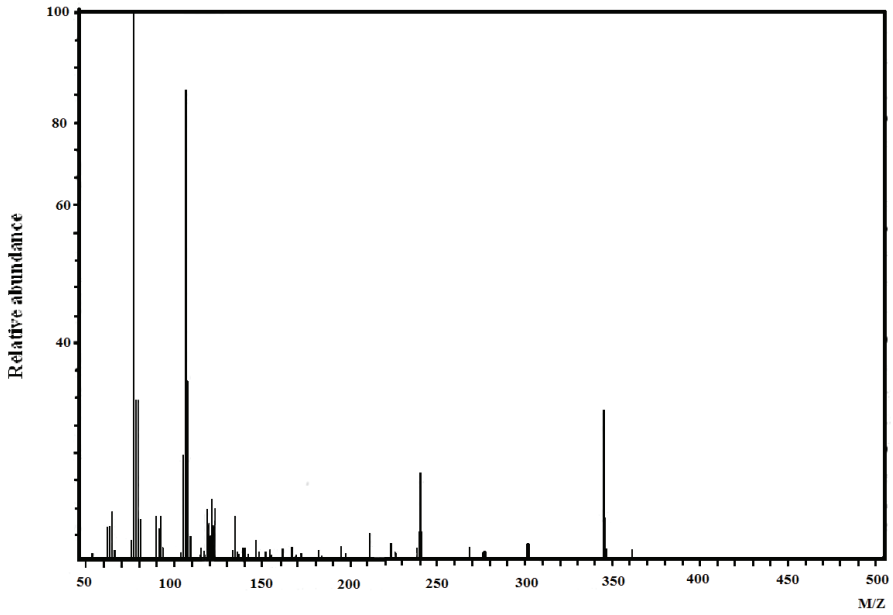

Fig. S-6. The mass spectrum of the ligand (H_2L) (**1**).

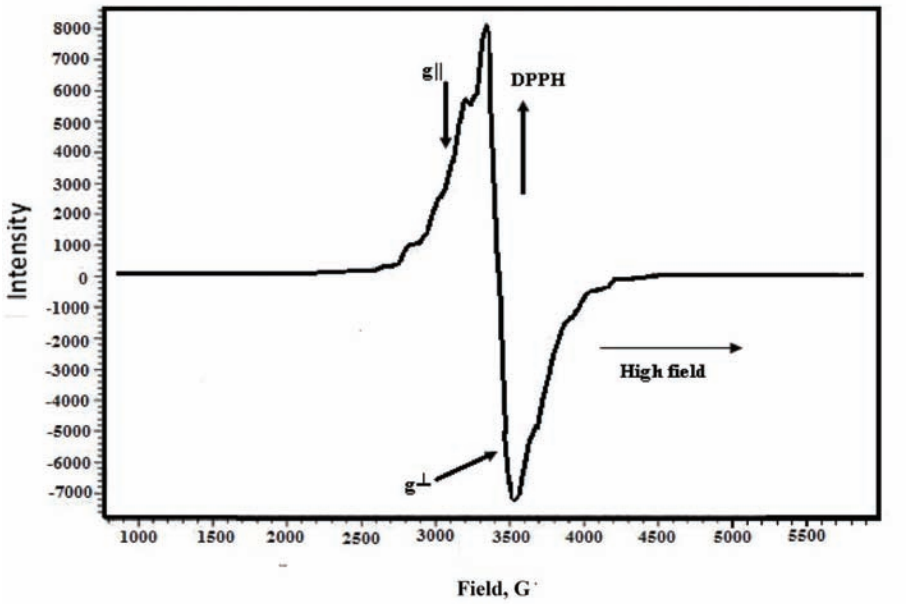

Fig. S-7. The ESR spectrum of the vanadyl(II) complex **2**.

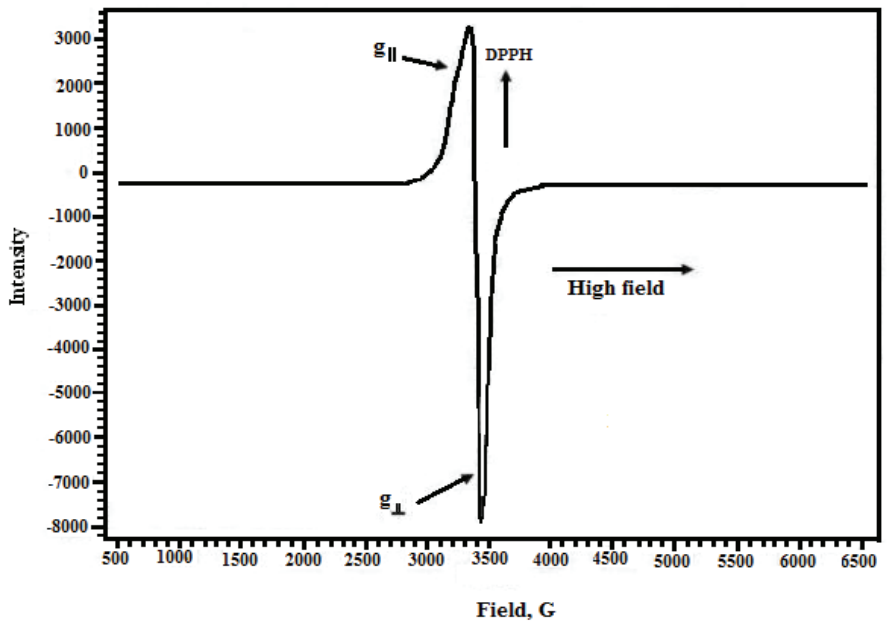

Fig. S-8. The ESR spectrum of copper(II) complex **3**.

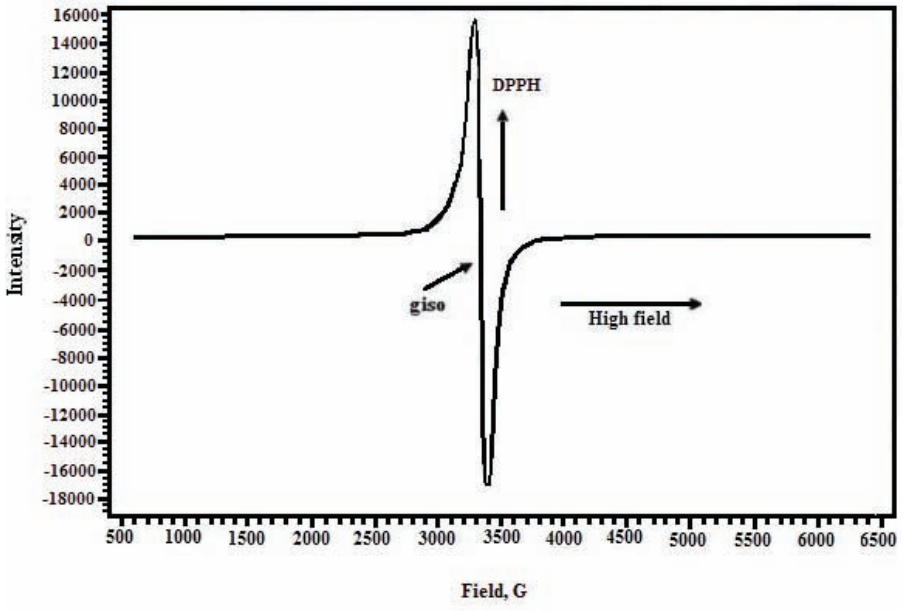

Fig. S-9. The ESR spectrum of copper(II) complex **6**.

Journal of the Serbian Chemical Society
JSCS-info@shd.org.rs • www.shd.org.rs/JSCS

J. Serb. Chem. Soc. 78 (1) 57–63 (2013)
JSCS–4395

UDC 547.313.2+547.466.4+547.073.1+546.228.5:548.7
Short communication

SHORT COMMUNICATION

Stereospecific ligands and their complexes. Part XIV. Crystal structure of the *O,O′*-dipropyl ester of *N,N′*-1,2-ethanediylbis--L-leucine, dihydrochloride

JELENA M. VUJIĆ[1], SANTIAGO GARCIA-GRANDA[2], LAURA MENENDEZ-TABOADA[2], SLAĐANA B. NOVAKOVIĆ[3] and SREĆKO R. TRIFUNOVIĆ[4*#]

[1]*Faculty of Agronomy, University of Kragujevac, Cara Dušana 34, 32000 Čačak, Serbia,* [2]*University of Oviedo, Faculty of Chemistry, Oviedo, Spain,* [3]*Vinča Institute of Nuclear Sciences, Condensed Matter Physics Laboratory, University of Belgrade, P. O. Box 522, 11001 Belgrade, Serbia and* [4]*Department of Chemistry, Faculty of Science, University of Kragujevac, Radoja Domanovića 12, 34000 Kragujevac, Serbia*

(Received 8 February, revised 24 April 2012)

Abstract: The bidentate *N,N′*-ligand precursor, the *O,O′*-dipropyl ester of *N,N′*--1,2-ethanediylbis-L-leucine, dihydrochloride, [(*S,S*)-H_4eddl]Cl_2, was prepared and its crystal structure is given herein. It crystallizes in a $P4_2$ space group of a tetragonal crystal system with a = 16.5620 (2) Å, b = 16.5620 (2) Å, c = 5.2240 (1) Å and Z = 2.

Keywords: crystal structure; tetragonal crystal system; *O,O′*-dipropyl ester of *N,N′*-1,2-ethanediylbis-L-leucine, dihydrochloride.

INTRODUCTION

R_2edda-type esters (edda = the ion of ethylenediamine-*N,N′*-diacetic acid) are of interest as ligands for a variety of opportunities for coordination of metal ions. Recently, the synthesis and characterization of platinum(II) and platinum(IV) complexes with *N,N′*-bidentate R_2eddp (R_2eddp = *O,O′*-dialkyl ethylenediamine-*N,N′*-dipropionate) and halide ligands were reported.[1–6] The work was extended by synthesizing chiral branched-chain esters, *(S,S)*-R_2eddp, and the corresponding platinum(II/IV) complexes.[7] Furthermore, most of the prepared ligands were used for the synthesis of the corresponding palladium(II) complexes.[8–10] Some of complexes, especially platinum(II) and platinum(IV) with *N,N*-bidentates, have demonstrated significant antitumoral activity.[2–7]

* Corresponding author. E-mail: srecko@kg.ac.rs
# Serbian Chemical Society member.
doi: 10.2298/JSC120208041V

Although a large number of R_2edda-type esters have been synthesized up to now, it was only possible to obtain single crystals suitable for X-ray analysis in the case of *O*,*O*′-diisopropyl ester of *N*,*N*′-1,2-ethanediylbis-L-alanine.[7]

The preparation and spectral characterization of the *O*,*O*′-dipropyl ester of *N*,*N*′-1,2-ethanediylbis-L-leucine, dihydrochloride was published earlier.[8] This paper reports the single crystal X-ray structure determination of *O*,*O*′-dipropyl ester of *N*,*N*′-1,2-ethanediylbis-L-leucine, dihydrochloride, [(*S*,*S*)-H_2Pr_2eddl]Cl_2.

EXPERIMENTAL

Chemistry

All reagents were of purity grade. *N*,*N*′-1,2-Ethanediylbis-L-leucine, dihydrochloride, [(*S*,*S*)-H_4eddl]Cl_2, was prepared as previously reported.[11]

Synthesis of O,O'-*dipropyl ester of* N,N′-*1,2-ethanediylbis-L-leucine, dihydrochloride, [(*S,S*)-H_2Pr_2eddl]Cl_2.

The ester was prepared using a previously described esterification reaction.[8] The ester was recrystallized from the warm 1-propanol and after cooling to room temperature and standing for several days, single crystals suitable for X-ray measurements were obtained.

X-Ray crystal structure determination

The diffraction data from a selected single crystal of [(*S*,*S*)-H_2Pr_2eddl]Cl_2 were collected at room temperature on an Oxford Diffraction Xcalibur Gemini S diffractometer equipped with CuKα radiation (λ = 1.54184 Å). The data were processed with CrysAlis software[12] and corrected for absorption by an analytical numeric method.[13] The crystal structure was solved by direct methods using Sir2002[14] and refined using SHELXL.[15] The refinement of the crystal structure revealed high isotropic displacement parameters for the carbon atoms of the propyl ester group, indicating severe disorder of this fragment. All attempts to model the disorder were unsuccessful and the temperature factors of the propyl ester C atoms were refined as isotropic. All H atoms were placed at the geometrically calculated positions with the D–H distances fixed at 0.98, 0.97 and 0.96 Å from C(sp^3) of methine, methylene and methyl, respectively, and at 0.90 Å from the N atom. The corresponding isotropic displacement parameters of the hydrogen atoms were equal to $1.2U_{eq}$ and $1.5U_{eq}$ of the parent C and N atoms. Geometrical calculations were performed with PARST97[16] and molecular graphics with ORTEP[17] and Mercury.[18] Details of the X-ray structural analysis are given in Table I.

TABLE I. Crystal data and structure refinement for [(*S*,*S*)-H_2Pr_2eddl]Cl_2

Empirical formula	$C_{20}Cl_2H_{42}O_4N_2$
Formula weight	445.47
Wavelength, Å	1.54184
Crystal system	Tetragonal
Space group	$P4_2$
Unit cell dimensions	
$a = b$ /Å	16.562(2)
c / Å	5.224(1)
Z	2
μ / mm^{-1}	2.215
V / $Å^3$	1432.9(3)

TABLE I. Continued

F(000)	484
D_{calc} / g cm^{-3}	1.032
Temperature, K	293
Crystal size, mm^3	0.07×0.02×0.01
Reflections collected	8570
Independent reflections	2869
Absolute structure parameter	0.05(6)
Goodness-of-fit on F^2	0.814
R_{int}	0.0663
R_1, wR_2 [$I > 2\sigma(I)$]	0.0769, 0.1911

RESULTS AND DISCUSSION

The title compound (Fig. 1) crystallizes in the chiral space group $P4_2$ with one-half of the molecule representing the asymmetric unit. The molecular halves are related by a twofold axis that passes through the mid-point of the central C10−C10^i bond ($i = -x + 1, -y, z$). The charge of the protonated ester molecule is balanced by chloride anions. Selected geometrical parameters are given in Table II. According to the values of the torsion angles C7−C6−C5−N1, C6−C5−N1−C10, C5−N1−C10−C10^i and N1−C10−C10^i−N1^i, which range from –167.2(9) to −178.8(8)°, the conformation of the aliphatic chain can be described as fully extended. The atoms of the C5/C6/C7/N1/C10 fragment are co-planar within 0.037(6) Å. A similar extended conformation of the chain and the co-planarity of the constituent atoms were observed in previously reported R_2edda-type esters.[7,9,10] In the present compound, the dihedral angle between the C5/C6/C7/ /N1/C10 best planes from the two molecular halves is equal to 32.6(5)°, indicating a slight mutual twist through the molecular center. Although severe dis-

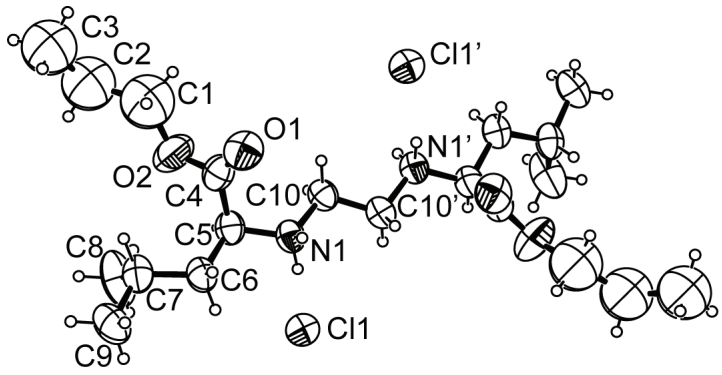

Fig. 1. Molecular structure of [(*S*,*S*)-H_2Pr_2eddl]Cl_2 with the atom labeling scheme. The displacement ellipsoids are plotted at the 40 % probability level. The twofold axis passes through the middle of C10−C10′ bond.

order prevents the clear localization of the C atoms of the propyl ester group, one can observe that the planar ester fragment C5/C4/O1/O2 (rms deviation of fitted atoms is 0.01) takes a significant turn with respect to the C5/C6/C7/N1/C10 plane. The dihedral angle formed between the corresponding best planes is equal to 74.1(3)°.

TABLE II. Selected bond lengths and angles

Bond lengths, Å		Bond angles, °	
C4−O1	1.479(18)	C5−C6−C7	113.5(6)
C4−O2	1.324(10)	C4−C5−N1	107.0(6)
C5−N1	1.491(8)	C5−N1−C10	115.8(5)
C5−C6	1.541(9)	O1−C4−O2	125.7(9)
C6−C7	1.531(9)	C5−C4−O1	127.4(8)

The molecular conformation is stabilized by two rather weak and bent intramolecular hydrogen bonds formed between the diamine and isopropyl C−H groups as donors and the oxygens of the ester group as acceptors (Table III). The crystal packing is, as expected, dominated by the hydrogen bonds formed between the charged components, the protonated amino nitrogen and the Cl anion. Both available N−H fragments of the amino group are utilized in the hydrogen bonding. These two rather strong N−H···Cl interactions (Table III) connect the molecules into a ribbon. In addition to the N−H···Cl hydrogen bonds, the molecules are interconnected by C5−H···O1 interactions (Fig. 2a). Although regarded as a secondary interaction, the C5−H···O1 displays a favorable directionality (Table III). Owing to the twofold symmetry, the molecules generate an identical set of interactions running in the opposite direction and reinforcing the connection between them. In general, two molecules inside the ribbon are connected with: four N−H···Cl interactions forming a motif described by Etter's graphset notation[19] as $R^4_2(14)$ and two C−H···O interactions forming a larger ring-like motif described as $R^2_2(18)$ (Fig. 2a). The interactions link the parallel molecules in the *c* direction; however taking into account the molecule length and its extended conformation, one can observe that the formed molecular ribbon expands through the entire *ac* plane. The described N−H···Cl hydrogen bonds, which engage the most polar parts of the molecules, are the main non-covalent interactions in this crystal structure. Similar contacts, leading to a similar molecular arrangement, were also observed in the crystal packing of two previously reported R_2edda·2HCl esters.[7,9] In the present crystal structure, the ribbons related by a fourfold axis direct their propyl ester fragments each to another, maximizing the nonbonding C−H contacts. As a result, the formation of a three-dimensional porous structure, with the parallel non-polar channels extended in the *c* direction, can be observed (Fig. 2b).

TABLE III. Hydrogen bonding geometry (Å and °). Symmetry codes: *i*) *x*, *y*, *z*; *ii*) *x*, *y*, *z*+1

Bond	D−H	D···A	H···A	D−H···A
C7−H7···O2^{i}	0.98	3.111(11)	2.57	114
C10−H10a···O1^{i}	0.97	3.119(10)	2.58	115
N1−H1a···Cl1^{i}	0.90	3.133(8)	2.25	166
N1−H1b···Cl1^{ii}	0.90	3.106(8)	2.25	158
C5−H5···O1^{ii}	0.98	3.303(10)	2.35	164

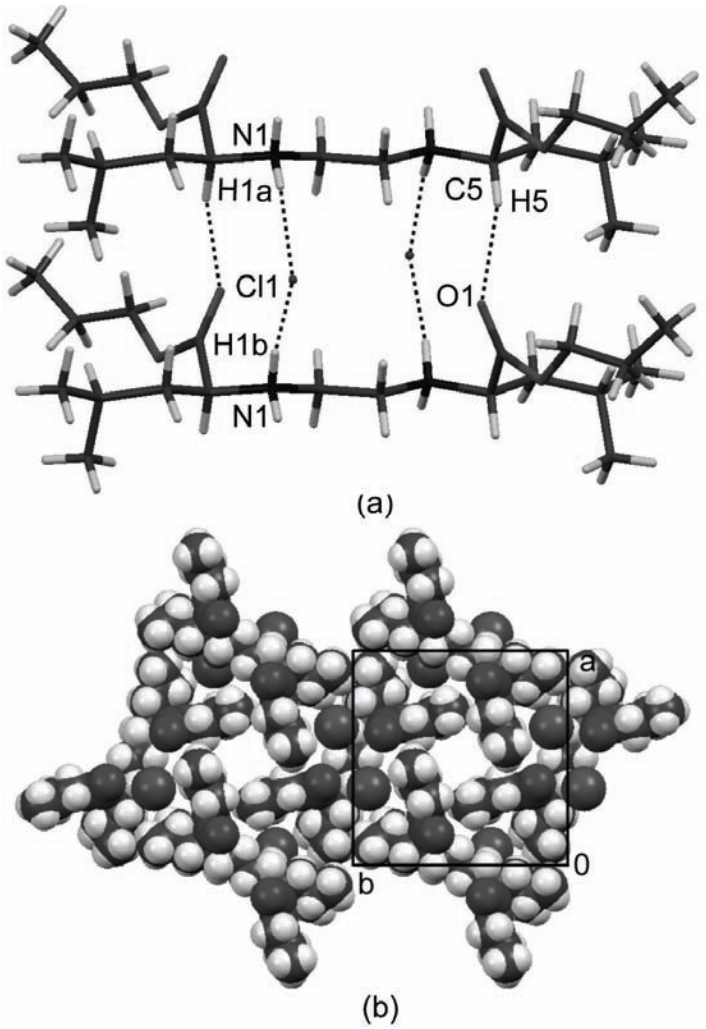

Fig. 2. a) Intermolecular N−H···Cl and C−H···O hydrogen bonding relates the molecules into ribbons; b) segment of the three-dimensional porous crystal structure.

CONCLUSIONS

O,*O'*-Dipropyl ester of *N*,*N*′-1,2-ethanediylbis-L-leucine was crystallized in the form of the dihydrochloride in a $P4_2$ space group of a tetragonal crystal system. The crystal form and the crystal packing are determined by strong intermolecular N1−H1a···Cl1, N1−H1b···Cl1 and C5−H5···O1 hydrogen bonds.

Supplementary data. CCDC 863095 contains the supplementary crystallographic data to this paper. These data can be obtained free of charge *via* www.ccdc.cam.ac.uk/conts/retrieving.html (or from the Cambridge Crystallographic Data Centre, 12, Union Road, Cambridge CB21EZ, UK; fax: +44 1223 336033).

Acknowledgement. The authors are grateful for the financial support to the Ministry of Education, Science and Technological Development of the Republic of Serbia (Project No. 172016).

ИЗВОД

СТЕРЕОСПЕЦИФИЧНИ ЛИГАНДИ И ЊИХОВИ КОМПЛЕКСИ. ДЕО XIV. КРИСТАЛНА СТРУКТУРА *O*,*O'*-ДИПРОПИЛ ЕСТРА *N*,*N'*-1,2-ЕТАНДИИЛБИС-L-ЛЕУЦИН--ДИХИДРОХЛОРИДА

ЈЕЛЕНА М. ВУЈИЋ[1], SANTIAGO GARCIA-GRANDA[2], LAURA MENÉNDEZ-TABOADA[2], СЛАЂАНА Б. НОВАКОВИЋ[3] И СРЕЋКО Р. ТРИФУНОВИЋ[4]

[1]Аїрономски факулшеш, Универзишеш у Країујевцу, Цара Душана 34, 32000 Чачак, [2]University of Oviedo, Faculty of Chemistry, Oviedo, Spain, [3]Инсшишуш за нуклеарне науке „Винча“, Лаборашорија за физику кондензоване маше рије,Универзишеш у Беоїраду, п. пр. 522, 11001 Беоїрад и [4]Инсшишуш за хемију, Природно–маше маши чки факулшеш, Универзишеш у Країујевцу, Радоја Домановића 12, 34000 Країујевац

Синтетисан је бидентатни *N*,*N'* лиганд прекурсор, *O*,*O'*-дипропил естар *N*,*N'*-1,2-етандиилбис-l-леуцин-дихидрохлорида, и испитивана је његова кристална структура. Наведени лиганд кристалише у просторној групи $P4_2$ тетрагоналног кристалног система са димензијама јединичне ћелије $a = 16.5620\ (2)$ Å, $b = 16.5620\ (2)$ Å, $c = 5.2240\ (1)$ Å и $Z = 2$.

(Примљено 8. фебруара, ревидирано 24. априла 2012)

REFERENCES

1. T. J. Sabo, G. N. Kaluđerović, S. R. Grgurić-Šipka, F. W. Heinemann, S. R. Trifunović, *Inorg. Chem. Commun.* **7** (2004) 241
2. G. N. Kaluđerović, D. Miljković, M. Momčilović, V. M. Đinović, M. Mostarica-Stojković, T. J. Sabo, V. Trajković, *Int. J. Cancer* **116** (2005) 479
3. S. Mijatović, D. Maksimović-Ivanić, J. Radović, D. Miljković, G. N. Kaluđerović, T. J. Sabo, V. Trajković, *Cell. Mol. Life Sci.* **62** (2005) 1275
4. G. N. Kaluđerović, H. Schmidt, S. Schwieger, C. Wagner, R. Paschke, A. Dietrich, T. Mueller, D. Steinborn, *Inorg. Chim. Acta* **361** (2008) 1395
5. G. N. Kaluđerović, H. Schmidt, D. Steinborn, T. J. Sabo, in: *Inorganic Biochemistry: Research Progress*, J. G. Hughes, A. J. Robinson, Eds., Nova Science Publishers, Hauppauge, NY, 2008, pp. 305–326

6. G. N. Kaluđerović, H. Kommera, S. Schwieger, A. Paethanom, M. Kunze, H. Schmidt, R. Paschke, D. Steinborn, *Dalton Trans.* (2009) 10720
7. B. B. Krajčinović, G. N. Kaluđerović, D. Steinborn, H. Schmidt, C. Wagner, Ž. Žižak, Z. D. Juranić, S. R. Trifunović, T. J. Sabo, *J. Inorg. Biochem.* **102** (2008) 892
8. J. M. Vujić, M. Cvijović, G. N. Kaluđerović, M. Milovanović, B. B. Zmejkovski, V. Volarević, N. Arsenijević, T. J. Sabo, S. R. Trifunović, *Eur. J. Med. Chem.* **45** (2010) 3601
9. B. B. Krajčinović, G. N. Kaluđerović, D. Steinborn, C. Wagner, K. Merzweiler, S. R. Trifunović, T. J. Sabo, *J. Serb. Chem. Soc.* **74** (2009) 389
10. B. B. Zmejkovski, G. N. Kaluđerović, S. Gómez-Ruiz, Ž. Žižak, D. Steinborn, H. Schmidt, R. Paschke, Z. D. Juranić, T. J. Sabo, *Eur. J. Med. Chem.* **44** (2009) 3452
11. L. N. Schoenberg, D. W. Cooke, C. F. Liu, *Inorg. Chem.* **7** (1968) 2386
12. Oxford Diffraction, CrysAlis CCD and CrysAlis RED Versions 1.171.32.24, Oxford Diffraction Ltd., Abington, UK, 2008
13. R. C. Clark, J. S. Reid, *Acta Crystallogr., A* **51** (1995) 887
14. M. C. Burla, M. Camalli, B. Carrozzini, G. L. Cascarano, C. Giacovazzo, G. Polidori, R. Spagna, *J. Appl. Crystallogr.* **36** (2003) 1103
15. G. M. Sheldrick, *Acta Crystallogr., A* **64** (2008) 112
16. M. Nardelli, *Comput. Chem.* **7** (1983) 95
17. L. J. Farrugia, *J. Appl. Crystallogr.* **30** (1997) 565
18. C. F. Macrae, P. R. Edgington, P. McCabe, E. Pidcock, G. P. Shields, R. Taylor, M. Towler, J. van de Streek, *J. Appl. Crystallogr.* **39** (2006) 453
19. M. C. Etter, *Acc. Chem. Res.* **23** (1990) 120.

Journal of the Serbian Chemical Society
JSCS-info@shd.org.rs • www.shd.org.rs/JSCS

J. Serb. Chem. Soc. 78 (1) 65–73 (2013)
JSCS–4396

UDC 536.5.004.12:533.6.013.7:547.854
Original scientific paper

Effect of temperature on rate of a spin-forbidden transition in uracil and thymine

MIHAJLO ETINSKI*#

Faculty of Physical Chemistry, University of Belgrade, Studentski trg 12–16, P. O. Box 47, 11158 Belgrade, Serbia

(Received 18 June 2012)

Abstract: The intersystem crossing rates of uracil and thymine molecules in interaction with a heat bath were studied by means of *ab initio* methods. The rates were calculated employing the time-dependent approach based on the correlation function. The normal modes of the singlet and triplet electronic states were related by the Duschinsky transformation. The correlation function was calculated using the Condon approximation for the spin–orbit matrix element and harmonic approximation for the nuclear motion. The excess vibrational energy in the initial singlet excited electronic state decreased the rate of triplet formation in uracil and thymine. This decrease was more pronounced for uracil. In addition, it was found that the change of the adiabatic energy gap could significantly modify the rate of triplet formation.

Keywords: excited states; intersystem crossing; correlation function.

INTRODUCTION

The ozone layer above the Earth ground protects living beings by absorbing harmful UV radiation below 290 nm. The UV radiation from 290 to 320 nm is partially absorbed while the UV radiation from 320 to 380 nm is not absorbed. The main cellular targets of UV radiation are nucleic acids.[1] Sequences containing two or several pyrimidine bases are hotspots prone to the formation of photolesions. These photolesions can change the genotype of cells and remove the normal capacity to inhibit cell growth. The most frequent photochemical reaction of nucleic acids is intrastrand pyrimidine dimerization. Although time-resolved infrared experiments[2] showed that the main dimerization product is formed in less than 1 ps in a sequence of thymine bases, indicating an ultrafast photochemical reaction on the singlet excited electronic potential surface, the triplet state mechanism is not necessarily excluded.[3] Essentially, in order to decrease the

* E-mail: etinski@ffh.bg.ac.rs
# Serbian Chemical Society member.
doi: 10.2298/JSC120618066E

yield of the dimerization, it is necessary that the excited state populations relax ultrafast to the ground electronic state. Nevertheless, it was shown that in the pyrimidine bases uracil, thymine and related compounds, a long-lived dark electronic state is formed to a minor extent.[4–8] The electronic structure of this long-lived state has been the subject of long and controversial debates. Recent theoretical work[9] and supersonic jet experiments[8] showed that this dark state is the lowest triplet state.

In previous studies,[9–14] the formation of the triplet state in the pyrimidine bases uracil, thymine and their derivatives were investigated. It was found that the lowest triplet state ($^3\pi\pi^*$) in uracil and thymine is formed *via* the lowest singlet excited state ($^1n\pi^*$). Two mechanisms were proposed for triplet formation upon initial excitation to the second excited singlet state ($^1\pi\pi^*$):[9] a) an internal conversion (IC) to the first excited singlet state ($^1n\pi^*$) followed by intersystem crossing (ISC) to the lowest triplet state ($^3\pi\pi^*$) and b) an ISC transition from the initially populated singlet ($^1\pi\pi^*$) state to the second triplet state ($^3n\pi^*$) followed by IC to the lower triplet ($^3\pi\pi^*$) state. Due to the fast depletion of the initial $^1\pi\pi^*$ state to the ground and $^1n\pi^*$ state, it was suggested that lowest triplet state is populated by the ISC process from the $^1n\pi^*$ state. In all studies[9–14] that were performed, the ISC process was initiated from the lowest vibrational level of the singlet electronic state. These cases corresponded to vibrationally cooled molecules. In this study, the way in which excess vibrational energy, due to interaction of uracil and thymine with a heat bath, modifies triplet formation is investigated. The heat bath was a solvent. In order to calculate the ISC rates, the time-correlation function method is employed.

The paper is organized as follows: in the next section, we present the computational details and a brief explanation of how ISC rates can be calculated when a molecule has excess of vibrational energy due to interaction with a heat bath are given. The complete explanation will be given elsewhere.[15] In the subsequent section, this method is applied to uracil and thymine and the results discussed. Finally, conclusions are given.

THEORETICAL METHODS AND COMPUTATIONAL DETAILS

Pure spin Born–Oppenheimer states $\left|S_a,\{\nu_{aj}\}\right\rangle$ and $\left|T_b^\alpha,\{\nu_{bk}\}\right\rangle$ were employed for the calculation of the ISC rate. Here, S_α is a singlet electronic state and T_b^α is an α fine-structure component of a triplet electronic state. $\{\nu_{aj}\}$ and $\{\nu_{bk}\}$ are vibrational states related to the S_α and T_b^α states. In this work, the potential surfaces were approximated by a harmonic potential. The normal modes of the triplet $\{Q_{T_i}\}$ and singlet $\{Q_{S_i}\}$ electronic states are related by the Duschinsky Transformation:[16]

$$Q_{T_i} = \sum_j J_{ij} Q_{S_j} + D_i \tag{1}$$

where J is the Duschinsky rotation matrix and D is the displacement vector.

If initially a molecule is in a thermal equilibrium with the heat bath, then the ISC rate constant is given as an ensemble average:

$$k = \sum_j p(E_{aj}) k(j \to k) \tag{2}$$

where $P(E_{aj})$ = $\exp(E_{aj}/k_BT)/Z$ is a canonical ensemble probability of the occupation of the initial vibronic level with an energy E_{aj}, Z is the canonical partition function, T is the temperature of the thermal bath, k_B is the Boltzmann Constant and $k(j \to k)$ is the ISC rate from the vibronic level with energy E_{aj} to the vibronic level with energy E_{bk}.

Assuming the Condon Approximation for the spin–orbit matrix elements, the ISC rate is given by:

$$k = \frac{2\pi}{Z} \left| \left\langle S_a \middle| \hat{H}_{SO} \middle| T_b^{\alpha} \right\rangle \right|^2 \sum_{k,j} \mathrm{e}^{-E_{aj}/k_BT} \left| \left\langle \{\nu_{aj}\} | \{\nu_{bk}\} \right\rangle \right|^2 \delta\left(E_{aj} - E_{bk}\right) \tag{3}$$

Transforming this expression to the Heisenberg Picture, one obtains an expression that contains the correlation function. Then, the ISC rate is calculated as the integral of the correlation function:

$$k = \frac{1}{Z} \left| \left\langle S_a \middle| \hat{H}_{SO} \middle| T_b^{\alpha} \right\rangle \right|^2 \int_{-\infty}^{\infty} F(t) \mathrm{d}t \tag{4}$$

where the correlation function is:

$$F(t) = \sqrt{\frac{\det(S_T^{-1} S_S^{-1} \Omega_S \Omega_T)}{\det(J^T \Omega_T B_T J + \Omega_S B_S) \det(J^T \Omega_T B_T^{-1} J + \Omega_S B_S^{-1})}} \times \\ \times \exp\{D^T [\Omega_T B_T J (J^T \Omega_T B_T J + \Omega_S B_S)^{-1} J \Omega_T B_T - \Omega_T B_T] D\} \mathrm{e}^{it\Delta E} \tag{5}$$

ΔE is the singlet–triplet adiabatic energy gap and the matrices S_S, B_S, S_T and B_T are diagonal matrices with the elements: $\sinh((1/k_BT - it)\omega_{Si})$, $\tanh(\omega_{Si}/(2(1/k_BT - it))$, $\sinh(it\omega_{Ti})$ and $\tanh(\omega_{Ti}it/2)$, respectively, ω_i is the normal mode frequency, indexes S and T label the normal modes of the singlet and triplet electronic states, t is time and the superscript T indicates the transposition of the matrix.

The geometries of the $S_1(n\pi^*)$ and $T_1(\pi\pi^*)$ states of uracil and thymine obtained with the CC2/cc-pVDZ level of theory[9] were used. The normal mode displacements of the T_1 state relative to the S_1 states of uracil and thymine in dimensionless harmonic oscillator coordinates are presented in Fig. 1. There are several low-frequency modes that are highly displaced in both uracil and thymine. In addition, the C_4–C_5 bond stretching has a very large displacement (2.84 in uracil and 2.85 in thymine). The Duschinsky matrices for the transition between the S_1 and T_1 states of uracil and thymine are presented in Fig. 2. Almost all modes are mixed. The mixing is particularly large for the low-frequency modes and the two highest frequency modes that represent N–H oscillation. In addition, some high-frequency modes are mixed with the low-frequency modes. The adiabatic energy gap between S_1 and T_1 electronic states of uracil and thymine, obtained at CC2/cc-pVDZ level, are 5150 and 6652 cm^{-1}, respectively.[9] The adiabatic energy gap and displacement of the normal modes are decisive parameters that contribute to the calculation of the ISC rates. The sum of the squares of all spin–orbit matrix elements between the S_1 state and all fine structure components of the T_1 state is 2391 cm^{-2} for uracil and 2319 cm^{-2} for thymine.[9] All ISC rates that will be presented in this work are the sum of the three ISC rates from the S_1 state to the three fine-structure components of the T_1

state. All normal modes were included in the calculations. The correlation function was calculated for the first 10 fs using 1000 points.

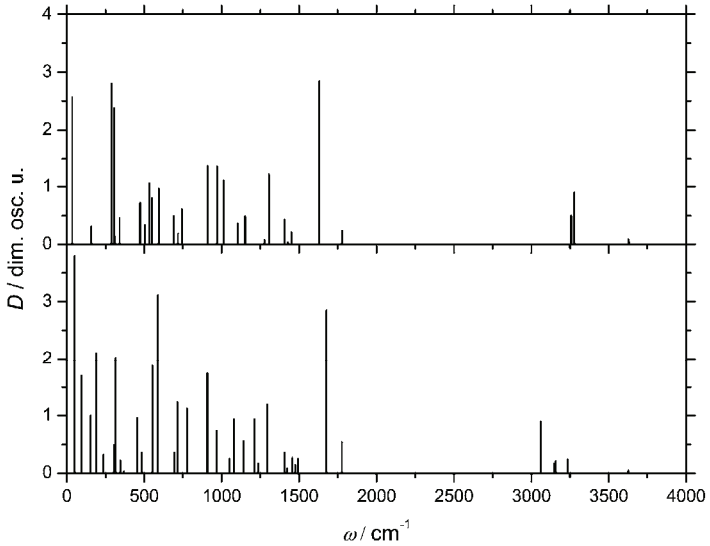

Fig. 1. Displacements of the T_1 normal modes relative to the S_1 normal modes in dimensionless harmonic oscillator coordinates for uracil (upper) and thymine (lower).

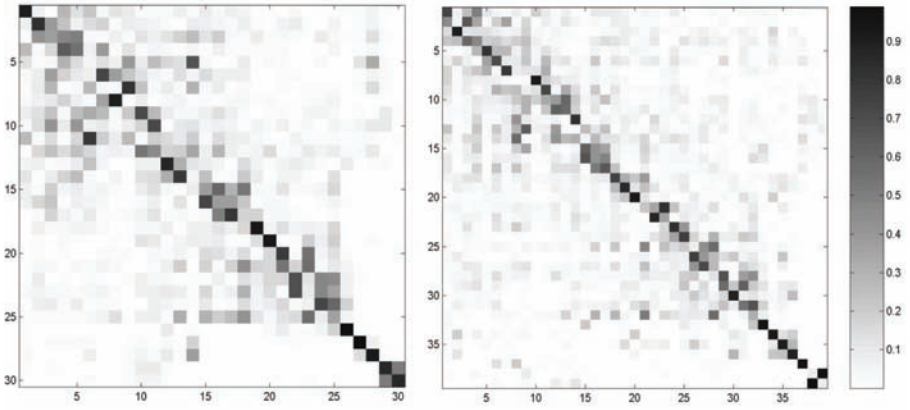

Fig. 2. Duschinsky matrix related to the transition between the S_1 and T_1 states of uracil (left) and thymine (right). In order to visualize the normal mode mixing, absolute values of the matrix elements are shown.

RESULTS AND DISCUSSION

If an electronic transition in a molecule is slower than the vibrational relaxation, then the normal modes of the electronic state will equilibrate with a heat

bath. This means that the heat bath will determine the average vibrational energy of the electronic state. Since the Boltzmann constant is $k_B \approx 0.7$ cm^{-1} K^{-1}, only the normal modes with the frequencies less than ≈250 cm^{-1} are more than singly occupied at 300 K. At higher temperatures, 400 and 600 K, this frequency is shifted to ≈300 and 500 cm^{-1}, respectively. This means that the heat bath can excite only low-frequency modes that include a pyrimidization of the ring atoms, an in-plane bending of the C=O bonds and a rotation and bending of the methyl group in thymine. Hence, these modes will have an excess of vibrational energy compared to the high-frequency modes. On the other hand, these modes significantly contribute to the ISC rate because they make a vibronic quasi-continuum in the triplet state.

The correlation functions for uracil and thymine calculated for different temperatures are presented in Fig. 3. In both molecules, the correlation functions decay to zero in approximately 5 fs. These fast decays are related to the large displacements of the normal modes. Since this is a multimode case with Duschinsky rotation, the normal modes with small displacements can also contribute to the correlation function. The correlation functions of thymine decay faster than the correlation function of uracil. This means that in thymine, the vibrational wavepacket on the triplet potential surface leaves the Franck–Condon zone faster than

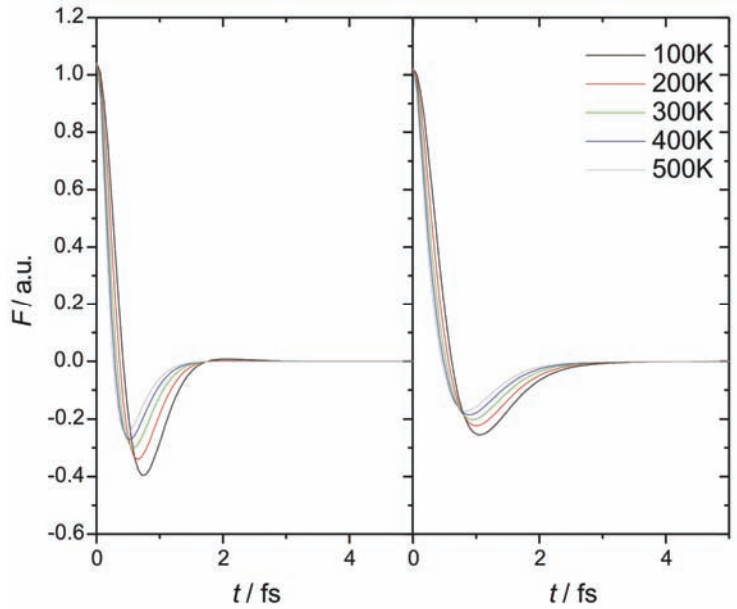

Fig. 3. Time dependence of the correlation function F for uracil (left) and thymine (right) for various temperatures. The adiabatic energy gap was 5150 cm^{-1} for uracil and 6652 cm^{-1} for thymine.

in uracil. In addition, the amplitude of the first oscillation is larger for thymine than for uracil. This amplitude for both correlation functions increases with increasing temperature. The same trend is valid for the decay of the first oscillation of the correlation function.

The correlation function at $t = 0$ should be exactly one but it is slightly higher for uracil and thymine. This is because the determinant of the Duschinsky matrices for uracil and thymine are 0.98 and 0.96, and not 1.00. Therefore, the normal modes of the triplet electronic state are not completely represented by the normal modes of the singlet electronic state without including rotations. This phenomenon is called the axis-switching effect.[17,18] Sando *et al.*[19] showed that the contribution of the nonlinear effect is in principal small for non-radiative transitions.

The ISC rate from the lowest vibrational level of the singlet electronic state (the $T = 0$ case) for uracil and thymine are 1.5×10^{10} and 2.5×10^{9}.[13,14] The ISC rates for uracil and thymine as a function of temperature are presented in Fig. 4. In accordance with the correlation function behavior, the rates decrease with increasing temperature. This means that the excess of vibrational energy in the S_1 state decreases the ISC rate for the formation of the triplet state. The explanation for this could be that the excited vibrational levels in the S_1 state have smaller

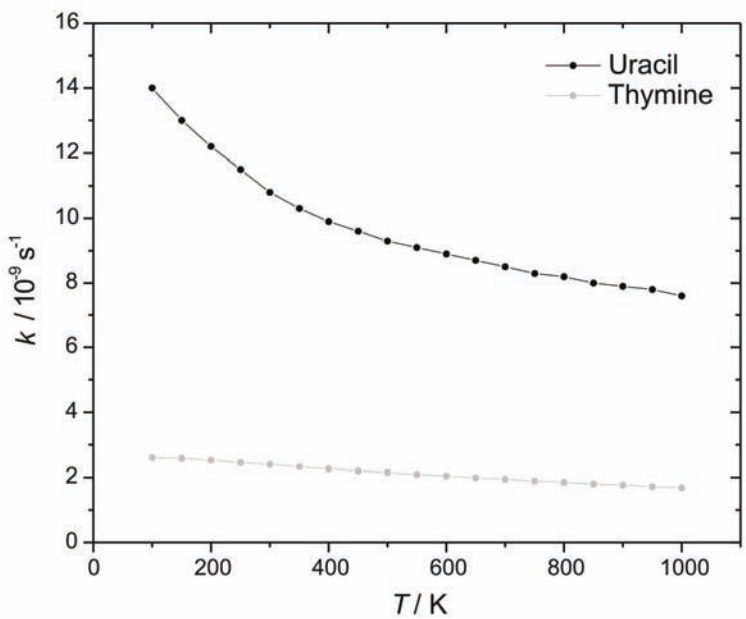

Fig. 4. Temperature dependence of the intersystem crossing rates for uracil and thymine. The adiabatic energy gap was 5150 cm^{-1} for uracil and 6652 cm^{-1} for thymine.

Franck–Condon integrals with the triplet vibrational level than the lowest vibrational state of the singlet state. The temperature dependence of the rate is more pronounced for uracil than for thymine. In the interval from 100 to 400 K, the rate decrease 30 % for uracil and 10 % for thymine. According to the energy gap law,[20] it is generally assumed that the rate of a non-radiative transition between two electronic states becomes larger if the energy difference between the states decreases. Thymine has a smaller singlet–triplet energy gap than uracil but the ISC rate is smaller. This is due to the large Duschinsky mixing. In this case, the energy gap law ceases to be valid.

A solvent can modify the adiabatic energy gap and it is of interest to see how the ISC rate depends on the adiabatic energy gap. The ISC rates of uracil and thymine as a function of the adiabatic energy gap calculated at 300 K are presented in Fig. 5. Up to 5000 cm^{-1}, the rates increase exponentially. For uracil, it changes two orders of magnitude while for thymine one order of magnitude. Hydration blue shifts the $S_1(^1n\pi^*)$ state by ≈4000 cm^{-1} and the $^3\pi\pi^*$ state by ≈800 cm^{-1}.[10] Hence, singlet–triplet energy gap is then increased by ≈3200 cm^{-1}. This would increase the ISC rate by an order of magnitude for uracil.

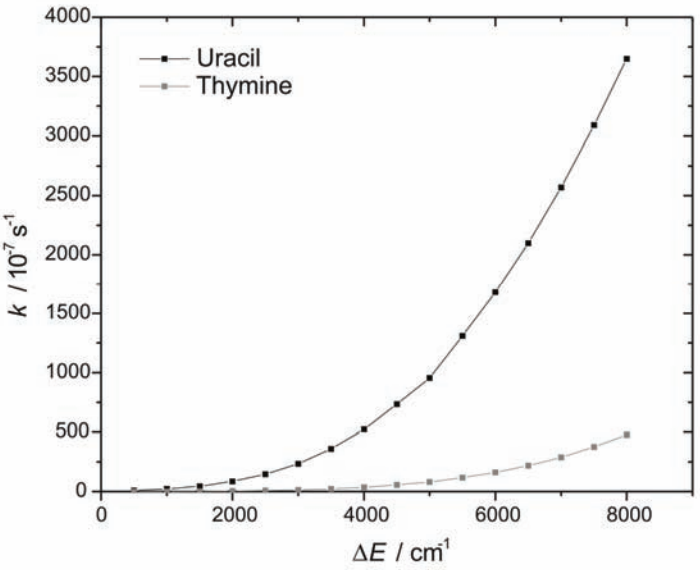

Fig. 5. The dependence of the intersystem crossing rates on the adiabatic energy gap for uracil and thymine. The temperature was 300 K.

CONCLUSIONS

The rate of formation of the lowest triplet state in uracil and thymine when the molecule has an excess vibrational energy due to interaction with a heat bath

was studied. In a previous paper on the spin-forbidden transitions in uracil, thymine and their methylated compounds,[9] two mechanisms for triplet formation were suggested, *i.e*., a) a non-radiative transition from the intermediate $^1n\pi^*$ state to the lowest triplet state and b) a transition from the initially populated $^1\pi\pi^*$ state to the second triplet state $^3n\pi^*$ followed by internal conversion to the lower triplet $^3\pi\pi^*$ state. In this work, the first mechanism was considered.

The intersystem crossing rates were calculated using the correlation function and canonical ensemble formalism. The normal modes of the triplet and singlet states were related by the Duschinsky transformation. The excess of the vibrational energy was controlled by the temperature of a heat bath. The correlation functions for both molecules decay in 5 fs. The correlation functions of thymine decay faster than the correlation functions of uracil. It was found that excess vibrational energy decreased the rate of triplet formation in uracil and thymine. This dependence was more pronounced for uracil. In addition, the rate of the triplet formation was more susceptible to changes in the adiabatic energy in uracil than in thymine.

Acknowledgement. The author acknowledges the Ministry of Ministry of Education, Science and Technological Development of the Republic of Serbia for financial support (Contract No. 172040).

И З В О Д

УТИЦАЈ ТЕМПЕРАТУРЕ НА КОНСТАНТУ БРЗИНЕ СПИНСКИ ЗАБРАЊЕНОГ ПРЕЛАЗА У УРАЦИЛУ И ТИМИНУ

МИХАЈЛО ЕТИНСКИ

Факултет за физичку хемију, Универзитет у Београду, Студентски трг 12–16, п. пр. 47, 11158 Београд

У раду су помоћу *ab initio* метода проучаване константе брзине интерсистемских прелаза у урацилу и тимину који интерагују са топлотним купатилом. Константе брзине су израчунате користећи временски зависна прилаз заснован на корелационој функцији. Нормални модови синглетног и триплетног електронског стања су повезани трансформацијом Душинског. Корелациона функција је израчуната користећи Кондонову апроксимацију за спин–орбитни матрични елемент и хармонијску апроксимацију за нуклеарно кретање. Вишак вибрационе енергије у почетном синглетном електронском стању смањује константу брзине настајања триплетног стања у урацилу и тимину. То смањење је израженије за урацил. Такође, нађено је да промена разлике адијабатских енергија електронски стања може значајно да утиче на брзину настајања триплетног стања.

(Примљено 18. јуна 2012)

REFERENCES

1. C. E. Crespo-Hernández, B. Cohen, P. M. Hare, B. Kohler, *Chem. Rev*. **104** (2004) 1977
2. W. J. Schreier, T. E. Schrader, F. O. Koller, P. Gilch, C. E. Crespo-Hernández, V. N. Swaminathan, T. Carell, W. Zinth, B. Kohler, *Science* **315** (2007) 625
3. W.-M. Kwok, C. Ma, D. L. Phillips, *J. Am. Chem. Soc*. **130** (2008) 5131

4. Y. He, C. Wu, W. Kong, *J. Phys. Chem., A* **107** (2003) 5143
5. Y. He, C. Wu, W. Kong, *J. Phys. Chem., A* **108** (2004) 943
6. M. Busker, M. Nispel, T. Häber, K. Kleinermanns, M. Etinski, T. Fleig, *ChemPhysChem* **9** (2008) 1570
7. J. González-Vázquez, L. González, E. Samoylova, T. Schultz, *Phys. Chem. Chem. Phys*. **11** (2009) 3927
8. M. Kunitski, Y. Nosenko, B. Brutschy, *ChemPhysChem*. **12** (2011) 2024
9. M. Etinski, T. Fleig, C. M. Marian, *J. Phys. Chem., A* **113** (2009) 11809
10. M. Etinski, C. M. Marian, *Phys. Chem. Chem. Phys*. **12** (2010) 4915
11. M. Etinski, C. M. Marian, *Phys. Chem. Chem. Phys*. **12** (2010) 15665
12. M. Etinski, J. Tatchen, C. M. Marian, *J. Chem. Phys*. **134** (2011) 154105
13. M. Etinski, *J. Serb. Chem. Soc.* **76** (2011) 1649
14. M. Etinski, *Hem. Ind.* **66** (2012) 165
15. M. Etinski, J. Tatchen, C. M. Marian, *in preparation*
16. F. Duschinsky, *Acta Physicochim. URSS* **7** (1937) 551
17. J. T. Hougen, J. K. G. Watson. *Can. J. Phys*. **43** (1965) 298
18. İ. Özkan. *J. Mol. Spec*. **139** (1990) 147
19. G. M. Sando, K. G. Spears. *J. Phys. Chem., A* **105** (2001) 5326
20. R. Englman, J. Jortner. *Mol. Phys*. **18** (1970) 145.

Journal of the Serbian Chemical Society
JSCS-info@shd.org.rs • www.shd.org.rs/JSCS
J. Serb. Chem. Soc. 78 (1) 75–83 (2013)
JSCS–4397
UDC 547.466.22:546.27'171.1:537.212
Original scientific paper

The effect of electric field on the interaction of glycine with (6,0) single-walled boron nitride nanotubes

DAVOOD FARMANZADEH* and SAMEREH GHAZANFARY

Faculty of Chemistry, University of Mazandaran, P. O. Box 453, Babolsar, I. R. Iran

(Received 12 April 2012)

Abstract: The interaction between the glycine molecule with the (6,0) zigzag model of single-walled boron nitride nanotubes (BNNTs) with H-terminated at the open end, has been investigated in the presence and absence of an external electric field (EF), using the DFT- B3LYP/6-31G* level of theory. The results demonstrated that glycine is chemisorbed on the (6,0) BNNT and this chemical adsorption can be significantly modified by the intensity of an external EF. It was found that increasing the EF strengthens the interaction between glycine and BNNT; thus, adsorption of glycine on BNNT could be controlled by the intensity of the EF. This result might be useful in the design of novel nano-devices, such as nano-sensors.

Keywords: glycine; density functional theory; boron nitride nanotube (BNNT); electric field.

INTRODUCTION

Boron nitride nanotubes (BNNTs) were first theoretically predicted by calculations and then their synthesis was reported in 1995.[1] Due to their large ionicity,[2] the properties of BNs are different from their carbon analogues.[3] BNNTs possess many unique properties, such as high thermal conductivity, chemical stability,[4] high oxidation resistivity,[5] and excellent mechanical properties,[6] which drastically differ from those of carbon nanotubes (CNTs). Therefore, BNNTs have been proposed as more suitable materials than CNTs for application in the nano-devices and molecular electronic circuits, and they can be used for the development of nanotube-based electronic devices, in material science and biotechnology.[7]

Recently much effort has been devoted to theoretical calculations with the aim of understanding the interaction between various molecules and BNNTs. It is well known, that theoretical studies can be very helpful in the understanding of the nature of interaction of BNNTs with other molecules. Modification of the

* Corresponding author. E-mail: d.farmanzad@umz.ac.ir
doi: 10.2298/JSC120419046F

electronic properties of nanotubes by interaction is an important issue for designing nano-devices based on nanotubes. Based on density functional theory (DFT) calculations, the adsorption of various aromatic molecules,[8] NH_3 and amino functional groups,[9] organic molecules,[10] nucleic acid bases,[11] hydrogen atoms,[12] O_2, N_2 and H_2O,[13] various metalloporphyrin[14] and transition metal atoms[15] on BNNTs were investigated. These studies indicated that the adsorption of atoms and molecules could effectively modify the electronic structures, and the physical and chemical properties of BNNTs.

Glycine, as the simplest of the α-amino acids,[16] is an important model compound in chemical physics, biophysics and biochemistry.[17] The –N–O–C(O)– structure, which occur in glycine, is a fundamental building block in α-amino acids and proteins.[18] In addition, the adsorption mechanism of amino acids and biological molecules onto nanotubes has attracted a lot of attention during the past years, since it is of great importance from both fundamental and applied points of view. Understanding the interaction between BNNTs and amino acids is important for the investigation the interaction mechanism between BNNTs and biomolecules.[19–21]

Modification of the structural and electrical properties by application of an external electric field is an important subject for the design of nano-devices. In previous studies,[22,23] it was found that the geometric and electronic structure of BNNTs can be modified by application of an external electric field; therefore it was considered of interest to investigate the BNNT–glycine system under the influence of an external electric field. In this study, the effect of external EF on the interaction of glycine molecule with SWBNNT (6,0) was investigated.

COMPUTATIONAL DETAILS

The quantum chemical calculations in this work were performed using the Gaussian 03 program package.[24] The structures of isolated BNNT, glycine and the BNNT–glycine complex were fully optimized by the DFT/B3LYP method with the 6-31G* basis set. The B and N dangling bonds at the two ends of (6,0) BNNT and the BNNT–glycine complex were saturated by hydrogen to avoid boundary effects. Geometric optimizations were performed until the maximum force and *rms* errors on all atoms were less than 0.00045 and 0.00030 Hartree/Bohr, respectively, which are the "normal" convergence criteria settings in Gaussian 03. The stationary point geometries were fully optimized and characterized as minima (no imaginary frequency) by vibration frequency calculations. The standard direction of the external electric field was along the positive X-axis (Fig. 1d). The numerical values of the applied static EF strengths were 50×10^{-4} and 100×10^{-4} a.u. (1 a.u. = 5.14224×10^{11} V m^{-1}).

Analysis of the electronic properties of the BNNT–glycine complex in the presence and absence of an EF were based on the adsorption energy, HOMO–LUMO gap, dipole moment and charge transfer (natural bond orbital (NBO) charge).

RESULTS AND DISCUSSION

Glycine adsorption on BNNT

The optimized structures for the pristine (6,0) BNNT and glycine are shown in Figs. 1a and 1b, respectively. To model the interaction between BNNT and the

glycine molecule, the glycine molecule was placed perpendicular to the BNNT at a height of 3.676 Å (Fig. 1c) and allowed to relax freely. The optimized structure of the BNNT–glycine complex is shown in Fig. 1d. After optimization, it was found that the glycine molecule preferred to orient parallel with respect to the surface of the BNNT, which is located at the end of the tube with the nearest distance being 1.726 Å.

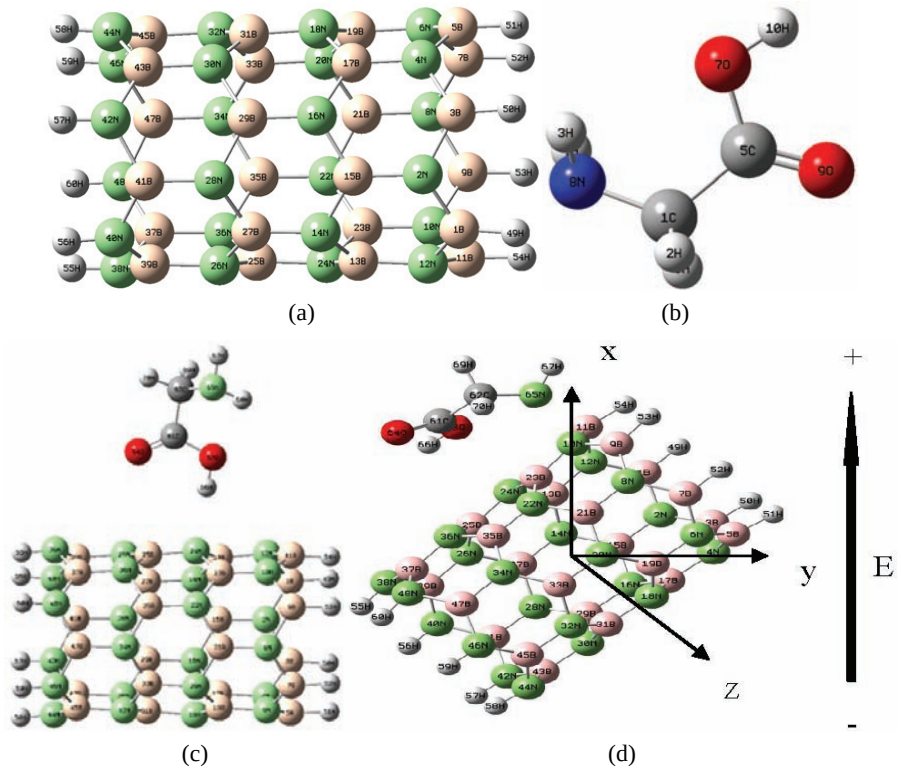

Fig. 1. The full optimized structure of a) BNNT, b) glycine, c) interaction of glycine with (6,0) BNNT and d) optimized structure of the BNNT–glycine complex at zero EF. The frame of axes used in this study is also shown.

First, the adsorption of glycine on (6,0) BNNT was investigated. The calculated values of the electronic energy of the glycine molecule, (6,0) BNNT and BNNT–glycine complex are reported in Table I, from which it can be seen that the energy of BNNT–glycine complex (–59989.291 eV) was lower in comparison to (6,0) BNNT (–52248.346 eV) and the glycine molecule (–7738.706 eV). These values indicate that the BNNT–glycine complex is energetically stable relative to the separated BNNT and glycine molecule.

TABLE I. *E*, band gap and dipole moment of BNNT, glycine and the BNNT–glycine complex at zero EF

Compound	*E* / eV	Band gap, eV	Dipole moment, D
BNNT	–52248.346	4.769	8.572
Glycine	–7738.706	5.376	1.297
BNNT–glycine	–59989.291	5.027	8.179

The adsorption energy of the glycine molecule on the (6,0) BNNT is defined by the following equation:

$$E_{ad} = E_{BNNT–glycine} – (E_{BNNT} + E_{glycine}) \quad (1)$$

where $E_{BNNT–glycine}$, E_{BNNT} and $E_{glycine}$ are the total energy of the BNNT–glycine complex, the total energies of the isolated glycine and isolated BNNT, respectively. $E_{ad} < 0$ denotes an exothermic adsorption, a negative E_{ad} corresponds to a stable adsorption structure and a larger negative adsorption energy means the configuration is more favorable from an energy viewpoint. The adsorption energy was larger than 0.5 eV, which supports the hypothesis that the adsorption mechanism was chemisorptions.[25–27] The adsorption energy of the BNNT–glycine complex at zero EF is reported in Table II. This result shows that the glycine molecule can be chemically adsorbed on the BNNT sidewall with exothermic adsorption energy of –2.237 eV.

TABLE II. Calculated E_{ad} and band gap of the BNNT–glycine complex, B–N bond length, transferred charge *Q* and dipole moment, in the presence and absence of an external EF

External EF	E_{ad} / eV	Band gap, eV	$R_{B11–N65}$ / Å	*Q* / e	Dipole moment, D
0	–2.237	5.027	1.726	0.331	8.179
50	–3.021	4.539	1.672	0.340	14.542
100	–4.126	4.041	1.663	0.343	22.657

Charge transfer is one of the key factors that facilities the adsorption of an adsorbate onto an adsorbent. The chemical adsorption of glycine onto a BNNT leads to a certain amount of charge transfer. To better understand the chemical adsorption of the glycine molecule onto BNNT, the transferred charge (*Q*) from glycine to (6,0) BNNT was calculated. A positive value corresponds to charge transfer from glycine to (6,0) BNNT. The *Q* of glycine molecule to BNNT using the NBO charge,[28–30] which is less sensitive to the selected basis sets than Mulliken[31] charge analysis, was obtained. The calculated values of *Q* at zero EF are reported in Table II, from which, it can be seen that the transferred charge in the absence of EF was significant (0.331 e).

It is essential to calculate the electronic properties of (6,0) BNNT before and after glycine molecule adsorption, to understand better the interaction of the glycine with BNNT. When glycine is adsorbed on the BNNT, the electronic properties of the tube and glycine are changed. The energy levels of the molecular

orbitals, especially the HOMO and LUMO, are excellent indicators of many molecular properties. Thus, the difference between the HOMO and LUMO, known as the band gap (E_{LUMO}–E_{HOMO}) was studied.

The calculated values of the band gap and dipole moment of the glycine molecule, (6,0) BNNT and the BNNT–glycine complex before application of an EF are given in Table I, according to which, the band gap of the pure (6,0) BNNT is 4.769 eV. The band gap increases to 5.027 eV upon glycine molecule adsorption onto the tube. In addition, the band gap of the BNNT–glycine complex is greater than that of the glycine molecule. The electric dipole moment of the free BNNT (8.572 D), glycine (1.297 D) and the BNNT–glycine complex (8.179 D) are presented in Table I. These results show that the polarization and electro-conductivity of the (6,0) BNNT in the presence of glycine molecule were changed.

The effect of an applied electric field on glycine adsorption

In this work, the adsorption of the glycine on the (6,0) BNNT was explored under the effect of an external EF. The calculated values of the adsorption energy (E_{ad}), B–N bond length ($R_{B11–N65}$) and charge transfer (Q) in zero, 50×10^{-4} and 100×10^{-4} a.u. EF intensity are reported in Table II. As can be seen, with increasing EF strength, the adsorption energy decreased from –2.237 in the zero external EF intensity to –3.021 and –4.126 eV at 50×10^{-4} and 100×10^{-4} a.u., respectively. These results show that the stability of the BNNT–glycine complex increased with the increasing EF intensity. In addition, an EF can easily modulate the adsorption energy of glycine adsorbed on BNNT.

Under the external electric EF, a single covalent B_{BNNT}–$N_{Glycine}$ bond is formed ($R_{B11–N65}$). The $R_{B11–N65}$ decreased from 1.726 Å in zero EF intensity to 1.672 and 1.663 for 50×10^{-4} and 100×10^{-4} a.u. EF strengths, respectively.

The optimized structure of BNNT–glycine complex under the applied external EF with 100×10^{-4} a.u. strength is shown in Fig. 2, according to which, the orientation of glycine on (6,0) BNNT changed under the external EF.

As can be seen in Table II, the transferred charge in zero EF intensity, 0.331 e, increased to 0.343 e at 100×10^{-4} a.u EF strength. These values show that the transferred charge increased with increasing external EF strength. Generally, these results show that interaction of glycine molecule with BNNT was enhanced with increasing external EF strength from zero to 100×10^{-4} a.u intensity.

One of the important applications of external EF on BNNTs is to modify the electronic structures and thus widen their potential applications. The calculated values of band gap of the BNNT–glycine complex for applied external EF from F = 0 to 100×10^{-4} a.u. are given in Table II, from which, it could be understood that with increasing field strength, the band gap decreased from 5.027 at zero external EF to 4.539 and 4.041 at 50×10^{-4} and 100×10^{-4} a.u., respectively. Thus, the electro-conductivity of the BNNT–glycine complex increased under an ex-

ternal EF. The change in the electro-conductivity of the BNNT–glycine system is an important process in the sensor industry.

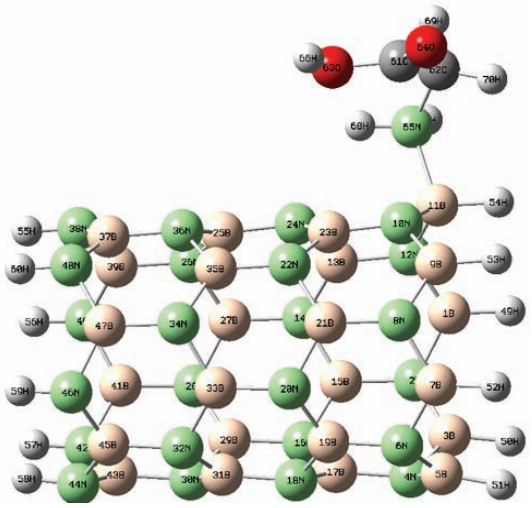

Fig. 2. The BNNT–glycine complex which response to the external EF with 100×10^{-4} a.u. strength is studied in this work at DFT-B3LYP/6--31G* level of theory.

On the other hand, an analysis of the spatial distribution of the frontier orbitals is one way to understand the molecular properties. To explain further the electrical properties of the BNNT–glycine complex under an external EF, the spatial distribution of the molecular orbitals (MOs), especially the frontier MOs including the HOMO and LUMO, were studied. The spatial distribution of the frontier orbitals was performed to obtain a better understanding on the interaction of glycine with (6,0) BNNT. The spatial distribution of the HOMO and LUMO of (6,0) BNNT and the BNNT–glycine complex under various external EF are illustrated in Fig. 3.

As shown in Fig. 3a, large amounts of the charge density of (6,0) BNNT are concentrated at the left and right ends of the tube, implying that the active sites of (6,0) BNNT probably lie in the ends of tube. In addition, this figure shows that the HOMOs and LUMOs of the BNNT–glycine complex are localized around the BNNT at all employed EF intensities. Fig. 3b shows that at zero EF, the major part of LUMO is distributed on the (6,0) BNNT near the glycine molecule and that the HOMO is localized over the whole of the (6,0) BNNT. According to Fig. 3, as the field strength increases to 100×10^{-4} a.u., the HOMO and LUMO are mainly localized at the end of the complex. Some small amount of the LUMO is localized around the B–N bond but there are no HOMO orbitals around the B–N bond.[32–36]

When an external electric field is applied on the BNNT–glycine system, rearrangements of its atomic charges lead to the separation of the positive and ne-

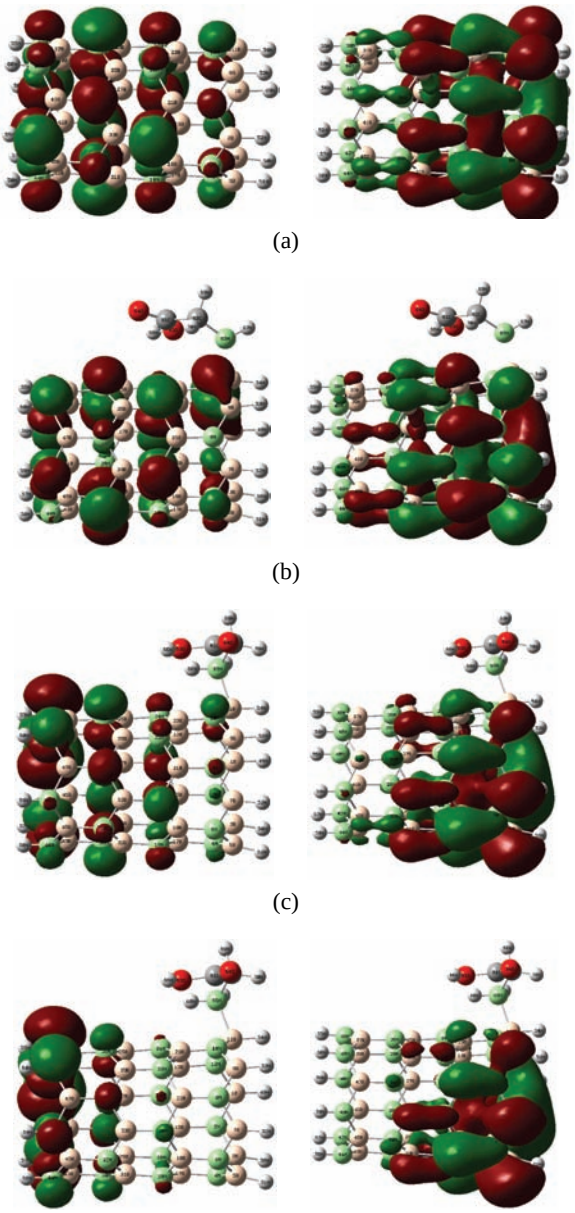

Fig. 3. Orbital spatial distribution of HOMO (right) and LUMO (left): a) optimized structure of (6,0) BNNT, b) the BNNT–glycine complex at zero EF, c) the BNNT–glycine complex at 50×10^{-4} a.u. and d) the BNNT–glycine complex at 100×10^{-4} a.u.

gative charges, which induces an electric dipole moment in the system. Thus, the study of the electric dipole moment under external EFs is important. The calculated values of the electric dipole moment (F in D) for applied external EFs from 0 to 100×10^{-4} a.u. are given in Table II. According to Table II, on application of an EF on the BNNT–glycine complex, the dipole moment increases from 8.179 D at zero EF to 22.657 D at 100×10^{-4} a.u. The significant changes in the electric dipole moment clearly predict that interaction of glycine molecule with (6,0) BNNT increases with increasing external EF intensity.

CONCLUSIONS

In summary, in this work, DFT calculations were performed on the BNNT––glycine complex on application of static electric fields. The glycine molecule is exothermally strongly adsorbed on the sidewall BNNT with high adsorption energy. Therefore, the BNNT–amino acid complex may be useful in the application of this class of biofunctional nanotubes to the design of amino acid delivery vessels. From these calculations, it was concluded that the electronic properties of the BNNT–glycine complex are modified with increasing EF intensity. This result may be useful in the application the BNNT–glycine system under the influence of an EF to the design of biosensor devices. In brief, study of this system under influence of EF intensity is important for the design and proposal of BNNT-based materials.

Acknowledgment. The support of the University of Mazandaran, Iran, through its research facilities and financial grants is acknowledged.

ИЗВОД

УТИЦАЈ ЕЛЕКТРИЧНОГ ПОЉА НА ИНТЕРАКЦИЈУ ГЛИЦИНА СА ЈЕДНОСЛОЈНОМ БОР-НИТРИДНОМ НАНОЦЕВИ ТИПА (6,0)

DAVOOD FARMANZADEH И SAMEREH GHAZANFARY

Faculty of Chemistry, University of Mazandaran, P. O. Box 453, Babolsar, I. R. Iran

Испитивана је интеракција између молекула глицина једнослојне бор-нитридне наноцеви, типа (6,0), у одсуству и у присуству спољашњег електричног поља. Примењен је DFT-B3LYP/6-31G* ниво теорије. Резултати показују да се глицин хемисорбира на наноцев и да на хемисорпцију значајно утиче јачина електричног поља. Нађено је да се појачањем електричног поља појачава интеракција између глицина и наноцеви. То значи да се адсорпција глицина може контролисати јачином електричног поља. Овај резултат би могао бити од користи за дизајнирање нових нано-уређаја, као што су нано-сензори.

(Примљено 12. априла 2012)

REFERENCES

1. M. Terrones, J. M. Romo-Herrera, E. Cruz-Silva, F. Muñoz-Sandoval, J. J. Velázquzar, H. Terrones, Y. Bando, D. Golberg, *Mater. Today* **10** (2007) 30

2. X. Wu, J. Yang, J. G. Hou, Q. Zhu, *Phys. Rev., B* **69** (2004) 153911
3. G. Y. Gou, B. C. Pan, L. Shi, *J. Phys. Chem., B* **112** (2008) 13571
4. Y. Li, Z. Zhou, J. Zhao, *J. Phys. Chem.* **127** (2007) 184705
5. G. Y. Gou, B. C. Pan, L. Shi, *ACS Nano* **4** (2010) 1313
6. W. He, Z. Li, J. Yang, J. G. Hou, *J. Chem. Phys.* **129** (2008) 024710
7. W. Sun, Y. Bu, Y. Wang, *J. Phys. Chem., B* **112** (2008) 15442
8. J. X. Zhao, Y. H. Ding, *Diamond Relat. Mater.* **19** (2010) 1073
9. X. Wu, W. An, X. C. Zeng, *J. Am. Chem. Soc.* **128** (2006) 12001
10. W. He, Z. Li, J. Yang, J. G. Hou, *J. Chem. Phys.* **128** (2008) 164701
11. S. Mukhopadhyay, S. Gowtham, R. H. Scheicher, R. Pandey, S. P. Karna, *Nanotechnology* **21** (2010) 165703
12. L. Feng, X. Yueyuan, Z. Mingwen, L. Xiangdong, H. Boda, J. Yanju, S. Chen, *Phys. Lett., A* **357** (2006) 369
13. J. X. Zhao, Y. H. Ding, *J. Phys. Chem., C* **112** (2008) 20206
14. J. X. Zhao, Y. H. Ding, *Mat. Chem. Phys.* **116** (2009) 21
15. X. Wu, X. C. Zeng, *J. Chem. Phys.* **125** (2006) 044711
16. M. F. Carvalho, R. A. Mosquera, R. Rivelino, *Chem Phys. Lett.* **445** (2007) 117
17. S. Maeda, K. Ohno, *Chem. Phys. Lett.* **398** (2004) 240
18. D. Yu, W. A. Rauk, D. A. Armstrong, *J. Am. Chem. Soc.* **117** (1995) 1789
19. C. K. Yang, *Comput. Phys. Commun.* **182** (2011) 39
20. S. Wenming, B. Yuxiang, *J. Phys. Chem., B* **112** (2008) 15442
21. M. Vivian, S. B. Fagan, I. Zanella, R. Mota, *Microelec. J.* **40** (2009) 877
22. D. Farmanzadeh, S. Ghazanfary, *Theor. Comput. Chem.* **1** (2011) 10
23. D. Farmanzadeh, S. Ghazanfary, *Struct. Chem.* **20** (2009) 709
24. *Gaussian 03*, Gaussian, Inc., Pittsburgh, PA, 2003
25. H. Chang, J. D. Lee, S. M. Lee, Y. H. Lee, *Appl. Phys. Lett.* **79** (2001) 3864
26. M. Chi, Y. P. Zhao, *Comput. Mat. Sci.* **46** (2009) 1085
27. S. H. Lim, J. Lin, Chem. *Phys. Lett.* **466** (2008) 197
28. A. E. Reed, R. B. Weinstock, F. Weinhold, *J. Chem. Phys.* **83** (1985) 735
29. E. D. Glendening, A. E. Reed, J. E. Carpenter, F. Weinhold, NBO Version 3.1, NBO website, http://www.chem.wisc.educ/~nbo5/
30. R. S. Mulliken, *J. Chem. Phys.* **23** (1955) 1833
31. Y. Ye, M. Zhang, H. Liu, X. Liu, J. Zhao, *J. Phys. Chem. Solids* **69** (2008) 2615
32. C. M. Chang, A. F. Jalbout, *Thin Solid Films* **518** (2010) 2070
33. A. D. Leon, A. F. Jalbout, V. A. Basiuk, *Chem. Phys. Lett.* **452** (2008) 306
34. N. Saikia, R. C. Deka, *Chem. Phys. Lett.* **500** (2010) 65
35. V. M. Menezes, S. B. Fagan, I. Zanella, R. Mota, *Microelec. J.* **40** (2009) 8.

Journal of the Serbian Chemical Society
JSCS-info@shd.org.rs • www.shd.org.rs/JSCS
J. Serb. Chem. Soc. 78 (1) 85–92 (2013)
JSCS–4398
UDC 544.174.2/.3:544.144.52:512.81
Original scientific paper

A study of the stretching vibrational spectra of $C_{120}O$ and $C_{120}O_2$ by *U*(2) Lie algebra

RUPAM SEN[1]*, ASHIM KALYAN[1] and RAMENDU BHATTACHARJEE[2]

[1]*Department of Physics, Srikishan Sarda College, Hailakandi-788151, India and* [2]*Department of Physics, Assam University, Silchar-788011, India*

(Received 31 January, revised 8 July 2012)

Abstract: The vibrational energy levels of the endohedral fullerene dimers $C_{120}O$ and $C_{120}O_2$ were calculated considering the local Hamiltonian of the Morse potential using algebra. Here, each bond of the molecules was replaced by a corresponding Lie algebra and finally the Hamiltonian was constructed considering the interacting Casimir and Majorana operators. The fundamental stretching modes of vibration of both dimers $C_{120}O$ and $C_{120}O_2$ were then calculated using this Hamiltonian to compare with the results of functional-based tight-binding (DF-TB) calculations.

Keywords: Lie algebra; vibrational spectra; $C_{120}O$; $C_{120}O_2$.

INTRODUCTION

In the last few years, theoretical studies of highly excited vibrational states of polyatomic molecules have been one of the most interesting topics for theoreticians and experimentalists because of the development of new laser spectroscopic techniques. Wulfman played a great role in the introduction of the algebraic approach to molecules. He was the pioneer who publish the first paper on the algebraic approach to molecules[1] (the algebraic approach to the Morse oscillator) in 1979. Later, in 1981, Iachello[2] used Lie algebraic method to study the spectra of molecules using *U*(4) algebra. The *U*(4) model takes rotation and vibration simultaneously into account but becomes intricate when the number of atoms in the molecules becomes more than four. After 1981, there was rapid progress in this field. Iachello *et al.*[3,4] proposed *U*(4) algebra to calculate the stretching and bending vibrational excitations of linear triatomic and tetratomic molecules. The situation up to 1995 in this perspective was reviewed in a paper by Iachello and Levine.[5] In next year, Stefano Oss presented a contemporary and comprehensive up-to-date review of the mathematical concepts, physical aspects, practical applications and numerical implementation of algebraic models[6] in

* Corresponding author. E-mail: rupamsen@yahoo.com
doi: 10.2298/JSC120131074S

molecular spectroscopy. Later, Iachello and Oss jointly[7] presented a brief review of the work realized in this field and also provided a concrete outlook of the algebraic method in the first decade of the 21st century. Recently, using the Lie algebraic method, Sarkar *et al.* reported better results[8,9] for the vibrational energy levels of different polyatomic molecules than those reported earlier. The *U*(2) algebraic model was particularly successful in explaining stretching vibrations of polyatomic molecules, such as tetrahedral, octahedral, endohedral and benzene-like molecules.[10] In the Lie algebraic method, there is provision for molecular vibrational energy to be studied by a normal and a local Hamiltonian. Using the powerful technique of the theoretical Lie algebraic group theory and by considering dynamical symmetry, the algebraic Hamiltonian was constructed. The application of the one-dimensional theoretical *U*(2) algebraic model enabled the analysis and interpretation of experimental and theoretical rovibrational spectra of different polyatomic molecules, which might facilitate the exploration of a new dimension in the field of molecular chemistry and nano-technology.

Till date, no extensive experimental study of the vibrational spectra of endohedral fullerene dimers $C_{120}O$ and $C_{120}O_2$ have been reported, but only functional-based tight-binding (DF-TB) theoretical calculations in which a study of the vibrational spectra of fullerene dimers $C_{120}O$ and $C_{120}O_2$ with their different energy bands were analyzed.[11] By using the one-dimensional *U*(2) algebraic model, which is an excellent alternative mathematical treatment for the determination of energy bands of fullerene dimers $C_{120}O$ and $C_{120}O_2$, the stretching vibrational energies of these dimers were determined and compared from a spectroscopic point of view.

THEORY: AN ALGEBRAIC APPROACH

Apart from Lie algebraic methods, two other well-defined methods already exist for the analysis of molecular vibrational spectra. These are:

1. The Dunham Expansion
2. The Potential Approach

Dunham Expansion approach was put forwarded by J. L. Dunham in 1932. Here, the molecular rotation-vibration spectrum is provided by the Dunham expansion. This is an expansion of energy levels in terms of vibration-rotation quantum numbers. For diatomic molecules, the expansion is:

$$E(v,J)=\sum_{i,j} y_{i,j}\left(v+\tfrac{1}{2}\right)^{i}\left[J\left(J+1\right)\right]^{j} \quad (1)$$

The Dunham Expansion approach has a few drawbacks. Here no Hamiltonian operator is available. Moreover, for large polyatomic molecules, one needs a large number of parameters are required to obtain by fitting a large experimental data base; these parameters are not always available. Furthermore, this expansion contains no information about the wave function of individual states. Thus, the matrix elements of the operators cannot be calculated directly. Lastly, the Dunham Expansion approach is unsuccessful for polyatomic molecules.

The second approach, called the Potential Approach provides more sophisticated analysis. Here, energy levels are obtained by solving the Schrödinger Equation with an interatomic potential. The potential is expanded in terms of interatomic variables. For diatomic molecules, a possible expansion is:

$$V(r) = \sum_n a_n \left(\frac{r - r_0}{b} \right)^n \tag{2}$$

Here, the coefficients are obtained by a fit to the experimental energy levels. The solution of the Schrödinger Equation also provides a wave function from which matrix elements of various operators can be calculated. In the Potential approach, all the calculations are either differentiations or integrations Moreover; this approach is very tiresome when the numbers of atoms are larger.

The third approach is the algebraic model in which each bond is represented by either one dimensional $U(2)$ or three dimensional $U(4)$ Lie algebra,[3-5] which are popularly known as the one dimensional and three dimensional vibron model, respectively. Among these, the $U(4)$ model effectively explains simultaneously the stretching and bending vibrational energies of medium- and large-sized molecules. However, the one dimensional $U(2)$ algebraic model is very successful in explaining independently the stretching and bending vibrational energies of medium- and large-sized molecules. This method is based on the idea of dynamical symmetry, which, in turn, is expressed through the language of Lie algebras.

In connection with molecular spectroscopy, the dynamical symmetries explored in this work constitute a big step forward over the conventional use of symmetry arguments, especially those concerning the description and classification of energy spectra denoting specific degeneracy patterns. The dynamical symmetries contain within themselves both the degeneracy aspects of a physical system and the complete mechanism for describing transitions among different states. All these tasks can be realized within the extremely compact and convenient framework of Lie groups and Lie algebras. The use of dynamical symmetry, a very powerful technique related to the dynamical group, leads to a conveniently simple form of the second-quantized Hamiltonian operator. The most important steps leading to the formulation of a dynamical symmetry are presented. This formulation should be thought of as a very effective, specialized version of the usual second quantized realization of a quantum problem. In such a realization: 1) the wave equation is replaced by an algebraic equation, 2) the wave functions are replaced with a Fock space and 3) the most general algebraic expansion, in terms of (boson) creation-annihilation operators, is restricted to invariant or Casimir operators of sub-algebras of the dynamical algebra. Such an "ultimate" algebraic structure turns out to be, for n-dimensional problems, the Lie algebra $U(n + 1)$. These three steps constitute the basic components for the definition of the dynamical symmetry realization of the Hamiltonian operator.

In this study, the $U(2)$ algebraic model which was introduced as an alternative approach to the traditional Dunham expansion and Schrödinger equation for polyatomic molecules, was used. The motivation for the construction of this algebraic model is the isomorphism of the one dimensional Lie algebra, $U(2)$, with that of the one dimensional Morse oscillator, which is a good description of a stretching vibration of a molecule. The Hamiltonian of the one dimensional Schrödinger Equation with Morse Potential is:[7]

$$h(p,x) = \frac{p^2}{2\mu} + D\left[1 - \exp(-\alpha x)\right]^2 \tag{3}$$

which can be put into one-to-one correspondence with the representation of the algebra $U(2) \supset O(2)$ characterized by the quantum numbers $|N_1, m\rangle$ with the provision that one takes only the positive branch of m, *i.e.*, $m = N_1, N_1–1, N_1–2,\ldots, 1$ or 0 for N_1 odd or even (N_1 is an integer). However, to obtain a complete description of molecular vibrations, both stretching and bending modes are required. This is achieved by considering the isomorphism of the $U(2)$ Lie algebra with the solution of the Schrödinger Equation with another potential called the Poschl-Teller potential. This potential is very applicable for the calculation of bending vibrations, where the Morse potential is inappropriate. The eigenstates of the Schrödinger Equation with Hamiltonian Operator are:

$$h(p,x) = \frac{p^2}{2\mu} - \frac{D}{\cosh^2 \alpha x} \tag{4}$$

This can also be put into one-to-one correspondence with the representation of $U(2) \supset O(2)$ characterized by the quantum numbers $|N_2, m\rangle$ with the provision that one takes only the positive branch of m. In the above equation, the coordinate x is the product of the radius of the bender r multiplied the bending angle θ, *i.e.*, $x = r\theta$. For the fullerene dimers, n $U(2)$ Lie algebra are introduced to describe n stretching bonds (C–C and C–O). The two possible chains[8-10] of molecular dynamical groups in these molecules are:

$$U^1(2) \otimes \ldots \otimes U^n(2) \supset O^1(2) \otimes \ldots \otimes O^n(2) \supset O(2) \tag{5}$$

$$U^1(2) \otimes \ldots \otimes U^n(2) \supset U(2) \supset O(2) \tag{6}$$

which correspond to local and normal coupling, respectively. The coupling to the final $O(2)$ group in the first chain is realized though different intermediate couplings $O^{ij}(2)$ and the second chain arises from all the possible couplings of $U^i(2)$groups to obtain a total $U(2)$ group, which in turn contains the final $O(2)$ group.[12] For these two situations, the Hamiltonian operator can be diagonalized analytically. Thus, the algebraic model Hamiltonian consider herein has the following form:[8,9]

$$H = E_0 + \sum_{i=1}^{n} A_i C_i + \sum_{i<j}^{n} A_{ij} C_{ij} + \sum_{i<j}^{n} \lambda_{ij} M_{ij} \tag{7}$$

If $\lambda_{ij} = 0$, the vibrations have a local behaviour. As the value of λ_{ij} increases, one goes more and more into normal vibrations. In Eq. (7), C_i is an invariant operator with eigenvalues $4(\nu_i^2 - N_i\nu_i)$ and the operator C_{ij}, known as the Casimir operator, contains diagonal matrix elements while the operators M_{ij}, known as the Majorana operators, have both diagonal and off-diagonal matrix elements.

Both the operators associated with coupling schemes involving algebras naturally arise from a systematic study of the algebraic formulation of the one-dimensional model for n interacting oscillators. Due to the restriction placed on the local uncoupled oscillators, the vibrational basis are represented as:

$$|\nu\rangle \equiv |\nu_1\nu_2\nu_3\ldots\nu_n\rangle \tag{8}$$

in which the aforementioned operators have the following matrix elements:

$$\begin{aligned}
\langle v|C_i|v\rangle &= -4\nu_i(N_i-\nu_i)\\
\langle v|C_{ij}|v\rangle &= -4(\nu_i+\nu_j)(N_i+N_j-\nu_i-\nu_j)\\
\langle v'|M_{ij}|v\rangle &= (\nu_i N_i+\nu_j N_j-2\nu_i\nu_j)\delta_{v'_i\nu_i}\delta_{v'_j\nu_j}\\
\langle v'|M_{ij}|v\rangle &= -[(\nu_i+1)(N_i-\nu_i)\nu_j(N_j-\nu_j+1)]^{1/2}\delta_{v'_i-\nu_i}\delta_{v'_j+\nu_j}\\
\langle v'|M_{ij}|v\rangle &= -[(\nu_j+1)(N_j-\nu_j)\nu_i(N_i-\nu_i+1)]^{1/2}\delta_{v'_i+\nu_i}\delta_{v'_j-\nu_j}
\end{aligned} \tag{9}$$

Here, in particular, the expressions above depend on the numbers N_i, popularly known as Vibron numbers (vibration rotation quantum number). Such numbers have to be seen as predetermined parameters of well-defined physical meaning, as they relate to the intrinsic anharmonicity of a single, uncoupled oscillator through a simple relation.

In purely local limit of N oscillators, these oscillators are somehow correlated with each other through the C_{ij} operators, which account for the (diagonal) cross-anharmonicities, represented by the following equation:

$$C_{ij} = C_i - N_{ij}\left(\frac{C_i}{N_i}+\frac{C_j}{N_j}\right), \text{ where } N_{ij} = N_i + N_j \tag{10}$$

In the special case of a pair of equivalent oscillators i and j ($N_i = N_j$), the above equation can be replaced by the following matrix elements:[13-15]

$$\langle \nu_i\nu_j|C_{ij}|\nu_i\nu_j\rangle = -4(\nu_i-\nu_j)^2 \tag{11}$$

i.e., the matrix elements do not depend on $N_i(N_j)$. As a result, C_{ij} would account for different contributions throughout different polyads and within the same polyad; the most important aspect of C_{ij} is the dependence of its matrix elements on the product $\nu_i\nu_j$.

Now, the quantum numbers ν_i correspond to the number of quanta in each oscillator, while V is the total vibrational quantum number given by

$$V = \sum_{i=1}^{n}\nu_i \tag{12}$$

For particular polyatomic molecules, the total vibrational quantum number is always conserved. The inclusion of C_{ij} and M_{ij} in the local Hamiltonian operator cannot affect the above conservation rule.

RESULTS AND DISCUSSION

In this study, we use the different algebraic parameters, *i.e.*, A, A', λ, λ' and N, were used to study the vibrational spectra of the endohedral fullerene dimers $C_{120}O$ and $C_{120}O_2$ molecules, where N is the vibron number.

The values of Vibron number (N) can be determined by the relation:

$$N_i = \frac{\omega_e}{\omega_e x_e} - 2, \quad i = 1,2..., \quad x_e = \frac{1}{N+2} \tag{13}$$

where ω_e and $\omega_e x_e$ are the spectroscopic constants[16,17] of polyatomic molecules of the stretching interaction of the molecule considered. This numerical value

must be seen as an initial guess, *i.e.*, depending on the specific molecular structure, changes in such an estimate can be expected, which, however, should not be larger than ±20 % of the original value of Eq. (13). It may be noted that during the calculation of the vibrational frequencies of the fullerene dimers $C_{120}O$ and $C_{120}O_2$, the value of N is kept fixed and not used as a free parameter.

To obtain a starting guess for the parameter A, the expression for the single-oscillator fundamental mode is used, which is given as:

$$E(\nu = 1) = -4A(N - 1) \tag{14}$$

Using Eq.(14), A can be obtained as:

$$A = -\frac{E_1}{4(N-1)} \tag{15}$$

To obtain an initial guess for the parameter λ, the role of which is to split the initially degenerate local modes, is obtained by considering the relation:

$$\lambda = \frac{E_3 - E_1}{2N} \tag{16}$$

and for the hyperfine splitting of the spectrum, the corresponding algebraic parameter is:

$$\lambda' = \frac{E_2 - E_1}{6N} \tag{17}$$

To obtain better results, a numerical fitting procedure (in a least-square sense) is required to obtain the parameters A, A', λ and λ' starting from the values as given by Eqs. (15)–(17). The initial guess for A' may be taken as zero.

The fitting algebraic parameters used in the study of vibrational spectra of the fullerene dimers $C_{120}O$ and $C_{120}O_2$ are given in Table I, whereas in Tables II and III are listed the calculated energies and their deviations from the results of a theoretical functional-based tight-binding (DF-TB) calculation.

TABLE I. Fitting algebraic parameters of the fullerene dimmers $C_{120}O$ and $C_{120}O_2$ (all the parameters are given in cm^{-1}, accept N, which is dimensionless)

Fullerene dimer	Vibron number, N	Stretching algebraic parameters		
		A	λ	λ'
$C_{120}O$	140	–0.9473	0.0175	0.0034
$C_{120}O_2$	140	–0.9367	0.0230	0.0050

TABLE II. Calculated energies (cm^{-1}) of the fullerene dimer $C_{120}O$

Normal level	I^{11}	II (this study)	Δ(I–II)	$100(I–II)/I$
ν_1	526.60	526.70	–0.10	0.00019
ν_2	529.50	529.55	–0.05	0.00009
ν_3	531.50	531.60	–0.10	0.00018

TABLE II. Continued

Normal level	I[11]	II (this study)	I–II	100(I–II)/I
ν_4	563.50	564.27	–0.77	0.00136
ν_5	568.30	567.90	0.40	0.00070
ν_6	573.40	572.90	0.50	0.00087
ν_7	576.30	576.93	–0.63	0.00109

TABLE III. Calculated energies (cm^{-1}) of the fullerene dimer $C_{120}O_2$

Normal level	I[11]	II (this study)	Δ(I–II)	100(I–II)/I
ν_1	520.80	520.85	–0.05	0.00009
ν_2	525.10	525.05	0.05	0.00009
ν_3	527.30	527.29	0.01	0.00001
ν_4	529.60	529.81	–0.21	0.00039
ν_5	563.70	564.25	–0.55	0.00097
ν_6	569.30	568.73	0.57	0.00100
ν_7	576.70	576.85	–0.15	0.00026

CONCLUSIONS

The algebraic model presented herein is a model of coupled one dimensional Morse oscillators describing the C–C, C–O stretching vibrations of the fullerene dimers $C_{120}O$ and $C_{120}O_2$. By making use of this algebraic model, the complicated integrations in the solution of coupled differential Schrödinger equations can be avoided. For the C–C and C–O stretching inter-bond interactions, this model can be useful in a simple and straightforward way and very reliable in the calculation with a small number of algebraic parameters. In this study, we presented only a small number of the fundamental modes of vibrations of $C_{120}O$ and $C_{120}O_2$ are presented, which are in good agreement with the results of functional-based tight-binding (DF-TB) calculations.[11] Hence, the method suggests that with the further advancement of this $U(2)$ algebraic model, other modes of vibrations of the molecules could also be explained and predicted for the interest of further experimental studies. This method has already successfully explained the vibrational spectra of many simple and polyatomic molecules. Thus, it can be concluded that the $U(2)$ algebraic method is a successful alternative theoretical approach to explore the hitherto unknown vibrational states of polyatomic molecules.

И З В О Д

ИСПИТИВАЊЕ ВИБРАЦИОНЕ СПЕКТРОСКОПИЈЕ ИСТЕЗАЊА $C_{120}O$ И $C_{120}O_2$ УЗ ПОМОЋ $U(2)$ ЛИЕВЕ АЛГЕБРЕ

RUPAM SEN[1], ASHIM KALYAN[1] и RAMENDU BHATTACHARJEE[2]

[1]*Department of Physics, Srikishan Sarda College, Hailakandi-788151, India и*
[2]*Department of Physics, Assam University, Silchar-788011, India*

Нивои вибрационих енергија димера ендохедралних фулерена $C_{120}O$ и $C_{120}O_2$ су израчунавани коришћењем $U(2)$ алгебре, узимајући у обзир локалне Хамилтонијане

Морзеових потенцијала. Свака молекулска веза је замењена одговарајућом Лиевом алгебром, а затим је, узимајући у обзир интеракције Казимир и Мајорана оператора, конструисан Хамилтонијан. Основни параметри вибрационог мода истезања оба димера су затим израчунати применом овог Хамилтонијана и упоређени са резултатима израчунавања методом функционалне густине и јаке везе (*functional-based tight-binding* - DFTB).

(Примљено 31. јануара, ревидирано 8. јула 2012)

REFERENCES

1. R. D. Levine, C. E. Wulfman, *Chem. Phys. Lett*. **60** (1979) 372
2. F. Iachello, *Chem. Phys. Lett*. **78** (1981) 581
3. F. Iachello, S. Oss, *Phys. Rev. Lett.* **66** (1991) 2976
4. J. Q. Chen, F. Iachello, J. L. Ping, *J. Chem. Phys.* **104** (1996) 815
5. F. Iachello, R. D. Levine, *Algebraic Theory of Molecules*, Oxford University Press, Oxford, UK, 1995
6. S. Oss, *Adv. Chem. Phys.* **93**(1996) 455
7. F. Iachello, S. Oss, *Eur. Phys. J., D* **19** (2002) 307
8. N. K. Sarkar, J. Choudhury, R. Bhattacharjee, *Mol. Phys.* **104** (2006) 3051
9. R. Sen, A. Kalyan, R. Das, N. K. Sarkar, R. Bhattacharjee, *Spectrosc. Lett.* **45** (2012) 273
10. S. R. Karumuri, N. K. Sarkar, J. Choudhury, R. J. Bhattacharjee, *Mol. Spectrosc.* **255** (2009) 183
11. M. Krause, L. Dunsch, G. Seifert, W. P. Fowler, A. Gromov, W. Krätschmer, R. Gutierez, D. Porezag, T. Frauenheim, *J. Chem. Soc., Faraday Trans.* **94** (1998) 2287
12. A. Frank, R. Lemus, R. Bijker, F. Perez-Bernal, JM. Arias, *Ann. Phys.* **252** (1996) 211
13. R. Sen, A. Kalyan, R. S. Paul, N. K. Sarkar, R. Bhattacharjee, *Acta Phys. Pol., A* **120** (2011) 407
14. R. Sen, A. Kalyan, N. K. Sarkar, R. Bhattacharjee, *Fullerenes Nanotubes Carbon Nanostruct.* **21** (2013) 403
15. R. Sen, A. Kalyan, N. K. Sarkar, R. Bhattacharjee, *Fullerenes Nanotubes Carbon Nanostruct.* **21** (2013) 429
16. K. Nakamoto, *Infrared and Raman Spectra of Inorganic and Coordination Compounds, Part A: Theory and Applications in Inorganic Chemistry*, Wiley, New York, 1997
17. K. P. Huber, G. Herzberg, *Molecular Spectra and Molecular Structure IV*: *Constants of Diatomic Molecules*, Van Nostrand Reinhold, New York, 1979.

Journal of the Serbian Chemical Society
JSCS-info@shd.org.rs • www.shd.org.rs/JSCS
J. Serb. Chem. Soc. 78 (1) 93–100 (2013)
JSCS–4399
UDC 546.659.3+546.657.3+546.131:66.061
Original scientific paper

Extraction of Sm(III) and Nd(III) with *N,N,N′,N′*-tetrabutyl-3-oxy-diglycolamide from hydrochloric acid

JINHONG YANG, YU CUI*, GUOXIN SUN, YONG NIE, GUANGMING XIA and GENGXIU ZHENG

School of Chemistry and Chemical Engineering, University of Jinan, Jinan, 250022, China

(Received 22 September 2011, revised 13 July 2012)

Abstract: The behavior of Sm(III) and Nd(III) during extraction with *N,N,N′,N′*-tetrabutyl-3-oxa-diglycolamide (TBDGA) in 70% kerosene–30 % *n*-octanol from hydrochloride acid was studied. The effects of temperature and the concentrations of hydrochloric acid and extractant on the distribution of the rare earth elements were investigated. The extraction mechanism was established and the stoichiometry of the main extracted species was confirm to be $SmCl_3$·2TBDGA and $NdCl_3$·2TBDGA for Sm(III) and Nd(III), respectively. The extraction distribution ratio decreased with increasing temperature, which demonstrates that the extraction reaction is exothermic. The IR spectra of the loaded organic phase and free extractant were recorded and are discussed.

Keywords: 3-oxa-diglycolamide; hydrochloric acid; stoichiometry; lanthanides; distribution ratio.

INTRODUCTION

The rare earth elements have an important position in the exploration and preparation of new functional materials due to their electronic configuration and changeable radius of their atom and ion. Therefore, pure and simple rare earth elements are necessary.[1] Solvent extraction has been the main means in partition and purification of rare earth elements due to its rapid reaction rates and good separation effects.[2,3]

Although tetrabutyl phosphate (TBP) has been used, 3-oxy-diglycolamides were selected as prospective extractants in this research project because they are widely used in nuclear fuel reprocessing. The products of radiolytic and hydrolytic degradation of amides are less detrimental to the extraction and separation processes than those of organic phosphorus extractants.[4,5] The amide ligands are completely incinerable, which implies that secondary wastes generated during

* Corresponding author. E-mail: chm_cuiy@ujn.edu.cn
doi: 10.2298/JSC110922077Y

nuclear waste treatment could be significantly reduced.[6,7] Moreover, they exhibited higher extractability than amides due to the soft ether oxygen atom.[8] The extraction behavior of actinides and lanthanides with 3-oxy-diglycolamides from nitric acid medium has been reported.[9–12] However, rare earth elements are usually recovered from hydrochloric acid medium. Therefore, it is important to study the extraction and separation of lanthanides with new extractants from hydrochloric acid medium. The extraction of lanthanides from hydrochloric acid media is very important for the hydrometallurgy and recycling process of lanthanides. To the best of our knowledge, there has only been one report[13] of the extraction performances of lanthanides from HCl with amides.

The effect of diluents on the extraction behavior of the neutral extractant was reported in a previous paper.[14] It was found that the extraction capacity was related to the polarity of the diluents. The extraction distribution ratios were lower in alkane and/or aromatic diluents than that in mixed diluents composed of a polar alcohol and an alkane. The extraction behavior of lanthanides with *N*,*N*,*N*′,*N*′-tetrabutyl-3-oxa-diglycolamide (TBDGA) employing a 70 % kerosene–30 % *n*-octanol mixture as diluent from a hydrochloric acid system was investigated in this work. Kerosene and *n*-octanol were selected they are cheaper than other solvents.

EXPERIMENTAL

Reagents

N,*N*,*N*′,*N*′-Tetrabutyl-3-oxy-diglycolamide (TBDGA) was laboratory synthesized in a three-step process.[15] The final product was characterized by elemental analysis and IR and ^{1}H-NMR spectroscopy and the purity was higher than 98 %. The other employed chemical reagents were all of A.R. grade.

Preparation of the Sm(III) and Nd(III) solutions

Sm_2O_3 (1.7436 g) was dissolved in 20 mL of 12.66 mol·dm^{-3} HCl solution and the solution was then evaporated carefully to dryness. The residue was dissolved in 2 mL 12.66 mol·dm^{-3} HCl and diluted to 100 mL with distilled water. The obtained solution contained 0.100 mol·dm^{-3} Sm^{3+} and 0.25 mol·dm^{-3} HCl. A series of 4.00×10^{-3} mol·dm^{-3} Sm^{3+} solutions were then prepared by quantitative dilution. The Nd(III) solutions were prepared in a similar method.

Extraction of Sm(III) and Nd(III) with TBDGA

In the studies of the extraction distribution of Sm(III) and Nd(III), solutions of the desired concentration of TBDGA in 70 % kerosene–30 % *n*-octanol were employed after pre-equilibration with the respective acidities. Equal volumes of organic and aqueous phases were agitated for 30 min (enough for equilibrium) at 25 °C under the desired experimental conditions. The two phases were then centrifuged and assayed by taking known aliquots (0.05––0.10 mL) from the aqueous phase. The concentrations of Sm(III) or Nd(III) remaining in the sample were determined by the Arsenazo-III visible spectrophotometric method[19] and those in organic phase were obtained by subtracting the aqueous concentrations from the total initial aqueous concentration of Sm(III) or Nd(III). The extraction distribution ratio (*D*) was cal-

culated as the ratio of the concentration of Sm(III) or Nd(III) in the organic phase to that in the aqueous phase.

Characterization of the extracted species

After the extracted species had been prepared, the TBDGA solution was shaken with a concentrated solution of $SmCl_3$ or $NdCl_3$, centrifuged and the organic phase separated. The organic solvent was removed and the IR spectra of the residue were recorded using an FTS-165 IR spectrometer in the range 400–4000 cm^{-1}. The scan times and the resolution were 60 and 2 cm^{-1}, respectively.

RESULTS AND DISCUSSION

Effect of HCl concentration

The effect of the concentration of HCl on the extraction behaviors of Sm(III) and Nd(III) with TBDGA are shown in Fig. 1. The distribution ratios of Nd(III) increased with increase in HCl concentration in the range of 1.00–5.00 mol dm^{-3}. However, the distribution ratios of Sm(III) increased to a maximum value at about 3.5 mol dm^{-3} HCl and then slowly decreased with further increase in the HCl concentration. This phenomenon is different from that reported in nitric acid medium.[12] That the distribution of both Sm(III) and Nd(III) increases significantly under low acidity conditions may be due to the co-ion effect which plays a crucial role. The coordinated anions formed by lanthanide ions and chloride anions under high acidity could not be extracted, which resulted in the slow distribution decrease for Sm(III). It is inferred that the extraction distribution of Nd(III) may reach a maximum value above 5 mol dm^{-3} HCl, which will be investigated further in future work.

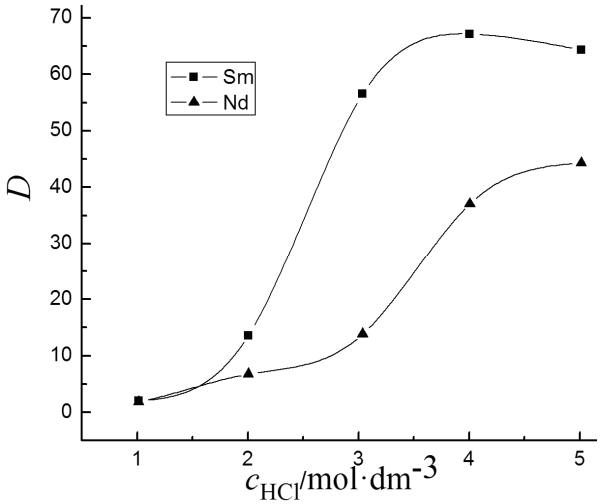

Fig. 1. Effect of the HCl concentration on the extraction distribution of Sm(III) and Nd(III). $c_{M^{3+}} = 4.00\times10^{-3}$ mol·dm^{-3}; $c_{TBDGA} = 0.10$ mol·dm^{-3}.

Effect of TBDGA concentration

The chemical reaction involved during the extraction of metal ions from hydrochloric acid medium by TBDGA in 70 % kerosene–30 % *n*-octanol can be described as follows:

$$M^{3+} + 3Cl^- + n\text{TBDGA} = MCl_3 \cdot n\text{TBDGA} \quad (1)$$

where n was determined by slope analysis method. The logarithm of the distribution ratio is plotted as a function of the logarithm of the initial concentration of TBDGA in Fig. 2. The distribution ratio increases with an increasing concentration of TBDGA.

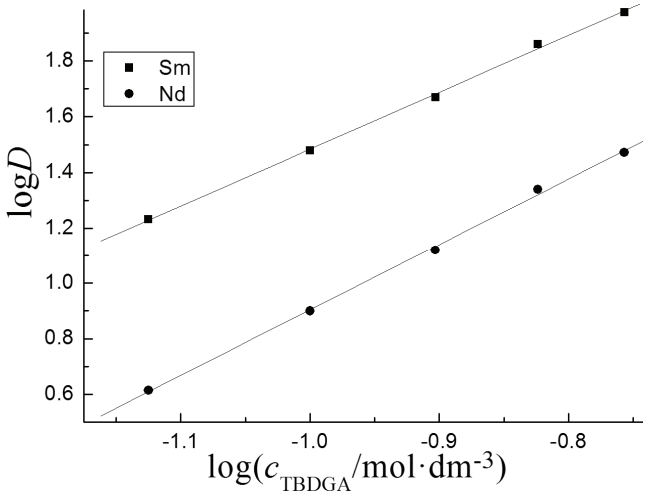

Fig. 2. Effect of the TBDGA concentration on the extraction distribution of Sm(III) and Nd(III). $c_{M^{3+}} = 4.00\times10^{-3}$ mol·dm^{-3}; $c_{HCl} = 2.50$ mol·dm^{-3}.

The plots of log D *vs*. log TBDGA for both Sm(III) and Nd(III) gave slopes of about 2, which suggests that the stoichiometries of the extracted species were $SmCl_3 \cdot 2$TBDGA and $NdCl_3 \cdot 2$TBDGA. Thus, the chemical reactions can be expressed as follows:

$$Sm^{3+} + 3Cl^- + 2\text{TBDGA} = SmCl_3 \cdot 2\text{TBDGA} \quad (2)$$

$$Nd^{3+} + 3Cl^- + 2\text{TBDGA} = NdCl_3 \cdot 2\text{TBDGA} \quad (3)$$

The apparent equilibrium constants for Sm(III) and Nd(III), K_{ex1} and K_{ex2}, respectively, are:

$$K_{ex1} = \frac{c_{SmCl_3 \cdot 2\text{TBDGA}}}{c_{Sm^{3+}} c^2_{\text{TBDGA}} c^3_{Cl^-} \gamma_{M^{3+}} \gamma^3_{Cl^-}} \quad (4)$$

$$K_{ex2} = \frac{c_{NdCl_3 \cdot 2TBDGA}}{c_{Nd^{3+}} c^2_{TBDGA} c^3_{Cl^-} \gamma_{M^{3+}} \gamma^3_{Cl^-}} \quad (5)$$

where $\gamma_{Sm^{3+}}$, $\gamma_{Nd^{3+}}$ and γ_{Cl^-} are the activity coefficients of Sm^{3+}, Nd^{3+} and Cl^-, respectively.

The total concentration of Sm(III) and Nd(III) in aqueous phase can be written:

$$c_M = c_{M^{3+}} \left(1 + \beta_1 c_{Cl^-}\right) \quad (6)$$

where β_1 is the coordination constant of metal ions with Cl^-. It is much more difficult for Cl^- to coordinate with Sm^{3+} and Nd^{3+} than with a water molecule. Therefore, Eq. (6) can be simplified as:

$$c_M \approx c_{M^{3+}} \quad (7)$$

The distribution ratio (D) is given by:

$$D = \frac{c_{M^{3+}(o)}}{c_{M^{3+}}} = \frac{c_{MCl_3 \cdot n TBDGA}}{c_{M^{3+}}} \quad (8)$$

Hence, K_{ex} can be written as:

$$K_{ex} = \frac{D}{c^3_{Cl^-} c^n_{TBDGA_{(o)}} \gamma_{M^{3+}} \gamma^3_{Cl^-}} \quad (9)$$

The values of $\gamma_{M^{3+}}$ and γ_{Cl^-}, calculated according to the Debye–Hückel Formula,[16] were 0.9011 and 0.9659, respectively. The values of log K_{ex} calculated from Eq. (9) are 2.30±0.12 for Sm^{3+} and 1.82±0.05 for Nd^{3+}.

Effect of temperature on the extraction distribution ratio of Sm(III) and Nd(III)

The effect of temperature on the extraction equilibrium is given in Fig. 3. The distribution ratio decreased with increasing temperature, which demonstrated that the extraction reaction is an exothermic process. The change in enthalpy, ΔH, in each case was evaluated using the Van't Hoff Equation:

$$\left[\frac{\partial \log D}{\partial (1/T)}\right]_p = \frac{-\Delta r H^\theta_m}{2.303R} \quad (10)$$

The values of enthalpy change obtained for the extraction of Sm(III) and Nd(III) were –68.54 and –35.70 kJ mol^{-1}, respectively. These values indicate that the extraction reaction is enthalpy favored.[17]

Spectroscopic studies of the extracted species

The IR spectrum of TBDGA and the extracted species are shown in Fig. 4. Compared with the free extractant, the C=O stretching vibration of the extracted

species were shifted to lower frequencies, to 1619 cm^{-1} for Sm(III) and to 1623 cm^{-1} for Nd(III). These results are consistent with the observation by Sasaki of the complex of Eu(III) with *N*,*N*,*N*′,*N*′-tetra(*n*-octyl)-3-oxy-diglycolamide (TODGA),[18] In addition, the C–O stretching band at 1134 cm^{-1} in spectrum of TBDGA was shifted slightly after extraction.[15] The above results indicate that the three oxygen atoms of the two carbonyl groups and alkoxyl group are all co-ordinated with Sm(III) and Nd(III) in the extracted species; in other words, TBDGA is a tridentate ligand.

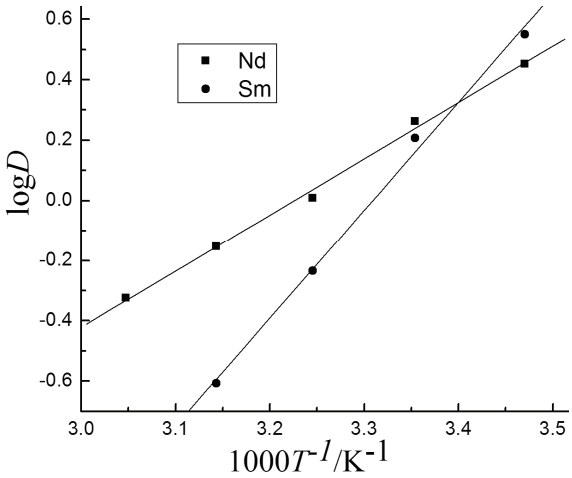

Fig. 3. Effect of temperature on the extraction distribution of Sm(III) and Nd(III). c_M^{3+} = = 4.00×10^{-3} mol·dm^{-3}; c_{TBDGA} = = 0.1 mol·cm^{-3}; c_{HCl} = 1.00 mol·dm^{-3}.

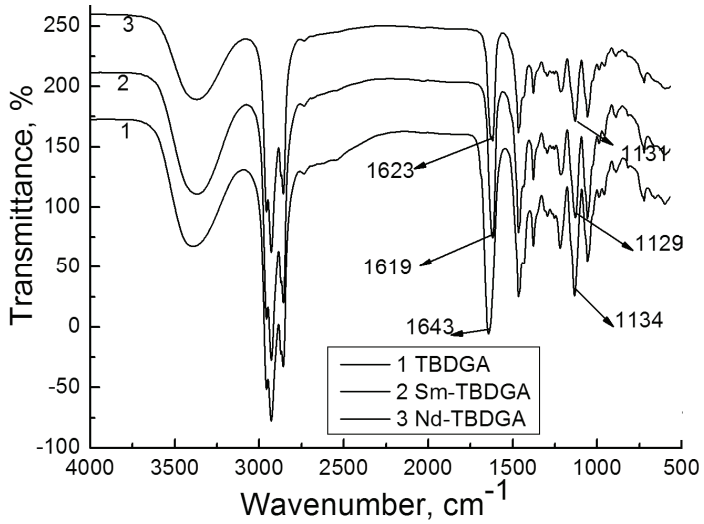

Fig.4. IR Spectra of the extractant and extracted species in 70 % kerosene–30 % *n*-octanol.

CONCLUSIONS

Sm(III) and Nd(III) can be extracted effectively from hydrochloric acid solution using TBDGA in 70 % kerosene–30 % *n*-octanol. The extractability of TBDGA for Sm(III) was higher than that for Nd(III). The distribution ratio increased with increasing concentration of HCl at low concentrations. The values of *D* increased with increasing TBDGA concentration. The stoichiometries of the extracted species can be described as $SmCl_3 \cdot 2TBDGA$ and $NdCl_3 \cdot 2TBDGA$. The extraction reactions are exothermic, and increasing temperature has a negative impact on the extraction process. From IR spectroscopy, it could be concluded that TBDGA forms tridentate complexes with Sm(III) or Nd(III) through its three oxygen atoms of carbonyl group and alkoxyl group.

Acknowledgments. The authors are grateful for the support from the National Nature Science Foundation of China (21077044 and 21171069) and Natural Science Foundation of Shandong Province (ZR2009BM046).

И З В О Д

ЕКСТРАКЦИЈА Sm(III) И Nd(III) ИЗ ХЛОРОВОДОНИЧНЕ КИСЕЛИНЕ ПОМОЋУ *N*,*N*,*N*′,*N*′-ТЕРАБУТИЛ-3-ОКСИ-ДИГЛИКОЛАМИДА

JINHONG YANG, YU CUI, GUOXIN SUN, YONG NIE, GUANGMING XIA и GENGXIU ZHENG

School of Chemistry and Chemical Engineering, University of Jinan, Jinan, 250022, China

Испитана је екстракција Sm(III) и Nd(III) из хлороводоничне киселин помоћу *N*,*N*,*N*′,*N*′-терабутил-3-окси-дигликоламида (TBDGA) у раствору 70 % керозина–30 % *n*-октанола. Истражен је утицај концентрације хлороводоничне киселине, концентрације екстранта и темпеаратуре на дистрибуцију ових ретких земаља. Установљен је екстракциони механизам и потврђена је стехиометрија основних екстрахованих врста: $SmCl_3 \cdot 2TBDGA$ за Sm(III) и $NdCl_3 \cdot 2TBDGA$ за Nd(III). Дистрибуциони однос екстракције се смањује са повећањем температуре, указујући да је реакција екстракције егзотермна. Снимљени су и дискутовани инфрацрвени (IR) спектри органске фазе и слободног екстранта.

(Примљено 22. септембра 2011, ревидирано 13. јула 2012)

REFERENCES

1. X. Huang, H. Li, C. Wang, G. Wang, X. Xue, G. Zhang, *Chin. J. Rare Metals* **31** (2007) 279
2. M. Atanassova, *J. Serb. Chem. Soc*. **73** (2008) 29
3. E. A. Mowafy, H. F. Aly, *Solvent Extr. Ion Exch*. **25** (2007) 205
4. G. Sun, Y. Cui, R. Jiang, R. Xu, S. Sun, *J. Serb. Chem. Soc.* **67** (2002) 653
5. M. Bao, G. Sun, *J. Radioanal. Nucl. Chem.* **231** (1998) 203
6. Y. Jin, L. Feng, S. Ding, C. Xia, W. Chen, G. Ye, *Chem. Res. Appl.* **14** (2002) 174
7. Y. Cu, G. Sun, Y. Li, Z. Zhang, S. Sun, *Chin. J. Inorg. Chem.* **21** (2005) 1723
8. G. M. Gasparini, G. Grossi, *Solvent Extr. Ion. Exch.* **4** (1986) 1233
9. D. Magnusson, B. Christiansen, J. P. Glatz, R. Malmbeck, G. Modolo, D. S. Purroy, C. Sorel, *Solvent Extr. Ion Exch.* **27** (2009) 26

10. M. T. Murillo, A. G. Espartero, J. Sanchez-Quesada, J. Mendoza, P. Prados, *Solvent Extr. Ion Exch.* **27** (2009) 107
11. M. Husain, S. A. Ansari, P. K. Mohapatra, R. K. Gupta, V. S. Parmar, V. K. Manchanda, *Desalination* **229** (2008),:294
12. Y. Zhang, Y. Cui, Y. Hu, G. Sun, *Chin. J. Inorg. Chem.* **26** (2010) 663
13. G. Wu, J. Yang, G. Xia, Y Cui, G Sun, *Chin, J. Inorg. Chem.* **27** (2011) 315
14. G. Yang, *Master Thesis*, University of Jinan, 2010
15. G. Sun, M. Liu, Y. Cui, M. Yuan, S. Yin, *Solvent Extr. Ion. Exch.* **28** (2010) 482
16. A. D. John, *Lange's Handbook of Chemistry*, McGraw-Hill, New York, 1978
17. S. M. Ghag, S. D. Pawar, *J. Serb. Chem. Soc*. **75** (2010) 1549
18. Y. Sasaki, P. Rapold, M. Arisaka, M Hirata, T Kimura, C Hill, G Cote, *Solvent Extr. Ion Exch.* **25** (2007) 187
19. H. Rohwer, N. Collier, E. Hosten, *Anal. Chim. Acta* **314** (1995) 219.

Journal of the Serbian Chemical Society
JSCS-info@shd.org.rs • www.shd.org.rs/JSCS
J. Serb. Chem. Soc. 78 (1) 101–114 (2013) UDC 546.185–034.1+669.14+621.793:544.351.3
JSCS–4400 *Original scientific paper*

Determination of surface coverage of iron-phosphate coatings on steel using the voltammetric anodic dissolution technique

JOVAN P. POPIĆ[1#], BORE V. JEGDIĆ[2#], JELENA B. BAJAT[3#], MIODRAG MITRIĆ[4] and VESNA B. MIŠKOVIĆ-STANKOVIĆ[3#*]

[1]ICTM-Department of Electrochemistry, University of Belgrade, Njegoševa 12, Belgrade, Serbia, [2]Institute GOŠA, Milana Rakića 35, 11000 Belgrade, Serbia, [3]Faculty of Technology and Metallurgy, University of Belgrade, Karnegijeva 4, P. O. Box 3503, 11120 Belgrade, Serbia and [4]Vinča Institute of Nuclear Sciences, P. 0. Box 522, 11001 Belgrade, Serbia

(Received 6 July, revised 13 September 2012)

Abstract: In this study, the effect of deposition time and concentration of $NaNO_2$ in the phosphate bath on the surface morphology of iron-phosphate coatings on low carbon steel was investigated using scanning electron microscopy (SEM) and atomic force microscopy (AFM). The composition of iron-phosphate coatings was determined using energy dispersive X-ray spectroscopy (EDS) and X-ray diffraction (XRD), while surface coverage was evaluated by the voltammetric anodic dissolution (VAD) technique in the borate solution. The addition of $NaNO_2$ to the phosphate bath significantly increased the surface coverage since better packed crystals of smaller size, which favour the phosphate nucleation, were obtained. It was also shown that prolonged deposition time increased the surface coverage, coating roughness and crystal size in the lateral direction, altering also the crystal shape from large platelets non-uniformly distributed on the steel surface during the initial time to better-packed laminated and needle-like structures during prolonged exposure.

Keywords: low carbon steel; iron-phosphate coatings; surface coverage; VAD; AFM.

INTRODUCTION

Corrosion resistance of a metal/organic coating system largely depends on the pre-treatment of the metal surface prior to organic coating deposition. The pre-treatment of the metal surface usually includes degreasing of the metal and formation of a conversion coating on the surface with the aim of increasing the corrosion resistance and adhesion strength between metal and organic coating. In practice, zinc-phosphate coatings, manganese-phosphate coatings, zinc-manga-

* Corresponding author. E-mail: vesna@tmf.bg.ac.rs
# Serbian Chemical Society member.
doi: 10.2298/JSC120706096P

nese-phosphate coatings and zinc-calcium-phosphate coatings have usually been used as conversion coatings on steel, aluminium, magnesium and zinc.[1–9] Iron-phosphate coatings showed less corrosion stability in respect to zinc-phosphate coatings,[5,10–12] but together with top organic coatings, good corrosion protection of steel could be achieved.[11,13–19] It was shown that steel pre-treatment with an iron-phosphate coating increased the adhesion strength of the organic coating, as well as the corrosion stability of the protective system, as compared to organic coating on a bare steel substrate.[3,13,14] The advantages of iron-phosphate pre-treatment are the simple and cheap equipment and waste water treatment.

The quality of the iron-phosphate layers greatly depends on the fraction of the total surface area covered by the phosphate coating. Various factors affect the surface coverage, in particular the composition of the deposition bath, bath temperature, deposition time, the morphology of the deposit and additives (accelerators) used in the electrolyte.

Various types of chemical accelerators for phosphating can be used, such as sodium nitrite, nitrates and chlorates.[1,3–5,10–12] Previous research[20,21] indicated that iron-phosphate coatings on steel surface do not have great surface coverage. It was shown that the addition of formic acid, sodium chlorate, or sodium nitrobenzenesulphonate in the phosphating solution increased the surface coverage of phosphate coatings.[17,18,20,22]

The surface coverage of phosphate coatings is usually measured using electrochemical methods: polarization resistance measurements,[23–25] electrochemical impedance spectroscopy,[24–26] corrosion potential and corrosion current measurements.[24,27] The voltammetric anodic dissolution (VAD) technique,[28–30] as an electrochemical method for the determination of surface coverage, has been used lately. This technique is based on the dissolution and passivation of a coated or uncoated metal surface.

In this work, the surface morphology of iron-phosphate coatings deposited on low carbon steel was investigated as a function of the deposition time and concentration of $NaNO_2$ in the phosphating bath. The surface coverage of these coatings was quantitatively determined using the VAD method, with the aim of obtaining iron-phosphate coatings with the highest surface coverage and, consequently, with better corrosion stability.

EXPERIMENTAL

Sample preparation

Low carbon steel panels (50 mm×25 mm×0.8 mm) were used as the substrate for iron-phosphate coating deposition. The chemical composition of the low carbon steel was (wt. %): C, 0.119; Si, 0.019; Mn, 0.250; P, 0.019; S, 0.014; Cr, 0.012 and Ni, 0.019.

Prior to the deposition of the iron-phosphate coatings, the steel panels were polished with SiC papers #220, #400 and #600, degreased in 0.2 g dm^{-3} nonylphenol ethoxylate at room temperature for 5 min and rinsed with distilled water. The iron-phosphate coatings were

formed chemically by immersion in the phosphating bath containing 0.92 g dm^{-3} H_3PO_4, 0.34 g dm^{-3} NaOH and 0.125 g dm^{-3} nonylphenol ethoxylate at 50 °C for different times (from 30 s to 15 min). The iron-phosphate coatings were deposited on steel in the phosphating bath without or with the addition of $NaNO_2$ as an accelerator, at different concentrations: 0.1, 0.5 and 1.0 g dm^{-3}. All solutions were prepared with analytical grade chemical compounds and deionised water.

Surface coverage measurements

The surface coverage of the iron-phosphate coatings on low carbon steel was determined using the electrochemical voltametric anodic dissolution (VAD) technique, in which the passivation charge of the substrate is measured. The VAD was recorded in 0.3 mol dm^{-3} H_3BO_3 + borax ($Na_2B_4O_7 \cdot 10H_2O$), pH 7.6, with a potential sweep rate of 2 mV s^{-1} starting from the open circuit potential (OCP), using a GAMRY Reference 600 potentiostat–galvanostat/ZRA.

Borate solution was chosen because when immersed in this solution during anodic polarization, low carbon steel actively dissolves at potentials near to the corrosive ones,[31-33] while further polarization leads to steel passivation. In addition, it was stated in the literature[28] that iron-phosphate coatings do not dissolve in neutral solutions.

Surface morphology

The surface morphology of the bare steel and iron-phosphate coatings on steel was investigated by atomic force microscopy (AFM), operated in the contact mode under ambient conditions, at a scan rate 0.7 Hz, scan angle 0, scan points 256 and scan lines 256 using an Asylum model MFP-3D microscope.

The microstructure of the iron-phosphate coatings was examined by scanning electron microscopy (SEM) using a JSM-6390 LV (JEOL) instrument. The compositional analysis was realized using an energy dispersive spectroscopy (EDS) attachment on the scanning electron microscope.

XRD measurements

X-Ray diffraction (XRD) measurements were performed on a Philips PW 1050 powder diffractometer with Ni filtered CuK_α radiation (λ = 1.5418 Å) and a scintillation detector within the 15−80° 2θ range in 0.05° steps with a scanning time of 45 s per step. The quailtative analysis of the samples was performed by XRD analysis based on the identification of the peaks using commercially available EVA software (DIFFRACplus EVA). The phases were identified using the Powder Diffraction File (PDF) database (JCPDS, International Centre for Diffraction Data).

RESULTS AND DISCUSSION

Surface morphology

The surface morphology of iron-phosphate coatings was investigated using the SEM and AFM techniques, commonly used in analyzing the surface morphology of coatings.[34,35] Low carbon steel was phosphated for different times: 5, 10 and 15 min, with the aim of investigating the influence of deposition time on the morphology and composition of the iron-phosphate coatings. Fig. 1 shows The SEM microphotographs of the bare steel (a) and of the iron-phosphate coatings deposited at different times (b, c and d). The sporadic small spots on the

bare steel (Fig. 1a) are probably the result of mechanical damage during polishing. The different surface coverage of steel with iron-phosphate coatings deposited for different phosphating times can be seen in Figs. 1b–1d. Small crystal nuclei of the iron-phosphate coating sporadically emerged during a deposition time of 5 min, while bigger crystals grew during longer deposition times.

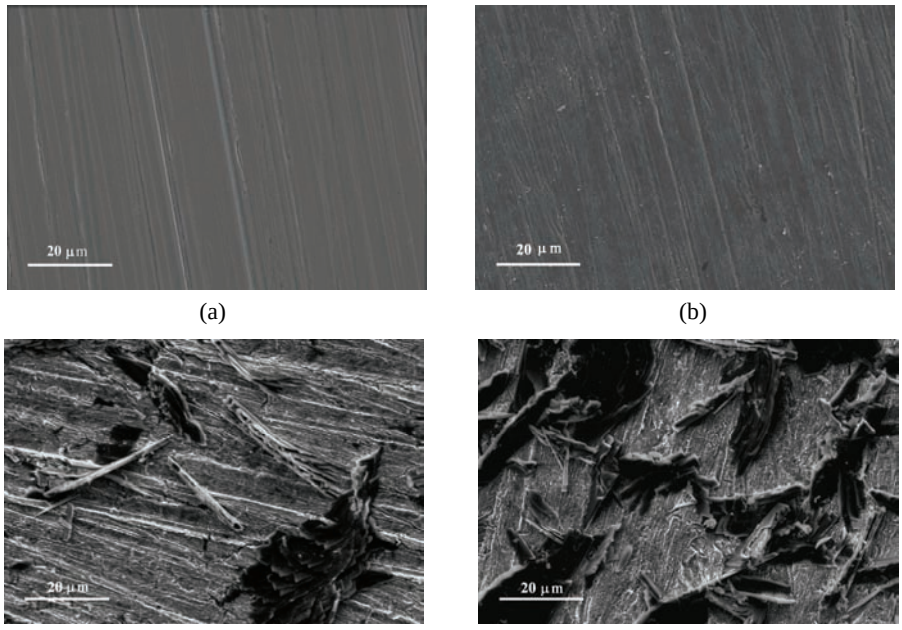

(a) (b)

(c) (d)

Fig. 1. Microphotographs of the steel surface prior to (a) and after phosphating for b) 5, c) 10 and d) 15 min.

The iron-phosphate crystals in the shape of platelets, non-uniformly distributed on the steel surface were obtained during a deposition time of 5 min (not shown). Their grain size, estimated by AFM, was 3–9 µm, while longer deposition times favoured lateral crystal growth of up to 15 µm during 15 min (Fig. 2 and Table I). Based on several AFM measurements on different surface spots, it could be observed that during prolonged deposition, the crystals grew in the normal direction only up to 1.2 µm in height, regardless of the deposition time. The values of surface roughness (*RMS*), derived from AFM images, are presented in Table I. The *RMS* value for the polished bare steel was 55 nm, while the *RMS* values of the iron-phosphate coatings deposited up to 10 min significantly increased to 280 nm. The observed increase in roughness is the result of the nucleation and growth of iron-phosphate crystals on the steel surface with prolonged

deposition time. It could also be noticed that the values of the *RMS* did not significantly change deposition times longer than 10 min were employed.

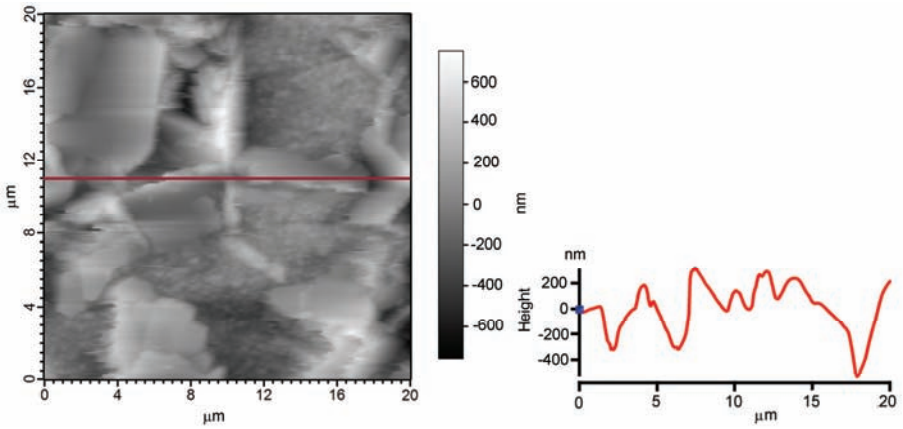

Fig. 2. AFM Image and height profile of the iron-phosphate coating on steel deposited during 15 min.

TABLE I. The values of *RMS*, grain size, passivation current, i_p, passivation charge density, Q_{pass}, surface coverage, Θ, and composition of the iron-phosphate coatings deposited with and without $NaNO_2$ in the plating bath

Substrate	Deposition time, min	$c(NaNO_2)$ g dm^{-3}	*RMS* nm	Grain size range µm	I_p µA cm^{-2}	Q_{pass} mC cm^{-2}	Θ %	Concentration at. %		
								O	P	Fe
Bare steel	–	–	55	–	294	12.3	0	–	–	–
Iron-phosphate coating	5	0	215	3–9	208	9.14	26.1	2.05	1.03	96.92
		0.1	–	–	122	5.48	55.3	–	–	–
		0.5	147	4–6	110	4.96	59.5	7.88	4.67	80.14
		1.0	–	–	95	4.30	64.9	–	–	–
	10	0	280	4–10	161	7.58	38.2	3.41	2.66	93.93
	15	0	270	5 –15	149	7.26	40.8	5.87	3.66	90.46

The EDS measurements provided information about the concentrations of particular elements on the surface of the phosphate coatings. The EDS spectra showed that the iron-phosphate coatings contained iron, oxygen and phosphorus. The semi-quantitative elemental compositions, obtained from the EDS analysis, are given in Table I. It could be noticed that the concentrations of oxygen and phosphorus increased with increasing deposition time, while that of iron decreased, indicating the growth of phosphate coatings with longer deposition time.

The phase composition of iron-phosphate coatings was determined by XRD analysis (Fig. 3). The phases present in the phosphate layers were mainly $FePO_4$ (according to PDF No. 01-072-2124 (ICSD 040863)), Fe_2O_3 (according to PDF

No. 00-052-1449) and Fe_3O_4 (according to PDF No. 01-079-0416 (ICSD 065338)).

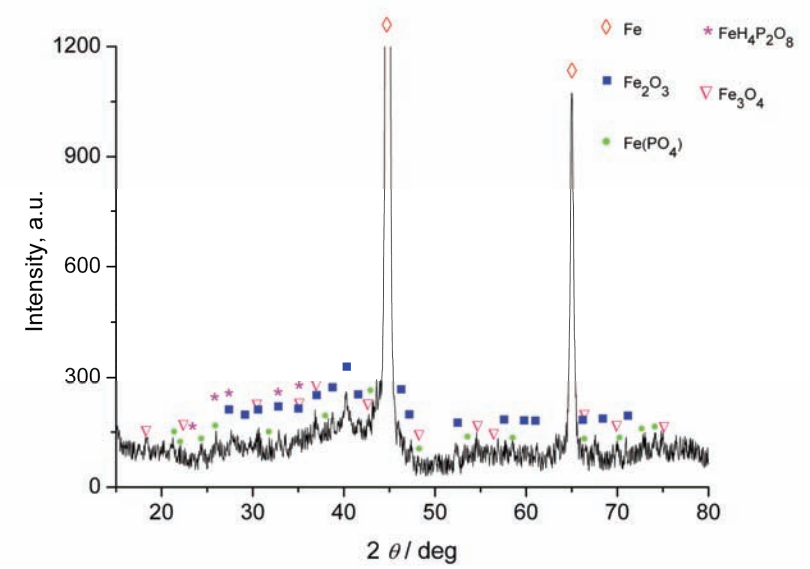

Fig. 3. XRD Pattern of an iron-phosphate coating on steel (deposition time: 5 min).

The formation of iron phosphate coating on steel occurs through reactions (1) and (2).[8] NaH_2PO_4 is formed from the H_3PO_4 and NaOH present in the plating bath:

$$Fe + 8NaH_2PO_4 + 4H_2O + 2O_2 \rightarrow 4Fe(H_2PO_4)_2 + 8NaOH \quad (1)$$

$$2Fe(H_2PO_4)_2 + 2NaOH + 1/2O_2 \rightarrow 2FePO_4 + 2NaH_2PO_4 + 3H_2O \quad (2)$$

In parallel, in the presence of oxygen (from the water-based phosphating bath), metallic iron is oxidized and $Fe(OH)_2$ and $Fe(OH)_3$ are formed on the iron surface. Iron hydroxides change gradually to iron oxide, Fe_2O_3 and Fe_3O_4, resulting in the formation of a passive film on the steel.[36]

Based on the AFM results, it could be concluded that two types of phosphate crystals were formed on the steel surface immersed in the phosphating solution: platelets, during initial deposition time, and laminated and needle-like crystals, during prolonged deposition times. The growth of iron-phosphate crystals starts with heterogeneous nucleation on the steel surface. Initially, the phosphate crystals grow in both the normal and lateral directions. During prolonged deposition, the crystals grow in the normal direction only up to 1.2 μm, regardless of the deposition time. Longer deposition times favour lateral crystal growth, up to 15 μm for a deposition time of 15 min (Table I). Extension of the phosphating time also

leads to the nucleation and growth of new crystals on the steel surface. In this way, longer deposition times result in greater surface coverage (Figs. 1 and 2) and greater amounts of phosphate deposit were obtained with greater amounts of oxygen and phosphorus, determined by EDS analysis (Table I). However, the iron-phosphate coating formed on the low carbon steel was not compact and the coating was significantly porous even after 15 min of phosphating.

Surface coverage

The surface coverage of iron-phosphate coatings on steel was determined by the VAD method in borate solution. Several solutions were tested but the borate solution was the most suitable. Namely, during anodic polarization in borate solution, steel is dissolved at potentials around the corrosion potentials, and during further polarization steel passivated.

Since the iron-phosphate coatings on steel contain iron phosphate and iron oxide,[5,8] their dissolubility in neutral borate solutions becomes questionable. However, bearing in mind that the rate of dissolution of Fe_2O_3 in slightly acidic and neutral solutions is very low,[20,31,33,37] this solution was adequate. Ptacek *et al.*[20] also showed that the rate of iron phosphate dissolution in slightly acidic solutions is very low. Thus, it was concluded that VAD method in borate solution could be used to determine the surface coverage of iron-phosphate coatings on steel.

Anodic polarization curves for bare steel and steel with iron-phosphate coatings in borate solution are shown in Fig. 4. During the anodic polarization of bare steel, the current passivation peak occurred at a potential of around –0.55 V.

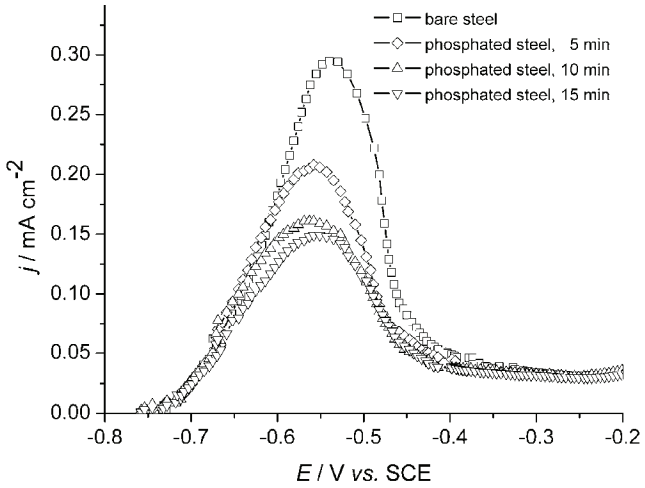

Fig. 4. Voltammetric anodic dissolution (VAD) curves in borate solution (pH 7.6) for bare steel and iron-phosphate coatings on steel, deposited during different deposition times.

The iron-phosphate coatings decreased the anodic dissolution of steel, as well as the anodic current passivation peaks (i_p). Increasing the coating deposition time resulted in decreased anodic dissolution of the steel. The values of anodic current passivation peaks, determined from VAD measurements for each phosphating condition, are given in Table I. The amount of passivation charge density (Q_{pass}) was calculated based on the measured experimental data, *i.e.*, from the value of the current of the anodic dissolution from the corrosion potential to the passivation peak and the duration of anodic dissolution until the passivation peak. Passivation charge density for bare steel surface was 12.26 mC cm^{-2}. This charge is defined as Q°_{pass} (the standard passivation charge density). The formation of the iron-phosphate coating on the steel surface led to a decrease in Q_{pass}.

Comparison of the passivation charge density of the bare substrate, Q°_{pass}, and that of the coated substrate, Q_{pass}, supplies the surface coverage, which is expressed by:

$$\Theta = 1 - \frac{Q_{pass}}{Q^{\circ}_{pass}} \quad (1)$$

where Θ is surface coverage, or the fraction of substrate area covered by the coating.

The values of the passivation charge density and surface coverage by the iron-phosphate coatings obtained during different phosphating times are given in Table I.

Based on the results presented in Fig. 4 and Table I, it could be concluded that the surface coverage by an iron-phosphate coating on the steel surface was greater when the deposition time was longer. The surface coverage by the iron-phosphate coating formed on the steel surface during 5 min was very low (26.1 %). A longer deposition time (10 min) resulted in increased surface coverage of iron-phosphate coating and the highest surface coverage (40.8 %) was obtained with the longest deposition time (15 min). It should be noted that even the highest surface coverage of 40.8 % is not actually significant, especially bearing in mind the long deposition time. The results of the electrochemically obtained surface coverage measurements (Fig. 4) are in a good agreement with the morphology of iron-phosphate coatings, shown in Figs. 1 and 2. This means that the application of the fast electrochemical method can very precisely determine the surface coverage of the iron-phosphate coating on the steel surface.

The effect of $NaNO_2$

Different amounts of $NaNO_2$ were added to the phosphating bath with the aim of accelerating the formation process of iron-phosphate coatings and obtaining better surface coverage by the deposited coatings. The anodic polarization

curves in borate solution are shown in Fig. 5. The obtained values of anodic current passivation peaks, passivation charge density and the surface coverage of the iron-phosphate coatings are given in Table I.

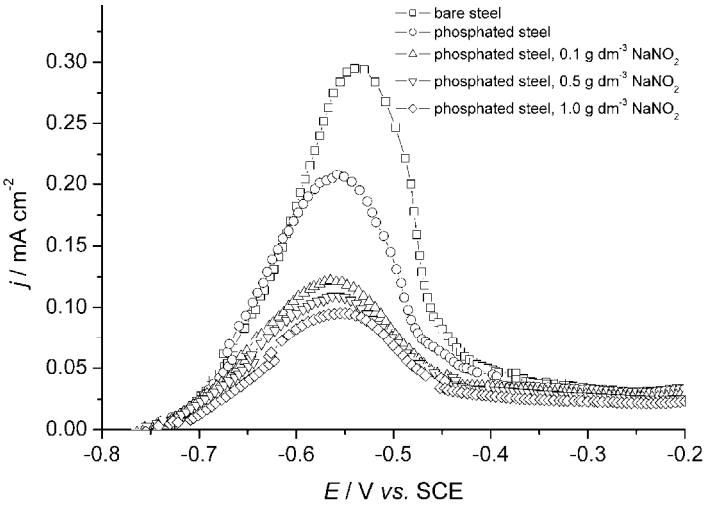

Fig. 5. Voltammetric anodic dissolution (VAD) curves in borate solution (pH 7.6) for bare steel and iron-phosphate coatings on steel deposited during 5 min without and with different concentrations of $NaNO_2$ in the plating bath.

Based on these results, it could be concluded that the addition of $NaNO_2$ to the phosphate solution significantly increased the surface coverage. Even a small amount of $NaNO_2$ (0.1 g dm^{-3} $NaNO_2$) in the plating bath increased the surface coverage from 26.1 to 55.3 % (Table I). On increasing the $NaNO_2$ concentration in the bath resulted in even higher surface coverage. The highest surface coverage (64.9 %) was obtained with 1.0 g dm^{-3} $NaNO_2$ in the bath. A concentration of 0.5 g dm^{-3} was chosen for further examination for both economical and environmental reasons, since the surface coverage did not significantly increase when the concentration of $NaNO_2$ was increased from 0.5 to 1.0 g dm^{-3}.

In order to monitor the nucleation and initial growth of iron-phosphate coatings deposited having $NaNO_2$ in the bath, the morphology of the coatings deposited from a bath with 0.5 g dm^{-3} of $NaNO_2$ during different times was analyzed (Fig. 6). It is evident that even after 0.5 min, centres of phosphate crystal nucleation had been formed (Fig. 6b). Extending the phosphating time to 1.0 min caused further growth of the single phosphate crystals (Fig. 6c). After 5.0 min of phosphating, the whole surface was covered with phosphate crystals. The iron-phosphate coatings deposited on the steel surface were mixtures of laminated and

needle-like structure, the needle-like structure of phosphate crystals being dominant (Fig. 6d).

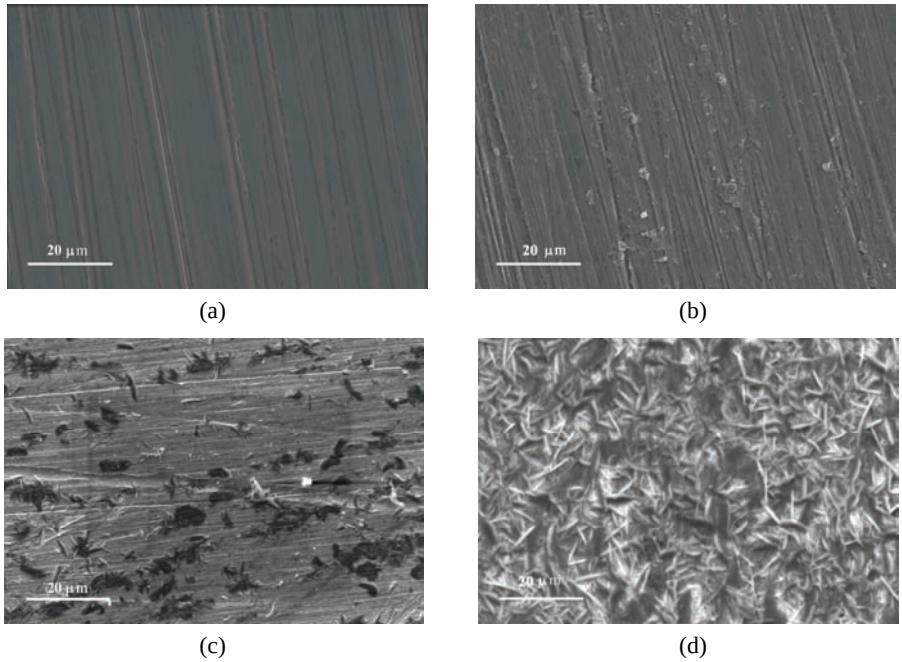

(a) (b)

(c) (d)

Fig. 6. Microphotographs of the steel surface prior to (a) and after phosphating with 0.5 g dm^{-3} $NaNO_2$ in the plating bath for b) 0.5, c) 1 and d) 5 min.

The EDS spectrum showed that iron-phosphate coating formed in the phosphate bath with $NaNO_2$ during 5 min contained iron, oxygen and phosphorus. The concentrations of the individual elements are presented in Table I (blank cells in Table I are for the samples where EDS analysis was not performed). Comparing these results with the results obtained for the iron-phosphate coatings deposited during the same time without the accelerator in the bath (Table I), it could be concluded that a significant increase in the concentration of phosphorus on the steel surface (nearly five times greater) was accomplished with the accelerator in the phosphating bath.

The values of the *RMS* and grain size of the iron-phosphate deposits obtained in the phosphating bath with 0.5 g dm^{-3} $NaNO_2$ for different phosphating time are presented in Table II. The AFM of the iron-phosphate coating confirmed that the centres of phosphate nucleation had been formed on the steel surface already after 30 s of phosphating. The size of formed phosphate nuclei were 0.3––0.7 μm (Table II). The surface roughness remained unchanged as compared to

that of the bare steel surface (52 nm, Table II). Extension of the phosphating time to 60 s led to an increase in the size of the phosphate crystals, which were as large as 3 μm. These crystals did not have a defined form and they were dispersed over the steel surface covering 20–30 % of the surface area. The surface roughness was increased and had a value of 127 nm. Further extension of the phosphating time to 5 min significantly increased the amount of phosphate crystals. The structure of these crystals could be defined as mostly laminated and needle-like structures with a size of the crystal ranging from 4 to 6 μm. Surface roughness has been slightly increased and amounts 147 nm.

TABLE II. The values of *RMS* and grain size of bare steel and iron-phosphate coatings on steel deposited with 0.5 g dm^{-3} $NaNO_2$ in the plating bath for different deposition times

Substrate	Deposition time, min	*RMS* / nm	Grain size range, μm
Bare steel	–	55	–
Iron-phosphate coating	0.5	52	0.3–0.7
	1.0	127	2–3
	5.0	147	4–6

Based on these results, it could be concluded that the presence of the accelerator $NaNO_2$ in the iron-phosphating bath resulted in a faster nucleation of phosphate crystals. The size of these crystals was smaller in comparison to those obtained in the phosphating solution without an accelerator. These results suggest that the $NaNO_2$ causes a decrease in the crystal size. Namely, the smaller crystal size obtained in the bath with $NaNO_2$ indicates that this additive has an effect on surface activation, favouring phosphate nucleation and leading to the formation of smaller crystals. In the presence of the accelerator, the concentration of phosphate crystals on the steel surface increased and crystals were more tightly packed. In addition, the roughness of the iron-phosphate coating decreased (Tables I and II). The higher concentration of phosphate crystals on the steel surface leads to an increase in the surface coverage of the iron-phosphate coating.

The higher surface coverage of iron-phosphate coatings on steel deposited with 0.5 g dm^{-3} $NaNO_2$ in the plating bath during 5 min is also shown in Fig. 5 and Table I. It was not only higher than the surface coverage of iron-phosphate coating deposited from the $NaNO_2$-free plating bath during the same deposition time, but also much higher even than the surface coverage of the iron-phosphate coating deposited from the $NaNO_2$-free plating bath during 15 min (Table I). Thus, based on all the presented results, it could be concluded that the addition of 0.5 g dm^{-3} $NaNO_2$ in the plating bath resulted in the completely different surface morphology of iron-phosphate coating on steel (Figs. 1b and 6d) of better surface coverage. Similar conclusions can be found in the literature for zinc-phosphate coatings on steel when $NaNO_2$ was used as an accelerator.[4,5,20,26,30,38–41]

CONCLUSIONS

It was shown that the growth of the phosphate crystals in both the normal and lateral direction, monitored by AFM, SEM and EDS, started with heterogeneous nucleation on the steel surface. The phosphate crystals, in the shape of platelets non-uniformly distributed on the steel surface, were formed during the initial deposition time in a $NaNO_2$-free bath. Extension of the phosphating time resulted in the formation of phosphate crystals with laminated and needle-like structures of increased roughness and increased phosphorous concentration, because of crystals growth. Consequently, the surface coverage determined from current passivation increased with prolonged deposition time. The addition of $NaNO_2$ to the phosphate solution significantly increased the surface coverage. The so-obtained crystals were of smaller size and more densely packed, which resulted in decreased coating roughness. They had laminated and needle-like structure with the needle-like structure prevailing, as compared to the platelets shape of the crystals obtained from a $NaNO_2$-free bath. Smaller crystal size indicates that this additive ($NaNO_2$) had an effect on surface activation, favouring phosphate nucleation and leading to the formation of smaller and better packed crystals.

Acknowledgement. This research was financed by the Ministry of Education, Science and Technological Development of the Republic of Serbia, Grant III 45019. The authors would like to thank Yao Xiong, Ph.D. student, Institute for Corrosion and Multiphase Technology, Ohio University, OH, USA, for helping in the AFM analyses, and Sanja Eraković, PhD student, Faculty of Technology and Metallurgy, University of Belgrade, for helping in the XRD analyses.

И З В О Д

ОДРЕЂИВАЊЕ ПОКРИВЕНОСТИ ПОВРШИНЕ ЧЕЛИКА ГВОЖЂЕ-ФОСФАТНИМ ПРЕВЛАКАМА АНОДНИМ РАСТВАРАЊЕМ ПРИМЕНОМ ЛИНЕАРНЕ ВОЛТАМЕТРИЈЕ

ЈОВАН П. ПОПИЋ[1], БОРЕ В. ЈЕГДИЋ[2], ЈЕЛЕНА Б. БАЈАТ[3], МИОДРАГ МИТРИЋ[4] и ВЕСНА Б. МИШКОВИЋ-СТАНКОВИЋ[3]

[1]ИХТМ – Центар за електрохемију, Универзитет у Београду, Његошева 12, Београд, [2]Институт ГОША, Милана Ракића 35, 11000 Београд, [3]Технолошко–металуршки факултет, Универзитет у Београду, Карнегијева 4, 11120 Београд и [4]Институт за нуклеарне науке Винча, Универзитет у Београду, п. пр. 522, Београд

У овом раду је, применом скенирајуће електронске микроскопије (SEM) и микроскопије међуатомских сила (AFM), испитиван утицај времена таложења и концентрације $NaNO_2$ у раствору за фосфатирање на морфологију гвожђе-фосфатних превлака на ниско-угљеничном челику. Састав гвожђе–фосфатних превлака је одређен применом енергетске дисперзионе атомске анализе (EDS) и дифракцијом X-зрака (XRD), док је покривеност површине одређивана анодним растварањем у боратном раствору применом линеарне волтаметрије (VAD). Показано је да додатак $NaNO_2$ у раствору за фосфатирање значајно повећава покривеност површине челика, јер се формирају боље паковани кристали, мање величине. Дуже време таложења такође повећава покривеност површине, као и храпавост превлаке и ширину кристала. Облик кристала се током дужег

времена таложења мења од кристала у облику већих плоча неуниформно распоређених на површини челика, ка боље пакованим ламинарним и игличастим кристалима.

(Примљено 6. јула, ревидирано 13. септембра 2012)

REFERENCES

1. A. Losch, E. Klusmann, J. W. Schultze, *Electrochim. Acta* **39** (1994) 1183
2. L. Fedrizzi, F. Deflorian, S. Rossi, L. Fambri, P. L. Bonora, *Prog. Org. Coat.* **42** (2001) 65
3. E. P. Banczek, P. R. P. Rodrigues, I. Costa, *Surf. Coat. Technol.* **202** (2008) 2008
4. E. P. Banczek, P. R. P. Rodrigues, I. Costa, *Surf. Coat. Technol.* **201** (2006) 3701
5. ASM Handbook, *Corrosion, Fundamentals, Testing, and Protection*, Vol. 13A, ASM International, OH, USA, 2005, p. 712–720
6. S. Q. Xu, Q. Li, Y. H. Lu, B. Chen, J. M. Fan, *Surf. Eng.* **26** (2010) 328
7. X. M. Song, G. Yu, H. B. Yi, L. Y. Ye, B. N. Hu, *Surf. Eng.* **26** (2010) 371
8. C. M. Wang, W. T. Tsai, Y. P. Lee, *Surf. Eng.* **24** (2008) 392
9. H. Nikdehghan, A. Amadeh, A. Honarbakhsh-Raouf, *Surf. Eng.* **24** (2008) 287
10. T. Biestek, J. Weber, *Electrolytic and chemical conversion coatings*, Portcullis Press, Redhill, Surrey, 1976, p. 180
11. B. Tepe, B. Gunay, *Prog. Org. Coat.* **62** (2008) 134
12. I. I. Hain, *Teoriya i praktika fosfatirovaniya metallov*, Himiya, Moskva, 1973, p. 68 (in Russian)
13. J. B. Bajat, V. B. Mišković-Stanković, J. P. Popić, D. M. Dražić, *Prog. Org. Coat.* **62** (2008) 201
14. B. V. Jegdić, J. B. Bajat, J. P. Popić, S. I. Stevanović, V. B. Mišković-Stanković, *Corr. Sci.* **53** (2011) 2872
15. L. Fedrizzi, E. J. Rodriguez, S. Rossi, F. Deflorian, *Prog. Org. Coat*. **46** (2003) 62
16. R. D. Armstrong, A. T. A. Jenkins, B. W. Johnson, *Corros. Sci*. **37** (1995) 1615
17. G. Gorecki, *Metal Finish*. **93** (1995) 36
18. G. Gorecki, *Corrosion* **48** (1992) 613
19. A. Albu-Yaron, Y. M. Aravot, *Thin Solid Films*, **232** (1993) 208
20. B. Ptacek, F. Dalard, J. J. Rameau, *Surf. Coat. Technol*. **82** (1996) 277
21. G. W. Critchlow, P. W. Webb, C. J. Tremlett, K. Brown, *Int. J. Adhes. Adhes*. **20** (2000) 113
22. C. Rajagopol, V. Subramanyan, V. Ramakishnan, K. Balakrishnan, *Paint India* **36** (1986) 16
23. D. Wang, P. Jokiel, A. Uebleis, H. Boehni, *Surf. Coat. Technol*. **88** (1996) 147
24. V. F. C. Lins, G. F. A. Reis, C. R. Aranja, T. Matencio, *Appl. Surf. Sci.* **253** (2006) 2875
25. L. Kwiatowski, *Surf. Eng.* **20** (2004) 292
26. A. Losch, J. W. Schultze, *J. Electroanal. Chem.* **359** (1993) 39
27. I. M. Notter, D. R. Gabe, *Corr. Sci.* **34** (1993) 851
28. H. A. Ponte, A. M. Maul, E. A. Alvarenga, *Mater. Res.* **5** (2002) 439
29. H. A. Ponte, A. M. Maul, *J. Appl. Electrochem.* **32** (2002) 641
30. E. P. Banczek, P. R. P. Rodrigues, I. Costa, *Surf. Coat. Technol.* **203** (2009) 1213
31. H. Kaesche, *Corrosion of metals*, Springer, Berlin, 2003, p. 209
32. N. Sato, M. Cohen, *J. Electrochem. Soc.* **111** (1964) 512
33. J. O' M. Bockris, D. M. Dražić, A. R. Despić, *Electrochim. Acta* **4** (1961) 325

34. G. Orhan, G. G. Gezdin, *J. Serb. Chem. Soc.* **77** (2012) 651
35. J. B. Bajat, S. Stevanović, B. M. Jokić, *J. Serb. Chem. Soc.* **76** (2011) 1537
36. H. Tamura, *Corros. Sci.* **50** (2008) 1872
37. P. E. Tegehall, N. G. Vannerberg, *Corros. Sci.* **32** (1991) 635
38. K. Ravichandran, H. Sivanandh, S. Ganesh, T. S. N. Sankara Narazanan, *Metal Finish.* **98** (2000) 48
39. G. Li, L. Niu, J. Lian, Z. Jiang, *Surf. Coat. Technol.* **176** (2004) 215
40. F. Fang, J. Jianf, S. Y. Tan, A. Ma, J. G. Jiang, *Surf. Coat. Technol.* **204** (2010) 2381
41. E. Klusmann, J. W. Schultze, *Electrochim. Acta* **48** (2003) 3325.

Journal of the Serbian Chemical Society
JSCS-info@shd.org.rs • www.shd.org.rs/JSCS
J. Serb. Chem. Soc. 78 (1) 115–127 (2013)
JSCS–4401
UDC 546.72+543.421+66.061+66.011
Original scientific paper

Optimization of a cloud point extraction procedure with response surface methodology for the quantification of iron by means of flame atomic absorption spectrometry

HOSSEIN ABDOLMOHAMMAD-ZADEH[1]*, ABDOLHOSSEIN NASERI[2] and GOLAMHOSSEIN SADEGHI[1]

[1]*Department of Chemistry, Faculty of Sciences, Azarbaijan University of Tarbiat Moallem, 35 Km Tabriz-Marageh Road, P. O. Box 53714-161, Tabriz, Iran and* [2]*Department of Analytical Chemistry, Faculty of Chemistry, University of Tabriz, Tabriz, Iran*

(Received 3 January, revised 21 May 2012)

Abstract: A simple micelle-mediated phase separation method has been developed for the pre-concentration of trace levels of iron as a prior step to its determination by flame atomic absorption spectrometry (FAAS). The method is based on the cloud point extraction (CPE) of iron using the non-ionic surfactant poly(ethyleneglycol–mono-*p*-nonylphenylether) (PONPE 7.5) without the addition of any chelating agent. Several variables affecting the extraction efficiency were studied and optimized utilizing a central composite design (CCD) and a three-level full factorial design. Under the optimum conditions, the limit of detection (*LOD*), limit of quantification (*LOQ*) and pre-concentration factor were 1.5 μg L^{-1}, 5.0 μg L^{-1} and 100, respectively. The relative standard deviation (*RSD*) for six replicate determinations at 50 μg L^{-1} Fe(III) level was 1.97 %. The calibration graph was linear in the range of 5–100 μg L^{-1}, with a correlation coefficient of 0.9921. The developed method was validated by the analysis of two certified reference materials and applied successfully to the determination of trace amounts of Fe(III) in water and rice samples.

Keywords: iron; ligand-less cloud point extraction; central composite design; full factorial design; flame atomic absorption spectrometry; rice samples.

INTRODUCTION

Iron is the fourth most abundant element in the earth's crust. There is an increasing interest in its determination due to its vital importance for living organisms and the consequent role in global carbon cycling. Iron deficiency in food may cause diseases, such as anemia. Many researchers and the World Health Organization (WHO) are therefore recommending fortification of food, mainly of

* Corresponding author. E-mail: h.abdol@azaruniv.edu
doi: 10.2298/JSC120103055M

grain products, with iron as one of the best options to combat its deficiency.[1] However, too much Fe is harmful and can be toxic when exposures exceed the physiological requirements. In drinking waters, a sanitary security limit for iron was restricted to 2 mg L^{-1} by the WHO.[2] Therefore, it is essential to establish simple, rapid, and efficient methods for the monitoring of iron at trace levels in environmental, biological and food samples.

Various methods have been developed for the trace determination of iron, including flame atomic absorption spectrometry (FAAS),[3–5] electrothermal atomic absorption spectrometry (ET–AAS),[6–9] inductively coupled plasma optical emission spectroscopy (ICP–OES),[10] inductively coupled plasma mass spectrometry (ICP–MS),[11,12] X-ray fluorescence,[13] spectrophotometry,[14,15] and electroanalytical techniques.[16–18] However, each of these methods have advantages/limitations regarding cost, interferences and especially limits of detection. In comparison with other instrumental analytical techniques, FAAS is less expensive, faster and widely available. However, it has a limited sensitivity regarding metal ions determination in complex matrices, such as biological and food samples. Therefore, a preliminary separation and pre-concentration step prior to its determination is often required.

Several techniques have been developed for the separation and pre-concentration of trace amounts of iron, including co-precipitation, ion-exchange separation, liquid–liquid extraction (LLE), solid phase extraction (SPE), and cloud point extraction (CPE). CPE is a separation and pre-concentration procedure that has been applied for trace metal determination in several different matrices.[19–22] Its major advantages are simple experimental procedures, low cost, high pre-concentration factors and environmental safety.[23] These aspects include it in a set of analytical methods in agreement with “green chemistry” principles. When a micellar solution of a nonionic or weakly polar surfactant is heated up, the polarity of the surfactant is decreased. Above a certain temperature, called the cloud point, the polarity is almost displaced and, hence, the surfactant molecules separate out from the aqueous phase. As a result, the clear solution becomes turbid and phase separation occurs. At the cloud point, the homogenous surfactant solution separates into two phases, one of which, called the surfactant-rich phase, contains most of the surfactant, while the other phase, called the aqueous phase, contains mostly water and surfactant monomers at a concentration near the critical micelle concentration (CMC). The hydrophobic compounds initially present in the solution and bound to the micelles will be extracted to the surfactant-rich phase, which leaves only a very small portion in the aqueous phase.[23]

Metal ions could be extracted into the surfactant-rich phase directly or after complex formation with a suitable ligand. Method development for ligand-less CPE requires the optimization of several experimental parameters, such as pH, concentration of surfactant, ionic strength, *etc*. In traditional strategies, only one

variable is changed whilst all the others remain constant. This approach does not allow the study of changes in the response that may occur when two or more factors are modified simultaneously. Furthermore, the optimization of the influencing parameters using "one variable-at-a-time" optimization method requires many experiments. Experimental design is an alternative to this strategy because it allows a large number of factors to be screened simultaneously and provides less ambiguous data. Furthermore, experimental designs combined with a response surface methodology help to visualize relationships between the responses and factor levels, which allow researchers to locate the region of the highest response values.[24]

In the present work, a ligand-less CPE method was developed for the separation and pre-concentration of Fe(III) in drinking water and rice samples prior to its determination by FAAS. In this CPE system, poly(ethyleneglycol–mono-*p*-nonylphenylether) (PONPE 7.5) was used as both the chelating agent and extractant. In addition, since the cloud point temperature for the employed ethanolic solution of the micellar system is around 25 °C, the requirement of a heating system to reach the phase separation was unnecessary. All these mentioned features are very important contributions because the majority of the methodologies reported in the literature require a heating step and a chelating reagent to realize the cloud point extraction process.[25] As a considerable number of variables can affect the extraction efficiency in a ligand-less CPE procedure, optimization and assessing of the proposed method were performed with the aid of experimental design and a response surface methodology (RSM). A central composite design (CCD) and a three-level full factorial design were employed for the determination of optimized experimental conditions for the ligand-less CPE of Fe(III) ions from real samples.

EXPERIMENTAL

Apparatus

A Varian model SpectrAA 220 (Mulgrave, Victoria, Australia) flame atomic absorption spectrometer, equipped with a deuterium lamp background correction and an iron hollow cathode lamp (operated at 15 mA) as the radiation source at the wavelength of 248.3 nm with 1 nm spectral band pass, was used. All of the absorbance measurements were performed using an air/acetylene flame at flow rates of 3.5 and 1.5 L min^{-1}, respectively. A centrifuge (Beckman GS-6, USA) was used to accelerate the phase separation process. The pH values were measured with a Metrohm pH meter (model 827, Switzerland), equipped with a combined glass electrode. A thermostated water bath (Julabo) model GMBH D-77960 was obtained from Germany. An electronic analytical balance (Mettler Toledo, PB303, Switzerland) was used for weighing the solid materials.

Standard solutions and reagents

All employed chemicals were of analytical-reagent grade and all solutions were prepared with deionized water (Shahid Ghazi Co., Tabriz, Iran). Stock solutions of iron and those used for the interference study (1000 μg mL^{-1}) were prepared by dissolving appropriate amounts of

their corresponding salts in deionized water. The working standard solutions were prepared daily by stepwise dilution of the stock standard solution with deionized water. Suprapur® HNO_3 (65 %), H_2SO_4 (95–98 %) and H_2O_2 (30 %), used for sample digestion, ethanol and sodium bicarbonate were purchased from Merck (Darmstadt, Germany).

As it is not possible to obtain a real aqueous solution of the surfactant PONPE 7.5 (Tokyo Kasei Industries, Chuo-Ku, Tokyo, Japan) since the cloud point of its micellar solution is markedly below room temperature, it was experimentally convenient to prepare a 3 % (v/v) working solution by mixing 1.5 mL surfactant PONPE 7.5 with 20.0 mL ethanol (Merck) in a 50.0 mL volumetric flask and diluting to 50.0 mL with deionized water.

A stock buffer solution (0.2 mol L^{-1}) was prepared by dissolving appropriate amounts of sodium bicarbonate in deionized water and adjusting to pH 6 by adding a dilute HNO_3 solution. A 2 mol L^{-1} $NaNO_3$ solution was used for the ionic strength study. Two standard reference materials, SRM 1549 (Non-Fat Milk Powder) and SRM 1566b (Oyster Tissue) (from the National Institute of Standards and Technology (NIST), Giathersburg, MD, USA) were used for validation of the presented method. The pipettes and vessels used for trace analysis were kept in 15 % (v/v) nitric acid at least overnight and subsequently washed three times with deionized water.

Sample preparation

Tap water was obtained from the drinking water system of Azarshahr, Iran. After sampling, a 50.0-mL aliquot of this sample was analyzed within 24 h of collection without previous treatment or filtration.

After milling in a glass mortar, an accurately measured amount (25 mg) of a powdered rice sample or a standard reference material (NIST SRM 1566b, Oyster Tissue) was heated to dryness on a hot plate at a fairly low temperature in the glass beaker containing a mixture of concentrated nitric acid 65 % (10 mL) and hydrogen peroxide 30 % (5 mL).[26] After cooling to room temperature, the residue was dissolved in a 1.0 mL of HNO_3 0.1 mol L^{-1}. After dilution with deionized water, the pH was adjusted to nearly 6 by the addition of a dilute NaOH solution. Then, the solution was transferred into a 50.0 mL volumetric flask and after dilution to the mark with the deionized water, the concentration of Fe(III) was determined as described in the section "General procedure". The same procedure was applied in the case of 1.0 g certified material (NIST SRM 1549) using concentrated sulfuric acid (10 mL) and nitric acid (4 mL) in the digestion step.

General procedure

For the cloud point extraction experiments, a 50.0 mL aliquot of a solution containing Fe(III) in the range of 5–100 μg L^{-1}, buffer solution (2×10^{-3} mol L^{-1}, pH 6), 0.5 mol L^{-1} $NaNO_3$ and 0.2 % (v/v) PONPE 7.5 were placed in a screw-cap conical-bottom polypropylene centrifuge tube. The mixture was diluted to 50 mL with deionized water. The resulting solution immediately became turbid at room temperature without heating. Phase separation was accelerated by centrifuging the tubes at 4000 rpm for 10 min. Subsequently, the aqueous phase was separated completely using a 10 mL syringe centered in the tube without cooling in an ice bath. Then, the surfactant rich phase was heated in a water bath and the residue was made up to 500 μL by adding 0.1 mol L^{-1} HNO_3 in ethanol to decrease the viscosity. Finally, the resultant solution was introduced into the flame of an AAS by conventional aspiration.

Data analysis

MINITAB (Minitab Inc.), release 14.0, statistical package was used for the experimental design, ANOVA and regression analysis of the experimental data. The fit quality of the

polynomial model equation was expressed by the regression coefficient R^2, and its statistical significance was checked by the Fisher *F*-test. The level of significance given as values of the probability (p) was less than 0.05.

RESULTS AND DISCUSSION

In this study, ligand-less CPE combined with FAAS was developed for the extraction and determination of Fe(III) ions in water and rice samples. The non-ionic surfactant PONPE 7.5 was used as both the extracting solvent and chelating agent. Based on previous studies, under appropriate conditions, PONPE 7.5 may form a complex with Fe(III) through its polyoxyethylene groups and thereby can be extracted into the surfactant-rich phase.[27] Complex formation between the ether linkages of PONPE 7.5 and some cations, such as Pb(II), Al(III) and Co(II), has also been reported by other researchers.[25,28,29]

Optimization of ligand-less CPE procedure

The aim of this study was to optimize the experimental conditions for high extraction efficiency of Fe(III) ions by employing the ligand-less CPE methodology. Different variables can affect the extraction efficiency in a ligand-less CPE procedure, *i.e.* surfactant concentration, pH, ionic strength, type of buffer and its concentration, equilibrium temperature, incubation time, and centrifugation time and speed, and in most cases they are optimized. Therefore, a multivariate approach is recommended for their optimization. However, some variables might not have a significant effect and thus can be neglected. Based on previous experience,[30] the equilibrium temperature and incubation time have no significant effect upon the extraction efficiency, and a centrifugation time of 10 min at 4000 rpm is sufficient for complete phase separation. Therefore, the influence of five factors on the extraction efficiency, namely surfactant concentration, pH, ionic strength, buffer type and its concentration were studied and optimized utilizing two optimization methods, *i.e.*, a central composite design (CCD) and a three-level full factorial experimental design. First, three factors (surfactant concentration, pH and ionic strength) were optimized using CCD, and in the second step, after obtaining the optimum pH value from CCD optimization technique, the buffer type and its concentration were studied and optimized utilizing a three-level full factorial design.

Central composite design (CCD)

An optimization procedure was applied in order to determine the exact values of the most important factors to obtain high extraction efficiency. Systematic optimization procedures are performed by selecting an objective function, finding the most important factors and investigating the relationship between the responses and factors by the so-called response surface methodology (RSM). In this study, CCD or Box–Wilson,[31] one of the most commonly used response surface

designs, was employed in order to determine the optimal conditions of the extraction process using a ligand-less CPE. Three independent variables, namely pH (X_1), the surfactant concentration (X_2), and ionic strength (X_3) were studied at five levels with four replicates at the central point. In the circumscribed CCD method, absolute upper and lower limits on certain factors are given, and these are specified as the star points. The coded levels of the variables and their real experimental values are given in Table I. The number of experiments in a CCD is defined by the expression: ($2^f + 2f + C$), where f is the number of variables and C is the number of central points.[32] In this study, f and C were set at 3 and 4, respectively. Therefore, 18 experiments had to be performed for the CCD. In order to obtain a good estimate of experimental error (pure error), the 18 experiments were performed in duplicate. The thirty-six experiments were randomized in order to minimize the effect of uncontrolled variables, and divided into six blocks to remove the expected variation caused by some change during the course of the experiment. This design permitted the response to be modeled by fitting a second-order polynomial, which can be expressed as the following equation:

$$y = \beta_0+\beta_1X_1+\beta_2X_2+\beta_3X_3+\beta_{12}X_1X_2+\beta_{13}X_1X_3+ \\ +\beta_{23}X_2X_3+\beta_{11}X_1^2+\beta_{22}X_2^2+\beta_{33}X_3^2 \quad (1)$$

TABLE I. The variables and their coded values used in the central composite design (CCD)

Variable name	Abbreviation	Coded variables levels				
		–2	–1	0	+1	+2
pH	X_1	2	4	6	8	10
PONPE 7.5 concentration, % v/v	X_2	0.06	0.12	0.18	0.24	0.3
Ionic strength, mol L^{-1}	X_3	0.05	0.25	0.45	0.65	0.85

where y is the response function (recovery percentage), X_1, X_2 and X_3 are the three chemical variables, referring to the pH, concentration of PONPE 7.5 and ionic strength, respectively), β_0 is the intercept, β_1–β_3 are the linear parameters, β_{12}–β_{23} represent the interaction parameters and β_{11}–β_{33} are the quadratic parameters. After fitting the above equation by least-squares regression, ANOVA and regression analysis were employed to assess the significance of the variables. Estimates of the 10 parameters contained in Eq. (1) obtained by the least squares matrix are given in Table II. The determination coefficient obtained for this model was satisfactory (R^2 = 0.9518) and the lack of fit was not significant. These results show that the obtained model is reliable. The random distribution of the residual plot (residual *vs*. observed results) also confirmed this reliability (data not shown). The levels of significance of the results, given as values of the probability (p), are also listed in Table II. Values of p less than 0.05 were considered as significant. Accordingly, among linear parameters, β_2 and β_3 were not significant. However, their related quadratic and interaction parameters, *i.e*.,

β_{22}, β_{33} and β_{13}, were significant. Based on the obtained results, all of three variables were proved to have a significant effect on the extraction.

TABLE II. Regression results and analysis of variance of the central composite design (CCD)

Parameter	Parameter estimate	*p*-value
β_0	46.56	0.01
β_1	16.23	0.00
β_2	149.60	0.21
β_3	–45.914	0.25
β_{11}	–2.06	0.00
β_{22}	–947.78	0.00
β_{33}	–52.33	0.03
β_{12}	17.47	0.08
β_{13}	7.52	0.01
β_{23}	189.93	0.06

CCD was used to determine the variables that have a higher impact on extraction recovery and adjust them to yield the maximum probable recovery. The results may be used to give an insight on the robustness of the method close to the optimum conditions and show possible variable interactions. In this respect, the selection of the optimum conditions was enabled using the response surface plots *vs.* the affecting parameters. The obtained regression models were used to calculate the response surface for each variable separately. The response surface plots for the extraction efficiency as a function of each pair of independent variables are shown in Fig. 1. The response plots were generated with one variable kept at its central level, and varying the others within the experimental range. The response surfaces obtained for the pH and surfactant concentration, while keeping the $NaNO_3$ concentration constant at 0.45 mol L^{-1}, are shown in Fig. 1a. As can be seen, these factors nonlinearly affect the response. The response reaches the maximum value when pH and concentration of PONPE 7.5 are 6 and 0.2 % (v/v), respectively. From the contour plot and the obtained results listed in Table II, there is no significant interaction between the two previously mentioned variables. Fig. 1b shows the response surface function developed by the model considering pH and ionic strength, while keeping the PONPE 7.5 concentration constant at 0.18 % (v/v). The response reaches the maximum value when 6.0 for pH and 0.5 mol L^{-1} of $NaNO_3$ for ionic strength were taken, and from the contour plot and the obtained results listed in Table II, there is a significant interaction between these two variables. The response surface function developed by the model considering the concentration of PONPE 7.5 and ionic strength, while keeping the pH value constant at 6.0 is shown in Fig. 1c, from which it can be seen that these factors nonlinearly affect the response. The response reaches the maximum value when 0.2 % (v/v) for the concentration of PONPE 7.5 and 0.5 mol L^{-1} $NaNO_3$ for the ionic strength were taken and from the contour plot and the ob-

tained results listed in Table II, there is no significant interaction between the two previously mentioned variables. The levels corresponding to the maximum response were selected as the optimum levels. Thus, the optimum conditions for ligand-less cloud point extraction were defined as: sample pH of 6.0, PONPE 7.5 concentration of 0.2 % (v/v) and ionic strength adjusted by 0.5 mol L^{-1} $NaNO_3$.

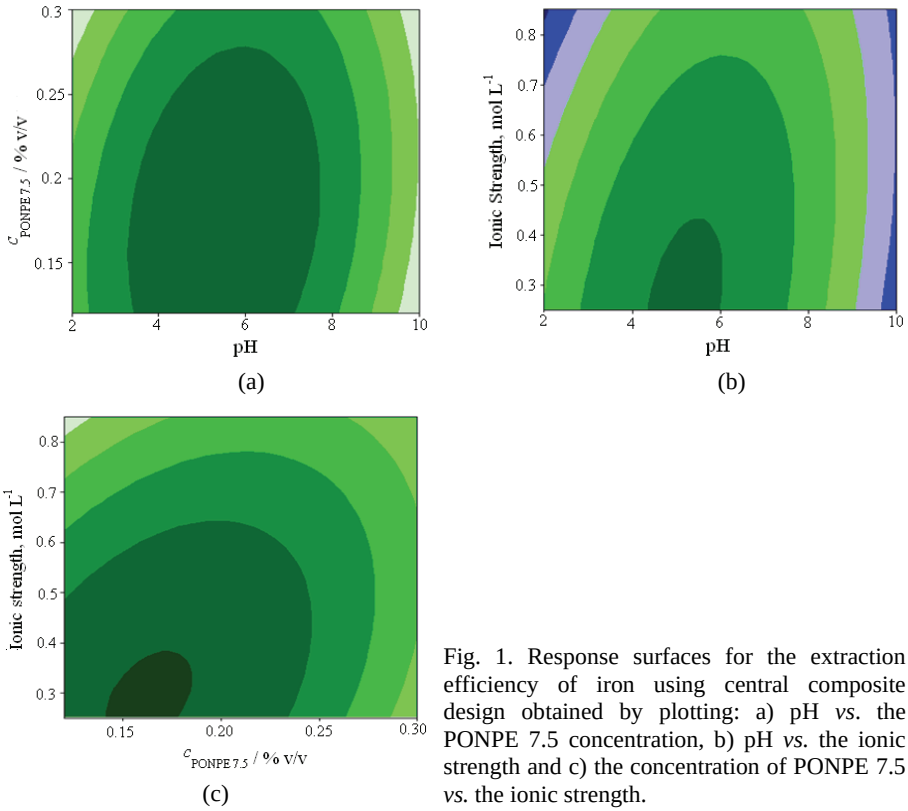

Fig. 1. Response surfaces for the extraction efficiency of iron using central composite design obtained by plotting: a) pH *vs.* the PONPE 7.5 concentration, b) pH *vs.* the ionic strength and c) the concentration of PONPE 7.5 *vs.* the ionic strength.

Full factorial design

Based on the obtained results from previous studies,[27,30,33] the type of buffer and its concentration are important variables that affect the extraction efficiency of ligand-less cloud point extraction of metal ions using the non-ionic surfactant PONPE 7.5. Hence, after obtaining the optimum value of the pH, it was necessary to find a suitable buffer and optimize its concentration. For this purpose, another kind of response surface methodology, three-level full factorial design (3^f), was used. Thus, two variables that could potentially affect the extraction efficiency were identified as the type of buffer and its concentration. Each

variable was studied at three levels (*i.e.*, acetate, phosphate and bicarbonate buffer solutions, as three levels of the first variable and 0.002, 0.006 and 0.01 mol L^{-1} buffer concentrations, as three levels of the second variable). Therefore, nine (3^2) experiments had to be performed and in order to obtain a good estimation of the experimental error, the nine experiments were performed in duplicate. The coded levels of the variables, together with their real experimental values, are given in Table III. This design permitted the response to be modeled by fitting a second-order polynomial and the optimum values of variables determined. From the obtained model and response surfaces (not shown here), 2×10^{-3} mol L^{-1} bicarbonate buffer solution was selected for the subsequent experiments.

TABLE III. Variables and values used for the three-level full factorial design

Variable name	Abbreviation	Coded factor levels		
		–1	0	+1
Type of buffer	X_1	Acetate	Phosphate	Bicarbonate
Buffer concentration, mol L^{-1}	X_2	0.002	0.006	0.01

Sample volume and pre-concentration factor

The Fe(III) concentration in real samples, such as natural waters, is usually low. Thus, the sample volume is one of the most important parameters in development of a pre-concentration method, since it determines the sensitivity enhancement of the technique. Thus, the effect of sample volume was examined in a range of 10–65 mL for 50 μg L^{-1} Fe(III) under optimum conditions. It was observed that extraction efficiency of Fe(III) was quantitative between 10–50 mL and for the higher sample volumes, extraction efficiency decreased. Subsequently, a sample volume of 50 mL was selected for the further experiments. Thus, by analyzing 0.5 mL of the final solution after the pre-concentration of 50 mL of sample solution, the pre-concentration factor was found to be 100.

Analytical figures of merit

Under the optimum conditions, a series of experiments were designed to determine the linear range, precision, detection limit and enrichment factor. The calibration graph was linear in the range of 5–100 μg L^{-1}, with a correlation coefficient of 0.9921. The regression equation was $A = 0.007c_{Fe} + 0.043$, where A is the absorbance and c_{Fe} is the Fe(III) concentration in μg L^{-1}. The limit of detection (*LOD*) and limit of quantification (*LOQ*) (n = 6), calculated as three times and ten times, respectively, the standard deviation of the blank signal divided by the slope of the calibration curve, were 1.5 and 5.0 μg L^{-1}, respectively. The relative standard deviation (*RSD*) resulting from the analysis of 6 replicates of 50 mL solution containing 50 μg L^{-1} Fe(III) was 1.97 %. As the amount of Fe(III) in the sample solution was measured with a final volume of 0.5 mL, the solution was concentrated by a factor of 100. Therefore, the enrichment factor,

defined as the ratio of between the volume of the initial sample solution and the final volume of the surfactant-rich phase, was 100.

Interferences

The effects of foreign species on the determination of Fe(III) ion were investigated by measuring the absorbance of the solutions containing 50 μg L^{-1} of this ion in the presence of various amounts of other ions. The tolerance limit was taken as the amount of added ion causing less than ±5 % relative error ($p < 0.05$ at the 95 % confidence level) in the determination of Fe(III) ion. The maximum tolerances to the investigated cations and anions are summarized in Table IV. It can be seen that most of examined cations and anions did not interfere with the extraction and determination. Therefore, the proposed method is selective for the determination of Fe(III). As shown later, these results allowed the interference-free determination of Fe(III) in water and rice samples.

TABLE IV. Tolerance limits of interfering ions in the determination of 50 μg L^{-1} of iron by means of FAAS

Coexisting ions	Interferent to analyte ratio
Na^+, K^+, Cs^+,Ca^{2+}, Mg^{2+}, Sn^{2+}, Cl^-, Br^-, I^-, NO_3^-, CO_3^{2-}	1000:1
Ni^{2+}, Cr^{3+}, Bi^{3+}, Zn^{2+}, Ba^{2+}, Co^{2+}, Sr^{2+}	500:1
VO_3^-, Ag^+, Cu^{2+}	100:1
Cd^{2+}, PO_4^{3-}, Pb^{2+}	50:1

Application of the method

To test the reliability of the method, it was applied for the determination of Fe(III) ions in water and rice samples. In order to verify the accuracy of the established procedure, recovery experiments were also performed by spiking the samples with different amounts of Fe(III) before any pretreatment. The obtained results are given in Table V. As can be seen, recoveries between 96.7 and 104.2 % were obtained, which confirm the accuracy of the proposed method. Additionally, the accuracy of the proposed procedure was verified by applying the method to the determination of Fe(III) in two standard reference materials, NIST SRM 1566b (Oyster Tissue), and NIST SRM 1549 (Non-Fat Milk Powder) with certified Fe(III) contents of 205.8±6.8 and 1.78±0.1 μg g^{-1}, respectively. The obtained value of Fe(III) found in the former standard using the proposed procedure was 207.2±5.3 μg g^{-1} (mean ± standard deviation, $n = 3$), which is in good agreement with the certified concentration. However, in the case of the SRM 1549 standard, the found Fe(III) concentration was lower than detection limit of the presented method. It can be concluded that the proposed method is accurate and could be employed for the determination of Fe(III) in complex matrices, such as water and biological and food samples.

TABLE V. Determination of iron in water and rice samples (results of recoveries of spiked samples and certified reference materials)

Samples	Found Fe[a], μg g^{-1}	Added Fe, μg g^{-1}	Found Fe[a], μg g^{-1}	Recovery[b], %
Tap water[c]	24.6±2.2[d]	10.0[d]	34.5±2.1[d]	99. 0
Mineral water[e]	6.1±0.4[d]	10.0[d]	16.2±0.6 [d]	101.0
Rice$_{(1)}$[f]	104.0±4.8	40.0	143.2±5.3	98.0
Rice$_{(2)}$[g]	118.0±6.5	40.0	159.7±7.1	104.2
Rice$_{(3)}$[h]	146.0±5.9	40.0	184.7±7.6	96.7
SRM 1549	1.78±0.1[i]	Not detected		–
SRM 1566b	205.8±6.8[i]	207.2±5.3[j]		0.68[k]

[a]Mean ± standard deviation, n = 3; [b]recovery (%) = 100(found–base)/added; [c]from drinking water system of Azarshahr, Iran; [d]μg L^{-1}; [e]from ZamZam Co. Tabriz, Iran; [f, g and h]grown in Thailand, Iran (Bafekr Co.) and India (Sella Co.), respectively, and obtained from a local market (Azarshahr, Iran); [i]certified value; [j]assayed value; [k]relative error

Comparison of the presented method with other CPE/FAAS procedures

A comparison of the presented method with other CPE/FAAS procedures is given in Table VI. Apparently, the presented method has a low *LOD*, high pre-concentration factor and these characteristics are comparable or even better than most of the other methods in Table VI. Besides the advantages of the multivariate optimization strategy, this methodology is a reproducible, simple and low cost method. Thus, the presented method could be used for Fe(III) determination in routine analytical laboratories.

TABLE VI. Comparison of the presented method with other proposed CPE methods coupled with FAAS

Complexing agent	Sample matrix	Sample volume, mL	*PF*[a]	Linear range μg L^{-1}	Detection limit, μg L^{-1}	*RSD* / %	Ref.
APDC[b]	Water	10	50	<100	3.5	1.8	34
APDC	Wine	10	NA [c]	<350	20	2.4	35
APDC	Water	250	NA	10−100	NA	NA	36
Ferron[d]	Environmental, biological	15	30	10−400	0.4	2.4	19
Ferron	Water, Milk	20	75	10−250	1.7	2.1	20
IYPMI[e]	Environmental, biological	15	30	10−300	2.8	2.0	21
Neutral Red[f]	Spice	25	98	2.5−200	0.7	2.1	22
Ligand-less	Water, Rice	50	100	5−100	1.5	1.97	This work

CONCLUSIONS

In this research, an effective method was developed for the extraction and determination of trace amounts of Fe(III) using a relatively straightforward procedure. A multivariate optimization strategy was used to obtain the optimum conditions for the extraction of Fe(III) by ligand-less CPE. Optimization of the CPE

variables was carried out using the central composite design (CCD) and three levels full factorial experimental design. The presented procedure does not require any chelating agent, long incubation time or cooling after centrifugation, and could be applied, as an inexpensive and wide spread technique for trace iron monitoring in routine analytical laboratories. Environmental pollution is limited to a very small amount of surfactant rich-phase. This fact is particularly attractive because the "green chemistry" concept can be employed here. Phase separation can be achieved at room temperature and the extraction efficiency is high, resulting in a low detection limit and high pre-concentration factor. The optimized ligand-less CPE coupled to FAAS enabled quantification of trace levels of Fe(III) in the different real samples with complicated matrices.

Acknowledgment. The financial support from the Research Council of Azarbaijan University of Tarbiat Moallem (AUTM, Iran) is gratefully acknowledged.

ИЗВОД

ОПТИМИЗАЦИЈА ПРОЦЕДУРЕ ЕКСТРАКЦИЈЕ СА ТАЧКОМ ЗАМУЋЕЊА МЕТОДОЛОГИЈОМ ОДГОВОРА ПОВРШИНА ЗА КВАНТИФИКАЦИЈУ ГВОЖЂА ПРИМЕНОМ ПЛАМЕНЕ АТОМСЕ АПСОПЦИОНЕ СПЕКТРОМЕТРИЈЕ

HOSSEIN ABDOLMOHAMMAD-ZADEH[1], ABDOLHOSSEIN NASERI[2] и GOLAMHOSSEIN SADEGHI[1]

[1]*Department of Chemistry, Faculty of Sciences, Azarbaijan University of Tarbiat Moallem,35 Km Tabriz-Marageh Road, P. O. Box 53714-161, Tabriz, Iran и* [2]*Department of Analytical Chemistry, Faculty of Chemistry, University of Tabriz, Tabriz, Iran*

Развијена је једноставна сепарациона метода за преконцентрацију трагова гвожђа, преко мицеларне фазе, која претходи одређивању помоћу пламене атомске апсорпционе спектрометрије. Метода је базирана на екстракцији са тачком замућења, уз коришћење нејонског сурфактанта полиетиленгликолмоно-*para*-нонилфенил етра без додавања хелирајућег агенса. Испитивано је неколико променљивих које утичу на ефикасност екстаркције и оптимизовано коришћењем централног композитног дизајна и потпуног факторског дизајна на три нивоа. Под оптималним условима граница детекције, граница квантификације и преконцентрациони фактор износе: 1,5 μg L^{-1}, 5,0 μg L^{-1} и 100, редом. Релативна стандардна девијација за шест поновљених одређивања за концентрацију Fe(III) од 50 μg L^{-1} износи 1,97 %. Калибрациона крива је линеарна у опсегу 5–100 μg L^{-1} са коефицијентом корелације од 0,9921. Развијена метода је валидирана анализом два сертификована референтна материјала и успешно примењене за одређивање трагова гвожђа Fe(III) у води и пиринчу.

(Примљено 13. јануара, ревидирано 21. маја 2012)

REFERENCES

1. L. M. G. Santos, R. G. O. Araujo, B. Welz, S. C. Jacob, M. G. R. Vale, H. Becker-Ross, *Talanta* **78** (2009) 577
2. WHO, *Guidelines for Drinking-water Quality, Recommendations*, vol. 1, 3rd ed., WHO Press, World Health Organization, Geneva, Switzerland, 2008, p. 390–391
3. P. Pohl, B. Prusisz, *Talanta* **71** (2007) 715
4. S. Soriano, A. D. Pereira Netto, R. J. Cassella, *J. Pharm. Biomed. Anal.* **43** (2007) 304

5. J. L. R. Junior, S. R. Oliveira, N. M. Caldas, J. A. Gomes Neto, *Anal. Chim. Acta* **627** (2008) 198
6. I. M. Dittert, J. S. A. Silva, R. G. O. Araujo, A. J. Curtius, B. Welz, H. Becker-Ross, *Spectrochim. Acta, B* **64** (2009) 537
7. A. Ohashi, H. Ito, C. Kanai, H. Imura, K. Ohashi, *Talanta* **65** (2005) 525
8. P. C. Aleixo, J. A. Nóbrega, *Food Chem.* **83** (2003) 457
9. F. G. Lepri, D. L. G. Borges, R. G. O. Araujo, B. Welz, F. Wendler, M. Krieg, H. Becker-Ross, *Talanta* **81** (2010) 980
10. A. Sapkota, M. Krachler, C. Scholz, A. K. Chebukin, W. Shotyk, *Anal. Chim. Acta* **540** (2005) 247
11. T. D. Saint' Pierre, L. F. Dias, S. M. Maia, A. J. Curtius, *Spectrochim. Acta, B* **59** (2004) 551
12. J. Jong, V. Schoemann, D. Lannuzel, J.-L. Tison, N. Mattielli, *Anal. Chim. Acta* **623** (2008) 126
13. L. S. G. Teixeira, R. B. S. Rocha, E. V. Sobrinho, P. R. B. Guimarães, L. A. M. Pontes, J. S. R. Teixeira, *Talanta* **72** (2007) 1073
14. P. C. Nascimento, C. L. Jost, M. V. Guterres, L. D. Del'Fabro, L. M. Carvalho, D. Bohrer, *Talanta* **70** (2006) 540
15. R. Ghavami, A. Najafi, B. Hemmateenejad, *Spectrochim. Acta, A* **70** (2008) 824
16. W. M. Moore, *Anal. Chim. Acta* **105** (1979) 99
17. G. Lu, X. Yao, X. Wu, T. Zhan, *Microchem. J.* **69** (2001) 81
18. M. H. Pournaghi-Azar, B. M. Fatemi, *Microchem. J.* **65** (2000) 199
19. M. Ghaedi, A. Shokrollahi, R. Mehrnoosh, O. Hossaini, M. Soylak, *Cent. Eur. J. Chem.* **6** (2008) 488
20. F. Shakerian, S. Dadfarnia, A. M. Haji Shabani, *J. Iran. Chem. Soc.* **6** (2009) 594
21. M. Ghaedi, A. Shokrollahi, K. Niknam, E. Niknam, M. Soylak, *Cent. Eur. J. Chem.***7** (2009) 148
22. Ç. A. Şahin, İ. Tokgoz, S. Bektas, *J. Hazard. Mater.* **181** (2010) 359
23. G. D. Matos, E. B. Reis, A. C. S. Costa, S. L. C Ferreira, *Microchem. J.* **92** (2009)135
24. Y. Hernández, M. G. Lobo, M. González, *Food Chem.* **114** (2009) 734
25. R. A. Gil, J. A. Gásquez, R. Olsina, L. D. Martinez, S. Cerutti, *Talanta* **76** (2008) 669
26. E. G. P. Silva, V. Hatje, W. N. L. Santos, L. M. Costa, A. R. A. Nogueira, S. L. C. Ferreira, *J. Food Comp. Anal.* **21** (2008) 259
27. J. L. Manzoori, H. Abdolmohammad-Zadeh, M. Amjadi, *Talanta* **71** (2007) 582
28. M. O. Luconi, M. F. Silva, R. A. Olsina, L. P. Fernández, *Talanta* **51** (2000) 123
29. L. L. Sombra, M. O. Luconi, L. P. Fernández, R. A. Olsina, M. F. Silva, L. D. Martínez, *J. Pharm. Biomed. Anal.* **30** (2003) 1451
30. J. L. Manzoori, H. Abdolmohammad-Zadeh, M. Amjadi, *J. Hazard. Mater.* **144** (2007) 458
31. G. E. P. Box, K. B. Wilson, *J. R. Stat. Soc., B* **13** (1951) 1
32. E. Morgan, *Chemometrics: Experimental Design*, Wiley, London, 1991
33. J. L. Manzoori, H. Abdolmohammad-Zadeh, M. Amjadi, *Microchim. Acta* **159** (2007) 71
34. D. L. Giokas, E. K. Paleologos, M. I. Karayannis, *Anal. Bioanal. Chem.* **373** (2002) 237
35. E. K. Paleologos, D. L. Giokas, S. M. Tzouwara-Karayanni, M. I. Karayannis, *Anal. Chim. Acta* **458** (2002) 241
36. D. L. Giokas, E. K. Paleologos, M. I. Karayannis, *Anal. Chim. Acta* **537** (2005) 249.

Journal of the Serbian Chemical Society
JSCS-info@shd.org.rs • www.shd.org.rs/JSCS

J. Serb. Chem. Soc. 78 (1) 129–136 (2013)
JSCS–4402

UDC 665.75+66.094.522.8:548.3+
549.514.6:547.313.2+547.269.1
Original scientific paper

Deep desulphurization of gas oil and model compounds by an anatase nanocomposite sandwich-type polyoxometalate as a novel, reusable and green nano mercaptan scavenger

ABDOLLAH FALLAH SHOJAEI[1], MOHAMAD ALI REZVANI[1]* and FAROKHZAD MOHAMADI ZONOZ[2]

[1]*Department of Chemistry, Faculty of Science, University of Guilan, Rasht 419961-3769, Iran and* [2]*Department of Chemistry, Hakim Sabzevari University, Sabzevar, 397, Iran*

(Received 12 January, revised 28 March 2012)

Abstract: The oxidative desulphurization of gas oil and model compounds that exist in gas oil with hydrogen peroxide/acetic acid using nanoparticle $(Bu_4N)_7H_3[P_2W_{18}Cd_4(Br)_2O_{68}]$–$TiO_2$ ($(Bu_4N)_7H_3[P_2W_{18}Cd_4]$–$TiO_2$) as a nano scavenger has been studied. This sandwich-type nanoparticle was shown to be able to scavenge hydrogen sulphide and mercaptans in high yields. The addition of acetic acid enhanced the conversion. This system provides an efficient, convenient and practical method for scavenging sulphur compounds. The $(Bu_4N)_7H_3[P_2W_{18}Cd_4]$–$TiO_2$ nanoparticle was a very active catalyst system for the oxidation of model compounds, while other polyoxometalate systems were much less active.

Keywords: polyoxometalates; desulphurization; anatase; scavenger; mercaptans.

INTRODUCTION

Deep desulphurization of transportation fuels has become an important research subject due to the increasingly stringent regulations and fuel specifications in many countries for environmental protection purpose.[1,2] Desulphurization techniques have been investigated widely, among which oxidetive desulphurization (ODS) is considered to be one of the promising new methods for super deep desulphurization of fuel oil.[3–5] In the ODS process, the refractory dibenzothiophene (DBT) and 4,6-dimethydibenzothiophene (4,6-DMDBT) are oxidized to their corresponding sulphones under mild conditions, which are subsequently removed by extraction, adsorption, distillation, or decomposition. Various oxidants have been used in ODS, such as NO_2,[1] O_3,[2] H_2O_2[3] and solid oxidizing agents.[4] Among these oxidants, H_2O_2 is mostly chosen as the oxidant as only water is

* Corresponding author. E-mail: marezvani2010@gmail.com
doi: 10.2298/JSC120112034S

produced as a by-product. Peracids produced *in situ* from organic acids, catalysts and H_2O_2 are reported to be very effective for the rapid oxidation of sulphur compounds in fuel oils under mild conditions. At present, several members of the sandwich-type heteropolyanion families, such $[P_2W_{18}M_4\ (H_2O)_2O_{68}]^{10-}$ and $[P_4W_{30}M_4(H_2O)_2O_{112}]^{16-}$ (M = Co(II), Cu(II) or Zn(II)) have been synthesized.[6–8] Their chemistry was discussed and recently, they have attracted much attention in the oxidative desulphurization (ODS) of gas oil.[9] The first cadmium-containing heteropolyanions, related to the mono lacunary anions of Keggin and Dawson structures (PW_{11} and P_2W_{17}) were synthesized by R. Contant.[10] In 1995, Kirby and Baker[11] reported the first sandwich-type heteropolyanions including Cd^{2+} based on the $[P_2W_{15}O_{56}]^{12-}$ defect structure, and later Bi *et al*.[12] prepared a series of dimeric polytungstates by reacting $[As_2W_{15}O_{56}]^{12-}$ with different metal ions, *i.e*., Cu(II), Mn(II), Co(II), Ni(II), Zn(II) and Cd(II). Herein, the synthesis of a new cadmium-containing heteropolyanion, in which two lacunary $PW_9O_{34}^{9-}$ units sandwich four cadmiums, is described.

Homogeneous catalysts cannot be separated from the reaction media and consequently, cannot be reused. Fixation of homogeneous catalysts onto a solid support may be a strategy to overcome this problem. Recently, supported heteropolyacids were synthesized and applied as effective catalysts in organic reactions.[13–16] Supporting heteropolyacids on solids with high surface areas improve their catalytic performance in various liquid–solid and solid surface heterogeneous reactions. Titanium dioxide is a wide-band-gap semiconducting material that has received intense scrutiny for a broad range of applications, thanks to its intriguing physicochemical properties and cheap, abundant, and reasonably non-toxic nature. TiO_2, also a widely used catalyst support as well as a catalyst itself, is known to enhance catalytic activity in many cases because of the strong interaction between the active phase and the support.[19] In continuation of research on the synthesis and application of polyoxometalates (POM) and anatase,[15–18] anatase TiO_2 crushed nano leaf coupled by a sandwich-type polyoxometalate was designed and synthesized at 100 °C *via* a sol–gel method under oil-bath conditions. The chemical characterization of this compound was accomplished by means of elemental analysis, infrared spectroscopy (IR), X-ray diffraction (XRD) analysis, transmission electron microscopy (TEM) and ^{113}Cd nuclear magnetic resonance (^{113}Cd-NMR) spectroscopy. The catalytic performances of these homogenous and heterogeneous catalysts were tested on the oxidative desulphurization of model sulphur compounds, such as benzothiophene (BT), dibenzothiophene (DBT), 4-methyldibenzothiophene (4-MDBT) and 4,6-dimethyldibenzothiophene (4,6-DMDBT) and gas oil using hydrogen peroxide/acetic acid as the oxidizing reagent. The POM–TiO_2 nanocomposites presented much higher catalytic activity than those of the corresponding unsupported polyoxometalates. The catalyst could be easily separated and reused at the end of reaction without a

significant loss of their catalytic activity, which suggests that the catalysts are stable under different conditions.

EXPERIMENTAL

All reagents and solvents used in this work are available commercially and were used as received, unless otherwise indicated. The model compounds and chemicals, including benzothiophene (BT), dibenzothiophene (DBT), 4-methyldibenzothiophene (4-MDBT), and 4,6-dimethyldibenzothiophene (4,6-DMDBT), solvent (*n*-heptane) for the experiments and analysis and hydrogen peroxide (30 vol. %) were obtained from Aldrich. The compound A-β-$Na_8HPW_9O_{34}\cdot 24H_2O$ (abbreviated as A-PW_9) and other catalysts $(NH_4)_{10}[P_2W_{18}Cd_4]$, $K_{10}[P_2W_{18}Cd_3Zn]$, $K_{10}[P_2W_{18}Cd_2Zn_2]$, $K_{10}[P_2W_{18}CdZn_3]$, $K_{10}[P_2W_{18}Zn_4]$, $K_6[P_2W_{21}O_{71}]$, $K_{10}[P_2W_{20}O_{70}]$ and $K_{14}[P_2W_{19}O_{69}]$, used for comparison, were prepared as previously described.[8,11] Their chemical characterization was accomplished by means of elemental analysis, IR, ^{31}P- and ^{113}Cd-NMR spectroscopy, which confirmed their structures. Titanium(IV) tetraisopropoxide and glacial acetic acid were obtained from Merck. Gas oil (density 0.8361 g mL^{-1} at 15 °C, total sulphur content 0.98 wt. %) was supplied from the terminal of the South Iranian Oil Company. Further properties of the gas oil are listed in Table I.

TABLE I. Properties of the south Iran (Kharg Island) gas oil; API GR. –API gravity (API – American Petroleum Institute); API = (141.5/Specific gravity) – 131.5; viscosity KIN – kinematic viscosity

Entry	Properties of gas oil	Method	Result
1	Specific gravity at 60/60 °F	ASTM D1298	0.8365
2	Density at 15 °C	ASTM D1298	0.8361
3	API GR. at 60/60 °F	Calculated	37.66
4	Flash point, °F	ASTM D93	142
5	Water content, vol. %	ASTM D4006	0.025
6	Total sulphur content, wt. %	ASTM D4294	0.98
7	Cloud point, °C	ASTM D2500	–4
8	Colour test	ASTM D156	1.5
9	Viscosity KIN at 50 °C. CST.	ASTM D445	2.8
10	Pour point, °C	ASTM D97	–9
11	Mercaptans, ppm	ASTM D3227	286
12	Distillation, °C	ASTM D86	
13	Initial Boiling Point, °C	ASTM D86	157.8
14	10 % Distillation, °C	ASTM D86	194.6
15	20 % Distillation, °C	ASTM D86	213.4
16	50 % Distillation, °C	ASTM D86	268.6
17	90 % Distillation, °C	ASTM D86	353.9
18	Final boiling point, °C	ASTM D86	384.9
19	Residue, vol. %	ASTM D86	1.5
20	Loss, vol. %	ASTM D86	1
21	Recovery, vol. %	ASTM D86	97.5

Preparation of the mercaptan scavenger

$(Bu_4N)_7H_3[P_2W_{18}Cd_4(Br)_2O_{68}]$ was prepared as follows. To a stirred solution of (0.216 g, 0.7 mmol) $Cd(NO_3)_2\cdot H_2O$ in 8 mL H_2O (pH adjusted to 6 with acetic acid), 1.0 g (0.35 mmol)

of A-PW_9 was added. The solution was carefully transferred into a microwave reactor vessel and irradiated at 1000 W for 5 min. This step was repeated 6 times. After cooling to room temperature, potassium chloride (1.2 g) was added to the solution and the mixture was stirred for 15 min and filtered. This solid was recrystallized from 20 mL of hot water and dried under vacuum. Then, to a stirred solution of 2.0 g (0.37 mmol) of the potassium salt of $[P_2W_{18}Cd_4(H_2O)_2O_{68}]^{10-}$ in 55 mL of warm distilled water, a solution of 1.0 g (3.7 mmol) of tetrabutyl ammonium bromide in 5.0 ml of H_2O was added. The mixture was stirred at 60 °C for 3 h and then the white precipitate was separated by filtration, recrystallized from acetonitrile and ether, and air dried (yield 0.65 g, 25 %). The results of the elemental analysis are presented in Table II.

Preparation of the nanomercaptan scavenger

The $(Bu_4N)_7H_3[P_2W_{18}Cd_4(Br)_2O_{68}]$–$TiO_2$ nanocomposite was prepared as follows. Titanium tetraisopropoxide was added to glacial acetic acid under stirring and a solution of $(Bu_4N)_7H_3[P_2W_{18}Cd_4(Br)_2O_{68}]$ in water was added dropwise. The mixture was stirred to dissolve any solid. Then, the sol was heated to 100 °C under oil bath conditions until a homogenous $(Bu_4N)_7H_3[P_2W_{18}Cd_4(Br)_2O_{68}]$–$TiO_2$ hydrogel was formed. Finally, the gel was filtered, washed with deionised water–acetone and dried in an oven at 50 °C overnight.

TABLE II. Elemental analysis of $(Bu_4N)_7H_3[P_2W_{18}Cd_4(Br)_2O_{68}]\cdot 27H_2O$

Element	P	W	Cd
Calcd., %	0.93	49.54	6.73
Found, %	0.88	49.33	6.79

Oxidative desulphurization (ODS) of model sulphur compounds

Some typical benzothiophenes and dibenzothiophenes, which represent easy, hard and very hard sulphur species to remove from gas oil, were selected to evaluate the catalysts and the reactivity of benzothiophenes and dibenzothiophenes in an oxidation reaction. A water bath was first heated up and stabilized at the desired reaction temperature (25–60 °C). The model sulphur compound (BT, DBT, 4-MDBT or 4,6-DMDBT was dissolved in *n*-heptane to make a stock solution with a sulphur content of 500 ppm. Then, 5 mL of the model sulphur compound and 0.06 mmol of the nano scavenger ($(Bu_4N)_7H_3[P_2W_{18}Cd_4(Br)_2O_{68}]$–$TiO_2$), as a catalyst, were mixed with 2 mL H_2O_2/acetic acid (peroxyacetic acid) (hydrogen peroxide/acetic acid molar ratio of 1.0) in a flask. The flask was immersed in the heating bath and stirred at 500 rpm for 2 h. After completion of the oxidation, the mixture was cooled to room temperature and 10 ml acetonitrile (MeCN) was added to extract the oxidized sulphur compounds. The two phases of MeCN and *n*-heptane were separated. The sulphur content in model sulphur compounds before and after the reaction was determined using X-ray fluorescence spectroscopy using a Tanaka X-ray fluorescence spectrometer RX-360 SH (ASTM D-4294 method). The ASTM D-4294 method covers the measurement of sulphur in fuels, such as diesel, naphtha, kerosene, residuals, lubricating base oils, hydraulic oils, jet fuels, crude oils, gasoline (all unleaded), and other distillates. Compared to other test methods for sulphur determination, the D-4294 test method has high throughput, minimal sample preparation, good precision, and is capable of determining sulphur over a wide range of concentrations. The equipment specified is in most cases less costly than that required for alternative methods. In the case of petroleum materials that contain suspended water, it is recommended that the water be removed before testing or that the sample be thoroughly homogenized and im-

mediately tested. The interference is greatest if the water creates a layer over the transparent film as it will attenuate the X-ray intensity for sulphur. One such method to accomplish the removal of water is to centrifuge the sample first under ambient sealed conditions, taking care that the sample integrity is not compromised.

Oxidative desulphurization (ODS) of gas oil

Oxidative desulphurization of the gas oil was accomplished in the same manner as used for the oxidation of the model sulphur compounds, *i.e.*, gas oil (sulphur 2300 ppm S, 10 ml) with 0.06 mmol catalyst and H_2O_2/acetic acid (hydrogen peroxide/acetic acid molar ratio of 1.0) at a temperature of 60 °C. After completion of the oxidation, the oxidized sulphur in the gas oil was extracted with acetonitrile at room temperature. The acetonitrile/oil ratio used was 1/2 by volume. The biphasic mixture was separated by decantation. The oil phase was separated and weighed to calculate % recovery of oil. The sulphur content in the oil before and after reaction was determined using an X-ray fluorescence spectrometer (ASTM D4294 method).

RESULT AND DISCUSSION

Effect of the catalyst structure

The effect of the nature of the catalyst on the oxidative desulphurization of DBT using hydrogen peroxide/acetic acid as the oxidant is shown in Table III. The sandwich type polyoxometalate-anatase nanoparticle catalyst $(Bu_4N)_7H_3[P_2W_{18}Cd_4(Br)_2O_{68}]$–$TiO_2$ and the unsupported $(Bu_4N)_7H_3[P_2W_{18}Cd_4]$ catalyst were very active systems for the oxidation of the model compound, while other studied polyoxometalates systems were much less active. It was shown that the order of the oxidation reactivity of the catalyst in the presence of hydrogen peroxide/acetic acid was: $(Bu_4N)_7H_3[P_2W_{18}Cd_4]$–$TiO_2$ > $(Bu_4N)_7H_3[P_2W_{18}Cd_4]$ > $(NH_4)_{10}[P_2W_{18}Cd_4]$ > $K_{10}[P_2W_{18}Cd_3Zn]$ > $K_{10}[P_2W_{18}Cd_2Zn_2]$ > $K_{10}[P_2W_{18}CdZn_3]$ > $K_{10}[P_2W_{18}Zn_4]$ > $K_6[P_2W_{21}O_{71}]$ > $K_{10}[P_2W_{20}O_{70}]$ > $K_{14}[P_2W_{19}O_{69}]$.

TABLE III. Effect of different catalysts in the oxidative desulphurization of DBT; conditions for desulphurization: 5 ml of DBT model oil (500 ppm S), 0.06 mmol catalyst, 2 ml H_2O_2/ /acetic acid, 5 ml extraction solvent, time 2 h and temperature 60 °C

Entry	Catalyst	DBT/catalyst	Oxidant/DBT	Residual sulphur, ppm	Sulphur removal, %
1	$(Bu_4N)_7H_3[P_2W_{18}Cd_4]$–$TiO_2$	100	10	8.4	98.32
2	$(Bu_4N)_7H_3[P_2W_{18}Cd_4]$	30	10	38.8	92.24
3	$(NH_4)_{10}[P_2W_{18}Cd_4]$	20	15	72.8	85.44
4	$K_{10}[P_2W_{18}Cd_2Zn_2]$[a]	20	15	84.8	83.04
5	$K_{10}[P_2W_{18}CdZn_3]$[a]	20	10	105.8	78.84
6	$K_{10}[P_2W_{18}Zn_4]$[a]	20	10	148.2	70.36
7	$K_6[P_2W_{21}O_{71}]$[b]	25	15	163.8	67.24
8	$K_{10}[P_2W_{20}O_{70}]$[b]	25	15	171.35	65.73
9	$K_{14}[P_2W_{19}O_{69}]$[b]	25	15	172.9	65.42

[a]synthesis of the catalyst is given in the literature;[2,19] [b]synthesis of the catalyst is given in the literature[3,14]

Reactivity of various sulphur compounds

The effect of the different soluble catalysts and $(Bu_4N)_7H_3[P_2W_{18}Cd_4(Br)_2O_{68}]$–$TiO_2$ in oxidative desulphurization of different sulphurs compounds are given in Table IV. The oxidation reactivity decreased in the order of DBT > 4,6-DMDBT > 4-MDBT > BT. BT exhibited the lowest reactivity, which was related to the different electron density on the sulphur atom. The difference in electron density on the sulphur atom of DBT and 4,6-DMDBT is very small. The oxidation reactivity was governed by the steric hindrance of the methyl groups, which become on obstacle for the approach of the sulphur atom to the catalytically active sites. The electron density for 4,6-DMDBT is the highest, but its oxidation reactivity was lower than DBT, this is due to the steric effect from the alkyl groups at the 4 and 6 positions.

TABLE IV. Effect of different catalysts in the oxidative desulphurization of various sulphur compounds; condition for desulphurization: 2 ml H_2O_2/acetic acid as the oxidant, 0.1 mmol catalyst, 5 ml acetonitrile as the extraction solvent, time 2 h and temperature 60 °C

Entry	Catalyst	Sulphur removal, %			
		DBT	4-MDBT	4,6-DMDBT	BT
1	$(Bu_4N)_7H_3[P_2W_{18}Cd_4]$–$TiO_2$	98.5	95.5	96	89
2	$(Bu_4N)_7H_3[P_2W_{18}Cd_4]$	92	90	91	84
3	$(NH_4)_{10}[P_2W_{18}Cd_4]$	86	87	87	79
4	$K_{10}[P_2W_{18}Cd_2Zn_2]$ [b]	85	86	85	77
5	$K_{10}[P_2W_{18}CdZn_3]$ [b]	83	85	84	75
6	$K_{10}[P_2W_{18}Zn_4]$ [b]	80	81	80	73
7	$K_6[P_2W_{21}O_{71}]$ [c]	75	73	73	72
8	$K_{10}[P_2W_{20}O_{70}]$ [c]	74	71	72	70
9	$K_{14}[P_2W_{19}O_{69}]$ [c]	70	69	71	68

[a]Synthesis of the catalyst is given in the literature;[2,19] [b]synthesis of the catalyst is given in the literature[3,14]

Oxidative desulphurization (ODS) of gas oil

The results of the oxidative desulphurization of oil gas are given in Table V. According to the obtained data, the total sulphur content (Entry 1) and the content of mercaptans (Entry 2) were much lower after the oxidation process, while numerous other properties of the gas oil remained unaffected. From the results obtained in this work, it was demonstrated that the nano mercaptan scavenger ($(Bu_4N)_7H_3[P_2W_{18}Cd_4(Br)_2O_{68}]$–$TiO_2$) can catalyze the oxidative desulphurization reaction in 2 h and can reduce the total sulphur content of gas oil from 0.98 to 0.087 wt. % and also reduce the content of mercaptans from 286 to 10 ppm.

Recycling of the catalyst

At the end of the oxidative desulphurization of the model sulphur compounds and gas oil, the catalyst was filtered off and washed with dichloromethane. In order to determine whether the catalyst would succumb to poisoning

and lose its catalytic activity during the reaction, the reusability of the catalyst was investigated. For this purpose, desulphurization reaction of gas oil and the model compounds were performed in the presence of fresh and recovered catalyst. Even after three runs of the reaction, the catalytic activity of $(Bu_4N)_7H_3[P_2W_{18}Cd_4(Br)_2O_{68}]$–$TiO_2$ was almost the same as that of fresh catalyst. The results are summarized in Tables V and VI for the oxidative desulphurization DBT and gas oil, respectively.

TABLE V. Oxidative desulphurization of gas oil using $(Bu_4N)_7H_3[P_2W_{18}Cd_4]$–$TiO_2$

Entry	Properties of gas oil	Before ODS	After ODS[a]	After ODS[b]
1	Total sulphur content, wt. %	0.98	0.087	0.092
2	Density at 15 °C	0.8361	0.8362	0.83690
3	Mercaptans, ppm	286	10	9
4	Flash point, °F	142	142	142
5	Water content, vol. %	0.025	0.025	0.025
6	Cloud point, °C	–4	–4	–4
7	Colour test	1.5	1.5	1.5
8	Viscosity KIN at 50 °C. cSt.	2.8	2.7	2.6
9	Pour point, °C	–9	–9	–9
10	Initial boiling point, °C	157.8	156.9	157.2
11	Final boiling point, °C	384.9	383.8	385.2

[a]Condition for desulphurization: 5 ml of gas oil (2300 ppm S), 0.06 mmol catalyst, 2 ml oxidant, 5 ml of extraction solvent, time 2 h and temperature 60 °C; [b]reuse of the catalyst in the desulphurization of gas oil

TABLE VI. Reuse of $(Bu_4N)_7H_3[P_2W_{18}Cd_4]$–$TiO_2$ for the oxidative desulphurization of DBT

Run	Sulphur removal, %
1	96
2	94
3	95

CONCLUSIONS

The $(Bu_4N)_7H_3[P_2W_{18}Cd_4(Br)_2O_{68}]$–$TiO_2$ nanocomposite was synthesized at a low temperature *via* a sol–gel method under oil-bath conditions. Fixing of $(Bu_4N)_7H_3[P_2W_{18}Cd_4(Br)_2O_{68}]$ with TiO_2 decreased the particle size of the crushed nano leaf of the anatase phase. The $(Bu_4N)_7H_3[P_2W_{18}Cd_4]$–$TiO_2$ nanocomposite was a very active catalyst system for the oxidation of model sulphur compounds and gas oil, while unmodified $(Bu_4N)_7H_3[P_2W_{18}Cd_4(Br)_2O_{68}]$ showed much lower activities. For this polyoxometalates/H_2O_2/acetic acid system, the oxidation reactivity decreased in the following order: DBT > 4,6-DMDBT > BT. The percent conversion increased when the amount of oxidant and catalyst were increased. The addition of acetic acid enhanced the oxidation.

ИЗВОД

ДУБОКА ДЕСУЛФУРИЗАЦИЈА ПЛИНСКОГ УЉА И МОДЕЛ ЈЕДИЊЕЊА АНАТАЗНИМ НАНОКОМПОЗИТНИМ ПОЛИОКСОМЕТАЛАТОМ СЕНДВИЧ ТИПА КАО НОВИМ, ОБНОВЉИВИМ И НЕШКОДЉИВИМ ПРИМАОЦЕМ МЕРКАПТАНА

ABDOLLAH FALLAH SHOJAEI, MOHAMAD ALI REZVANI И FAROKHZAD MOHAMADI ZONOZ

Department of Chemistry, Faculty of Science, University of Guilan, Rasht 419961-3769, Iran

Проучавана је оксидативна десулфуризација плинског уља и индивидуалних модел једињења која се налазе у плинском уљу, водоник пероксидом/сирћетном киселином уз примену наночестица $(Bu_4N)_7H_3[P_2W_{18}Cd_4(Br)_2O_{68}]$–$TiO_2$ ($(Bu_4N)_7H_3[P_2W_{18}Cd_4]$–$TiO_2$)) као примаоца меркаптана. Показано је да су ове наночестице сендвич-типа способне да вежу водоник-сулфид и меркаптане уз високе приносе. Додавање сирћетне киселине је побољшало конверзију. Овај систем омогућава ефикасан, погодан и практичан метод за везивање сумпорних једињења. Наночестице $(Bu_4N)_7H_3[P_2W_{18}Cd_4]$–$TiO_2$ су се показале као врло активан катализаторски систем за оксидацију модел једињења, док су се други полиоксометалатни системи показали много мање активним.

(Примљено 12. јануара, ревидирано 28. марта 2012)

REFERENCES

1. D. Huang, Y. J. Wang, *Ind. Eng. Chem. Res*. **45** (2006) 1880
2. D. Huang, *Ind. Eng. Chem. Res*. **46** (2007) 1447
3. M. M. Q. Simoes, C. M. M. Conceic, J. A. F. Gamelas, *J. Mol. Catal., A* **144** (1999) 461
4. J. Toufaily, M. Soulard, J.-L. Guth, J. Patarin, L. Delmote, *Colloids Surfaces, A* **316** (2008) 285
5. M. H. Lim, C. F. Blanford, A. Stein, *Chem. Mater*. **10** (1998) 467.
6. S. Tangestaninejad, V. Mirkhani, M. Moghadam, I. Mohammadpoor-Baltork, E. Shams, H. Salavati, *Ultrason. Sonochem*. **15** (2008) 438
7. W. Bu, L. Wu, A. Tang, *J. Colloid Interface Sci*. **26** (2004) 472
8. R. G. Finke, M. W. Dreoge, P. J. Domaille, *Inorg. Chem*. **26** (1987) 3886
9. T. J. R. Weakley, R. G. Finke, *Inorg. Chem*. **29** (1990) 1235
10. R. Contant, *J. Chem. Res*. **24** (1984) 120
11. J. F. Kirby, L. C. W. Baker, *J. Am. Chem. Soc*. **117** (1995) 10010
12. L. H. Bi, E. B. Wang, J. Peng, R. D. Hung, L. Xu, C. W. Hu, *Inorg. Chem*. **39** (2000) 671
13. G. Maayan, R. Popovitz-Biro, R. Neumann, *J. Am. Chem. Soc*. **128** (2006) 4968
14. X. Yu, L. Xu, X. Yang, *Appl. Surf. Sci*. **254** (2008) 4444
15. A. Fallah Shojaei, M. A. Rezvani, M. Heravi, *J. Serb. Chem. Soc*. **76** (2011) 955
16. A. Fallah Shojaei, M. A. Rezvani, M. Heravi, *J. Serb. Chem. Soc.* **76** (2011) 1
17. R. Harutyunyan, M. A. Rezvani, M. M. Heravi, *Metal-Org. Nano-Metal Chem*. **41** (2011) 94
18. A. Fallah Shojaei, M. H. Loghmani, *Chem. Eng. J*. 157 (2010) 263
19. A. Pearson, H. Jani, K. Kalantar-Zadeh, S. K. Bhargava, V. Bansal, *Langmuir* **27** (2011) 6661
20. S. Sakthivel, M. V. Shankar, M. Palanichamy, B. Arabindoo, D. W. Bahnemann, V. Murugesan, *Water Res*. **38** (2004) 3001
21. Y. Yang, Q. Wuc, Y. Guoa, C. Hu, *J. Mol. Catal., A* **225** (2005) 203.

Journal of the Serbian Chemical Society
JSCS-info@shd.org.rs • www.shd.org.rs/JSCS

J. Serb. Chem. Soc. 78 (1) 137–154 (2012)
JSCS–4403

UDC 546.763+539.196+547.992:
543.422.3:543.51
Original scientific paper

A study of chromium interaction with *O*-donor humic-like ligands using electrospray-ionization mass spectrometry

DARKO H. ANĐELKOVIĆ[1]*, RUŽICA S. NIKOLIĆ[1], DEJAN Z. MARKOVIĆ[2], TATJANA D. ANĐELKOVIĆ[1], GORDANA M. KOCIĆ[3], ZORAN B. TODOROVIĆ[2] and ALEKSANDAR LJ. BOJIĆ[1#]

[1]*Faculty of Sciences and Mathematics, University of Niš, Višegradska 33, 18000 Niš, Serbia,* [2]*Faculty of Technology, University of Niš, Bulevar oslobođenja 124, 16000 Leskovac, Serbia and* [3]*Faculty of Medicine, University of Niš, Bulevar dr Zorana Đinđića 81, 18000 Niš, Serbia*

(Received 20 March, revised 3 July 2012)

Abstract: A study of the interaction of chromium with *O*-donor humic-like ligands war performed using electrospray-ionization mass spectrometry (ESI--MS) and ultraviolet/visible (UV/Vis) spectrophotometry. The heterogeneity of the functional groups justifies the use of model compounds of humic substances. For studying the interaction of chromium with humic substances, benzoic, salicylic, phthalic and citric acid, which include *O*-donor atoms also present in heterogeneous and polydispersed ligands, such as humic and fulvic acids, were used as model substances. The intensity of the interaction is correlated with the acid–base and electron-donor properties, geometric and steric characteristics, and the number and the positions of the *O*-donor atoms in the investigated ligands. UV/Vis data describing chromium interaction with humic-like ligands was placed in correlation with ESI-MS data of the complexes, both in quantitative and in qualitative terms. UV/Vis spectroscopy and ESI-MS quantification showed a large difference in the information they yield in describing the interaction of chromium(III) with the ligand, the ESI-MS technique being more informative. ESI-MS Technique can be used for quantitative analysis of the system Cr(III)–ligand. ESI-MS ion current chromatograms of 20 μL loop injections of systems Cr(III)–ligand, indicate a stabile peak and signal integrity.

Keywords: chromium; interaction; humic; ligand; electrospray-ionization mass spectrometry.

INTRODUCTION

The presence of heavy metals in nature has a negative impact on human health and the environment. Their state, form, mobility, sorption and bioavail-

* Corresponding author. E-mail: darko.andjel@gmail.com
# Serbian Chemical Society member.
doi: 10.2298/JSC120320071A

ability depend on the physical and chemical environmental conditions in which they are located, and on the nature of all chemical species, present in that environment, with which they can interact. Thus, the migration of heavy metals from soil into groundwater is strongly dependent on the terrestrial conditions, such as physical and chemical characteristics of soil, clay mineral content and the presence of natural organic matter - humic substances.[1,2]

Humic substances are complex organic molecules formed by the decomposition of plant, animal and/or microbial material. They are ubiquitous and persistent in the biosphere, playing an important role in the mobilization of metal ions in soil and aquatic environments, and influencing the bioavailability and toxicity of these ions. By creating a water-soluble complex between HS and metal ions, an increase in the concentration of ions in the groundwater and other natural waters, far above their solubility, could be expected. In addition, the possibility that complexation of humic substances in solid phase could mobilize metals present in landfills, which leads to their penetration into the biosphere,[3–6] should be taken into consideration.

Chromium is an essential, yet toxic trace element depending on its valence state and the nature of the ligand to which it is bound. Chromium in the environment can be found in two oxidation states +3 and +6, which have different chemical, physicochemical and biochemical reactivity. Cr(VI) chemical species are more soluble, mobile and bioactive than Cr(III) chemical species.[7,8]

In natural environments, such as soil, chromium primarily interacts with soil organic matter – humic substances.[9–11] The heterogeneity of functional groups and their versatility justifies the use of model compounds of humic substances. “Hard” binding sites are the most common in the humic structure, with mainly oxygen in carboxylic and phenolic binding sites as the donor atom.[12–14] As model substances for studying the interaction of chromium with humic substances, benzoic, salicylic, phthalic and citric acid, which include all *O*-donor atoms of heterogeneous and polydispersed ligands, such humic and fulvic acids, were used. Therefore, an investigation of the interactions of chromium with each individual *O*-donor atom ligand, with a further investigation of the complex mixture of *O*--donor atoms in humic acid, present a good methodology for defining the interactions of metals with polyfunctional, polydispersed and polyelectrolytic ligands, such as humate macromolecules.[15–17]

Electrospray-ionization mass spectrometry, ESI-MS is used for the detection and characterization of one or more ionic species in solution, and has been confirmed as very useful in studies of various complex systems.[18] In the case of metal–ligand coordination interactions, it is often used for verification of the stoichiometry of a newly synthesized complex,[19] that do not participate in the liquid phase equilibrium, and after decomposition do not produce other molecular species (if it is still the case, the created equilibrium is usually ignored).

Studies of solution equilibrium, simultaneous detection, identification and quantification of numerous species, the distribution of which depends on pH, the stoichiometric concentration, *etc*. are less routine, although very interesting applications of ESI-MS.

Another convenient feature of ESI-MS is its low detection limit; thus, concentrations down to 10^{-6} mol L^{-1} can be detected.[20–22]

This paper deals with a study of the interaction of chromium(III) with *O*-donor humic-like ligands by ESI-MS and UV/Vis spectrophotometry. Application of ESI mass spectrometry is a novelty in the study of the interactions of chromium and model humic ligands.

UV/Vis spectrophotometric characterization of the chromium complexes with *O*-donor humic-like ligands was correlated with the ESI-MS characterization of the complexes, in both quantitative and qualitative terms.

The aim of this study was to closer define processes that chromium ions in interaction with humic substances in the system soil/water can undergo. This research contributes to complex processes of chromium translocation in the groundwater systems, *i.e.*, leaching from the soil, after which the chromium could be further transported and dispersed in the biotic and abiotic systems of the natural environment.

EXPERIMENTAL

Chemical reagents, solutions, instrumentations

All reagents used were *p.a.* or HPLC grade purity. Salicylic, benzoic, phthalic and citric acid were purchased from Aldrich (USA). Methanol, purchased from Baker (Analyzed Reagent Bio), was of HPLC grade purity. As a source of chromium(III), crystalline chromium(III) chloride hexahydrate (Merck, Germany) was used. The employed glass and plastic laboratory ware were rinsed with 4.0 mol L^{-1} hydrochloric acid (Baker Analyzed), then with 0.6 mol L^{-1} nitric acid (Environmental Grade Anachemia) and finally with purified water (< 0.1 μS cm^{-1}) to remove trace metals and other contaminants.

Standard stock solutions of the ligands were prepared by weighing the respective acid with an accuracy of ±0.0001g and dissolving in methanol. The solutions were kept in a refrigerator at 4 °C. Working solutions were made by dilution of the standard solutions in a methanol/water mixture (50/50, v/v). Working solutions of the ligand–chromium mixtures were prepared in polyethylene vials of 5, 2 and 1.5 cm^3 (Eppendorf, Germany) previously washed with 0.1 mol L^{-1} HCl, deionized water and methanol to remove any adsorbed surface impurities and reduce the plastic additives in the working solutions.

Spectrophotometric characterization in the UV/Vis region was performed on a double beam UV/Vis spectrophotometer (Shimadzu UV-1650 PC). The ESI-MS investigation was performed on a LCQ Deca Ion Trap Mass Spectrometer (Thermo Finnigan, USA) with auxiliary equipment.

Experimental procedure for the UV/Vis characterisation of the Cr–ligand interactions

A mixture of methanol and deionized water (< 0.1 μS cm^{-1}) in ratio 50/50 (v/v) was used as the blank. Samples with the appropriate ligand and Cr(III) in the same solvent mixture, were recorded 30 min after mixing the components, to ensure the formation of the complex in

solution, considering the relatively low concentration range of the components. In the preparation of the samples of ligand, and ligand–chromium(III) mixtures, any pH adjustment was avoided so as not to disrupt the equilibrium in the reaction mixture. Otherwise, the occurrence of secondary chemical reactions and the formation of various coordination compounds with buffer components could not be excluded.

For the obtained spectral curves (Fig. 1), the areas of the surface integrals for all spectral curves were calculated and compared. The calculation was performed in order to obtain the relative area difference ($\Delta P_{\%}$) between the area of the binary ligand–Cr(III) system (P_2) and

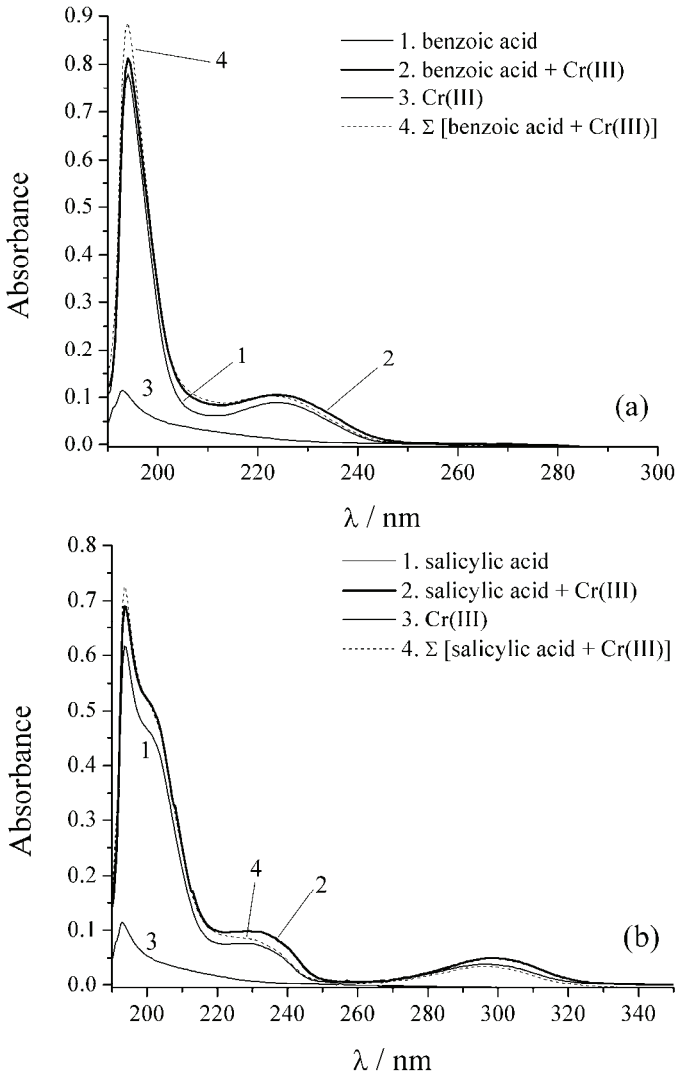

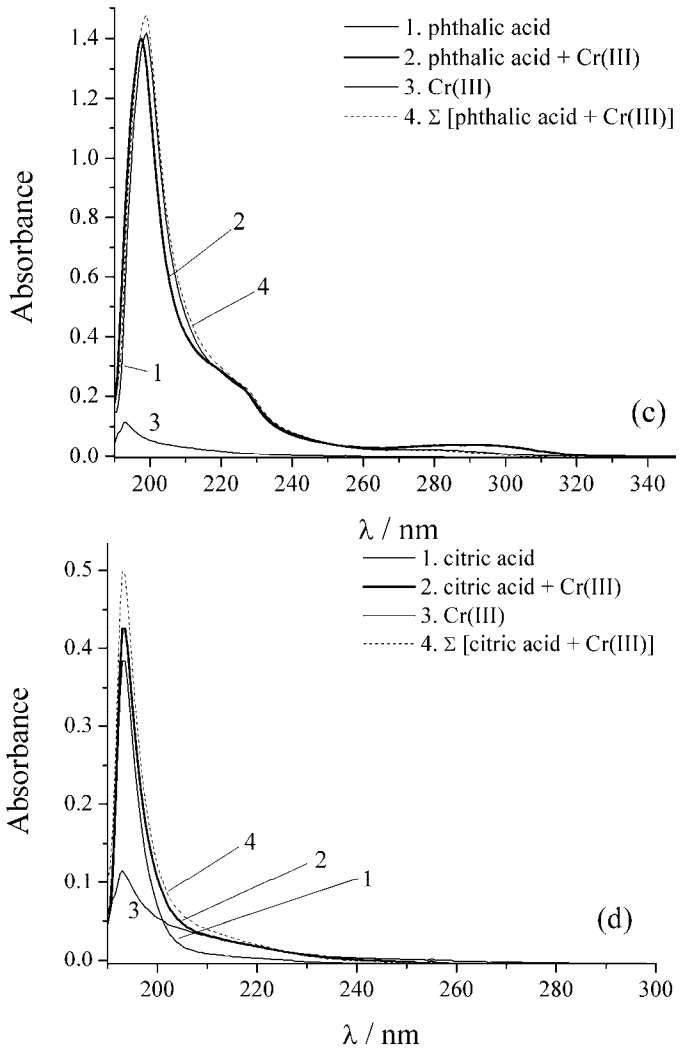

Fig. 1. UV/Vis Spectra of the ligands: benzoic (a), salicylic (b), phthalic (c) and citric acid (d). 1 – ligand solution, 2 – ligand + Cr(III) solution, 3 – Cr(III) solution and 4 – mathematical sum of ligand spectrum and chromium spectrum. l = 1 cm, solvent: CH_3OH/H_2O = 50/50.

the area of the arithmetical summation of the two spectra of the monocomponent systems, *i.e.*, the solution of ligand and the solution of Cr(III) (P_4), according to Eq. (1):

$$\Delta P_{\%} = \frac{P_2 - P_4}{P_2} \times 100 \quad (1)$$

The correlation coefficient (r) was calculated for range of wavelengths in which the absorption occurred, from λ_{min} = 190 nm to λ_{max} = 245 – 330 nm, depending on the ligand.

The sum of absolute values of absorbance differences for every binary ligand–chromium system was calculated for the wavelength (λ_i), according to Eq. (2):

$$S_{\Delta A} = \sum_{\lambda_{min}}^{\lambda_{min}} \mathrm{abs}\left(x_i - y_i\right) \quad (2)$$

where the wavelength range was 190 to 245–330 nm, in which the absorption was observed. The parameter $S_{\Delta A}$ could be calculated in this way as all the data were equidistant following the abscise (wavelength), because all spectra were recorded with an identical sampling interval of $\Delta\lambda$ = 0.5 nm.

The sum of squares of the absorbance differences ($S^2_{\Delta A}$) for the specific wavelength (λ_i), between two series of spectral curves data, was calculated according Eq. (3):

$$S^2_{\Delta A} = \sum_{\lambda min}^{\lambda max} \left(x_i - y_i\right)^2 \quad (3)$$

Experimental procedure for the ESI-MS characterisation of the Cr–ligand interactions

Monocomponent solutions of ligands were made in pre-washed polyethylene Eppendorf tubes 1.5–5 cm^3, with the solvent methanol/water (50/50, v/v). Binary systems of chromium(III)-chloride and the corresponding ligands were obtained in the same way, in the same solvent, by dilution of the concentrated stock solutions. All the obtained solutions were stored in the cold (4 °C) and dark. The presence of 50 % deionized water in the solvent was intended to facilitate the desolvation electrospray process and provide better ion yields.

Solutions of pure ligands were analyzed by ESI-MS immediately after preparation, while the two-component systems of chromium(III) and ligands were analyzed after maturation for at least 30 min after mixing of the components, in order to allow sufficient time for chemical interaction. Bearing in mind that, compared to UV/Vis spectrophotometric analysis, ESI-MS is much more time-consuming, it was ensured that the prepared working solutions were not older than a few hours, in order to avoid side-reaction products. Considering the chemical nature of all the investigated ligands and their relative chemical stability at a given pH, it was assumed that the formation of side products due to photolysis or catalytic degradation did not occur to an extent that could jeopardize the relevance of the results.

By using the ICIS® module of Xcalibur™ 1.3 software, the areas of each ESI-MS ion current chromatogram of 20 µL loop injection for the defined mass range of ligand (P_1) and ligand–chromium solution (P_2) were calculated (Fig. 2).

In order to quantitatively describe the interaction between ligand and chromium(III), the comparison of the obtained areas P_1 and P_2 in Fig. 2., *i.e.*, the difference of areas $\Delta P_{(1–2)\%}$ was performed following Eq. (4):

$$\Delta P_{(1–2)\%} = \frac{P_1 - P_2}{P_1} \times 100\ \% \quad (4)$$

The areas are presented in absolute non-dimensional (arbitrary) units of the Xcalibur™ software (count–second units) that have no physical meaning.

Bearing in mind that the chromium concentration was constant in all the binary systems but ligand concentrations were different, normalization of all the $\Delta P_{(1–2)\%}$ values was performed, providing, the corrected relative area differences $\Delta P_{ESI\%}$, expressed as in Eq. (5):

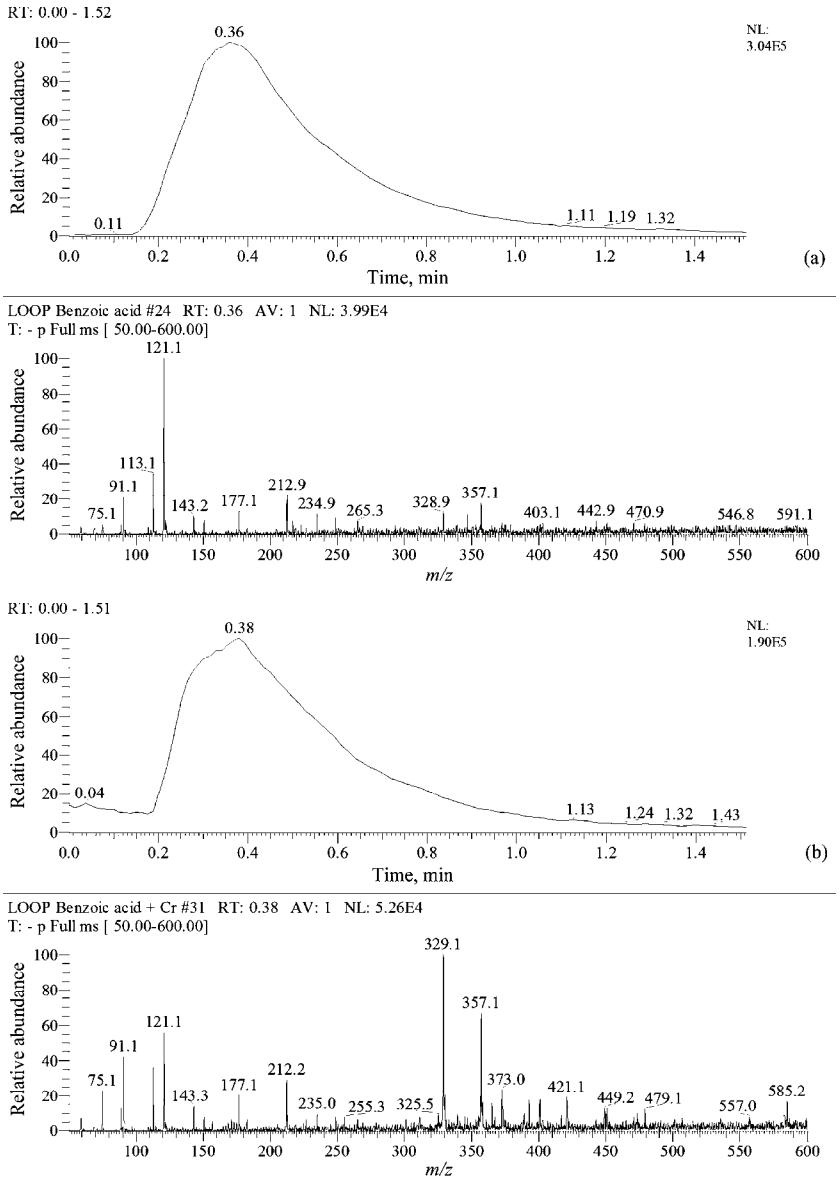

Fig. 2. a) ESI-MS Ion current chromatogram for mass range *m/z* 120–122 of the loop injection of ligand without chromium: benzoic acid, c = 7.00 μmol L^{-1}; b) ESI-MS ion current chromatogram for mass range *m/z* 120–122 of the loop injection of ligand with chromium: benzoic acid, c = 1.00 μmol L^{-1} and chromium, c = 9.0 μmol L^{-1}. Solvent: CH_3OH/H_2O = 50/50, negative ionization mode, flow rate = 100 μL min^{-1}.

$$\Delta P_{\mathrm{ESI\%}} = \Delta P_{(1-2)\%} \frac{c_{\max}(\mathrm{ligand})_m}{(1/n)\sum_{i=1}^{n}\left[c_{\max}(\mathrm{ligand})_i\right]}\ \%, \quad \frac{1}{n}\sum_{i=1}^{n}\left[c_{\max}(\mathrm{ligand})_i\right] = 11.696\ \mu\mathrm{mol\ L^{-1}} \quad (5)$$

where $c_{\max}(\mathrm{ligand})_m$ is maximum ligand concentration (μmol L^{-1}) in the ligand–chromium system, while the denominator presents the average maximal concentration of the investigated ligands, *i.e.*, 11.696 μmol L^{-1}.

The obtained $\Delta P_{\mathrm{ESI\%}}$ values were used for comparison of the interactions between chromium(III) and the ligands. A higher $\Delta P_{\mathrm{ESI\%}}$ value confirms stronger interaction in the investigated binary system.

RESULTS AND DISCUSSION

UV/Vis analysis of the Cr(III)–ligand system

The results of UV/Vis spectrophotometric studies of chromium(III) interaction with benzoic, salicylic, phthalic and citric acids are shown in Fig. 1. The obtained UV/Vis spectra of the investigated ligands correspond well with literature data.[23]

Spectra of benzoic acid and binary system chromium(III)–benzoic acid (Fig. 1a) have very similar absorption profiles, with a small positive (λ > 225 nm) or negative difference (λ, 204–225 and 193–202 nm) between spectrum of the binary system and mathematical sum of the spectra of the separate components. Neither shifts of the absorption maximum and minimum nor do significant absorbance (A) changes exist, which indicates small coordination or interaction between the ligand and metal ion, or a similarity in the electronic configuration of the free and bound ligand, in terms of orbital energy and the probability of electronic transitions.

In contrast to benzoic acid, salicylic acid showed difference in spectra of free salicylic acid and binary system of chromium(III)–salicylic acid, expressed in bands, 220–250 nm and 275–325 nm, in terms of increasing the absorption (A) (Fig. 1b). A bathochromic shift of $\Delta\lambda$ = 2 nm could be seen in the spectrum of complexed salicylic acid at λ = 298 nm, while the other bands did not change their positions.

The binary system Cr(III)–phthalic acid showed suppression of the absorbance, except at 266–317 nm, where the absorbance increased with the appearance of a poorly defined peak at $\lambda_{\max}$ = 293 nm (Fig. 1c). The most prominent peak below 200 nm is, in comparison to the other investigated ligands, bathochromically shifted by approximately $\Delta\lambda$ = 6 nm, and also the molar absorption coefficient (ε) shows the highest value compared to the other ligands.

The spectra of citric acid and citric acid complexed with chromium(III) showed a similarity of the spectral curves, as well as the lack of a bathochromic effect; only a pronounced peak was located at $\lambda_{\max}$ = 193 nm (Fig. 1d). The slightly lower absorption intensity of the complex in solution compared to the mathema-

tical sum of the spectra of the individual components (hypochromic effect) can be noted, indicating a lower probability of excitation of electrons in the resulting complex, while the absorption at λ > 240 nm decreased due to the absence of π-conjugated electrons and low energy excitation chromophores.

The differences in the spectra can indicate the existence of interaction and/or coordination in the binary systems of ligand–Cr(III) because there is no basis for assuming that some other causes could lead to the measurable hypochromic, hypsochromic, bathochromic or hyperchromic shifts under the given conditions of the measurements. The hypothesis that the presence of Cr(III) could lead to the catalytic degradation of ligand or redox reaction with the ligand is unlikely because to the short preparation and maturation time of the system (about 30 min), relatively low redox potential (positive or negative) of the ligands and chromium(III), low concentrations and mild pH of the solutions. In addition, in the case of structural degradation of the ligand molecules in the presence of chromium(III) chloride, it would be expected that the spectra of the resulting products would be of significantly different in shape and intensity and would not show, for example, the hyperchromic effect while maintaining approximately the same shape of the spectrum.

The calculated parameters, the relative difference between the areas ($\Delta P_{\%}$), the linear correlation coefficient (r), the sum of the absolute values of the absorbance difference ($S_{\Delta A}$) and the sum of the squares of the absorbance difference ($S_{\Delta A}^2$), according Eqs. (1)–(4), are presented in Table I. These parameters can be considered only as qualitative or, at most, as semi-quantitative indicators of the chromium(III)–ligand interaction, bearing in mind the differences in the spectra, *i.e.*, the intensities and shifts of the positions of λ_{max} and A depend on the nature of the ligands, the characteristics of the molecular orbitals, changes in bond energies and electronic configuration of the complex in relation to the individual types of ligands and metal ions, the stability constants of complexes in the circumstances, *etc.*

TABLE I. Comparative overview of the differences in the numerical quantifiers of UV/Vis spectra between the monocomponent system (ligand solution) and the binary system (ligand––Cr(III) solution)

Ligand	ΔP / %	r	$S_{\Delta A}$	$S_{\Delta A}^2$	Range λ / nm
Benzoic acid	3.629	0.99756	1.5490	0.06964	190–255
Salicylic acid	8.542	0.99808	2.9655	0.05298	190–330
Phthalic acid	–3.056	0.98782	9.0534	1.01692	190–320
Citric acid	–6.011	0.99790	1.3350	0.05400	190–245

Generally, a larger $\Delta P_{\%}$, lower r, higher $S_{\Delta A}$ and larger $S_{\Delta A}^2$ reveal significant interaction between the ligand and chromium(III), to the extent to which

the physicochemical nature of the process observed in the binary system can be reflected in the UV/Vis absorption characteristics.

Overall, the UV/Vis spectral characterization in terms of the observation of the interaction in the different systems can have only qualitative or semi-quantitative character because, despite the statistical analysis of systems, it could not provide the correct conclusions about the strength of the interaction of chromium(III) and the observed series of ligands.

Even if the difference in the spectrum of the ligand and the analog spectrum of Cr(III)–ligand is small or negligible, a coordination interaction can not be excluded with certainty because the formed UV/Vis absorption systems with their own new electronic configuration may be similar to the absorption of the unbound ligand and therefore differences in the UV/Vis spectrometric analysis are difficult to distinguish.

Based on the previous discussion, it could be stated that UV/Vis spectroscopy could be employed for a fast, easy to perform and preliminary study of interactions due to the simplicity of the preparation of the solutions, a low-cost instrument and the easiness of the interpretation of the experimental results.

ESI-MS Analysis of the Cr(III)–ligand system

A preliminary ESI-MS investigation of ligand solutions by flow injection analysis showed that the selected polarity ESI source coincides with the ionization characteristics of the molecules, which are expected based on their structure. Thus, ligands with *O*-donor atoms with a tendency to deprotonize because of the presence of OH and COOH groups were examined in the ESI negative polarity mode.

Quantification was performed by calculating the area of ESI-MS ion current chromatograms of loop injections for an appropriate mass range (*m/z* molecular ion ±1.0) obtained by analyzing series of mono-component (ligand without chromium) and two-component systems (ligand with chromium). The recorded MS spectra of the mono- and two-component systems in the case of benzoic acid––Cr(III) are shown in the Fig. 2. The areas of the ESI-MS selected mass range ion current chromatograms of the loop injection that are considered in the calculation are shown in Fig. 2. The same procedure was repeated for the other three ligands: salicylic, phthalic and citric acid, the spectra of which are not presented in the paper.

The values of ion current chromatogram peak areas are plotted *vs*. the ligand concentrations and a two-variable correlation was described by linear fitting (Fig. 3).

The quantification was based on the fact that all areas of the chromatograms are in direct function of the peak intensities obtained by observing the signal of ions in the required mass range *m*/*z*. In binary systems in which there is interaction of the ligand with chromium(III), the intensity of the observed characteris-

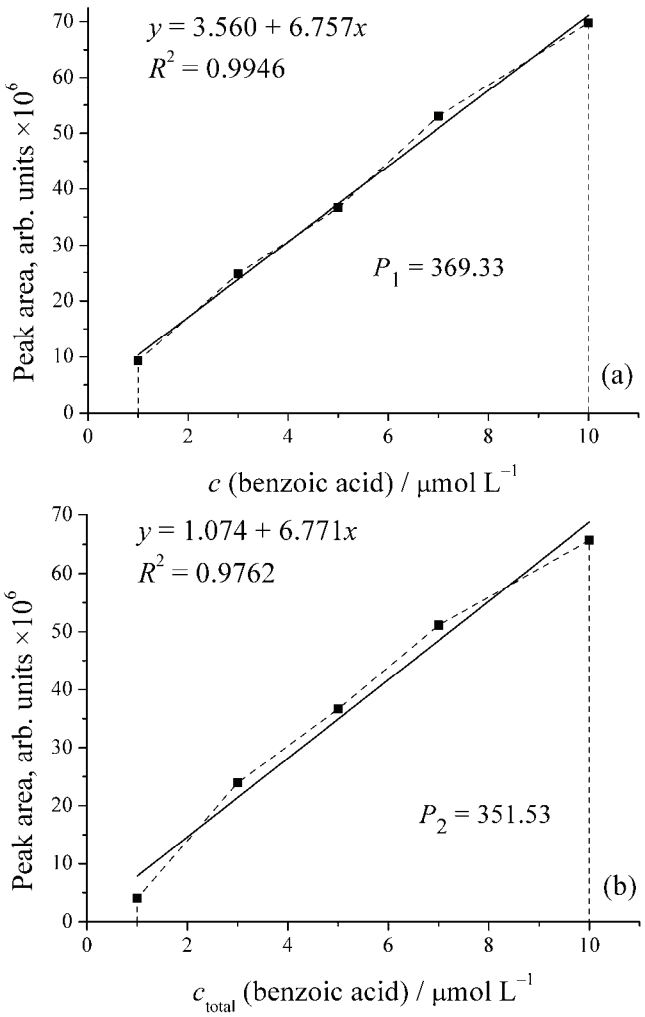

Fig. 3. a) Plot of the peak areas of the ESI-MS ion current chromatograms of the loop injection of benzoic acid (without chromium) for the mass range *m/z* 120–122 *vs*. ligand concentration; b) plot of the peak areas of the ESI-MS ion current chromatograms of the loop injection of the benzoic acid–chromium system (with chromium) for the mass range *m/z* 120––122 *vs*. the ligand. concentration. Solvent: CH_3OH/H_2O = 50/50, negative ionization mode.

tic ion is reduced, because the coordination bonding or other interactions of chromium(III) and ligand change the molecular and ionic composition of the sample. The creation of new ionic species with chromium, also results in a decrease of concentration of the monitored ligand ions because of mass balance preservation. This leads to a reduction in the number of ions generated in a unit of time, in the

case of the analysis of binary systems with sufficient interactions. Simultaneously, by a similar but not by quite identical dependence, there is a reduction in the concentrations of other ionic species that have a ligand molecule incorporated as a component (adducts and/or dimers), since all the species present are in dynamic equilibrium in the injected solution and are desolvated in the ESI source. This proportion is eventually reflected in lower signal intensities of the selected ions registered by the MS detector, because the ESI source is sensitive to concentration and not to the total amount of injected analyte. In this way, in binary systems of the ligands with chromium(III), for identical ligand concentrations, proportionally smaller area of the chromatographic peak are obtained, and the relative decrease in area can be related to the strength of the interaction of chromium and the observed ligand because of a decrease in the monitoring ion concentration in the inlet capillary of the ESI source.

It should be noted that, for a variety of fundamental and methodological reasons, changes in area of chromatogram peaks of loop injections can be treated as valid only in a relative comparison, in the analysis of the system of ligand––Cr(III), with an identical ESI source, ion optics, MS analyzer parameters and the same conditions of pH, ionic strength, solvent, *etc*. Comparison of the absolute values of the area of chromatogram peaks between the different compounds (ligands) is not valid without a special study and knowledge of the complete stoichiometry of the investigated solutions, the equilibrium relationship between species, evaluation of their reactivity and stability in the desolvation and ionization processes, determination of specific response factors, *etc*.

The values $\Delta P_{(1–2)\%}$ and $\Delta P_{\mathrm{ESI}\%}$, calculated according to Eqs. (4) and (5), for the series of ligands are presented in Table II. In the group of studied *O*-donor ligands, the strength of ligand–Cr(III) interaction follows the decreasing order: citric acid > phthalic acid > salicylic acid > benzoic acid.

TABLE II. Values of $\Delta P_{(1–2)\%}$ and $\Delta P_{\mathrm{ESI}\%}$ obtained by ESI-MS

Ligand	$\Delta P_{(1–2)}$ / %	ΔP_{ESI} / %
Benzoic acid	4.8	4.1
Salicylic acid	54.5	54.8
Phthalic acid	60.8	63.7
Citric acid	63.0	66.5

The minimum value of $\Delta P_{\mathrm{ESI}\%}$ of 4.1 % among the studied *O*-donor ligands, can be explained by the fact that ionized benzoic acid with one carboxyl group in the molecule has no ability to build a high stability complex with chromium(III). The first reason is that, compared to all the examined *O*-donor ligands, it is the weakest acid (pK_a = 4.21),[24] which means that in the methanol/water matrix it has the greatest tendency to bind H_3O^+ to the conjugate anion (benzoate), which possess ligand properties. As ligands act as bases, acids and

metal ions in water-containing solutions, this may lead to competition between the protons and chromium(III) ions for the ligand. If the interaction between ligand and protons is strong, protonation of ligand occurs, leading to a decrease in the coordination interaction with chromium(III).

The other investigated *O*-donor ligands have, in comparison to benzoic acid, an order of magnitude larger acidity constants (citric acid, pK_{a1} = 3.09; phthalic acid, pK_{a1} = 2.98 and salicylic acid, pK_{a1} = 2.97)[23] allowing them stronger interactions with the chromium cations in the studied binary systems. These acidity constants are valid for aqueous solutions of these compounds, while in a mixture of methanol/water 50/50 (v/v), the corresponding constants are about 6–10 times smaller because of the lower basicity of methanol compared to water, although this does not interfere substantially in the above-described relative relations. Groups in the *ortho*-positions, such as –OH (salicylic acid), by its +*R* effect, lower the acidity of the neighboring –COOH groups, but also by its strong –*I* effect, lower the electronic density of the carboxyl groups, which favor deprotonation. In the case of citric, salicylic and phthalic acid anions, stabilization is enhanced by the presence of intramolecular hydrogen bonds.

In addition to the above-discussed acid–base characteristics, ligand dentate is another important factor in the formation of chromium complexes. Benzoic acid, or benzoate, can be considered as a bidentate ligand because of the presence of carboxylate anions. However, due to the slightly higher effective ionic radius of Cr(III) ions (61.5 pm), four-atom cyclic structures are not stabile and benzoic acid can be considered as a monodentate ligand. On the contrary, salicylate and phthalate ($HPht^-$, Pht^{2-}) are typical bidentate ligands with the possibility of creating five- or six-membered ring structures with Cr(III), which is more suitable for ligand field stabilization of the octahedral coordination sphere of chromium ions.

Salicylic acid with an OH group in the *ortho*-position possesses two binding sites with three *O*-donor atoms (ambidentate ligand), which significantly enhances its interaction with chromium compared to that of benzoate. It should be noted that further deprotonation of the OH groups in the salicylate is present to a very small extent ($pK_{a2} \approx 13.80$); hence, this structure can be excluded from further consideration. The deprotonized carboxyl group and the *ortho*-OH group of salicylate may, with low steric hindrance, form a stable bidentate complex with chromium, which is confirmed by the higher value of $\Delta P_{ESI\%}$ = 54.78 %.

Phthalic acid with two COOH groups in the 1,2-position is subject to two-step deprotonation and can appear as a monodentate or bidentate ligand at the pH values of the investigated solutions, providing for complexes of different stoichiometric composition and type. The forms of the neutral ligand, phthalate and hydrogenphthalate (H_2Pht, Pht^{2-} and $HPht^-$) are more convenient for coordination of Cr(III) than salicylate, as evidenced by the higher value $\Delta P_{ESI\%}$ = 63.72 %.

As a consequence of intermolecular hydrogen bonds, there is a tendency of dimerization of hydroxycarboxylic and dicarboxylic acids, especially in non-polar solvents, which therefore have the possibility of forming open or cyclic dimeric forms, (H_4L_2) in neutral or ionized form ($H_3L_2^-$, $H_2L_2^{2-}$, *etc*.). This variety of forms with electron-donor ability favors the formation of different interactions with the chromium in the observed binary systems, which has the consequence of significantly reducing the concentration of the monitored analyte ions in solution and the relatively high values of $\Delta P_{ESI\%}$ for the *O*-donor ligands, except for benzoic acid.

Citric acid as a natural three-carbon acid with four acidic hydrogen atoms (H_4Cit) plays an important role in the transport processes of chromium(III) in soil systems and may represent a good model system for studying the properties of natural organic matter. Despite its aliphatic character, it possesses substantial acidity due to the strong *–I* effect, because of which the adjacent –COOH groups act on one another. The effect is strong enough to disable the partial dissociation of the carboxylic H-atom from the $–CH_2$ group. In addition to the polar effect, statistically there is greater probability that one of the three equivalent carboxyl groups will dissociate and give protons. However, the citrate forms, in contrast to other *O*-donors, and most of the other studied ligands, form typical chelate complexes, which further favor coordination with chromium. In addition, there is the possibility of forming a homoleptic complex series of the type $[CrCit_2]^{n+/-}$, because the steric hindrances are relatively small and the flexible conformation of the σ-bonds allows favorable orientation for the formation of chromium coordination octahedron with oxygen. For these reasons, citric acid shows the highest value $\Delta P_{ESI\%}$ = 66.46% among the studied *O*-donors, indicating it has the strongest interaction with Cr(III) in the series of studied ligands.

Comparing a series of studied systems of chromium(III) with ligands, the values of $\Delta P_{ESI\%}$ are in good correlation with the acid–base and electron-donor properties, geometric and steric characteristics and molecular structures of the investigated compounds.

The general evaluation of the application of ESI-MS technique for the quailtative and quantitative analysis of metal–ligand systems, based on the presented results, is that it can be considered that the idealized descriptions and theoretical considerations and advantages of ESI-MS techniques often do not match with the real conditions, which may affect the evaluation of the results obtained by ESI-MS technique for defining metal–ligand interactions. During the ESI soft ionization process, the composition of the solution can be changed in relation to the initial equilibrium conditions: a) the volume changes due to spray evaporation, which increases the concentration of species and the modification of ionic strength of solution, b) there is a variation of the temperature in the droplet spray, due to the high temperature that exists in the ESI source and the constant evapo-

ration from the droplet surface, c) changing the pH, as influenced by changes in temperature and concentration in the spray and as a result of redox reactions in the solution in the capillary ion source, especially in systems with redox-active ligands and metal ions, while redox reactions may also occur in the other parts of the ES chamber, not only in the capillaries. The ions produced in the ESI source may be subject to a variety of reactions in the gas phase, before they reach the mass analyzer/detector. Among the factors that can complicate the ESI-MS analysis are the facts, which were also confirmed in this study, that solvent molecules can be added to (or taken away from) the central metal ion, the ligand or during the process of ionization. Ion adducts that do not normally occur in the solution can be formed in the process of ionization, as observed in the present study of the investigated studied systems. The formation of pseudo molecular or adduct ions (*e.g.*, with Na^+) is very common in ESI-MS analyses. They do not compromise the analysis but make the recognition the origin of some peaks difficult. Despite the soft ionization characteristic of ESI-MS, fragmentation or polymerization phenomena can still play role (*e.g.*, with salicylic acid and other systems). In addition, the number of acidic protons in the metal–ligand complex cannot be determined. ESI-MS Spectra are sensitive to instrumental parameters for source and ion optics (recording conditions), such as spray voltage, capillary temperature, capillary voltage, ion optics potentials (tube lens offset) and the cone voltage. Change in these parameters can have an impact on the results for a given system. Different ions can show different response factors. The composition of solutions that can be subjected to the analysis is conditioned by significant limitations: no application of high ionic strengths, even relatively low concentrations of non-volatile components can be disturbing (*e.g.*, Na^+, Ca^{2+} and Mg^{2+}); the method requires the addition of an organic solvent to the aqueous solution before analysis, which can be somewhat disruptive to the equilibrium state in solution.

Despite these interfering factors, the ESI-MS technique was used in studies of metal–ligand systems, as evidenced by literature references. ESI-MS was applied not only to the speciation of particular elements,[24,25] which can be defined by phenomenon of coordination interactions, but also in the domain of studying the non-covalent interactions between biomacromolecules.[26,27]

In phase of determining the research methodology, it is necessary to define whether ESI-MS can provide qualitative determinations, giving reliable data on the number and stoichiometry of metal–ligand species in solution. It is necessary to know whether the ESI process introduces interference in equilibria, and whether gas-phase reactions occur and what are their products. Equilibrium misbalance can occur only if the metal–ligand system is kinetically unstable in the time range of ESI process, *i.e.*, about 0.01 sec. As for gas-phase reactions, they can occur under a variety of specific conditions and hence a simple conclusion on this issue cannot be given.

In addition, for quantification purposes, it is important to determine whether the ESI-MS technique can be successfully applied for the quantification, *i.e.*, if it provides a proper determination of the concentrations of the species in solution. For this application, besides the above-mentioned requirements (kinetic inertia and absence of gas phase reactions), it is essential to know the response factors of the individual ions. However, the different approaches proposed for their calculations are still not reliable enough, and in most papers, equivalence of the response factors is assumed, which is a relatively debatable assumption, except in cases of similar types of identical charge (for example, host–guest systems). Finally, an acceptable method for assessing the usefulness of ESI-MS results is comparison of the ESI-MS results with those from available conventional techniques, such as potentiometry and other methods.

In terms of qualitative results, this comparison often gives good matches. Thus, it would seem that in most cases equilibrium misbalance and gas-phase reactions do not occur to a significant extent, or if they occur at all, then they do not modify the stoichiometry of the species present in the initial solution, but change only their quantitative relations. Therefore, the ESI-MS technique may be considered as a relevant and reliable technique for qualitative analysis of metal––ligand system.

With regard to the quantitative application ESI-MS, rigorous comparison with other techniques can be realized only with the correction of activity coefficients, due to the different composition of the solution ionic strength, while currently there is no generally applicable method for overcoming the problem of response factors. In summary, the ESI-MS technique, for now, cannot be considered as a completely reliable application for the quantitative determination of metal–ligand system (this of course is not true for quantitative analytical applications in other fields, *e.g.* with HPLC and other separation techniques), but due to some unique features, in combination with other techniques, ESI-MS is still a valuable source of data for a better understanding of the equilibrium of metal–ligand systems. In this paper, quantification by the employed techniques, UV/Vis spectroscopy and ESI-MS showed a large difference in the informativness of the experimental results, in favor of the ESI-MS technique, which is related to the fundamental limitations of the UV/Vis method. A comparative view of UV/VIS and ESI-MS method for the study of interactions in metal–ligand systems is given in Table III.

TABLE III. Comparison of the suitability of the UV/Vis and ESI-MS techniques for investigations of metal–ligand systems

Technique	Species number determination	Stoichiometry determination	Equilibrium constant determination	Detection limit mol L^{-1}
UV/Vis	Not ideal	Acceptable	Good	10^{-5}
ESI-MS	Good	Excellent	Problematic	10^{-6}

CONCLUSIONS

Chromium(III) interacted with the investigated *O*-donor humic-like ligands. The intensity of the interaction of chromium(III) with the *O*-donor humic-like ligands was correlated with the acid–base and electron-donor properties, geometric and steric characteristics, and the number and position of the *O*-donor atoms in the investigated ligands. The intensity of the interaction of chromium with the *O*-donor ligands followed the order: citric acid > phthalic acid > salicylic acid > benzoic acid, which correlates with the number of *O*-donor atoms in the structure. The study of the possibility of chromium interaction with humic model substances, benzoic, salicylic, phthalic and citric acid is a good method for defining the interaction with polyfunctional, polydispersed, polyelectrolyte ligand, such as humic macromolecules. UV/Vis spectroscopy and ESI-MS quantification showed a large difference in their ability to define the interaction of chromium(III)–ligand; the ESI-MS technique being superior. The ESI-MS technique with loop injection can be used for quantitative analysis of the system Cr(III)–ligand under certain circumstances. The ESI-MS ion current chromatograms of loop injection indicated a stabile peak and signal integrity for both the total ion current and the range of *m*/*z* values.

Acknowledgement. This study was supported by the Ministry of Education, Science and Technological Development of the Republic Serbia and was performed as a part of the Project TR 31060.

И З В О Д

ИНТЕРАКЦИЈА ХРОМА СА О-ДОНОР ХУМАТНИМ МОДЕЛ ЛИГАНДИМА ЕЛЕКТРОСПРЕЈ МАСЕНОМ СПЕКТРОМЕТРИЈОМ

ДАРКО Х. АНЂЕЛКОВИЋ[1], РУЖИЦА С. НИКОЛИЋ[1], ДЕЈАН З. МАРКОВИЋ[2], ТАТЈАНА Д. АНЂЕЛКОВИЋ[1], ГОРДАНА М. КОЦИЋ[3], ЗОРАН Б. ТОДОРОВИЋ[2] и АЛЕКСАНДАР Љ. БОЈИЋ[1]

[1]*Природно–математички факултет,Универзитет у Нишу,Вишеградска 33, 18000 Ниш,*
[2]*Технолошки факултет,Универзитет у Нишу, Булевар ослобођења 124, 16000 Лесковац и*
[3]*Медицински факултет, Универзитет у Нишу, Булевар др Зорана Ђинђића 81, 18000 Ниш*

Проучавање интеракције хрома са *O*-донор хуматним модел лигандима вршено је коришћењем електроспреј-јонизационе масене спектрометрије (ESI-MS) и ултраљубичасте/видљиве (UV/Vis) спектрофотометрије. Хетерогеност функционалних група оправдава примену модел једињења хуминских супстанци. Као модел супстанце за проучавање интеракције хрома са хуминским супстанцама коришћене су бензоева, салицилна, фтална и лимунска киселина, које садрже *O*-донор атоме, а који се налазе и у хетерогеном и полидисперзном лиганду, каква је хуминска или фулво киселина. Интензитет интеракције је у корелацији са ацидо–базним и електрон-донорским особинама, геометријским и стерним карактеристикама, као и бројем и положајем *O*-донор атома у испитиваним лигандима. UV/Vis карактеризација интеракције хрома са хуматним модел лигандима је доведена у корелацију са ESI-MS карактеризацијом комплекса, у квалитативном и квантитативном смислу. UV/Vis спектроскопија и ESI-MS квантификација су показале информативну разлику у погледу дефинисања интеракција хром–лиганд, и то у корист ESI-MS технике. ESI-MS техника се може користити за квантитативну ана-

лизу система Cr(III)–лиганд. ESI-MS хроматограми јонске струје добијени инјектирањем 20 μL система Cr(III)–лиганд, показују стабилне пикове и интензитете сигнала.

(Примљено 20. марта, ревидирано 3. јула 2012)

REFERENCES

1. H. E. Allen, C. P. Huang, G. W. Bailey, A. R. Bowers, *Metal Speciation and Contamination of Soil*, Lewis Publishers, Ann Arbor, Michigan, 1995, p. 7
2. M. Linde, *PhD Thesis*, Swedish University of Agricultural Sciences, Uppsala, 2005
3. E. Tipping, C. Woof, *J. Soil. Sci.* **42** (1991) 437
4. E. Tipping, M. A. Hurley, *Geochim. Cosmochim. Acta* **56** (1992) 3627
5. R. A. Griffin, A. K. Au, R. R. Frost, *J. Environ. Sci. Health* **12** (1977) 431
6. D. G. Kinniburgh, W. H. V. Riemsdijk, L. K. Koopal, M. Borkovec, M. H. Benedetti, M. J. Avena, *Colloids Surf., A* **151** (1999) 147
7. B. R. James, R. J. Bartlett, in *Chromium in Natural and Human Environments*, J. O. Nriagu, E. Nieboer, Eds., Wiley Interscience, New York, 1988, p. 265
8. R. J. Bartlett, *Environ. Health Perspect.* **92** (1991) 17
9. J. Kotas, Z. Stasicka *Environ. Pollut.* **107** (2000) 263
10. R. J. Bartlett, J. M. Kimble, *J. Environ. Qual.* **5** (1976) 379
11. R. J. Bartlett, J. M. Kimble, *J. Environ. Qual.* **5** (1976) 383
12. T. Andjelkovic, J. Perovic, M. Purenovic, S. Blagojevic, R. Nikolic, D. Andjelkovic, A. Bojic, *Anal. Sci.* **22** (2006) 1553
13. T. Andjelkovic, R. Nikolic, A. Bojic, D. Andjelkovic, G. Nikolic, *Maced. J. Chem. Chem. Eng.* **29** (2010) 215
14. T. Arunachalam, R. Bhakyaraj, A. K. Sasi, *E-J. Chem.* **6** (2009) 743
15. E. Nakayama, T. Kuwamoto, S. Tsurubo, H. Tokoro, T. Fujinaga, *Anal. Chim. Acta* **130** (1981) 289
16. L. Bois, A. Ribes, M. Petit-Ramel, M. F. Grenier-Loustalot, *Chem. Ecol.* **19** (2003) 263
17. T. D. Burns, T. G. Spence, M. A. Mooney, L. A. Posey, *Chem. Phys. Lett.* **258** (1996) 669
18. P. Kebarle, L. Tang, *Anal. Chem.* **65** (1993) 972A
19. W. Henderson, M. J. Taylor, *Inorg. Chim. Acta* **277** (1998) 26
20. Y. Bai, F. R. Song, M. L. Chen, J. P. Xing, Z. Q. Liu, S. Y. Liu, *Anal. Sci.* **20** (2004) 1147
21. D. Baron, J. G. Hering, *J. Environ. Qual.* **27** (1998) 844
22. Z. L. Cheng, K. W. M. Siu, R. Guevremont, S. S. Berman, *J. Am. Soc. Mass Spectrom.* **3** (1992) 281
23. *NIST database*, National Institute for Standards and Technology, Gaithersburg, MD, USA
24. J. A. Dean, *Lange's Handbook of Chemistry*, McGraw Hill, New York, 1992
25. I. I. Stewart, *Spectrochim. Acta, B* **54** (1999) 1649
26. H. Chassaigne, V. Vacchina, R. Lobinski, *TrAC, Trends Anal. Chem.* **19** (2000) 300
27. J. L. Beck, M. L. Colgrave, S. F. Ralph, M. M. Sheil, *Mass Spectrom. Rev.* **20** (2001) 61
28. A. J. R. Heck, R. H. H. Van den Heuvel, *Mass Spectrom. Rev.* **23** (2004) 368.